UNDERSTANDING THE MECHANICAL BEHAVIOR OF CLAYEY MATERIAL FOCUSED ON DEVELOPING/DIMINISHING OF ANISOTROPY AND DISTURBANCE OF STRUCTURE

By

Imran KHAN

Supervisor: Dr. Kentaro Nakai

A dissertation submitted in partial fulfillment of the requirements for the degree of Doctor of Philosophy,

Geotechnical Engineering Laboratory
Department of Civil and Environmental Engineering,
Nagoya University,
Nagoya, Japan.

March, 2020

異方性の発達／消滅と構造の乱れに着目した
粘性土の力学挙動の把握

カン　イムラン

令和　2年 3月

ABSTRACT

The earthquake damage prediction is mainly focused on the seismic instability of sandy foundations, although the clayey foundation could also be vulnerable to earthquake damage. Previously for the dynamic problem, the conventional clay is safe but recently investigated results showed that clay foundation showed loss of rigidity and cause damages due to earthquake. If the past earthquake damage is examined carefully, although there are not many cases like liquefaction damage of sandy foundation, earthquake damage of clayey foundation can be also observed.

Naturally deposited clays/sands are mostly found in structured, and usually also in overconsolidated states. Furthermore, they exhibit what is more or less a condition of anisotropy. In an artificial/remolded sample, the soil skeleton structure is disturbed but in naturally soil, the soil skeleton structure is developed. In order to deal with naturally deposited materials, it is very important to know about soil skeleton structure, especially structure and anisotropy.

The main purpose of this research is to understand the work of soil skeleton structure especially for anisotropy and structure and to know the mechanical properties of clay and the developing/diminishing of anisotropy. Naturally deposited soil has a highly developed structure as compared to remolded soil, so during the deposition process, anisotropy is considered to be also highly developed. The knowledge of development/diminishing of anisotropy are very important, to understand the mechanical behavior of natural soil and the work of soil skeleton structure with ongoing plastic deformation is important.

Another important aim is to artificially produce the soil sample having similar characteristics to those of naturally deposited soft clay in the laboratory. Because it is very important to grasp both static and dynamic mechanical properties of naturally deposited clayey materials and it can be achieved by carrying out various systematic experiments using the undisturbed soil samples.

Since the cyclic shear strength varies depending on the loading rate, it is important to conduct experiments using a suitable loading rate. Therefore, it is important to obtain experimental results at the lowest possible loading rate so that the internal state of the specimen can be treated as homogeneous and uniform. Therefore, reconstituted clayey

samples were subjected to undrained cyclic triaxial compression/extension tests with loading rate from 1.0Hz to 0.0042Hz by stress control, and 0.01%/min by strain control to determine the undrained cyclic shear behavior of clayey soil under a drastically changed loading rate. Finally, the final values of excess pore water pressure after the homogenization process was the same regardless of the loading rate. This means that if sufficient time is left after cyclic loading, the final mean effective stress value becomes equal regardless of the loading rate.

Triaxial tests were carried out using the vertical and the horizontal extraction specimen of the reconstituted clay and silty clay, for accumulating experimental facts of the development of anisotropy during the preliminary consolidation process and the influence of the anisotropy on the shear behavior. The vertical sample shows larger peak strength as compared to horizontal, because of the development of anisotropy on the compression side. As the confining pressure increases, the difference between the peak strength of vertical and horizontal becomes smaller and smaller which indicates that the anisotropy diminished and intensity ratio decreases. By comparing clay and silty clay, silty clay materials lose their anisotropy at lower confining pressure (600kPa) as compared to clay materials (1800kPa). Therefore, the grain sizes have a significant effect on the developing and diminishing of anisotropy. Another important fact observed was critical state index is decreasing and becomes constant as confining pressure increases.

In the past, according to the results of laboratory experiments, it has been found that destabilization such as liquefaction phenomenon does not occur in clayey soil because clayey soil maintains relatively high rigidity and strength even after cyclic loading. It is common that the soil was in the state of "high water content", "high sensitivity", and "soft" where the earthquake damage occurred. The difference between a natural deposited sample and a reconstituted sample is considered to be the degree of development of "soil skeleton structure" that develops over a long period of deposition process over several tens of thousands of years. Therefore, the influence of the disturbance of soft clay due to cyclic loading is grasped from undrained triaxial compression tests and importance/implication of soil skeleton structure, it was observed that it can be understood that the degradation of structure and accumulation of over consolidation occur during the cyclic loading.

It is difficult to prepare the number of homogeneous soft clay samples, due to the

problem of variability of quantities during sedimentation, disturbance during sampling and high expense of the boring surveys. Therefore, the influence on mechanical properties when hydration reaction controlled cement is added to clayey soil and also describe the results of examining the influence of calcium leaching on the mechanical properties of cemented cohesive soil. By using the remolded sample, focused on the cementation reaction, in order to artificially produce the soil sample having similar characteristics to those of naturally deposited soft clay. By doing so, while maintaining the reproducibility of the specimen, it might be possible to perform a large number of systematic experiments, and to conduct such model experiments as impossible in the past, in order to artificially produce the sample having similar characteristics to those of naturally deposited soft clay.

As a result, the solidification effect was so strong that localized failure occurred in the soil specimen due to cracking followed by a sudden decrease of shear stress with no increase in excess pore water pressure. So, in terms of the necessity to reduce the solidification effect, a newly attempted method was introduced “addition of hydration reaction controlled cement” and “calcium leaching” to represent similar characteristics of soft clay material. It was concluded that the addition of cement makes it possible to reproduce the characteristics of naturally deposited soft clay to some extent, such as high sensitivity ratio and high compressibility ratio and by using pre-curing cement and stirring the mixture for a while, the solidification action of the hydrated product was destroyed and by controlling the hydration reaction, it showed ductile behavior. Moreover, by using calcium leaching smooth stress in shearing behavior-strain curve and softening behavior were achieved.

ACKNOWLEDGEMENTS

Though only my name appears on the cover of this dissertation, a many great people have contributed to its production. I owe my gratitude to all those people who have made this dissertation possible and because of whom my Doctoral experience has been one that I will cherish forever.

Foremost, I would like to thanks to my sweet great Almighty Allah for his continuous blessings on me, as without his blessing it was impossible for me to complete my thesis. All the Respect to our beloved Holy Prophet Muhammad (Peace be upon him) and their Ahl E Bait (A.S), who after a lot of hardships and difficulties, made us able to recognize our ALLAH and to distinguished virtue and evil.

After thanks to Almighty Allah, I would like to express my sincere gratitude to my respected advisor Associate professor. Kentaro Nakai for his continuous support during my PhD study and research, for his patience, motivation, enthusiasm, and immense knowledge. Dr. Kentaro Nakai is one of the best supervisor/ teacher/ human being, that I have had in my life. His guidance helped me in all the time of my research and writing of this thesis. I could not have imagined having a better advisor and mentor for my PhD study. His patience and support helped me overcome many crisis situations and finish this dissertation. I am also thankful to him for encouraging, the use of correct grammar and consistent notation in my writings and for carefully reading and commenting on countless revisions of this manuscript. I am grateful to him for holding me to a high research standard and enforcing strict validations for each research result, and thus teaching me how to do research. I hope that one day I would become as good advisor to my students as Dr. Kentaro Nakai has been to me. I wish such a teacher-student relationship and friendship to be everlasting.

My appreciation also for having granted me the opportunity to attend a number of conferences inside Japan. The experiences will forever remain memorable and treasured in my heart. The valuable suggestions that I received during the research progress presentations were helpful in the development of the thesis. I wish to show my sincere gratitude to the dissertation committee, Professor Masaki Nakano, Professor Toshihiro

Noda, and Professor Feng Zhang of Nagoya Institute of Technology (NIT), for their continuous guidance, positive, and invaluable suggestions which have helped me in achieving the targeted research goals and also for taking time off their busy schedule in order to review my thesis.

Likewise, I would like to acknowledge the positive comments that I received form Professor Akira Asaoka, Emeritus Professor of Nagoya University, for his valuable suggestions and motivation. I would like to express my sincere gratitude to Associate Professor Shotaro Yamada for his conscientious and patient instruction. I can always receive enlightening suggestion and always encourage me with his nice smile. I would like to express my sincere gratitude to Assistant Professor Takahiro Yoshikawa and Assistant Professor Takayuki Sakai for his conscientious and kind support, I really like talking with both of them as they make me laugh.

I would like to acknowledge Mr. Mizukami, Hori, Hayano san and the other entire lab member who were very kind to me during my stay in japan and I really appreciate their help. Also, many friends have helped me stay sane through these difficult years. Their support and care helped me overcome setbacks and stay focused on my graduate study. I greatly value their friendship and I deeply appreciate their belief in me. I am also thankful to Isono and Sachiko san (Nani Chan) and Tsujimura family (Osaka homestay), who are really kind to me and never made me feel, that I am lonely here in Japan. Also, I would like to pay tribute to Nusrat Fateh Ali Khan, whose beautiful qawali/songs were always with me during my Ph.D. journey and Sheikh Abdul Rahman Al Sudais for his beautiful voice which makes me relax, when I got stress during my research.

This research is financially supported by the Monbukagakusho Scholarship Program, provided by the Ministry of Education, Science, and Culture (MEXT) of Japan and I would like to express my special acknowledgment here and to Nagoya University, Japan.

Last but not the least; I would like to thank my parents, my brother and sister who always stand beside me whenever I need them, I really appreciate their help.

Imran KHAN
Nagoya University
Nagoya, Japan

TABLE OF CONTENTS

Chapter 1

INTRODUCTION

1.1 RESEARCH BACKGROUND

Soft clays belong to the well-known category of problematic soils. Such soils are mainly encountered under layered deposits in coastal areas. The lack of bearing capacity, high compressibility and very long time of consolidation are three typical properties of soft clays. Several problems as related to soft clays exist from field investigation to their modelling behavior.

Since the liquefaction damage to sandy soils has been noticed by the Niigata and the Alaska Earthquake in 1964 [1, 2], the earthquake damage prediction of the ground / soil structure has been mainly focused on the seismic instability of the sandy foundations. On the other hand, even if the clayey soil which has an N-value of zero or contains a large amount of sand / silt, as soon as it is classified as "clay", it has been often considered that earthquake damage does not occur and it has been virtually modeled as an elastic material in the past. However, in fact, it is not the case that earthquake damage has not really occurred on clayey foundations.

Previously for dynamic problem the conventionally clay is safe but recently investigated results showed that clay foundation showed loss of rigidity and cause damages due to earthquake. If the past earthquake damage is examined carefully, although there are not many cases like liquefaction damage of sandy foundation, earthquake damage of clayey foundation can be also observed and statically soft clay foundation showed large settlement as the compressibility is large. Clay shows static and dynamic problems. A static problem includes; The Nagashima area, during the embankment construction, consolidation settlement was about 2 meters. In total, over 3 meters of consolidation settlement has existed for 40 years as shown in Figure 1.1 and soil profile in Figure 1.2.

Chapter 1

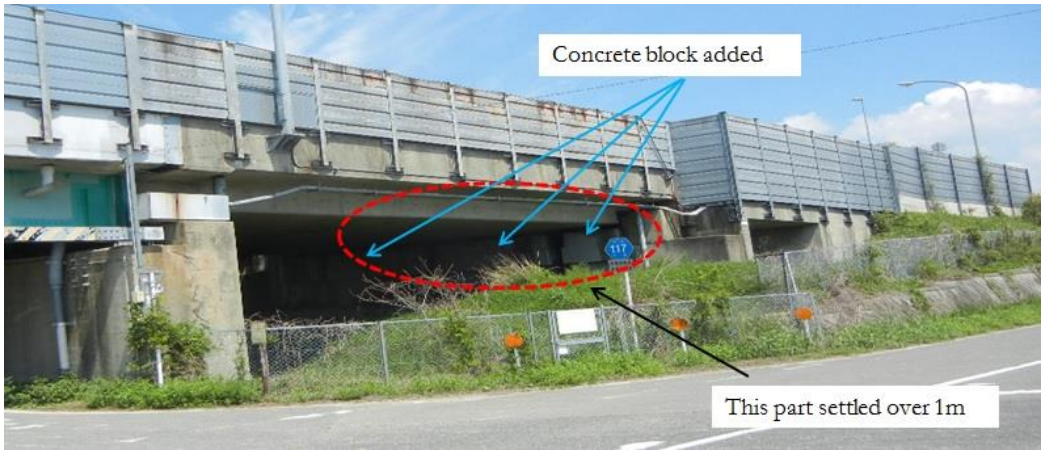

Fig. 1.1 Nagashima bridge

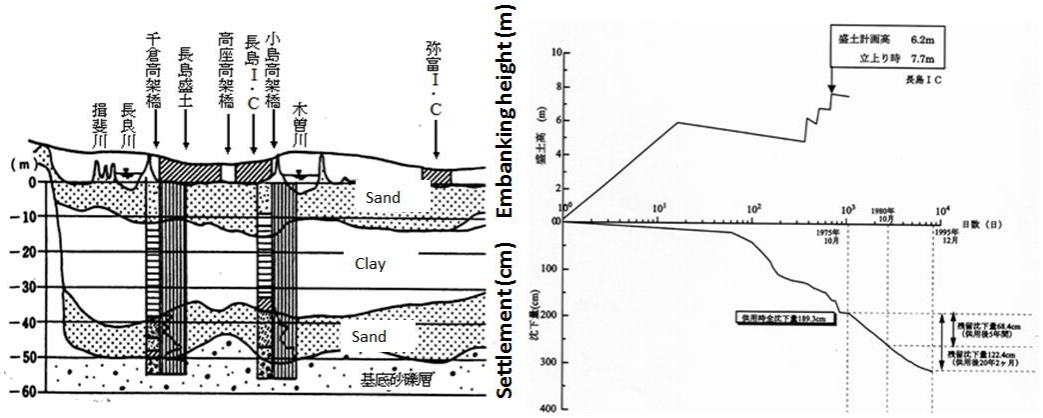

Fig. 1.2 Soil profile of Nagashima area

It is known that the damage to the clayey foundation at the time of the Mexico City earthquake in 1985 caused tremendous human and structural damage in Mexico City far from the epicenter. Mexico City is located on the ground made by reclaiming of old Texcoco Lake, and soft volcanic ashy clay was deposited thickly. This soft clay lost its bearing capacity during the earthquake, causing overturning damage to structures [3, 4]. In addition to the structural damage during the earthquake, the settlement of the clay layer accelerated immediately after the earthquake, and continued for a long time [5].

Similar earthquake damage, thought to be caused mainly by clayey soil, has also been observed both in Japan and abroad. Long-term continuous settlement damage of the Niigata plain by the off the coast of Miyagi earthquake in 1978 [6], shown in Figure 1.3

and Chuetsu earthquake in 2007 [7], shown in Figure 1.4 and the settlement acceleration of Port Island by the 1995 Southern Hyogo Prefecture Earthquake [8]. Also, the soil sampling (disturbed and undisturbed samples) was done by 21 m borehole at the site due to the collapsed of Margalla Tower, Islamabad in 2005 Earthquake, Pakistan. The grain size distribution and the electric resistivity test results showed that the soil beneath the tower was mainly clayey and silty soil as shown in Figure 1.5. In recent years, collapse of soil structures in the Kathmandu Valley caused by the Nepal earthquake in 2015, shown in Figure 1.6 and 1.7. Graben-like cracks in the Aso caldera caused by the Kumamoto earthquake in 2016 could be also considered to be earthquake damage of clayey material.

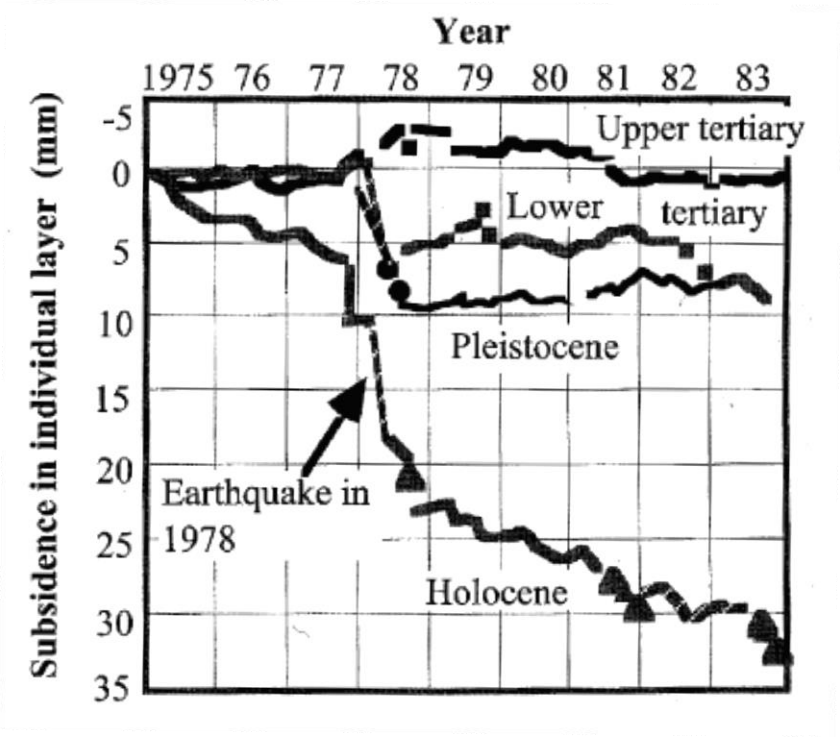

Fig.1.3 1978 Off the Coast Miyagi Prefecture earthquake

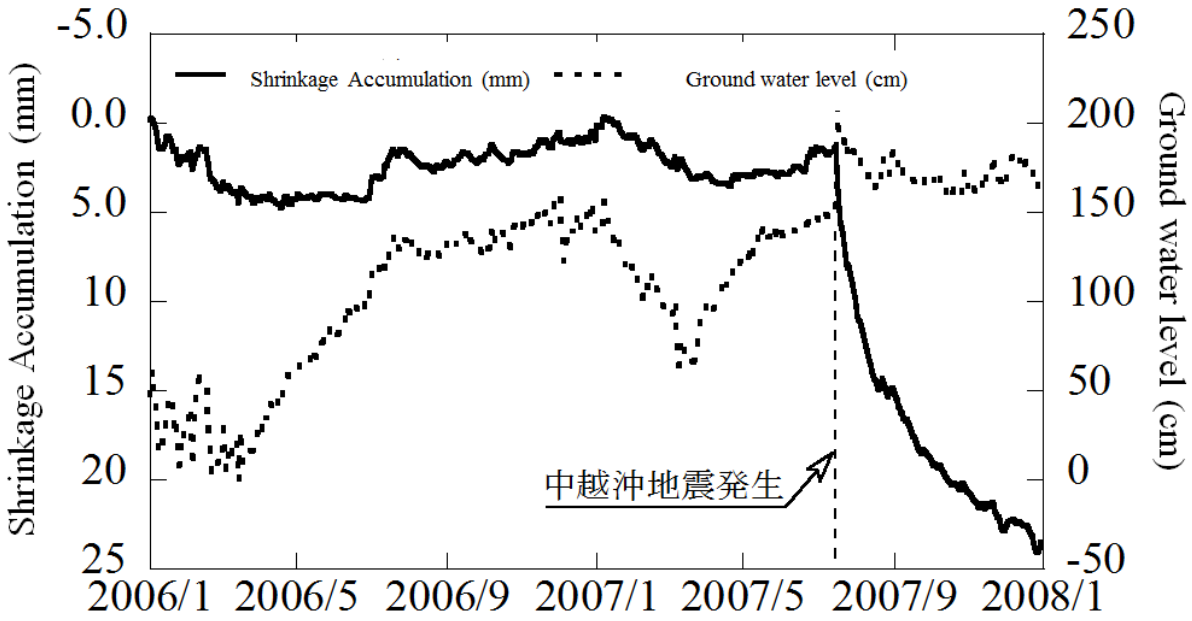

Fig. 1.4 Modified figure of 2007 Chuetsu-oki earthquake (Isobe et.al)

Depth (m)	Plasticity Index	Liquid Limit	USCS	Soil type	AASHTO	Soil type
1.5	5	16	CL-ML	Silty Soil	A-2-4	Silty or Clayey Soil
3.5	6	20	CL - ML	Silty Soil	A-2-4	Silty or Clayey Soil
8.5	12	23	CL	Clayey Soil	A-2-6	Silty or Clayey Soil
10.5	6	19	CL-ML	Silty Soils	A-2-4	Silty or Clayey Soil
14	8	28	CL	Clayey Soil	A-2-4	Silty or Clayey Soil
20.5	15	29	CL	Clayey Soil	A-2-6	Silty or Clayey Soil

Before Collapse

After Collapse

Fig. 1.5 Soil Classification by unified soil classification system (USCS)

(Collapsed of Margalla Tower, Islamabad in 2005 Earthquake, Pakistan)

Chapter 1

Fig 1.6 2015 Nepal Earthquake

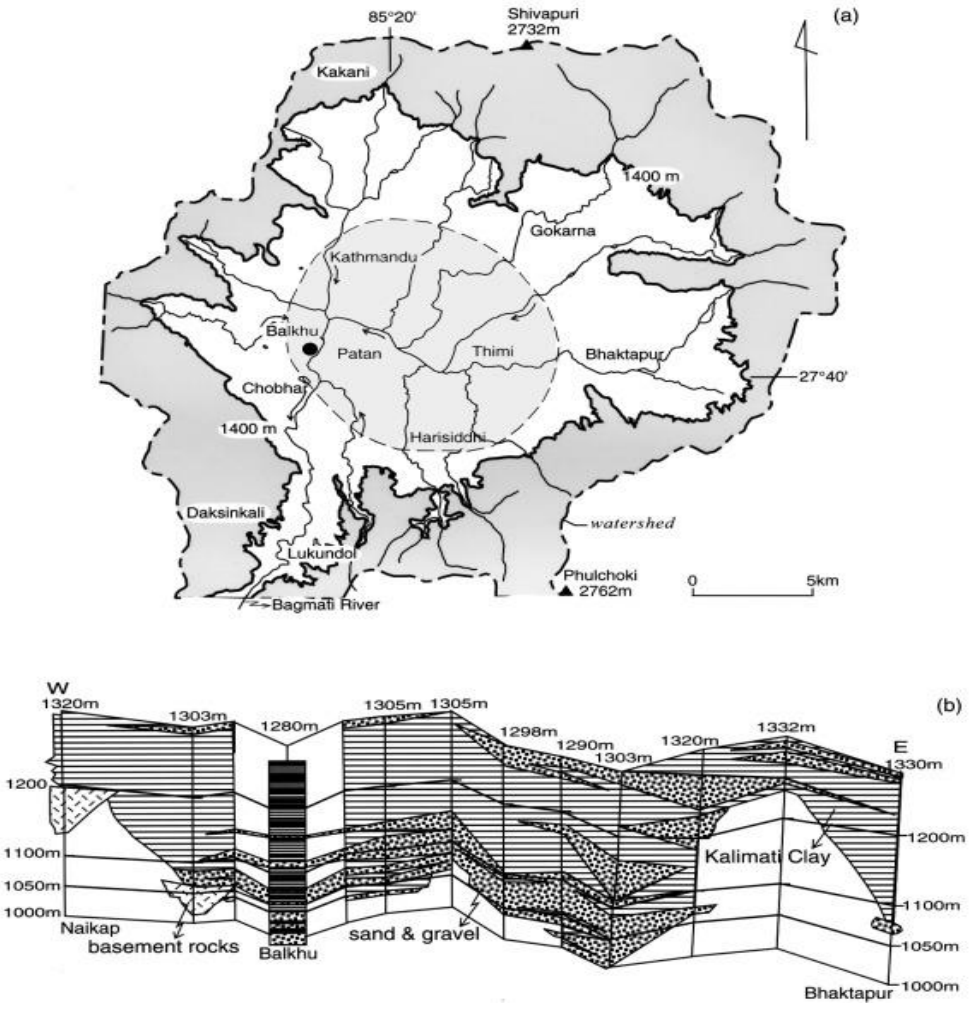

Fig 1.7 Soft Lake deposits in Kathmandu valley

(Softening of soft and sensitive clays/ (some of the black clayey soils "Kalimati").

Chapter 1

Naturally deposited clays/sands are mostly found in structured, and usually also in overconsolidated states. Furthermore, they exhibit what is more or less a condition of anisotropy. In remolded soil sample, the soil skeleton structure is disturbed but in naturally soil, the soil skeleton structure is developed. In order to deal with naturally deposited materials, it is very important to know about soil skeleton structure, especially structure and anisotropy shown in Figure 1.8

Based on the SYS cam clay model, both clay and sand can be expressed using the soil skeletal structure concept, and the difference between them is described as the difference in how the soil skeleton structure changes per unit plastic deformation. In the case of loosely packed sand with a particularly high structure, the mean effective stress easily decreases to zero and liquefies because sand has a remarkably lowered structure. On the other hand, the clay has a slower structure lowering, so the average effective stress will not decrease to near zero, but consolidation will proceed over a long period of time with the dissipation of excess water pressure accumulated by repeated loading. In order to grasp the dynamic behavior of natural sedimentary ground, it is important to understand the concept of soil skeletal structure and its change (accompanying plastic deformation). The detailed explanation of soil skeleton structure is explained in Appendix A2.

Naturally deposited soil possessed soil skeleton structure as shown below;

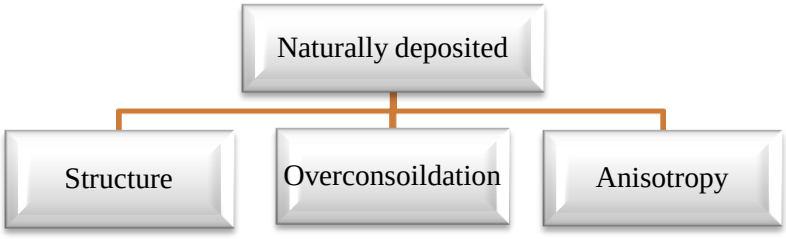

Fig. 1.8 Schematic diagram of soil skeleton structure.

1.2 RESEARCH OBJECTIVE

The main aim for this research was to understand the work of soil skeleton structure especially for anisotropy and structure, and to know the mechanical properties of clay and the developing/diminishing of anisotropy. Natural deposited soil have highly developed structure as compared to remolded soil, so during deposition process, anisotropy is considered to be also highly developed. The knowledge of development/diminishing of anisotropy are very important, to understand the mechanical behavior of natural soil and

the work of soil skeleton structure with ongoing plastic deformation are important.

Another, important aim is to artificially produce the soil sample having similar characteristics to those of naturally deposited soft clay in the laboratory. Because, it is very important to grasp both static and dynamic mechanical properties of naturally deposited clayey materials and it can be achieve by carrying out various systematic experiments using the undisturbed soil samples. However, it is difficult to prepare a number of homogeneous soft clay samples, due to the problems of the variability of quantities during sedimentation, sampling disturbance and high expense of boring survey. Therefore, in this study, we focused on cementation reaction, to artificially produce the soil sample having similar characteristics to those of naturally deposited soft clay.

1.3 OUTLINE OF THE THESIS

The flow chart of the thesis is given in Figure 1.9.

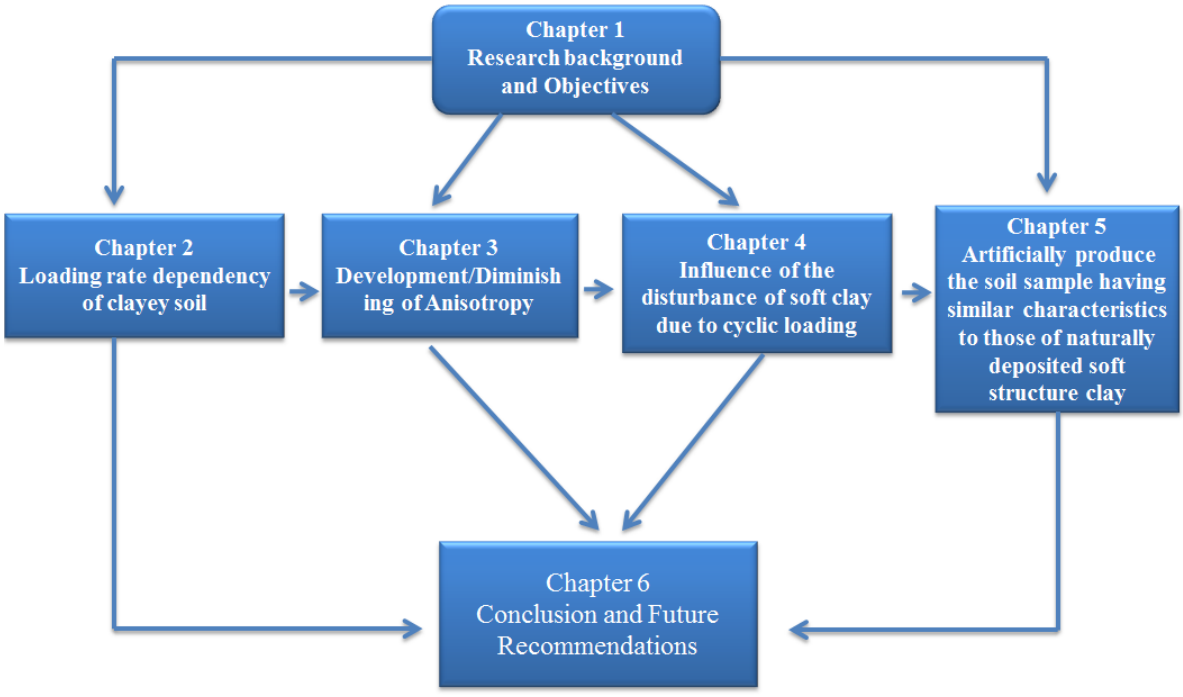

Fig. 1.9 Flow chart of thesis

The structure of this thesis is given as follows:
In the chapter 1, the research background, research objective and the outline of dissertation are discusses.

Chapter 1

In the chapter 2, to understand the undrained cyclic shear behavior of clayey soil under a drastically changed loading rate are discussed. There are various types of external cyclic forces, such as earthquake motion, coastal waves, and traffic loads, which are actual problems. These all have different loading cycles from rapid loading to slow loading. Since the cyclic shear strength varies depending on the loading rate, it is important to conduct experiments using a suitable loading rate compared with the target problem. Since clay material has low permeability, there is a difference in excess pore water pressure migration depending on the loading rate. Especially when the loading rate is high, the pore water does not migrate sufficiently during cyclic loading and the excess pore water pressure distribution inside the specimen becomes non-uniform.

In the chapter 3, importance of anisotropy are discussed. Soft/sensitive/high water content clay of undergoes large settlement during static as well as dynamic loading. Natural deposited soil have highly developed structure as compared to remolded soil, natural deposited soil have highly developed structure as compared to remolded soil, so during deposition process, anisotropy is also considered to be also highly developed. The knowledge of development/diminishing of anisotropy are very important, to understand the true behavior of naturally deposited soil and the work of soil skeleton structure with ongoing plastic deformation. For that purpose, triaxial tests were carried out using the vertical and the horizontal extraction specimen of the reconstituted clay and silty clay, for accumulating experimental facts of development of anisotropy during the preliminary consolidation process and the influence of the anisotropy on the shear behavior.

In the chapter 4, the dynamic problems are focused and the influence of the disturbance of soft clay due to cyclic loading is grasped from undrained triaxial compression tests and importance/implication of soil skeleton structure is discussed. In the past, according to the results of laboratory experiments, it has been found that destabilization such as liquefaction phenomenon does not occur in clayey soil because clayey soil maintains relatively high rigidity and strength even after cyclic loading. It is common that the soil was in the state of "high water content", "high sensitivity", and "soft" where the earthquake damage occurred. The difference between a natural deposited sample and a reconstituted sample is considered to be the degree of development of "soil skeleton structure" that develops over a long period of deposition process over several tens of thousands of years.

In the chapter 5, the influence on mechanical properties, when hydration reaction controlled cement is added to clayey soil and also describe the results of examining the influence of calcium leaching on the mechanical properties of cemented cohesive soil will

be discussed. By using the remolded sample, and the necessity to reduce the solidification effect, a newly attempted method was introduced “addition of hydration reaction controlled cement” and “calcium leaching”, in order to artificially produce the soil sample having similar characteristics to those of naturally deposited soft structure clay. Various tests were conducted to achieve the required results.

In the chapter 6,the conclusions of this research study are sumerized and future work are reommended to improve the stduy.

REFERENCES

1. Page, R., Aftershocks and microaftershocks of the great Alaska earthquake of 1964. Bulletin of the Seismological Society of America, Vol. 58, No.3, 1968, pp.1131-1168.

2. Satake, K., and Abe, K., A fault model for the Niigata, Japan, earthquake of June 16, 1964. Journal of Physics of the Earth, Vol. 31, No. 3, 1983, pp.217-223.

3. J. Merlos and M. P. Romo, Fluctuant bearing capacity of shallow foundations during earthquakes, Soil Dynamics and Earthquake Engineering, No.26, 2006, pp.103-114.

4. Mendoza, M. J., Foundation engineering in Mexico City; Behavior of foundations, Proceeding of International Symposium on Geotechnical Engineering of Soft Clay, Vol.2, 1987, pp.351-367.

5. Leonardo Zeevaert., Foundation Engineering for Difficult Subsoil Conditions, Van Nostrand Reinhold Company, 1972, pp. 521.

6. Towhata, I., Geotechnical Earthquake Engineering, Springer, 2008, pp.359.

7. Isobe, K., Ohtsuka, S. and Takahara, T., Study on long-term subsidence of soft clay due to 2007 Niigata Prefecture Chuetsu-Oki Earthquake, Proceedings of 18th ICSMGE, 2013, pp.1499-1502.
8. Kazama, M., Yamaguchi, A., and Yanagisawa, E., Seismic behavior of an underlying alluvial clay on man-made islands during the 1995 Hyogoken-Nambu earthquake., Soils and Foundations, Vol.38(Special), 1998, pp 23-32.

Chapter 2

UNDRAINED CYCLIC SHEAR BEHAVIOR OF CLAY UNDER DRASTICALLY CHANGED LOADING RATE

2.1 INTRODUCTION

There are various types of external cyclic forces, such as earthquake motion, coastal waves, and traffic loads, which are actual problems. These all have different loading cycles from rapid loading to slow loading. Since the cyclic shear strength varies depending on the loading rate, it is important to conduct experiments using a suitable loading rate compared with the target problem. In other words, it is important to treat as an initial boundary value problem. In the development of a constitutive equation, it is important to grasp the element characteristics of the material accurately. Therefore, it is important to obtain experimental results at the lowest possible loading rate so that the internal state of the specimen can be treated as homogeneous and uniform.

If the past earthquake damage is examined carefully, although there are not many cases like liquefaction damage of sandy foundation, earthquake damage of clayey foundation can be also observed. During Mexico earthquake in 1985 soft clay lost its bearing capacity during the earthquake, causing overturning damage to structures [1, 2] and , the settlement of the clay layer accelerated immediately after the earthquake, and continued for a long time [3].

Laboratory tests on the dynamic properties of clayey soil have been conducted since earthquake damage of clayey foundation began to be noticed. In general, it is known that clayey soil shows a marked loading rate dependency in monotonic shear behavior due to its low permeability [7-11]. Also, in order to overcome such a problem as non-uniformity of pore water pressure distribution inside the specimen and to treat the experimental results as “element behavior,” it is common to apply load as slowly as possible for static loading test. Therefore, in order to investigate the undrained cyclic shear characteristics of clayey soil, it is necessary to evaluate the effect of loading rate in mind [12-17]. However, the range of the loading rate of the cyclic loading test that has been performed so far is narrower than that of the static loading test. Furthermore, many of the experiments so far have focused on the cyclic shear strength during cyclic loading, but few experiments have been conducted to observe in detail, the dissipation process of excess pore water pressure after cyclic loading that became non-uniform during cyclic loading.

As a basic experiment of clayey material, the purpose of this section is to understand the undrained cyclic shear behavior of clayey soil under a drastically changed loading rate.

Since clay material has low permeability, there is a difference in excess pore water pressure migration depending on the loading rate. Especially when the loading rate is high, the pore water does not migrate sufficiently during cyclic loading and the excess pore water pressure distribution inside the specimen becomes non-uniform. Therefore, the specimen was left for a while in an undrained condition after cyclic loading, until the excess pore water pressure distribution inside the specimen became uniform.

2.2 PHYSICAL PROPERTIES OF SAMPLE USED IN THE EXPERIMENT

Over 90% is occupied by fine particles (silt / clay), and it is classified as “CL” (low liquid limit clayey soil) by Japanese classification of geomaterials [18]. The water content of the slurry-like sample, was adjusted to twice the liquid limit (w=90%), and the sample was thoroughly stirred and degassed. Then, it was placed in a pre-consolidation tank, and one-dimensional consolidation was performed at a vertical stress of 200kPa for one week to prepare a reconstituted sample. Figure 2.1 shows the grain size distribution and Table 2.1 shows the physical properties of the sample used in the experiment respectively.

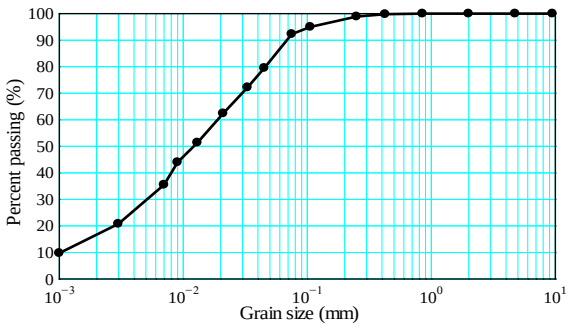

Fig.2.1 Grain size distribution

Table 2.1 Physical properties of the sample

Soil particle density ρ_s (g/cm^3)	2.69
Liquid limit w_L (%)	45.8
Plastic limit w_p (%)	25.3
Plasticity index I_p	20.5

2.3 MONOTONIC SHEAR BEHAVIOR WITH DIFFERENT LOADING RATE

Monotonic drained and undrained triaxial compression tests under various constant axial strain rates were conducted. Confining pressure was set to 300kPa (back pressure 200kPa, lateral pressure 500kPa) so that normal consolidated state could be achieved for all specimens. All the experimental results shown below had a B-value of 0.95 or higher and the specimen size was 35 mm to 80mm. Figure 2.2 shows the results of drained triaxial compression tests conducted at various loading rates, 0.002, 0.10, 0.130 and 1.300 %/min from lower to faster loading respectively. The lower the axial strain rate, the greater the failure or maximum shear strength. In Case-[4], the loading rate of which was the highest, there was almost no volumetric change during shearing, even though the test was conducted under drainage conditions. As the loading rate became lower, volumetric change during shearing tended to occur. Therefore, the shear strength

increased as the loading rate decreased.

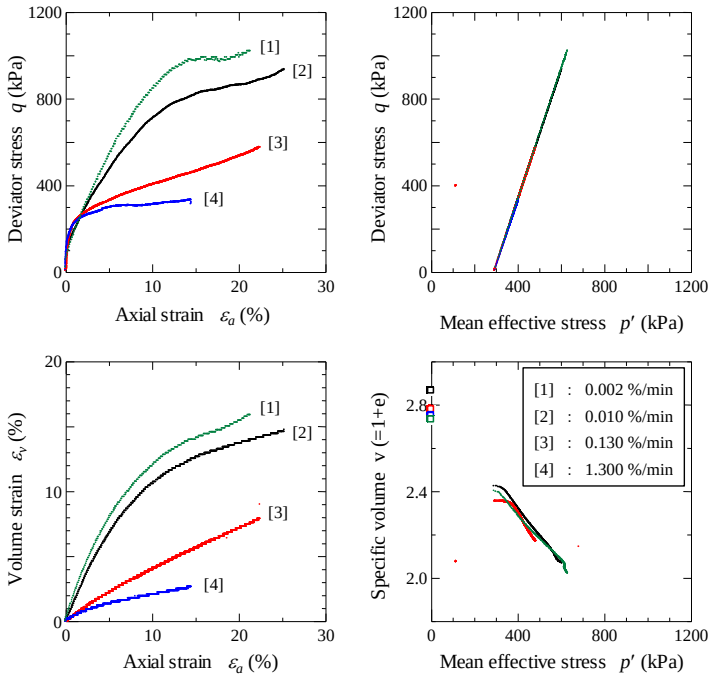

Fig. 2.2 Drained triaxial compression tests with different loading rate

Figure 2.3 shows the results of undrained triaxial compression tests conducted at various loading rates. Contrary to drained shear behavior, a higher the axial strain rate correspond to a, greater failure or maximum shear strength. This is due to the migration of pore water. Because excess pore water pressure was generated non-uniformly inside the specimen along with shearing, a gradient occurred in the water pressure, and pore water migration occurred inside the specimen even though the total volume was constant [19]. If the loading rate is high and the excess pore water pressure distribution is more non-uniform, the water pressure gradient becomes larger, and pore water migration is likely to occur. However, in Case-[4], because the loading rate is high, there would be almost no migration of pore water, and the specific volume would remain in a uniform state.

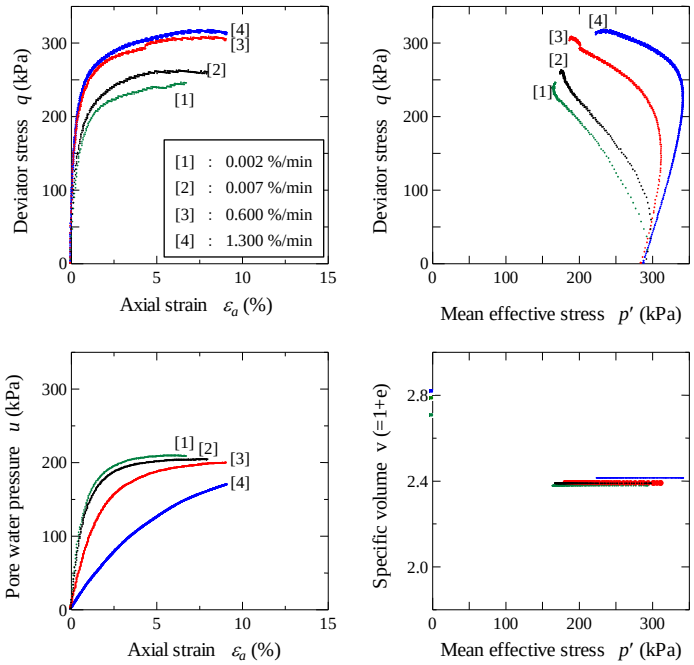

Fig. 2.3 Undrained triaxial compression tests with different loading rate

On the other hand, when the loading rate is low, pore water migration occurs, and thus the specific volume becomes non-uniform inside the specimen. Since the specific volume of the entire specimen did not change under undrained conditions, the shear strength became stronger when the specific volume was uniform. Furthermore, it can be seen that mean effective stress *p*' increased in the effective stress path at the initial stage of loading as the axial strain rate increases. In particular, at the most rapid loading rate (Case-[4]), the effective stress path almost coincided with the total stress path (*q*/*p*'=3). If the axial strain rate was sufficiently low, the pore water pressure distributed uniformly. However, when the axial strain rate was high, the pore water pressure accumulated in the center of the specimen and was unlikely to occur at both ends. Because pore water pressure was measured at the lower end of the specimen, the pore water pressure could not be measured accurately or be measured smaller value when the axial strain rate is higher. As a result, *p*' at the beginning of loading became larger.

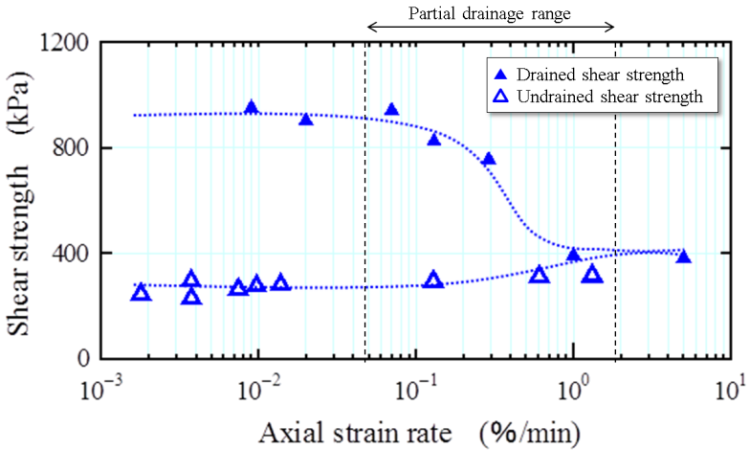

Fig. 2.4 Shear strength with different drainage condition and loading rate

Figure 2.4 shows a summary of the loading rate effect. The drained shear tests draw an inverted S-shaped curve, and the undrained shear tests draw an S-shaped curve, and the drained shear strength is greater than the undrained one. At a high loading rate of 1.0×10^{0} %/min or higher, pore water migration does not occur, so the shear strength matches regardless of drainage conditions. However, if the loading rate is 1.0×10^{-2} %/min or less, pore water migration sufficiently occurs, and neither drained nor undrained shear strength changes any more. When the loading rate is between these values, the shear strength changes due to the partial drainage effect accompanying the migration of pore water.

Nakano [11] focused on the experimental fact that the loading rate range in which drained and undrained shear strength changed were almost equal, and one of the causes of the loading rate effect was that the specimen was non-uniform due to the difference in pore water migration. Asaoka and Noda [20] found that mode-switching occurred due to the migration of excess pore water which resulted in the difference of drained and undrained shear strength through the numerical analyses. Thus, it has been shown both experimentally and numerically that the non-uniformity of excess pore water pressure distribution caused by differences in loading rates has a great influence on the shear strength.

2.4 UNDRAINED CYCLIC SHEAR BEHAVIOR WITH DIFFERENT LOADING RATE

Many experiments have been conducted to understand the dynamic properties of clayey soil. In order to understand the effect of loading rate on undrained cyclic shear behavior, undrained cyclic triaxial compression / extension tests were conducted under constant stress amplitude conditions. Confining pressure was set to 300kPa (back

pressure 200kPa, lateral pressure 500kPa) so that a normal consolidation state could be achieved. All the experimental results shown below had a B-value of 0.95 or higher. Stress amplitude was given by 120kPa (stress amplitude ratio = 0.4). Loading conditions are shown in Tables 2.2 and 2.3. Cases -A to E were performed by stress control with a sinusoidal waveform changing the loading rate from 1.0×10^{0} Hz to 4.2×10^{-4} Hz. Case-F was carried out by strain control with a constant rate 1.0×10^{-2} %/min, which is considered to be low enough that the pore water migration occurs sufficiently. In all cases, cyclic loading was stopped when DA (double amplitude) exceeded 5%. Then, the specimen was left for a while in an undrained condition after cyclic loading, until the value of pore water pressure (mean effective stress *p*') converged.

Table 2.2 Loading rate under stress control

Case	Loading rate	
	Frequency (Hz)	Period (s)
A	1.0×10^{0}	1
B	1.0×10^{-1}	10
C	5.0×10^{-2}	20
D	1.7×10^{-3}	600
E	4.2×10^{-4}	2400

Table 2.3 Loading condition under strain control

Case	Loading rate (%/min)
F	1.0×10^{-2}

2.4.1 Undrained Cyclic Shear Behavior

First, shear behavior during cyclic loading is described. Experimental results (stress ~ strain curves and stress paths) are shown in Figures 2.5 to 2.10. Mean effective stress is calculated using the pore water pressure measured at the lower end of the specimen as a representative value.

In Case-A, the loading rate of which is high (1.0×10^{0}), the *p*' hardly decreased (excess pore water pressure was hardly measured) during cyclic loading. Moreover, the effective stress path almost coincided with the total stress path (*q*/*p*'=3). As mentioned in section 2.3, excess pore water pressure measured at the lower end of the specimen decreased when the axial strain rate was high. Similar to the change of effective stress,

axial strain was also hardly generated at the initial stage of cyclic loading, but the strain progressed gradually as cyclic loading continued. In Case-B, the loading rate (1.0×10^{-1}) of which is 10 times lower than Case-A, decrease of p' became obvious compared with Case-A. Mean effective stress tended to decrease relatively early in the initial cyclic loading and eventually converged. Axial strain was also more likely to occur than in Case-A, but the tendency for strain to be small during the initial stage of loading and gradually increase was the same. It can be seen that as the loading rate decreased from Case-B to Case-E, the p' decreased more with the cyclic loading and axial strain also tended to be generated at the same time. In Case-F, which loaded slowly (1.0×10^{-2}) enough to cause sufficient pore water migration, showed the largest decrease of p' at the initial loading stage compared with other conditions. Furthermore, axial strain also increased from the beginning of the loading.

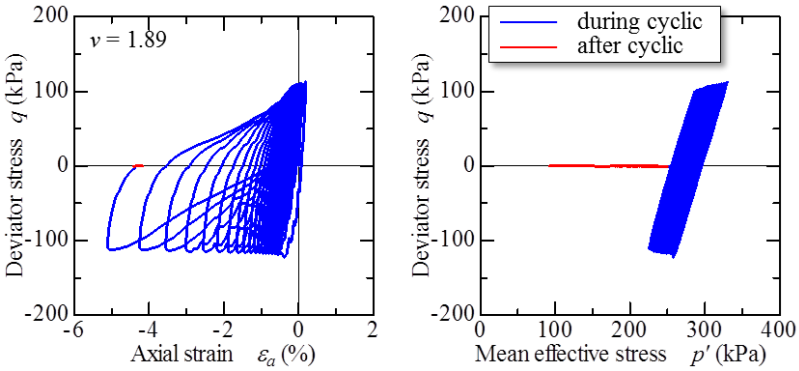

Fig. 2.5 Case-A (stress control with 1.0×10^{0} Hz)

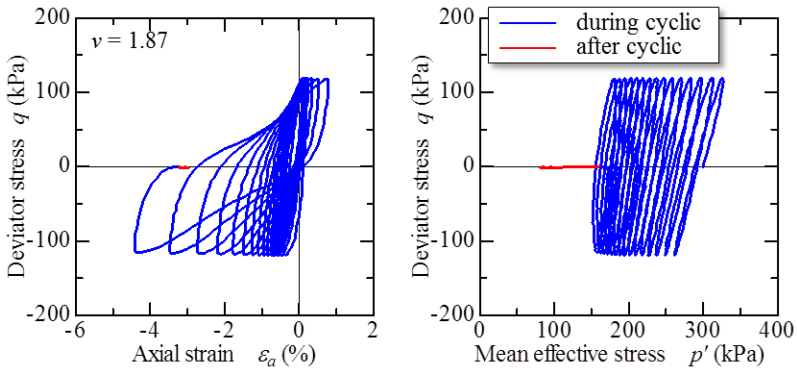

Fig. 2.6 Case-B (stress control with 1.0×10^{-1} Hz)

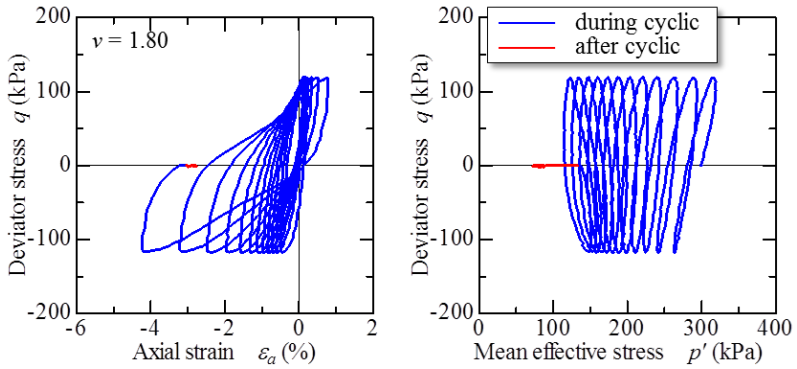

Fig. 2.7 Case-C (stress control with 5.0×10^{-2} Hz)

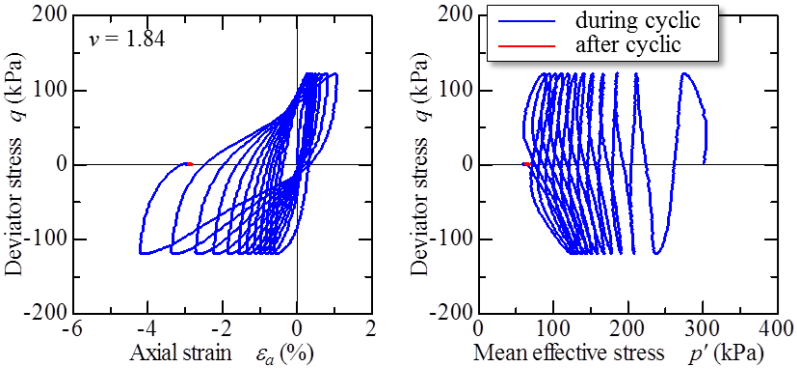

Fig. 2.8 Case-D (stress control with 1.7×10^{-3} Hz)

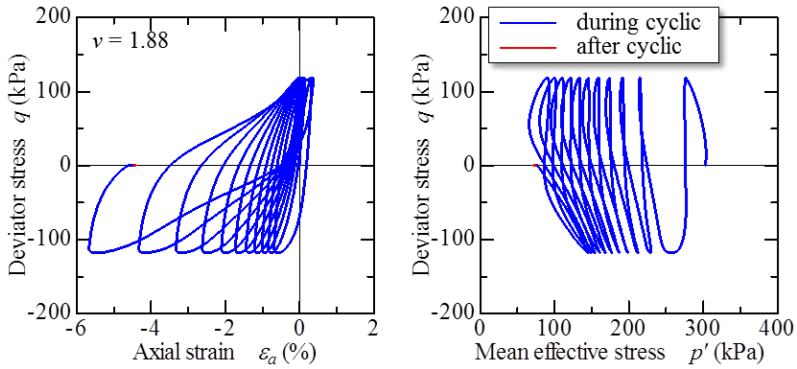

Fig. 2.9 Case-E (stress control with 4.2×10^{-4} Hz)

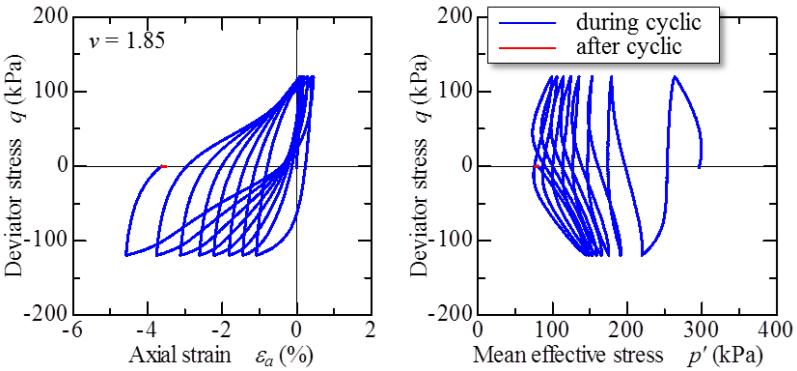

Fig. 2.10 Case-F (strain control with 1.0×10^{-2} %/min

Figure 2.11 shows the relationship between the number of cycles and the progress of maximum / minimum axial strain. Axial strain was unlikely to occur at the beginning of cycles, but when the number of cycles increased to some extent, the axial strain progressed at an accelerated rate. In addition, the higher the loading rate, the more strain began to generate even if the number of cycle is small. The strain progress was more pronounced on the extension side than on compression side. This is due to the anisotropy effect which was developed during the pre-consolidation process. Because the pre-consolidation load was applied in the vertical direction, the specimen might be more resistant/stronger to compression side than the expansion side.

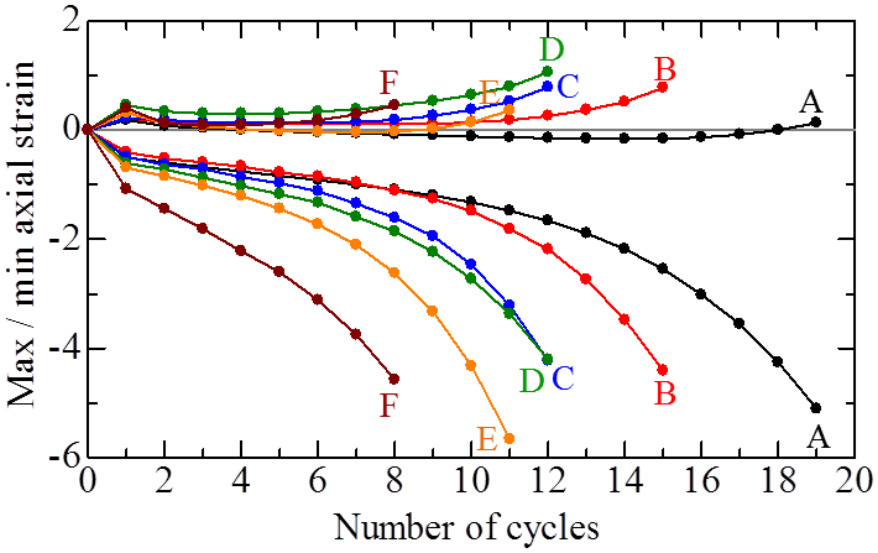

Fig. 2.11 Progress of axial strain with increasing cycles

Table 2.4 shows the number of cycle when DA reached 2% and 5%. As the loading rate became lower, the number of cycles that corresponds to DA=2% and 5% clearly decreased. Undrained cyclic shear strength is often evaluated by the number of cycles to reach a given DA. It can be seen that the undrained cyclic shear strength varied greatly depending on the loading rate, and that the cyclic shear strength decreased as the loading rate became lower.

Table 2.4 Number of cycle until predetermined DA

Case	Number of cycle	
	DA=2%	DA=5%
A	14	19
B	11	15
C	9	12
D	8	12
E	7	11
F	4	8

2.4.2 Excess Pore Water Pressure Uniformity Process after Cyclic Loading

Next, uniformity process in excess pore water pressure after cyclic loading are examined. Figure 2.12 shows the relationship between the number of cycles and the excess pore water pressure (measured at the bottom end of the specimen).

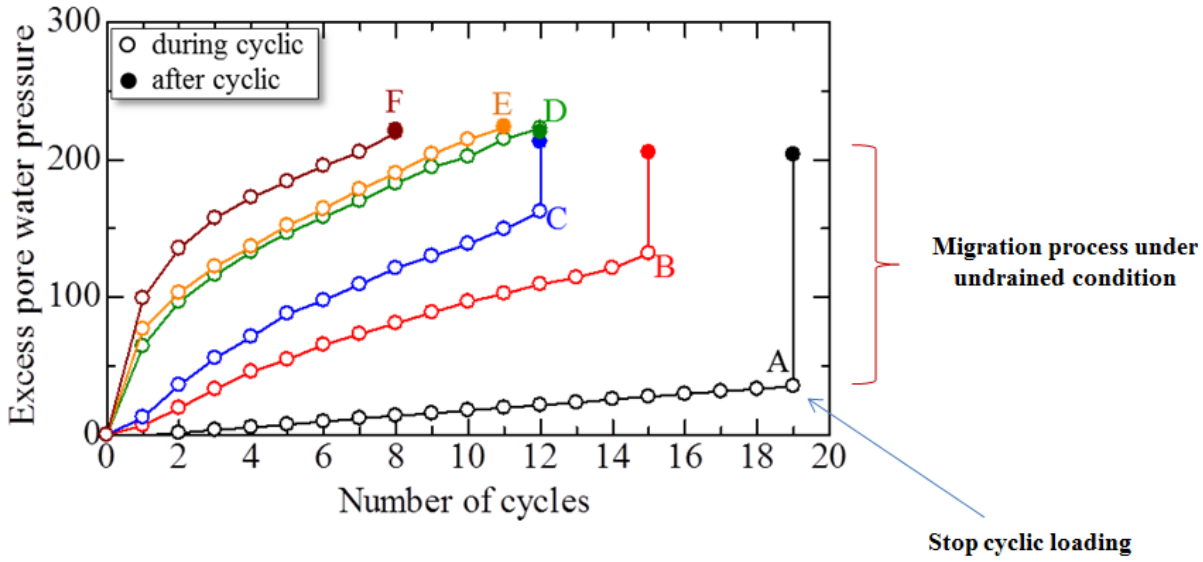

Fig. 2.12 Excess pore water pressure change with increasing cycles

Case-A, which has the most rapid loading rate, generated small excess pore water pressure during cyclic loading. As the loading rate became lower, the excess pore pressure increased with ongoing cyclic loading. Figure 2.12 also shows the change in excess pore water pressure after stopping cyclic loading (denoted by filled circle marks), while maintaining the undrained condition. In Case-A, excess pore water pressure increased greatly after cyclic loading. The lower the cyclic loading rate, the less the excess pore water pressure rose after cyclic loading, and there was almost no change after Case-D. As mentioned in Chapter 3., when the cyclic loading rate was high, the excess pore water pressure distribution inside the specimen became non-uniform during shearing. The increase of excess pore water pressure was measured in the process of uniforming the excess pore water pressure distribution after cyclic loading. In all experimental results from Cases A to F, cyclic loading was stopped at DA=5%. Considering the uniformity process of the excess pore water pressure, the final value of excess pore water pressure seems to be the same in all cases or slightly larger if the loading rate is lower. This means that if sufficient time is left after cyclic loading, the final mean effective stress value becomes equal regardless of the loading rate.

2.5 COMPRESSION BEHAVIOR AFTER CYCLIC LOADING

Excess pore water pressure accumulated by undrained cyclic loading will dissipate and show consolidation when the specimen is changed to a drained condition. Until now, attempts have been made to understand the compression behavior of clayey soil subjected to cyclic loading, and the relationship with the compression index or swelling index has been studied [13, 21-23]. Therefore, after the excess pore water pressure change ceased after cyclic loading, the drainage valve was opened while maintaining isotropic stress condition and the volume change of the specimen was measured.

Table 2.5 shows the slopes of the compression lines obtained through the reconsolidation process. The slopes were calculated from two points: before and after opening the valve. Regardless of the cyclic loading rate, the values of the recompression gradient were the same, and the average value is 0.04.

Table 2.5 Slopes of compression line obtained through reconsolidation process

Case	Recompression gradient
A	0.043
B	0.041
C	0.034
D	0.044
E	0.040
F	0.044

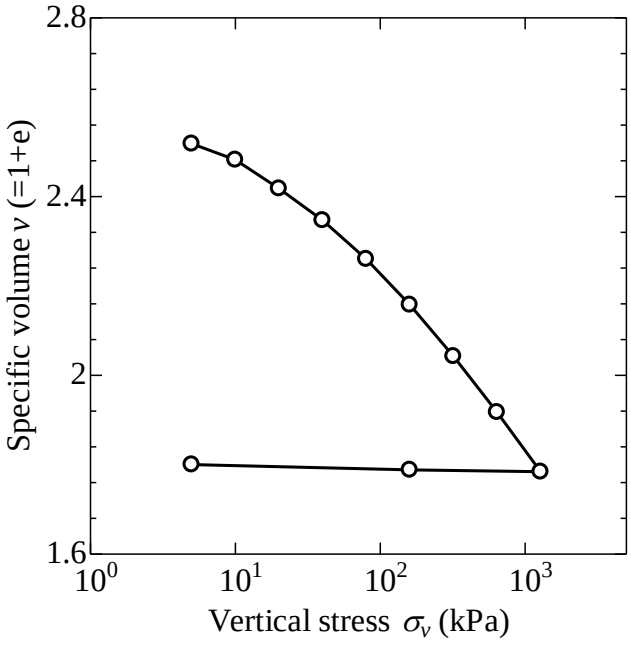

Fig. 2.13 Standard consolidation test

Figure 2.13 shows experimental results from a standard consolidation test using reconstituted specimens. Compression index *Cc* and swelling index *Cs* obtained from the results were 0.590 and 0.020 respectively. The slopes of the compression line after cyclic loading was smaller than the compression index *Cc* and was equal to or slightly larger than the swelling index *Cs*. This means that the amount of compression after cyclic loading would be determined based on the swelling index. However, there might be a risk of underestimating the amount of compression unless the decrease in *p*' due to uniformity

2.6 DISCUSSION AND CONCLUSION

This chapter shows the results of undrained cyclic triaxial compression/extension tests of reconstituted clay specimens with different loading rates, which were conducted as basic experiments for grasping the dynamic characteristics of clayey materials. The loading rate was changed drastically from 1.0Hz to 0.0042Hz by stress control, and 0.01%/min by strain control which was considered to be low enough that pore water migration occurs sufficiently during shearing.Moreover, observation of the uniformity process of excess pore water pressure after cyclic loading, and a re-compression test after cyclic loading were also conducted. The following results were obtained from the experimental results.

(1) The degree of strain evolution varied depending on the loading rate. Because undrained shear strength is often evaluated by the number of cycles to reach a given DA (double amplitude), this experimental fact indicates that the undrained shear strength also varies depending on the cyclic loading rate. The lower the loading rate is, the weaker the strength becomes.

(2) In the triaxial test apparatus, mean effective stress *p*' is calculated using the excess pore pressure measured at the lower end of the specimen as a representative value. When the cyclic loading rate is high, the pore water does not migrate sufficiently and the distribution of the excess pore water pressure inside the specimen becomes non-uniform (the measured value of the excess pore water pressure becomes small). Therefore, the (apparent) effective stress path varies depending on the loading rate. When the loading rate is high, the effective stress path hardly decreases during the cyclic loading.

(3) During the uniformity process after cyclic loading, the measured value of excess pore water pressure at the end of the specimen increased (mean effective stress decrease). Higher the cyclic loading rates generated, greater excess pore water pressure. However, the final values of excess pore water pressure after the homogenization process was the same regardless of loading rate or slightly larger if the loading rate was lower. This

means that if sufficient time is left after cyclic loading, the final mean effective stress value becomes equal regardless of the loading rate.

(4) Slopes of compression lines after cyclic loading were equal regardless of the cyclic loading rate and this value was smaller than the compression index C_c, and equal to or slightly larger than the swelling index C_s. This means that the amount of compression after cyclic loading would be determined based on the swelling index. However, there might be a risk of underestimating the amount of compression unless the decrease in p' due to uniformity process of excess pore water pressure is taken into account.

In this chapter reconstructed samples were used, but experiments using undisturbed samples from the naturally deposited condition will be discuess in chapter 4 to understand the effects of soil skeletal structure and its disturbance.

REFERENCES

1. Towhata, I., Geotechnical Earthquake Engineering, Springer, 2008, pp.359.
2. Isobe, K., Ohtsuka, S. and Takahara, T., Study on long-term subsidence of soft clay due to 2007 Niigata Prefecture Chuetsu-Oki Earthquake, Proceedings of 18th ICSMGE, 2013, pp.1499-1502.
3. Matsuda, H. and Nagira, H., Decrease in effective stress and reconsolidation of saturated clay induced by cyclic shear, Journal of JSCE, No. 659, III-52, 2000, pp. 63-75.
4. Skempton, A. W. and Bishop, A. W., Soils, Chapter X of Building Materials, North Holland Publ. Co., Amsterdam, 1954, pp.417-482.
5. Vaid, Y. P. and Campanella, R. G., Time-dependent behavior of an undisturbed clay, The University of British Columbia Soil Mechanics Series, No.33, 1977.
6. Sekiguchi, H., Nishida, Y. and Kanai, F., Analysis of partially-drained triaxial testing of clay, Soils and Foundations, Vol.21, No.3, 1981, pp.53-66.
7. Tonosaki, A., Akaishi, M., Saitoh, H. and Inada, M., Effects of loading speed and dilatancy of saturated clays, Soils and Foundations, Vol.27, No.4, 1987, pp.200-203, in Japanese.
8. Nakano, M., Analysis of undrained and partially drained shear behavior of clay and its application to embankment design on soft ground, Doctoral Dissertation, Nagoya University, 1993, in Japanese.
9. Procter, D. C. and Khaffaf, J. H., Cyclic triaxial tests on remoulded clays, Journal of Geotechnical Engineering, ASCE, Vol.110, No.10, 1984, pp.1431-1445.

10. Matsui, T., Ohara, H. and Ito, T., Effects of dynamic stress history on mechanical characteristics of saturated clays, Journal of JSCE, No.257, 1977, pp.41-51, in Japanese.
11. Yasuhara, K., Yamanouchi, T. and Hirao, K., Cyclic strength and deformation of normally consolidated clay, Soils and Foundations, Vol.22, No.3, 1982, pp. 77-91.
12. Hyodo, M., Shinomiya, K., Yasufuku, N. and Murata, S., Cyclic strengths of clay and sand by strain rate controlled cyclic triaxial test, Journal of JSCE, No.523, III-32, 1995, pp.9-18, in Japanese.
13. Yamamoto, Y. and Hyodo, M., The rate effect of cyclic shear characteristics of clays, Journal of JSCE, No.645, III-50, 2000, pp.63-76, in Japanese.
14. Byung-Woong Song., Yasuhara, K. and Murakami, S., An estimating method for post-cyclic strength and stiffness of fine-grained soils in direct simple shear tests, Journal of the Korean Geotechnical Society, Vol.20, No.2, 2004, pp.15-26.
15. The Japanese Geotechnical Society, Japanese Geotechnical Society Standards – Laboratory testing standards of Geomaterials , 2015.
16. Asaoka, A., Nakano, M. and Noda, T., Soil-water coupled behavior of saturated clay near/at critical state, Soils and Foundations, Vol.34, No.1, 1994, pp.91-105.
17. Asaoka, A. and Noda, T., Imperfection-sensitive bifurcation of Cam-clay under plane strain compression with undrained boundaries, Soils and Foundations, Vol.35, No.1, 1995, pp.83-100.
18. Suzuki, T., Settlement of saturated clays under dynamic stress history, Journal of the Japan Society of Engineering Geology, Vol.25, No.3, 1984, pp.21-31, in Japanese.
19. Yasuhara, K. and Andersen, K. H., Recompression of normally consolidated clay after cyclic loading, Soils and Foundations, Vol.31, No.1, 1991, pp.83-94.
20. O'Reilly, M. P., Brown, S. F. and Overy, R. F., Cyclic loading of silty clay with drainage periods, Journal of Geotechnical Engineering, ASCE, Vol.117, No.2, 1991, pp.354-362.

Chapter 3

ANISOTROPY AND ITS EFFECT ON THE GRAIN SIZE

3.1 INTRODUCTION

In artificial/remolded sample, the soil skeleton structure is disturbed but in naturally soil, the soil skeleton structure is developed. In order to deal with naturally deposited materials, it is very important to know about soil skeleton structure, especially structure and anisotropy. In this chapter anisotropy will be discussed in detail.

Anisotropy refers to the directional dependence of material properties. The anisotropy of clays and silty clay intimately connected with their structure, which depends on the environmental conditions during which the soil is deposited as well as the stress changes subsequent to deposition. Neglecting the anisotropy of soil behavior may lead to highly inaccurate predictions of soil response under loading. The knowledge of development/diminishing of anisotropy are very important, to understand the true behavior of naturally deposited soil.

Soft/sensitive/high water content clay of undergoes large settlement during static as well as dynamic loading. Natural deposited soil have highly developed structure as compared to remolded soil, natural deposited soil have highly developed structure as compared to remolded soil, so during deposition process, anisotropy is considered to be also highly developed. Also, the large settlement occurred maybe due to anisotropy effect as they still remain even at high confining pressure particularly for clayey soil. So, in order to understand the mechanical behavior of natural soil and the work of soil skeleton structure with ongoing plastic deformation the knowledge of anisotropy are very essential.

Many soil mechanics theories assume that the behavior of soils is isotropic to apply in geotechnical engineering problems. However, several natural soils behave as an anisotropic material and they have anisotropy imposed through the processes by which they were formed. Gravity influences soil formations and the vertical direction consequently retains importance with the variation of properties reflecting this vertical significance. It is well known that natural soils are often deposited in horizontal layers and then subjected to anisotropic stress leading to preferred orientation of the particles. As a consequence, most natural soil deposits possess an inherently anisotropic structure which causes variation in deformation-strength characteristics as the loading direction changes.

Hoque et al. investigated the anisotropy in elastic deformation of granular materials by

measuring local strains in both vertical and horizontal direction with static cyclic loading as in Figure 3.1. He found that vertical Young's modulus is greater than horizontal Young's modulus at isotropic stress level [1]. Islam et al. investigated the strength anisotropy in both vertical and horizontal directions by trimming the specimens at different angles so as to obtain the test samples of different orientations, compared to the depositional direction and then subjected to unconfined compression tests and direct shear tests for both the horizontal and vertical planes from undisturbed clay masses. He concluded that the clay samples collected from different places and different depths showed different coefficients of anisotropy in different laboratory tests [2].

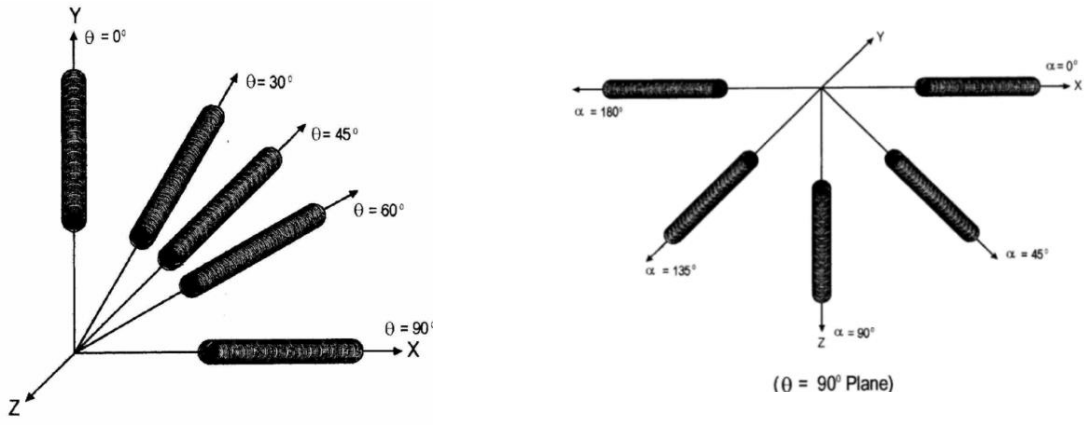

Angle in Vertical Plane Angle in Horizontal Plane

Fig. 3.1. Definition of the angle α in the vertical and horizontal plane (Hoque et al.)

Similarly, Attom, M. F. et al, investigated experimentally the effect of anisotropy on the shear strength properties of clayey soil. Unconfined compression tests were conducted on all soil samples. It was found that the unconfined compressive strength values were greater in the vertical direction than in the inclined and horizontal directions, and increased as the over consolidated ratio increased. It was also noticed that the failure strain in the horizontal samples was smaller than in the vertical samples. The test results indicate that a correlation can be developed to determine the anisotropy factor based on depth and overconsoildation ratio. Anisotropy factor is defined as the ratio of the unconfined compressive strength in the inclined or horizontal direction to the unconfined compressive strength in the vertical direction. The anisotropic behavior of clayey soils almost disappeared at greater depth for both unconfined compressive strength and failure strain, which means that soil, will become somehow isotropic as [3], shown in Figure 3.2.

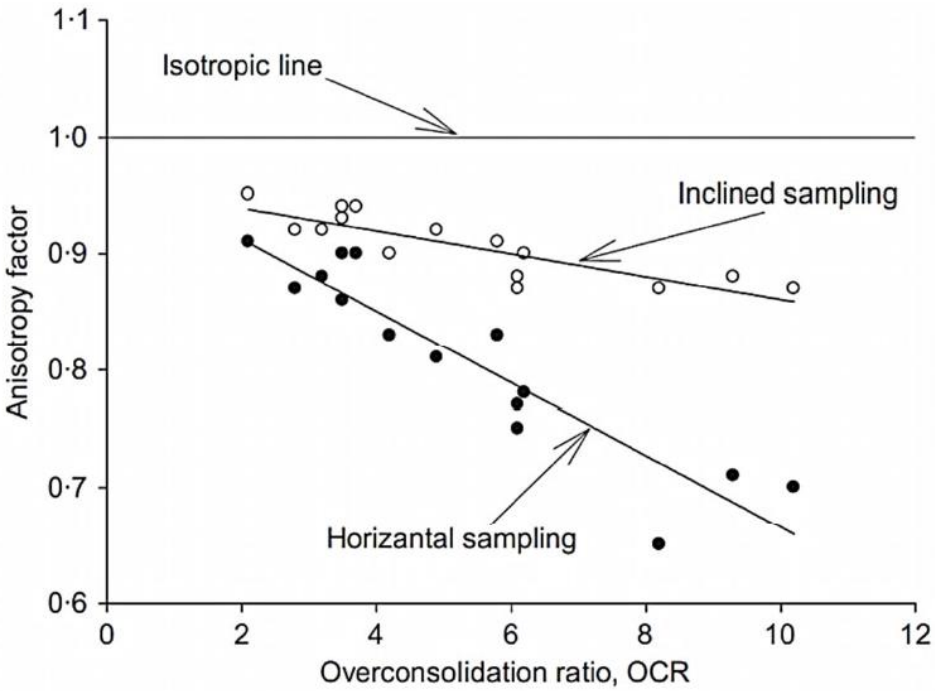

Fig.3.2. Effect of overconsoildation ration on anisotropy (Attom, M. F. et al)

There have been some similar studies related to this research [4-9] and numerous experimental studies on the effects of anisotropy have been conducted focusing on the shear strength, however, there is not much to explain how the anisotropy develops or disappears with ongoing plastic deformation and it effect on shear behavior

In this chapter, triaxial tests were carried out using the vertical and the horizontal extraction specimen of the reconstituted clay and silty clay, for accumulating experimental facts of development of anisotropy during the preliminary consolidation process and the influence of the anisotropy on the shear behavior. Pre-consolidation pressure of 200kPa applied to induced initial anisotropy. Undrained shear triaxial test was performed with different isotropic stresses on clay (50 to 1800kPa) and silty clay (50,300 and 600kPa), and undrained shearing was carried out under constant axial strain rate of 0.0056(mm/min) for clay was 2 days as the permeability of clay is very low and slow ,loading applied in order to get the uniform distribution of excess pore water pressure as explained in chapter 2 and 0.0112(mm/min) for silty clay 6hrs, as the permeability of silty clay is not as low as compared to clay. Moreover, the comparison of clayey and silty clay and how the grain size affects the development/diminishing of anisotropy are discussed.

3.2 EXPERIMENTAL WORK

Physical properties and grain size distribution of the clay and silty clay used in the

experiment are shown in Table 3.1 and Figure 3.3 respectively. After thorough stirring and degassing at a water content of 1.5 times the liquid limit, applied pre-consolidation pressure of 200kPa for one week for clay and two days for silty clay, because of the low permeability of clay. The sample was stir and degassed to destroy the structure of the specimen as in this chapter the focus is on Anisotropy.

Table 3.1 Physical properties of soil.

Description	**Clay**	**Silty-clay**
Liquid Limit w_L (%)	81.4	45.82
Plastic Limit w_p (%)	43.7	25.37
Plasticity index I_p	37.7	20.44
G_s(g/cm^3)	2.65	2.65

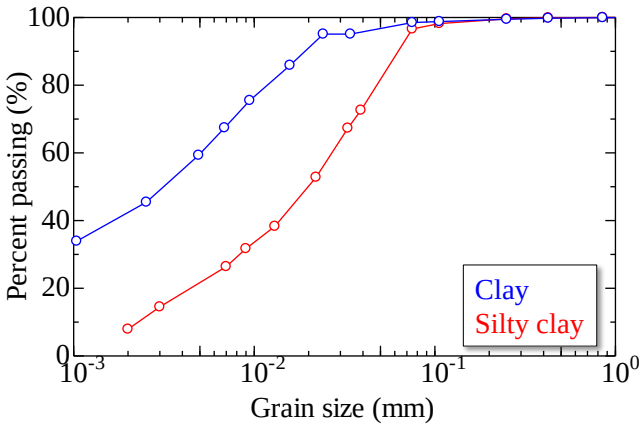

Fig.3.3 Grain size distributions

The method of extracting the sample from the preliminary consolidation tank is the following; specimen pulled out so that the axis was in the vertical direction is vertical specimen and the specimen extracted so that the axis is in the horizontal direction is horizontal specimen, shown below in schematic Figure 3.4.

Fig. 3.4 Extracting vertical and horizontal specimen

By extracting the reconstituted sample from different directions, samples with different initial anisotropy were prepared. Five types of isotropic stress of 50, 100,300,600 and 1800kPa were applied on clay and three isotropic stresses of 50, 300 and 600kPa were applied on silty clay. Both the clay and silty clay were isotopically consolidated for 24hrs.

The saturation (B-Values) of each samples were confirmed to be 0.96 or higher. After isotropic consolidation and undrained shearing was carried out under constant axial strain of 0.0056(mm/min) for clay (2days) and 0.0112(mm/min) for silty clay (6hrs.).These axial strain rate were considered to be slow enough to maintain element behavior (the distribution of excess pore water pressure inside the specimen is uniform) during shearing and the equipment used for experiment was triaxial equipment, shown in Figure 3.5. Detailed explanation of the triaxial equipment and procedure to do the experiment is explained in Appendix 1.

Fig.3.5 Triaxial equipment

3.2.1 Development/Diminishing of Anisotropy in Clay

The stress-strain relationship and effective stress path of vertical and horizontal specimen with different confining pressures of clay, 50 to 1800kPa are shown in Figures 3.6 to 3.10 respectively. Isotropic stresses of 50kPa and 100kPa are considered to be in fully remolded and overconsolidated conditions because the pre-consolidation pressure was 200kPa and, the isotropic stresses of 300kPa and above are considered to be in fully remolded and normal consolidated condition.

In all specimens, the effective stress is constant when the axial strain reaches 20%, because the strain applied was so slow to achieve the uniform distribution of excess pore water pressure inside the specimen, so it is considered that the specimen reached a critical state. In the case of the normal consolidated condition, the effective stress path exhibits typical behavior with an increasing of q with decreasing of p'.

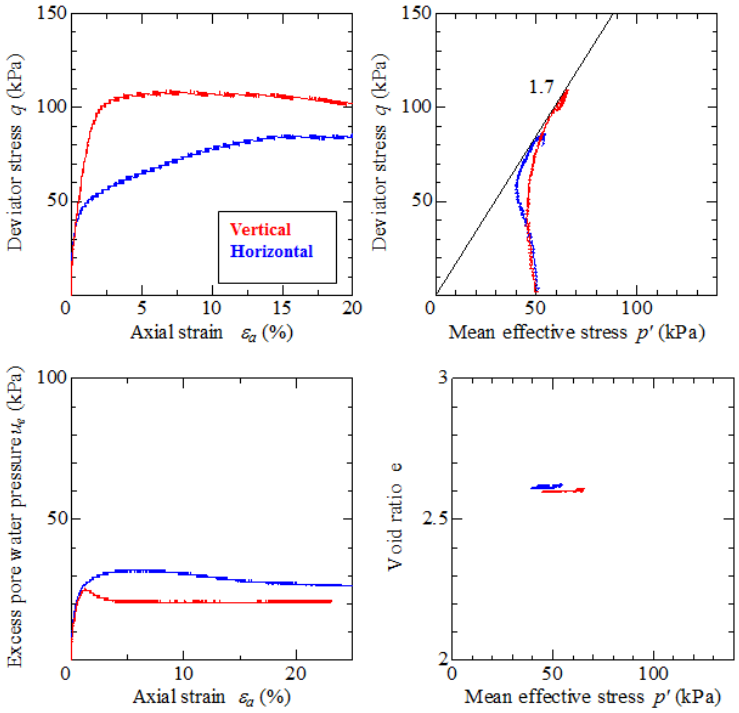

Fig. 3.6 Confining pressure 50kPa (clay)

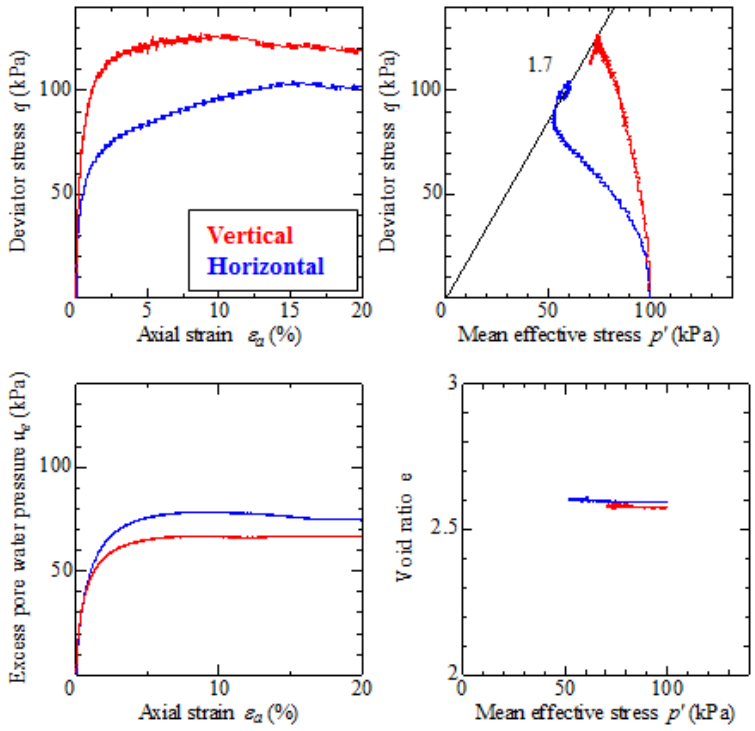

Fig. 3.7 Confining pressure 100kPa (clay)

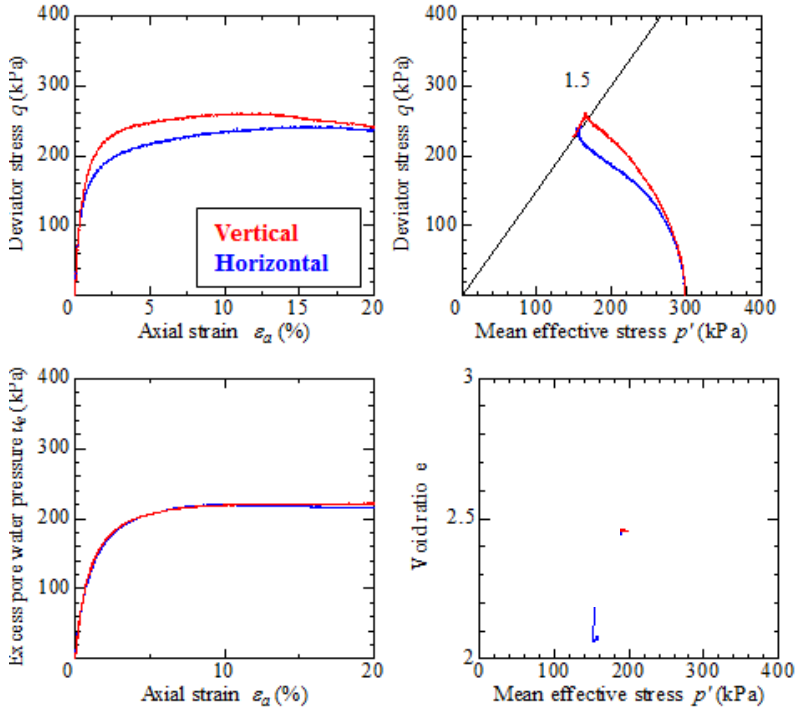

Fig. 3.8 Confining pressure 300kPa (clay)

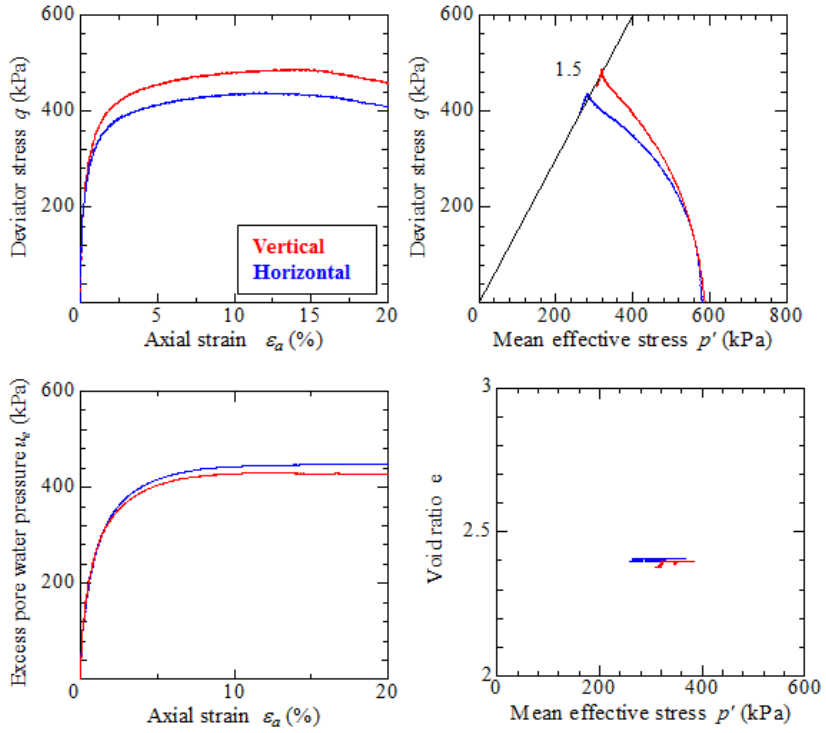

Fig. 3.9 Confining pressure 600kPa (clay)

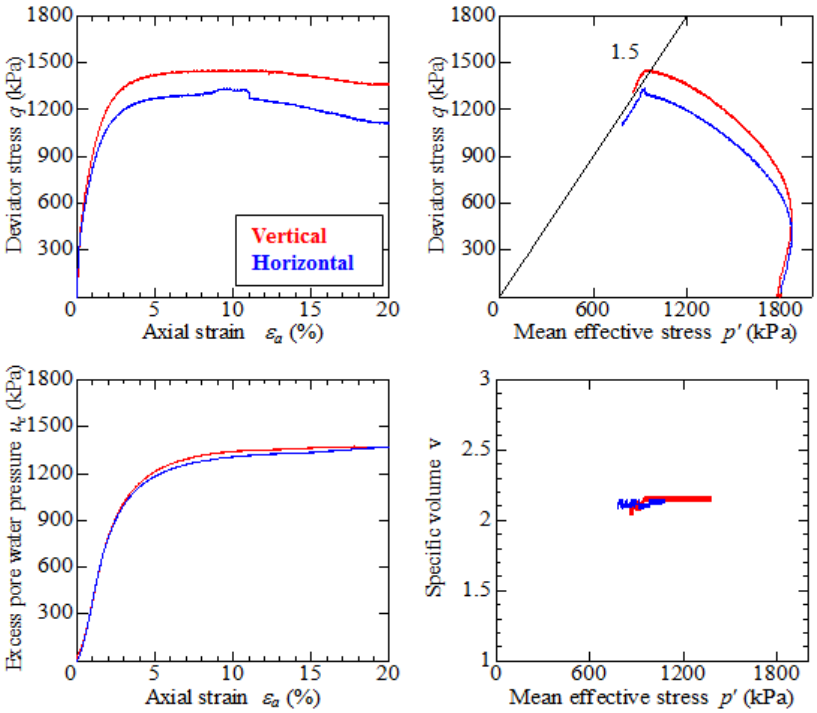

Fig. 3.10 Confining pressure 1800kPa (clay)

Figure 3.11 summarizes the difference of shear strength in vertical and horizontal direction at the time of axial strain was 5% and 10% of axial strain (almost critical state). By comparing the shear/peak strength of samples of clay, it was observed that vertical sample shows larger peak strength as compared to horizontal because of the development of anisotropy on the compression side. As the confining pressure increases, the difference becomes smaller and smaller which indicate that the anisotropy disappears/diminished and intensity ratio decreases.

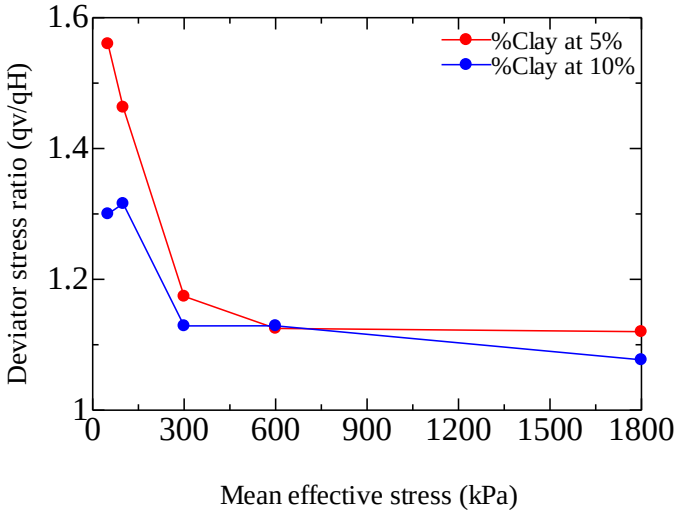

Fig. 3.11 Difference in vertical and horizontal shear strength of clay

However, even at 300, 600, and 1800kPa, the same degree of strength difference remains. So it was found that even if we have applied high isotropic consolidation pressure, anisotropy was not completely diminished. Figure 3.12 summarizes the clayey samples that the critical state index (slope of critical state line) is changing with increasing confining pressure. Also it was observed that, critical state index is decreasing and become constant as confining pressure increases.

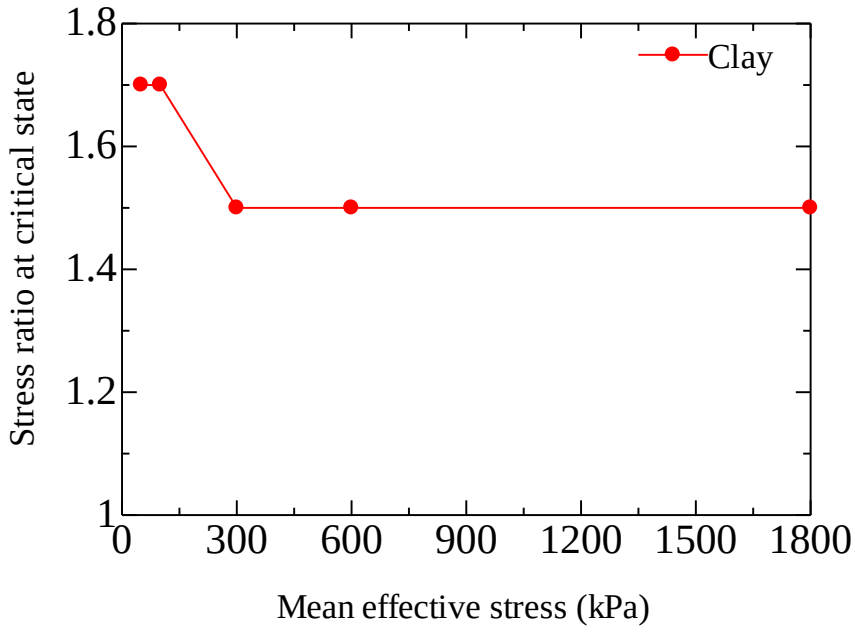

Fig. 3.12 Difference in critical state index of clay

3.2.2 Development/Diminishing of Anisotropy in Silty Clay

The stress-strain relationship and effective stress path of vertical and horizontal specimen with different confining pressures of silty clay at 50 to 600 kPa are shown in Figures 3.13 to 3.15 respectively. Isotropic stress of 50kPa is considered to be in fully remolded and overconsolidated condition. The isotropic stresses of 300kPa and 600kPa are considered to be in remolded and normal consolidated condition. In the case of silty clay specimens, unlikely clay specimens, q continues to increase even when the axial strain reaches 20%. Moreover, the effective stress path of the normal consolidated condition turns to an increase of q with increasing of p' after increasing of q with decreasing of p'.

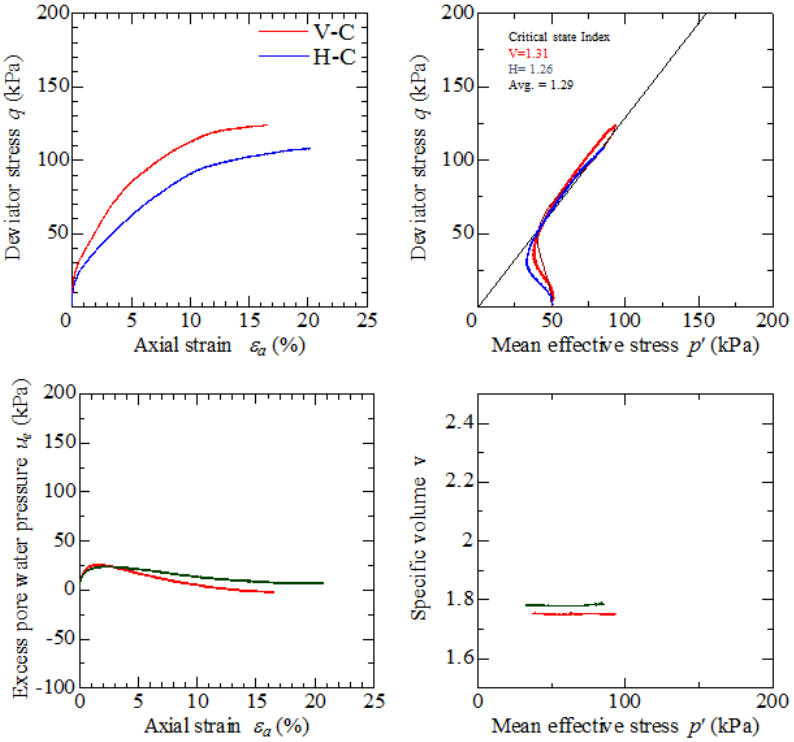

Fig. 3.13 Confining pressure 50kPa (silty clay)

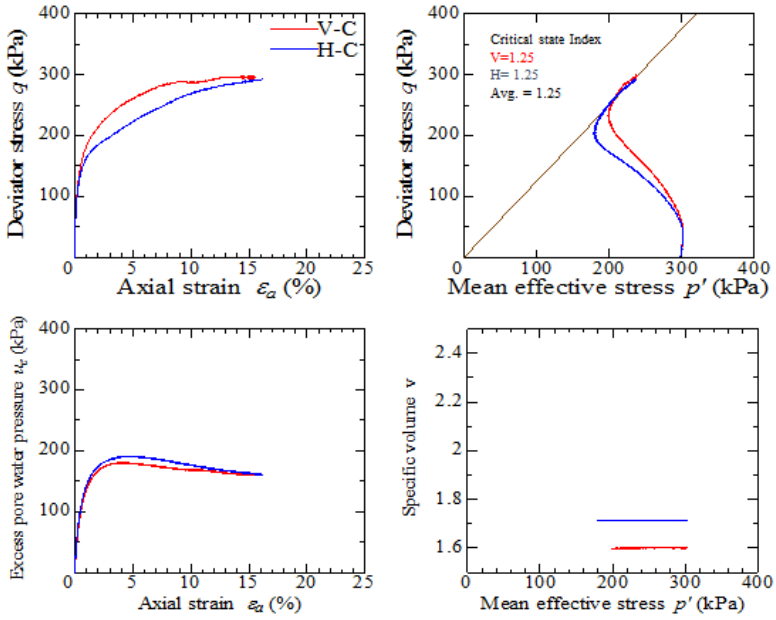

Fig. 3.14 Confining pressure 300kPa (silty clay)

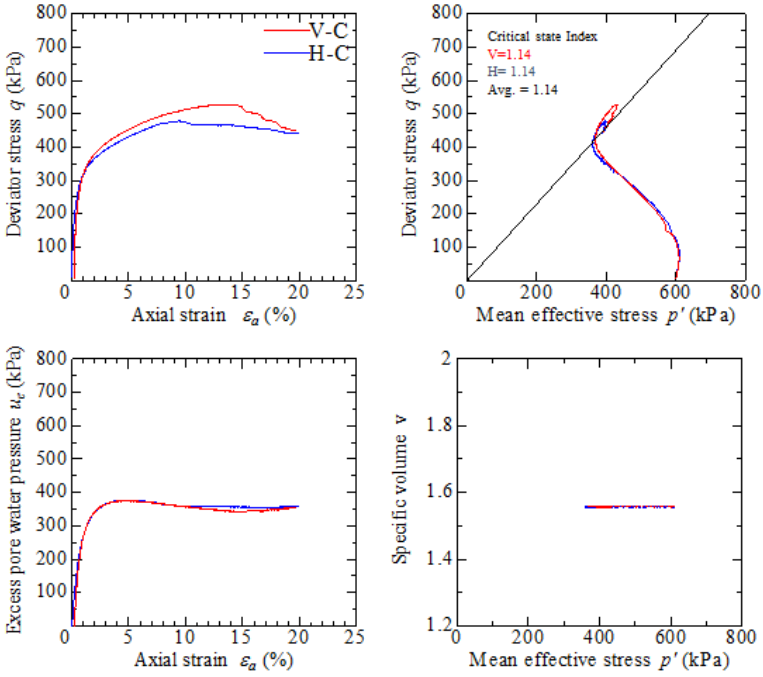

Fig. 3.15 Confining pressure 600kPa (silty clay)

Fig 3.16 summarizes the difference of shear strength in vertical and horizontal direction at the time of axial strain was 5% and 10%. By comparing the shear/peak strength of samples of silty clay, it was observed that vertical sample shows larger peak strength as compared to horizontal because of the development of anisotropy on the compression side. As the confining pressure increases, the difference becomes smaller and smaller which indicate that the anisotropy disappears/diminished and intensity ratio decreases. Moreover, the anisotropy almost diminished at confining pressure of 600kPa. Compared with the clay specimen in Fig.3.11, it can understand that anisotropy disappears with small isotropic pressure.

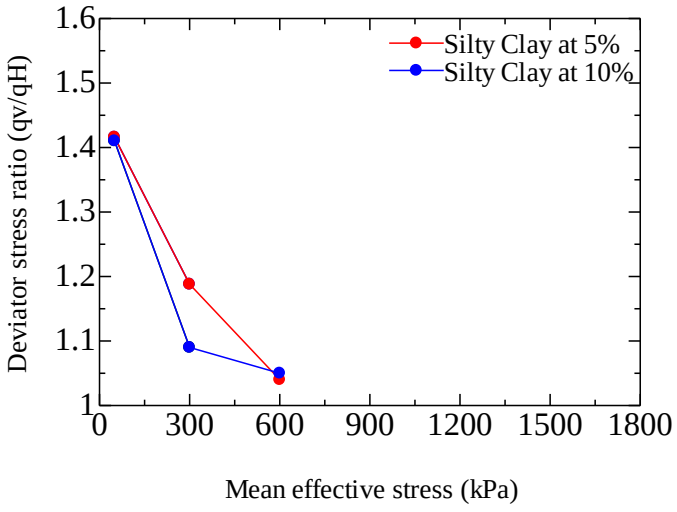

Fig. 3.16 Difference in vertical and horizontal shear strength of silty clay

The silty clay samples, the critical state index are changing with increasing confining pressure same as in clayey specimen is summarizes in Figure 3.17.

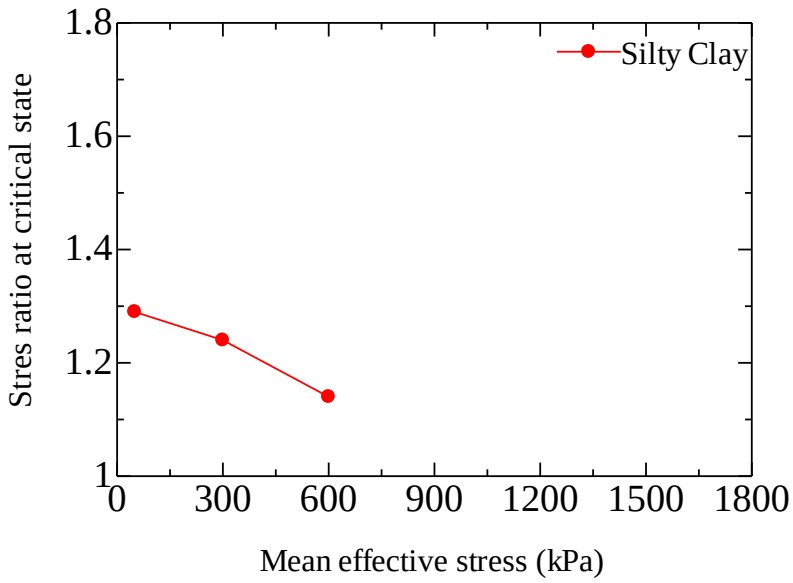

Fig. 3.17 Difference in critical state index of silty clay

3.3 COMPARISON OF CLAY AND SILTY CLAY

The clay and silty clay samples, difference in vertical and horizontal shear strength at 5% of axial strain are summarize in Figure 3.18. Values were taken at 5% because, in case of silty clay sample, localized failure (sudden decrease and discontinuous curve in stress-strain relationship) can be observed after 5% of axial strain, especially within high confining pressure and therefore, it is difficult to recognize as element behavior furthermore.

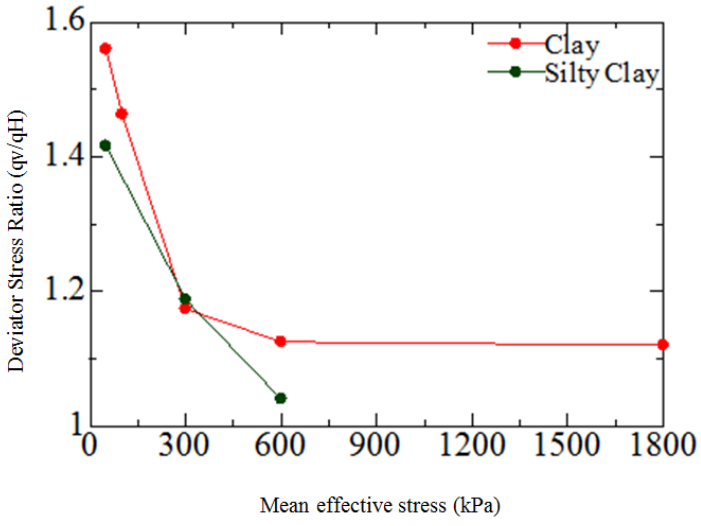

Fig. 3.18 Difference in vertical and horizontal shear strength

As indicated above, both vertical samples shows larger peak strength as compared to horizontal because of the development of anisotropy on the compression side. As the confining pressure increases, the difference becomes smaller and smaller which indicate that the anisotropy disappears/diminished and intensity ratio decreases. It was found that even if we have applied high isotropic consolidation pressure, anisotropy was not completely diminished specially in case of clay soil but in case of silty clay they lose their anisotropy at rapid rate as compared to clayey materials, at confining pressure of 600kPa. So, it is concluded that the grain size has significant effect on the diminishing of anisotropy, and silty material shows rapid change in anisotropy compared with clay material.

Figure 3.19 summarizes the clay and silty clay samples changing of critical state index with increasing confining pressure. Comparing clay and silty clay, critical state index is larger for clay material because of strong anisotropy effect. Another important fact observed that, critical state index is changing with different confining pressure. The critical state index decreases as the anisotropy disappear with an ongoing increase of isotropic pressure.

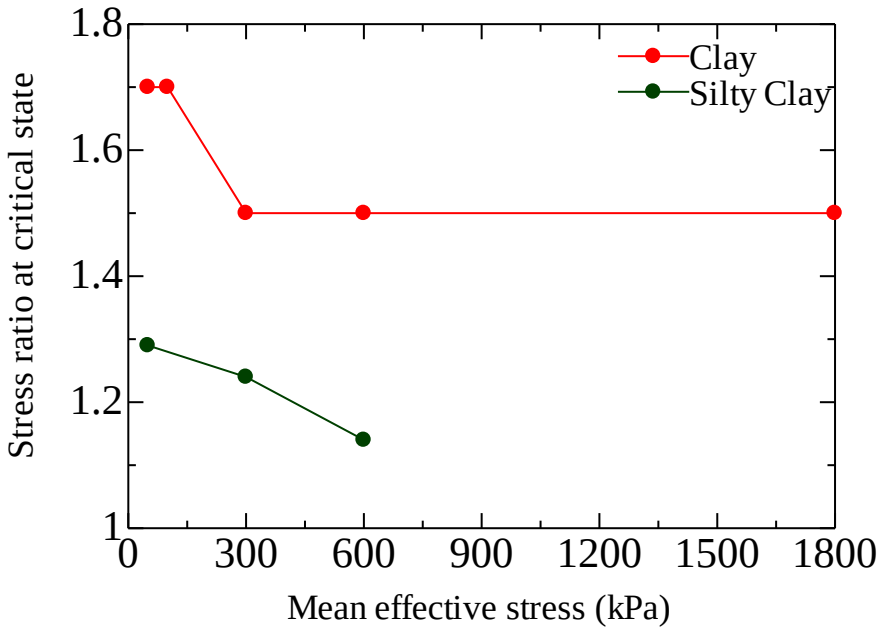

Fig.3.19 Difference in critical state index

To describe the effect of anisotropy in the numerical simulation, the rotational hardening concept [10] was often used. However, when introducing the rotational hardening concept directly to the original Cam clay model that is so-called as the Sekiguchi-Ohta model [11], the critical state index did not change even if the anisotropy develops and

disappears. On the other hand, when introducing the rotational hardening concept to the modified Cam clay model, critical state index changes according to the plastic deformation. Figures 3.20 and 3.21 show the change of yield surface and critical state line in $q \sim p'$ plane of Sekiguchi-Ohta model and modified Cam clay model with rotational hardening [12] during undrained shearing respectively. The soil is in the normal consolidated condition, considering only the development of anisotropy.

In the Sekiguchi-Ohta model, the critical state line does not change when anisotropy develops, whereas, in the Modified Cam-clay model, critical state line changes (critical state index increases) as the anisotropy develops. Furthermore, in the case of the Modified Cam Clay model, the phenomenon of increasing q accompanied by an increase in p' in the effective stress path can be reproduced due to the effect of rotational hardening. From this viewpoint, modified Cam clay model can considered to be more suitable to use as compared to the original Cam clay model in order to represent the work of anisotropy.

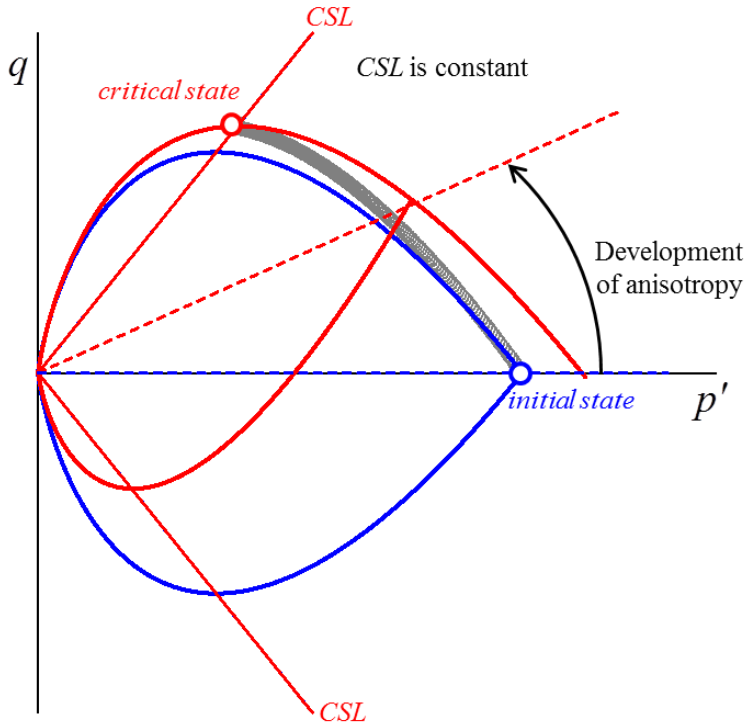

Fig. 3.20 Sekiguchi-Ohta model

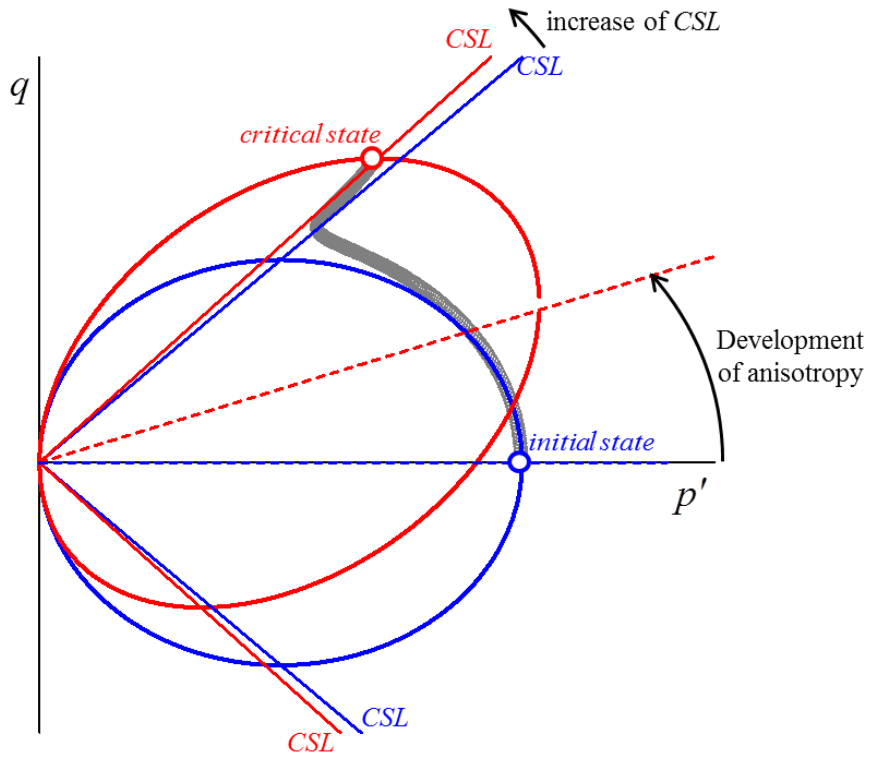

Fig.18 Modified Cam-clay model with rotational hardening

3.4. CONCLUSION

In this chapter from a series of experimental results, it is concluded that anisotropy developed in the preliminary consolidation process, and anisotropy disappears due to isotropic consolidation. Nevertheless, it does not completely disappear even under high confining pressure i.e. 1800kPa, especially in case of clay. However, if we compare clay and silty clay soil, silty clay materials lose their anisotropy at lower confining pressure i.e. 600kPa, as compared to clay materials. Therefore, the grain sizes have significant effect on the developing and diminishing of anisotropy.

Another important fact observed was that critical state index (slope of critical state line) is decreasing and become constant as confining pressure increases. Moreover, modified Cam clay model can considered being more suitable to use as compared to the original Cam clay model in order to represent the work of anisotropy.

Further experiment will be performed to observe the effect of cyclic shear test to evaluate the development/diminishing of anisotropy. Moreover, based on experimental facts, we will validate the constitutive model and add some improvement if necessary.

Chapter 3

REFERENCES

1. Islam M. S. and E Haque., Strength Anisotropy in Undisturbed Dhaka Clay, Journal of Geotechnical Engineering, Vol.1, No.1, 2011, pp. 7-15.
2. Hoque E. and Tatsuoka F., Anisotropy in elastic deformation of granular materials, Soils and Foundations, Vol.38, No.1, 1998, pp. 163-179.
3. Attom M.F. and Al-Akhras N.M., Investigating anisotropy in shear strength of clayey soils, Proceedings of the Institution of Civil Engineers: Geotechnical Engineering Vol.161, No. 5, 2008, pp 269–273.
4. Karstunen M, and Koskinen M., Plastic anisotropy of soft reconstituted clays, Canadian Geotechnical Journal, Vol.45, No.3, 2008, pp 314-328.
5. Duncan J. M., Anisotropy and stress reorientation in clay, Journal of Soil Mechanics and Foundations Division ASCE, Vol.92 No. SM 5, 1966, pp. 81-103.
6. Atkinson J. H., Anisotropic elastic deformations in laboratory tests on undisturbed London Clay, Geotechnique, Vol.25, No.2 1975, and pp 357-374.
7. Liu W., Shi M., Miao L., Xu L., and Zhang, D., Constitutive modeling of the destructuration and anisotropy of natural soft clay, Computers and Geotechnics, Vol.51, 2013, pp 24-41.
8. Graham J. and Houlsby G. T., Anisotropic elasticity of natural clay. Géotechnique, Vol.33, No.2, 1983, pp 165-180.
9. Rowshanzamir M. A. and Askari A. M., An investigation on the strength anisotropy of compacted clays, Applied Clay Science, Vol. 50, No.4, 2010, pp 520-524.
10. Hashiguchi K. and Chen Z.P., Elastoplastic constitutive equations of soils with the subloading surface and the rotational hardening, International Journal for Numerical and Analytical Methods in Geomechanics, Vol.22, No.3, 1998, pp.197-227.
11. Sekiguchi H. and Ohta H., Induced anisotropy and time dependency in clays, Constitutive Equations of Soils (Proc. 9th Int. Conf. Soil Mech. Found. Eng., Spec. Session 9), Tokyo, 1977, pp.229-238.
12. Asaoka A., Noda T., Yamada E., Kaneda K., and Nakano M., An elasto-plastic description of two distinct volume change mechanisms of soils, Soils and Foundations, Vol.42, No.5, 2002, pp.47-57.

Chapter 4

INFLUENCE OF SOIL DISTURBANCE DUE TO CYCLIC LOADING ON UNDRAINED SHEAR BEHAVIOR OF SOFT CLAY BASED ON SOIL SKELETON STRUCTURE CONCEPT

4.1 INTRODUCTION

Modern large cities are frequently exposed to natural and man-made risks which affect many aspects of urban development. Political, social, economic, geographical, morphological, geological conditions and others determine the way in which hazards can be faced in practice, and authorities will generally seek means for eliminating or mitigating these risks and their effects. These conditions combine in various ways to preclude or limit the effectiveness of public policies for hazard management.

In a volcanic ash-like viscous land plate with high water content ratio, high plasticity (wn = 300-400%), horizontal movement of intense structure destroys the ground and the structure that the support capacity has been lost collapses over a wide area. In the viscous land board which did not lead to destruction and large deformation at the time of the earthquake, the settlement continued for a long period immediately after the earthquake and thereafter.

If past earthquake damage is examined carefully, although there are not many cases of liquefaction damage to sandy foundation, earthquake damage to clayey foundation is reported. Figure 4.1 shows an apartment building in Mexico City that was destroyed in the 1985 Mexico earthquake [1, 2]. Mexico City is located in a basin, on land where Lake Tescoco was reclaimed, and its soil profile is composed of extremely soft volcanic ash-like clay. This area was famous for its massive earthquake damage, despite its distance of 300 km from the epicenter. It is said that soft clayey soil was severely disturbed by the earthquake motion which was amplified and accumulated in the basin. In soft clayey foundations, not only instabilities during earthquakes but also large deformations after earthquakes might occur. Figure 4.2 shows the relationship between the amount of land subsidence and time observed in the Mexico basin during the 1957 Mexico earthquake [3]. Land subsidence, which was once approaching convergence, showed a surge and acceleration during the earthquake. It has been confirmed by the investigation that this settlement occurs in highly plastic volcanic ash clay with extremely high water content. Earthquake damage, which is thought to be caused mainly by clayey soil, has also been observed both in Japan and abroad. Examples include the long-term continuous subsidence damage of the Niigata plain from the earthquake off the coast of Miyagi earthquake in 1978 and Chuetus earthquake in 2007, settlement acceleration of Port Island from the Great Hanshin earthquake in 1995,

collapse of soil structures on the Kathmandu Valley from the 2015 Nepal earthquake, and Graben-like cracks in the Aso caldera from the 2016 Kumamoto earthquake. On September 19, 2017, earthquake (M_w=7.1), earthquake occurred exactly 32 years after the 1985 Michoacan Earthquake that hit the Pacific Coast of Mexico City.

Strangely, many of the buildings that survived in 1985 succumbed to the tremors from the magnitude 7.1 in 2017 earthquake. That's because the two earthquakes produced different kinds of shaking. In 1985, the damage concentrated in the central part, while the southern part did not exhibit significant losses. In overall, it was observed that buildings that collapsed in 1985 had longer natural periods than those that collapsed this time. Most of the structural damage concentrated in zones II (Sandy and silty layers) and III (soft soils), where the previous 1985 Earthquake have also caused numerous collapses and the pattern of damage is similar to that experienced in 1985. Soil profile of Mexico City (east-west cross section) is shown in Figure 4.2.

Fig. 4.1 Overturn damage of upper structures due to decreased bearing capacity of clayey foundation

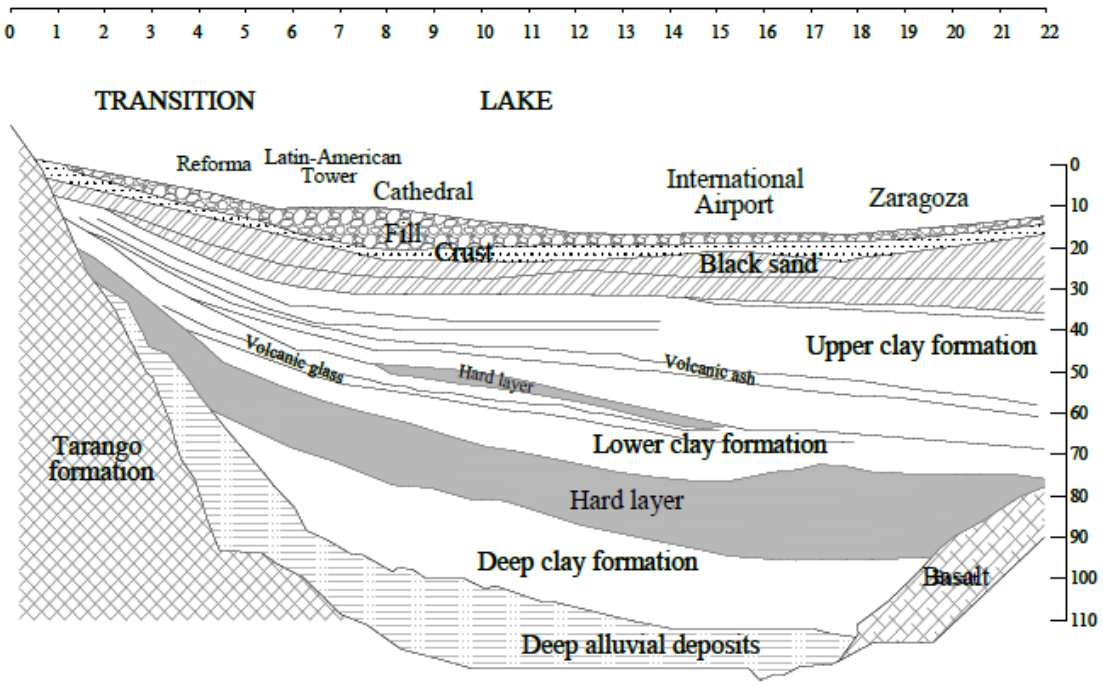

Fig. 4.2 Soil profile in Mexico City (east-west cross section)

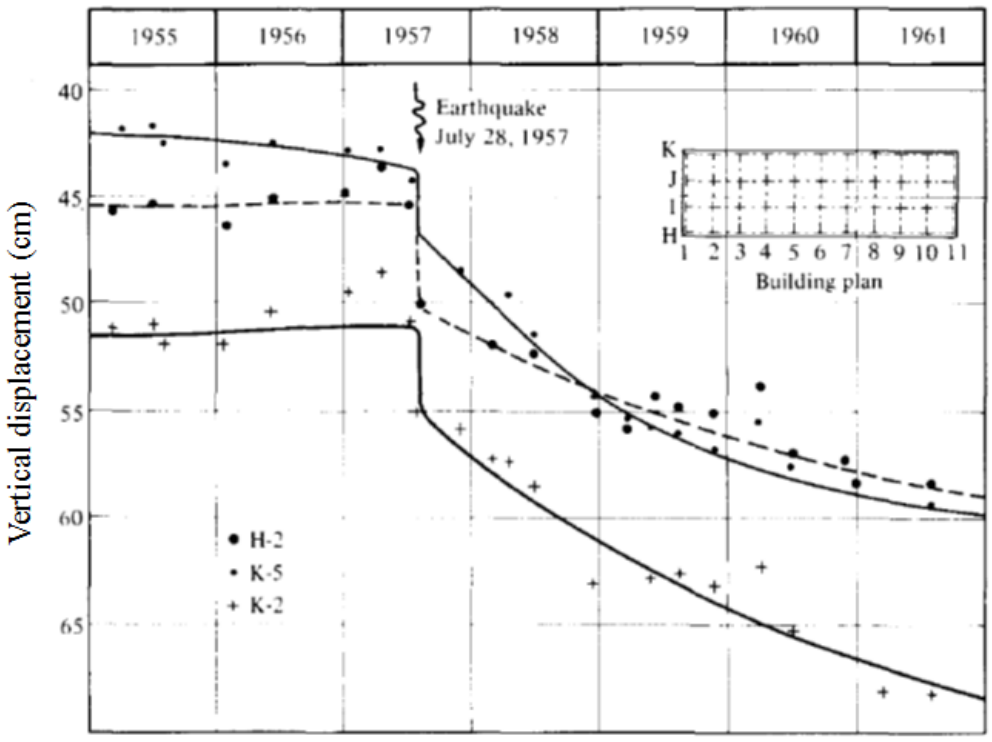

Fig. 4.3 Effect of an earthquake on the settlement of a building (Leonardo Zeevaert, 1972)

A case history is shown in Figure 4.3 for a heavy building placed on an undercompensated foundation, from which it is observed that the building, after being practically stabilized, started to settle strongly after the earthquake.

The investigation of this case demonstrated that the static shear stresses added to the dynamic shears induced during the earthquake of July 1957 reached the ultimate shear strength of the silty clay deposit; therefore, partial damage took place in the soil skeleton structure, giving as a result an increase in the compressibility of the, material that produced the consolidation phenomenon observed. Finally, it is important to mention that the value of the shear modulus of elasticity should be determined, as accurately as possible, in good undisturbed soil samples.

However, earthquake damage does not occur in every clayey foundation. It is common that the soil was in the state of "high water content", "high sensitivity", and "soft" where the earthquake damage occurred. In the past, according to the results of laboratory experiments, it has been found that destabilization such as liquefaction phenomenon does not occur in clayey soil because clayey soil maintains relatively high rigidity and strength even after cyclic loading. However, it is considered that the soil sample used in these experiments is not an undisturbed sample collected while maintaining the naturally deposited condition, but an artificial sample in which the once disturbed soil is reconstituted. The difference between a natural deposited sample and a reconstituted sample is considered to be the degree of development of "soil skeleton structure" that develops over a long period of deposition process over several tens of thousands of years. Therefore, in this chapter, the influence of the disturbance of soft clay due to cyclic loading is grasped from undrained triaxial compression tests and importance/implication of soil skeleton structure is discussed.

4.2 SOIL SAMPLE USED IN THE EXPERIMENT AND ITS MONOTONIC MECHANICAL BEHAVIOR

The clay sample used in this study is alluvial clayey soil deposited in Anpachi, Gifu in Japan and the cross-sectional view of the site is shown in Figure 4.4. There is a sand layer As1 at a depth of 5m to 15m, but the clay layer is dominant to the deep part. The clay layers can be divided into four layers from Ac1 to Ac4, but each layer has a small *N*-value and is in a soft condition. The average *N*-value of each layer is shown in Table 4.1. One of the important characteristics is that even in deep Ac4 where the overburden pressure is large, averaged *N*-value is as small as 1. Therefore, in this study, the Ac4 (Figure 4.4) was used as an experiment target and thin-wall sampling was conducted so as to disturb the sample as little as possible.

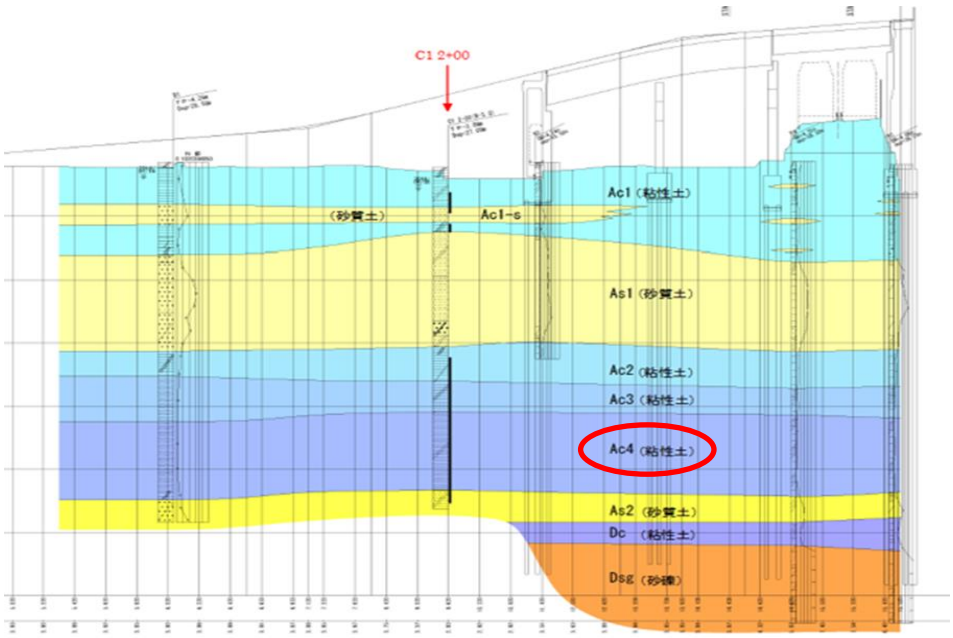

Fig. 4.4 Cross-sectional view of the sampling point

Table 4.1 Averaged *N*-value of each layer

	Depth	Averaged *N*-value
Ac1	0m – 5m	1
Ac2	15m – 18m	4
Ac3	18m – 20m	3
Ac4	20m – 32m	1

4.2.1 Physical property

The grain size distribution and a list of physical properties of the clayey sample are shown in Figure 4.5 and Table 4.2 respectively. The fines content is almost 100%, and the clay and silt contents are almost equal. The table shows that the liquid index I_L exceeds 1.0. The liquid index is expressed by equation 4.1 and is an index that indicates the relative hardness of the sample within a condition of natural water content w_n. When I_L exceeds 1.0, it indicates that the soil is in a liquid condition, and it can be seen that this clayey soil was deposited at high water content and in a very soft condition.

$$I_L = \frac{w_n - w_p}{w_L - w_p} \tag{4.1}$$

w_n: natural water content

w_L: liquid limit (water content ratio at which soil moves from a plastic state to liquid state)

w_p: plastic limit (water content ratio at which soil moves from semi-solid state to plastic

state)

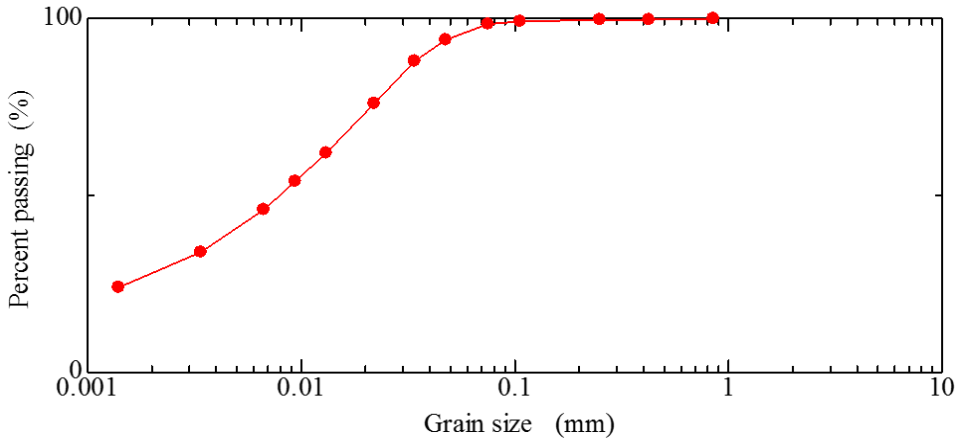

Fig. 4.5 Grain size distribution

Table 4.2 Physical properties

Soil particle density ρ_s (g/cm^3)	2.69
Liquid limit w_L (%)	54.0
Plastic limit w_p (%)	25.8
Plasticity index I_p	28.2
Natural water content w_n (%)	54.4
Liquid index I_L	1.01

4.2.2 Compression behavior

The experimental results of standard consolidation tests using an undisturbed sample and a remolded sample are shown in Figure 4.6. The remolded sample was prepared by repeatedly squashing the undisturbed sample. The remolded sample is in the normally consolidated state from the initial loading stage, and the normal consolidation line can be obtained. On the other hand, since undisturbed samples are unloaded during sampling, they are initially in the overconsolidated state. When vertical stress is less than the overburden pressure (170kPa), compressibility is small. However, when vertical stress exceeds overburden pressure and the sample reaches a normal consolidation state, compressibility becomes large. The compression line of the undisturbed sample shows bulky behavior outside the normal consolidation line in the normally consolidated state, and gradually approaches the normally consolidation line as the vertical stress increases. The degree of bulkiness is quantitatively defined as structure [4, 5]. From the experimental results, it can be seen that the undisturbed sample, which had a large structure at the beginning, loses its structure with the increase of vertical stress and approaches the normally consolidated state. The characteristics of

the soft clayey soils are 1) bulky behavior outside of the normal consolidation line, and 2) larger compressibility compared to remolded samples.

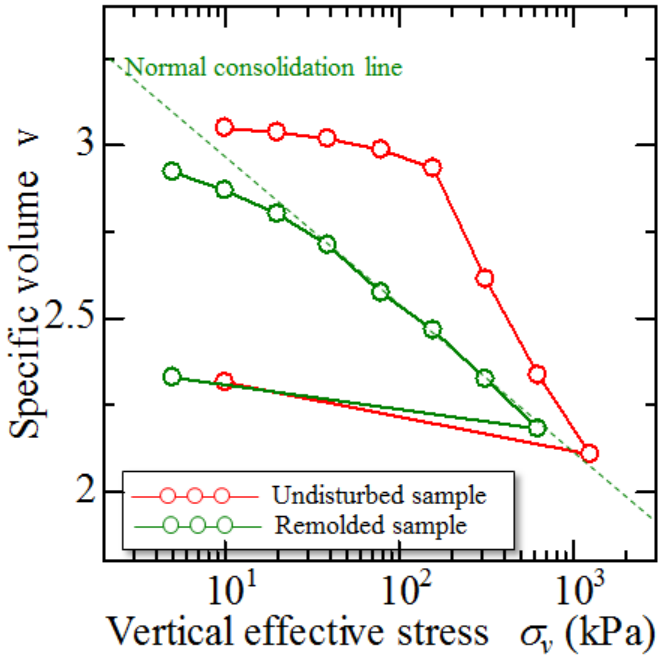

Fig. 4.6 Standard consolidation test

4.2.3 Monotonic undrained shear behavior

The experimental results of undrained triaxial compression tests using undisturbed samples and the initial condition of each sample are shown in Figure 4.7 and Table 4.3 respectively. Confining pressure was implemented in four ways, 45kPa, 100kPa, 170kPa, and 400kPa, with the overburden pressure (170kPa) of the sample in the middle. After isotropic consolidation for 24 hours, undrained shearing was carried out under constant axial strain rate of 0.007 mm/min. This axial strain rate was considered to be slow enough to maintain element behavior (the distribution of excess pore water pressure inside the specimen is uniform) during shearing. From the initial specific volume, it can be seen that although there is some variation, it is about 3.0 and the density is low. Deviator stress q – axial strain ε_a relationship shows that q decreases smoothly after reaching a peak in all tests. q – mean effective stress p' relationship indicate that the low confining pressure (A-1: 45kPa) specimen in the overconsolidated state shows "rewinding behavior" such as an increase of q with a decrease of p' to an increase of q with an increase of p' and then a decrease of q with a decrease of p'. On the other hand, specimens in the slightly overconsolidated state (A-2: 100kPa, A-3: 170kPa) and normally consolidated state (A-4: 400kPa) show "sorrow behavior" such as decrease of q with a decrease of p' after the increase of q with a decrease of p'. In addition, when the undisturbed sample shows softening (decrease of q), the excess pore

water pressure u_w rises smoothly (generation of positive excess pore water pressure) in any sample. Such strain softening behavior is caused by the fact that the highly developed structure is lowered by the loading, which is a typical feature of the naturally deposited soft clay.

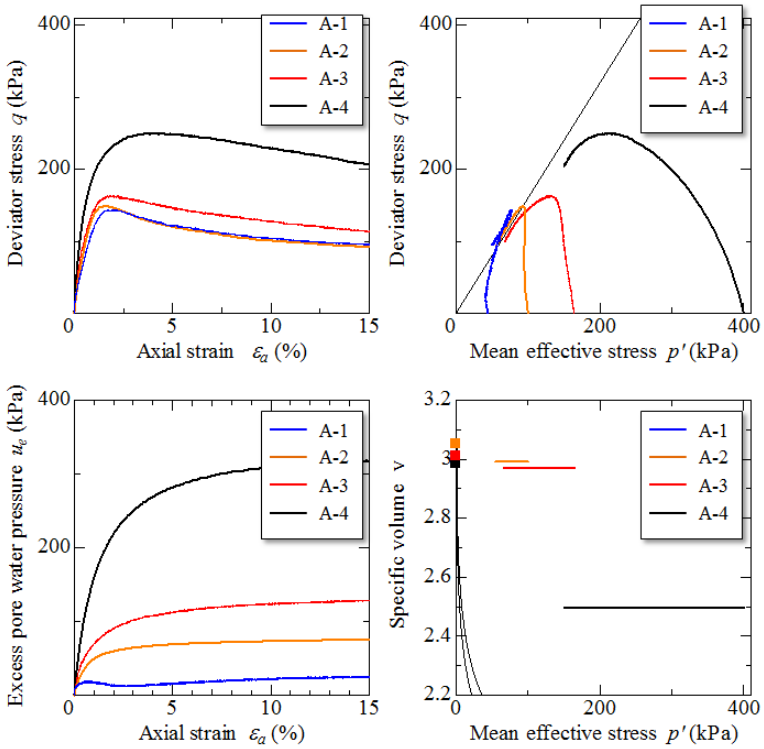

Fig. 4.7 Undrained triaxial compression tests

Table 4.3 Initial condition

Test name	Confining pressure (kPa)	Specific volume before consolidation	Specific volume after consolidation
A-1	45		
A-2	100	3.05	2.99
A-3	170	3.01	2.97
A-4	400	2.99	2.50

4.3 UNDRAINED SHEAR BEHAVIOR OF SOFT CLAYEY SOIL SUBJECTED TO CYCLIC LOADING

4.3.1 Test procedure

In this section, “disturbance” is given to a soft clayey specimen by cyclic shear using a triaxial apparatus. After that, the monotonic undrained shear test is carried out to understand the influence of cyclic loading history on the mechanical behavior of soft

clay. The clay sample used in this experiment is the same as the previous section 4.2. Generally, in the laboratory testing, cyclic loading is provided by stress control, but in the case of stress control, axial strain develops with cyclic loading and necking failure of the specimen occurs. And, it is not possible to apply multiple cyclic loading while maintaining the element property. Therefore, in this study, by applying cyclic loading with strain control, it was possible to give multiple cyclic loading without causing localized deformation of the specimen. Undrained cyclic shear behavior of clayey soil under stress and strain control are shown in Figures 4.8 and 4.9 respectively.

Both results indicate a decrease of *p'* and rigidity with the number of cycles. But it is obvious that in case of stress control, axial strain gradually develops at the extension side and eventually reaches failure. On the other hand, in case of strain control, the specimen can gradually lose its mean effective stress and rigidity without the development of axial strain. Specific experimental procedures are shown below.

1) Isotropic consolidation was performed at 170kPa which is almost equal to overburden pressure for 1 day.

2) Undrained cyclic compression/extension shear test with axial strain control was performed with its half amplitude of 1.0%. The loading rate is 14.4mm/min.

3) Cyclic loading was stopped at a certain number of cyclic loading and the specimens were left for a 4 hours while under undrained conditions, so the excess pore water pressure inside the specimen would become uniform.

4) After sufficient time, monotonic undrained shearing was carried out at a constant strain rate of 0.007mm/min.

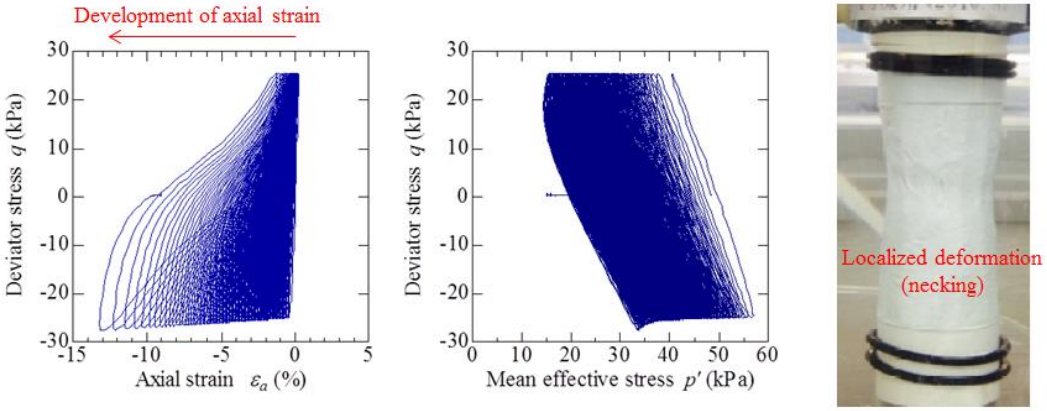

Fig. 4.8 Cyclic loading by stress control

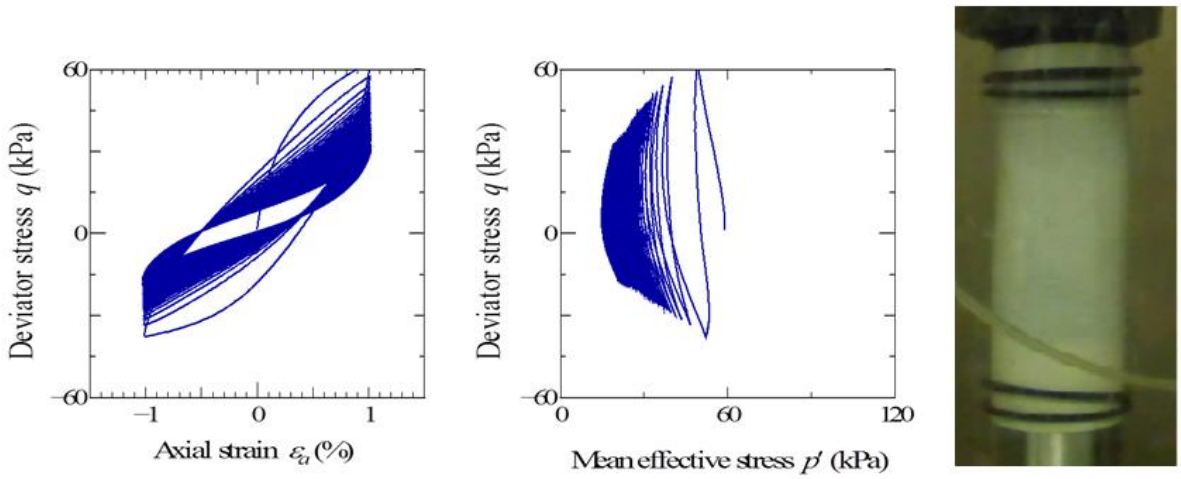

Fig. 4.9 Cyclic loading by strain control

4.3.2 Monotonic undrained shear behavior with cyclic loading history

The experimental results of undrained triaxial compression tests with cyclic loading history and the initial condition of each sample are shown in Figure 4.10 and Table 4.4. After isotropic consolidation at a confining pressure of 170 kPa, the undrained cyclic shear history was given by the method explained in 4.3.1. The test results for A-3 has no cyclic loading history (same as the result shown in Figure 4.7), B-2 is 100 cyclic loading history, and B-1 is 6500 cyclic loading history. The mean effective stress after cyclic loading is 100 kPa for B-2 and 45 kPa for B-1. The *p'* for B-1 and B-2 specimen is different because the cyclic loading was stopped at B-2 and then applied again for B-2 specimen. The pore water pressure in the specimen is not sufficiently migrated during cyclic loading, and the pore water pressure distribution may be uneven. Therefore, after giving a cyclic loading history, the cock was left to stand until no change in pore water pressure occurred. After a sufficient time (4 hours), the undrained shear test was conducted at a constant axial strain rate of 0.007 mm/min. The experimental results without cyclic loading are listed again in Figure 4.10 for easy comparison.

The comparison of the difference between the cyclic loading shows that the stiffness at the initial stage of shearing decreases as the cyclic loading history increases. This is because, as apparent from Figure 4.9, the stiffness is lowered by the cyclic shear history. It is also clear that the peak strength decreases with the increase of cyclic history, and the degree of strain softening also decreases. The soil sample used in this study is not "remolded clay" but "naturally deposited clay with highly developed soil skeleton structure". It is thought that this soil skeleton structure was "disturbed" by cyclic loading and the undrained shear strength decreased.

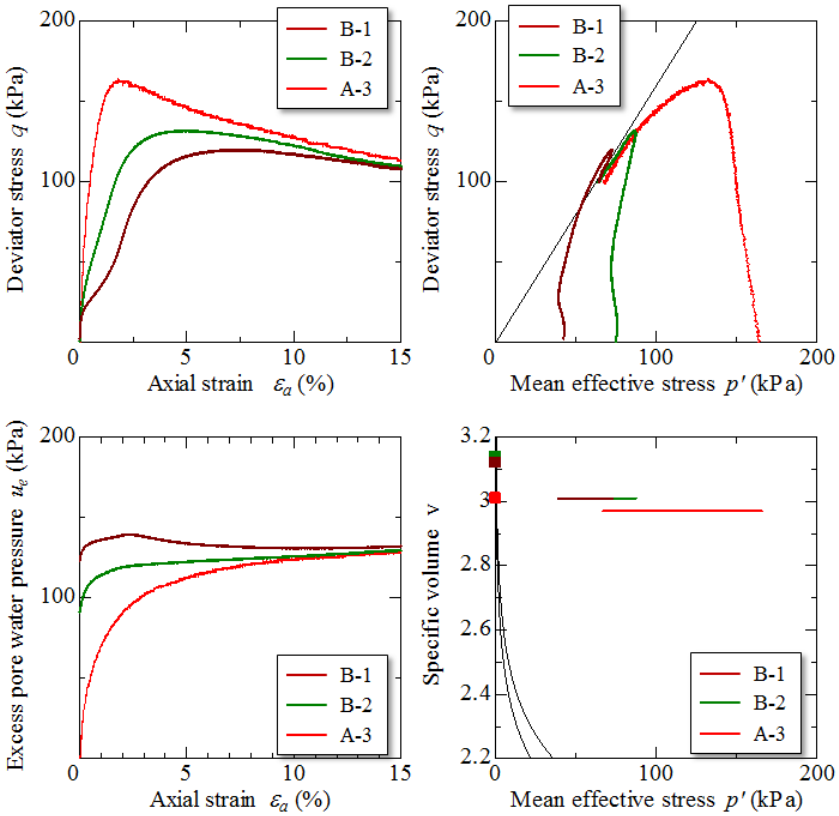

Fig. 4.10 Undrained shear behavior with cyclic loading history

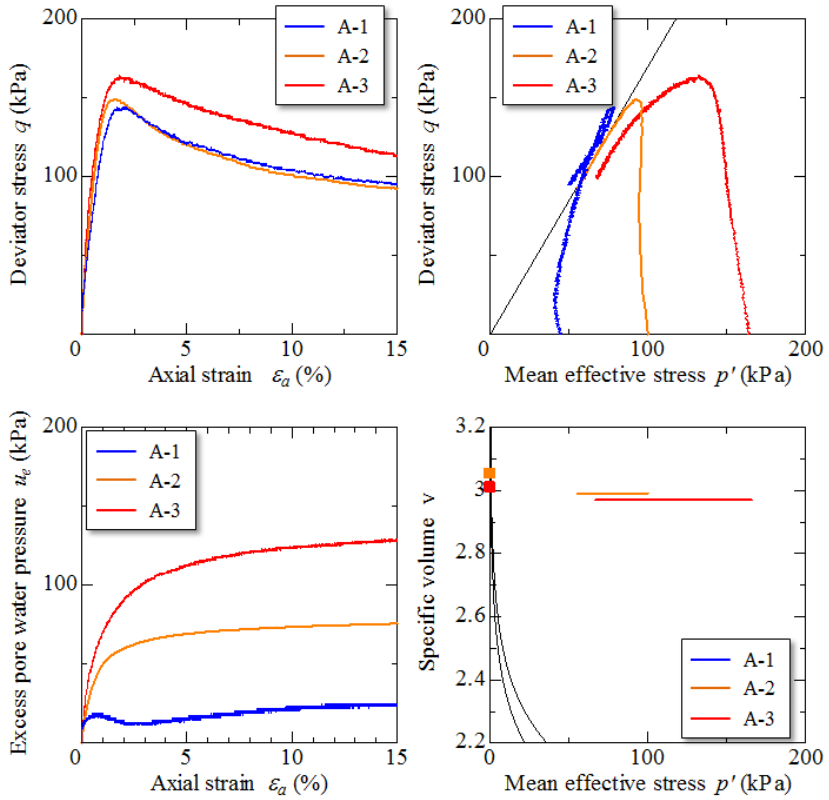

Fig. 4.11 Undrained shear behavior without cyclic loading history

Table 4.4 Initial condition

Test name	Loading	Confining pressure (kPa)	Specific volume before consolidation	Specific volume after consolidation
B-1	Cyclic	45	3.12	3.01
B-2	Cyclic	100	3.14	3.01
A-3	Isotropic	170	3.01	2.97

The results of A-1 with no cyclic loading history and B-1 with cyclic loading history are shown in Figure 4.12. Initial mean effective stress and specific volume are almost equal. As it is clear when the two are put together that the cyclic loading history makes (1) the initial stiffness smaller, (2) the undrained shear strength decreases, and (3) the degree of strain softening decreases. The rigidity of B-1 is lower than the A-1 but the residual strength of B-1 is still higher and they don't converge on same point, the reason might be because of not same void ratio and condition of the preparation of the specimen, as A-1 is under isotropic condition but B-1 is under cyclic loading history.

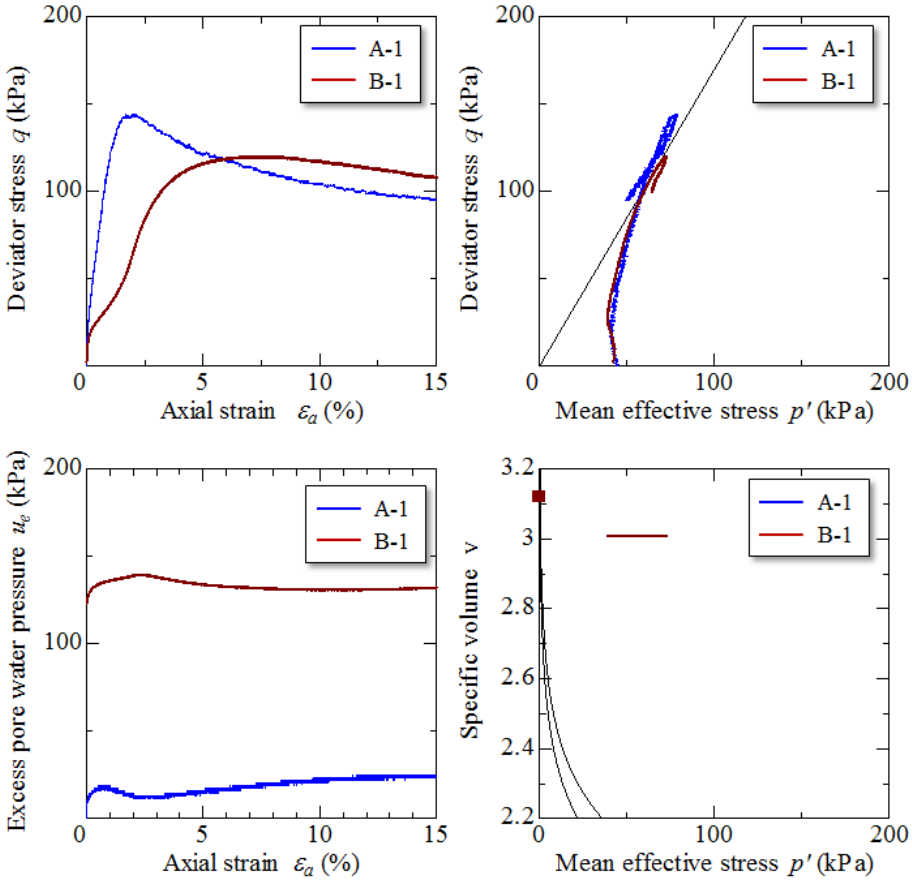

Fig. 4.12 Comparison of the cyclic loading history

4.4 DESCRIPTION OF SOIL DISTURBANCE ASSOCIATED WITH CYCLIC LOADING BASED ON THE SOIL SKELETON STRUCTURE CONCEPT

To date, the authors of this paper have been developing an elasto-plastic constitutive model namely super/subloading Yield Surface Cam-clay model with rotational hardening, abbreviated as SYS Cam-clay model [4-6], which describes the soil skeleton structure of the soil in three terms, "structure," "overconsolidation," and "anisotropy," and describes the development of the soil skeleton structure with ongoing plastic deformation progress. The SYS Cam-clay model makes it possible to describe the mechanical behavior of natural deposited soil by introducing the soil skeleton structure concept. In addition, the mechanical behavior of soil, from typical clay to sand, can be expressed in a unified manner using a single model taking into account the difference in the development rate of the soil skeleton structure. Here, the experimental results obtained in section 4.3, are reproduced using the SYS Cam-clay model, focusing on the function of the structure among the soil skeleton structures. The mechanical behavior of sensitive soft clay under cyclic loading is explained based on the soil skeleton structure concept.

4.4.1 Determination of the material constants

Material constants are determined by reproducing the static behavior of clay using SYS Cam-clay model. Several experiments have been conducted as shown in 4.2.2 and 4.2.3, but it is assumed that the degree of soil skeleton structure is the same at the time of sampling because all of them are close in sampling point and sampling depth. Therefore, it was assumed that p' = 10kPa, which corresponds to the time of sample removal from the sampler, was the common initial stress state. From this point, 1) standard consolidation test and 2) undrained shear under arbitrary isotropic consolidation pressure was performed to reproduce the experimental results. The material constants and initial values are shown in Table 4.5, and the reproduction results of the standard consolidation test and the undrained triaxial compression test are shown in Figures 4.13 and 4.14. Although the undrained shear strength under a confining pressure of 400kPa appears larger, it can be said that the calculation results can be well reproduced from one set of material constants and initial values from compression behavior to shear behavior.

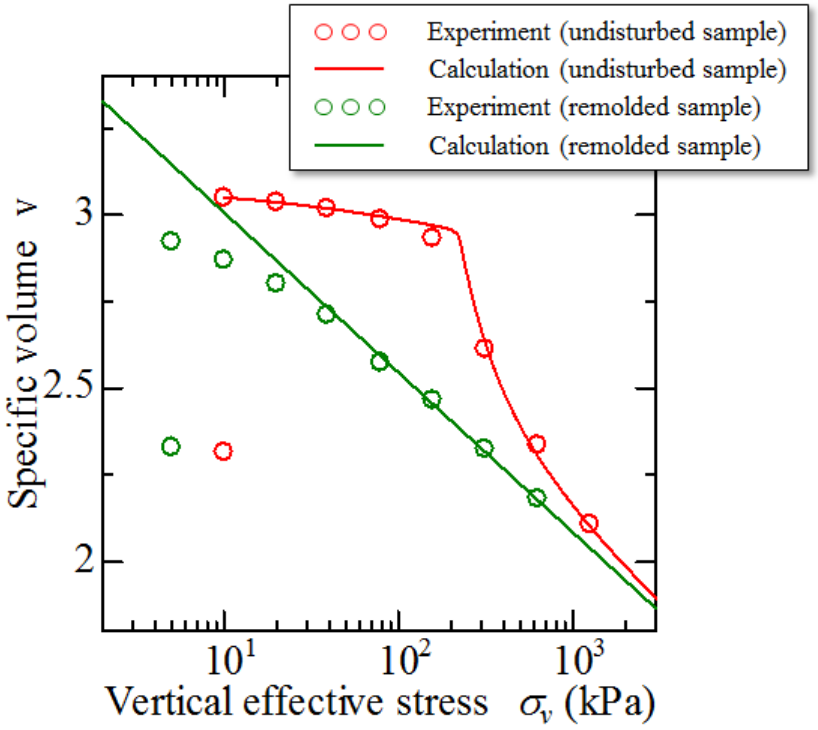

Fig. 4.13 Calculation result of standard consolidation

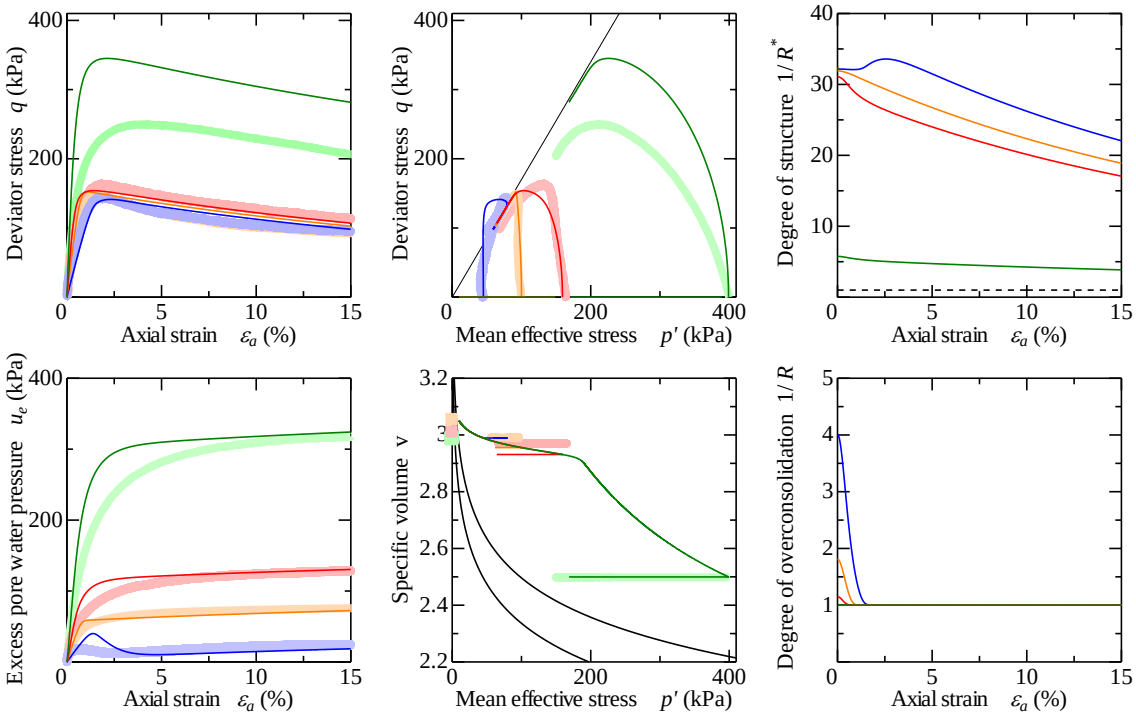

Fig. 4.14 Calculation result of undrained shear tests

Table 4.5 Material constant and initial conditions

Elasto-plastic parameter	
Compression index λ	0.20
Swelling index κ	0.04
Critical state index M	1.70
Intercept of NCL N	2.50
Poisson's ratio ν	0.10
Evolutional parameter	
Degradation parameter of structure a(b=c=1.0)	0.55
Degradation parameter of structure c_s	0.2
Degradation parameter of overconsolidation m	30.0
Evolution parameter of $\boldsymbol{\beta}$	0.0
Limit of rotation m_b	0.0
Initial condition	
Specific volume v_0	3.05
Mean effective stress p'_0	10.0
Stress ratio η_0	0.0
Degree of structure $1/R^*_0$	32.3
Degree of overconsolidation $1/R_0$	18.0
Degree of anisotropy ζ_0	0.0

4.4.2 Reproduction of undrained shear behavior without cyclic history

The reproduction results of the undrained triaxial compression tests without cyclic loading history where the confining pressure is less than 170kPa (Except from Figure 4.14) are shown in Figure 4.15. If the specific volume is equal, the experimental fact that "the undrained shear peak strength is equal regardless of the confining pressure" can be reproduced well. Table 4.6 shows the initial values after isotropic consolidation at each confining pressure. Before isotropic consolidation (p' = 10 kPa) is common, but the degree of structure changes with the difference in the isotropic consolidation process. From the table 4.6, as the confining pressure increases, the degree of overconsolidation decreases and approaches the normally consolidated state, but the degree of structure hardly changes. The structure is expressed as "bulk" against the compression line of the remolded sample, but it has the characteristic that it is difficult to decay by isotropic stress.

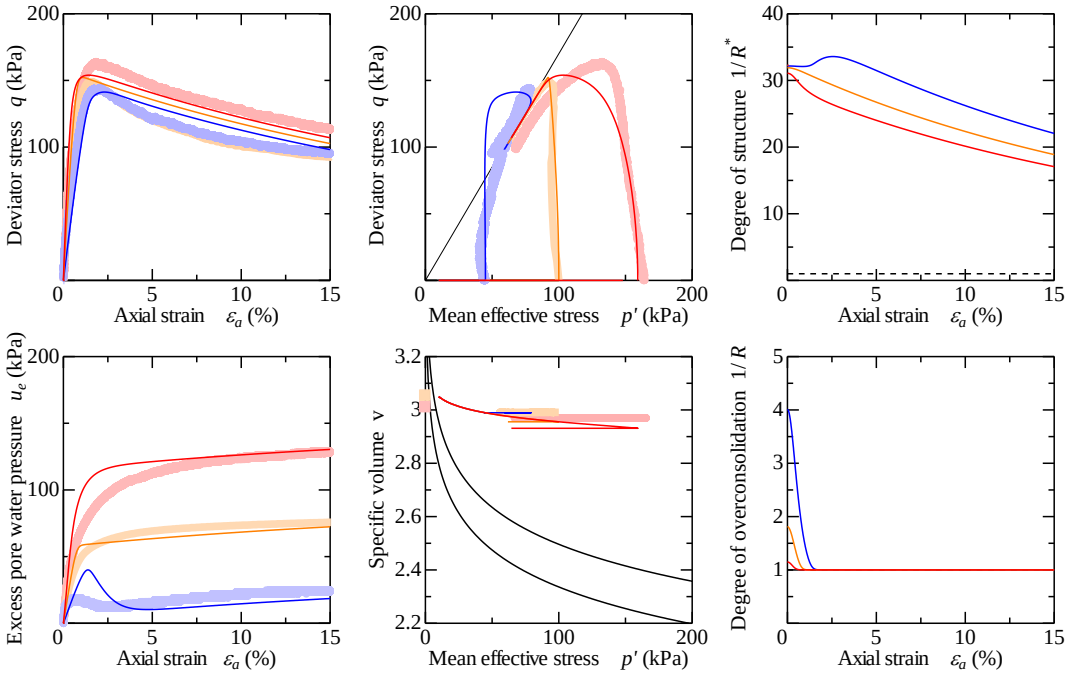

Fig. 4.15 Calculation result of undrained shear tests without cyclic loading history

Table 4.6 Initial values after isotropic consolidation

	A-1S	A-2S	A-3S
Specific volume v_0	2.99	2.96	2.93
Mean effective stress p'_0	45.0	100.0	170.0
Stress ratio η_0	0.0	0.0	0.0
Degree of structure $1/R^*_0$	32.2	31.9	31.1
Degree of overconsolidation $1/R_0$	4.00	1.81	1.15
Degree of anisotropy ζ_0	0.0	0.0	0.0

4.4.3 Reproduction of undrained shear behavior with a cyclic history

The calculation results of undrained cyclic shear with strain control are shown in Figure 4.16. The stiffness decreases as the cyclic history increases, and the behavior in which the effective stress decreases can be reproduced. Here, when focusing on the degree of the structure and the degree of overconsolidation, it can be seen that the degree of the structure decreases and the degree of overconsolidation increases as the cyclic loading history increases. In other words, it can be understood that the degradation of structure and accumulation of overconsolidation occur during the cyclic loading.

The calculation results of monotonic undrained shear behavior stopping the cyclic

loading after an arbitrary number of cyclic loading are shown in Figure 4.17. The experimental fact that "the undrained shear peak strength is reduced by the cyclic history" can be reproduced. Table 4.7 shows the initial values before undrained shear at each confining pressure. The degree of overconsolidation and the structure both decrease as the cyclic loading history increases (as the mean effective stress decrease because pore water pressure increases). The structure was not degraded by isotropic compression, but the structure was significantly degraded by cyclic shear. Therefore, it is clear that the decrease in undrained shear peak strength due to the number of cyclic loading is reproduced as the degree of the structure is small.

A reproduction of the experimental results shown in Figure 4.10 is shown in Figure 4.17. These are excerpts from the calculation results shown in Figs. 4.15 and 4.17. Comparing Tables 4.6 and 4.7, it can be seen that because of the different loading history, the degree of soil skeleton structure is different although they are almost in the same stress and specific volume state. If there is no cyclic history, the degree of overconsolidation and the degree of structure are both high. On the other hand, when there is a cyclic history, the degree of overconsolidation and the degree of structure are smaller than those without cyclic history. In other words, soil disturbance caused by cyclic loading can be described as the reduction of structure and overconsolidation. Such a decrease in undrained shear peak strength due to soil disturbance is a phenomenon that can be explained for the first time by incorporating the structural concept, suggesting the necessity/importance of the "structural concept".

Table 4.7 Initial values after cyclic loading

	B-1S	B-2S	A-3S
Specific volume v_0	2.93	2.93	2.93
Mean effective stress p'_0	45.0	75.0	170.0
Stress ratio η_0	0.0	0.0	0.0
Degree of structure $1/R^*_0$	18.9	22.7	31.1
Degree of overconsolidation $1/R_0$	3.40	2.15	1.15
Degree of anisotropy ζ_0	0.0	0.0	0.0

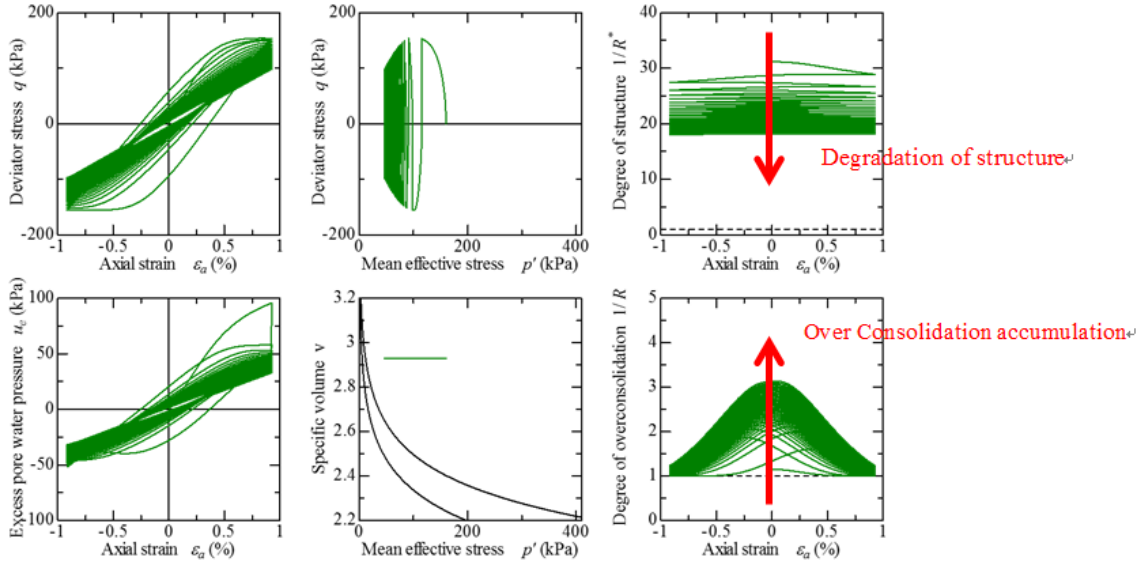

Fig. 4.16 Calculation result of cyclic undrained shear tests

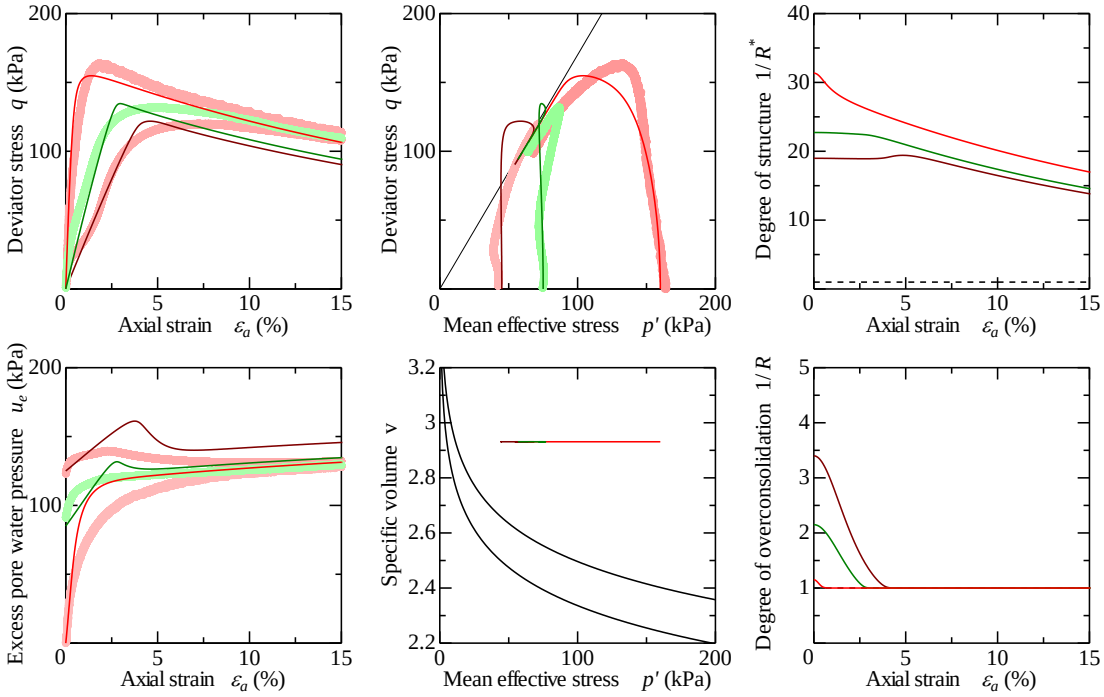

Fig. 4.17 Calculation result of undrained shear tests with cyclic loading history

4.5 CONCLUSIONS

(1) In this chapter, in the monotonic undrained triaxial test, the strain softening behavior was observed, which is a typical feature of the naturally deposited soft clay.

(2) By applying cyclic loading with strain control, it was possible to give multiple cyclic loading without causing localized deformation of the specimen as compared to stress control which showed the necking failure of the specimen.

(3) It is clearly observed, that with the increase of the cyclic loading history, (1) the initial stiffness smaller, (2) the undrained shear strength decreases, and (3) the degree of strain softening decreases.

(4) It was observed in that in undrained shear isotropic test, as the confining pressure increases, the degree of over consolidation decreases and approaches the normally consolidated state, but the degree of structure hardly changes, because it has the characteristic that it is difficult to decay by isotropic stress.

(5) The stiffness decreases as the cyclic history increases, and the behavior in which the effective stress decreases can be reproduced. Here, when focusing on the degree of the structure and the degree of over consolidation, it can be seen that the degree of the structure decreases and the degree of over consolidation increases as the cyclic loading history increases. In other words, it can be understood that the degradation of structure and accumulation of over consolidation occur during the cyclic loading.

REFERENCE

1 Mendoza, M. J., Foundation engineering in Mexico City; Behavior of foundations, Proceeding of International Symposium on Geotechnical Engineering of Soft Clay, Vol.2, 1987, pp.351-367.

2 J. Merlos and M. P. Romo, Fluctuant bearing capacity of shallow foundations during earthquakes, Soil Dynamics and Earthquake Engineering, No.26, 2006, pp.103-114.

3 Leonardo Zeevaert., Foundation Engineering for Difficult Subsoil Conditions, Van Nostrand Reinhold Company, 1972, pp. 521.

4 Asaoka, A., Noda T., and Kaneda, K., Displacement/traction boundary conditions represented by constraint conditions on velocity field of soil, Soils and Foundations,

Vol. 38, No. 70, 19989, pp 173-181.

5 Asaoka A., Nakano M., and Noda, T., Superloading yield surface concept for highly structured soil behavior. Soils and Foundations, Vol. 40, No. 2, 2000, pp 99-110.

6 Asaoka, A., Noda, T., Yamada, E., Kaneda, K., and Nakano, M., An elasto-plastic description of two distinct volume change mechanisms of soils, Soils and Foundations, Vol. 42, No. 5, 2002, pp 47-57.

Chapter 5

EXPERIMENTAL ATTEMPT TO PRODUCE SOFT CLAYEY SPECIMEN BY ADDING HYDRATION REACTION CONTROLLED CEMENT OR LEACHING OF CALCIUM

5.1 INTRODUCTION

Since liquefaction damage to sandy ground has attracted attention from the Niigata Alaska Earthquake 1964 [1-2], the earthquake damage prediction in the field of geotechnical engineering is the instability phenomenon of sandy ground, that is, liquefaction. It is the center, and the sticky land has not received much attention. Therefore, even if the cohesive soil has an N value of zero or contains a large amount of sand / silt, as soon as it is classified as "cohesive soil", it is considered that earthquake damage to the ground does not occur / does not need to be considered. , Cohesive soil has been modeled as "elastic" in effect. On the other hand, when the past earthquake damage such as the Mexico earthquake (1957, 1985), Nepal earthquake (2015), Miyagi prefecture earthquake (1978), Niigata prefecture Chuetsu earthquake (2007), etc. is examined, Figure 5.1 shows an apartment in Mexico City that was destroyed in the 1985 Mitokan earthquake in Mexico. Mexico City is originally located on the basin where the Lake Tescoco was reclaimed, and its soil quality is composed of volcanic ash-like extremely soft cohesion. The area is famous for the occurrence of huge earthquake damage despite the fact that it is 300 km away from the epicenter, but as the cause, the seismic movement is amplified and stagnated in the basin, and not only during the earthquake but also the earthquake.

Fig. 5.1 Mexico Apartment (Earthquake 1985)

After that, it is said that the soft and viscous soil was violently disturbed by receiving repeated vibration for a long time, and the supporting power was lost and Figure 5.2 shows the relationship between the amount of land subsidence and time observed at Port Island during the 1995 Hyogoken Nanbu Earthquake. Land subsidence, which was once approaching convergence after the completion of Port Island landfilling, showed a surge and acceleration during the earthquake. Although this settlement occurs in the marine alluvial clay Ma13 layer in Osaka Bay, it has been confirmed by the investigation that the clay layer was in a sensitive and high water content state, and the increase of the overburden load by the landfill and its polarization [3]. It is thought that the strong vibration received under the applied load reduced the stiffness of the ground respectively.

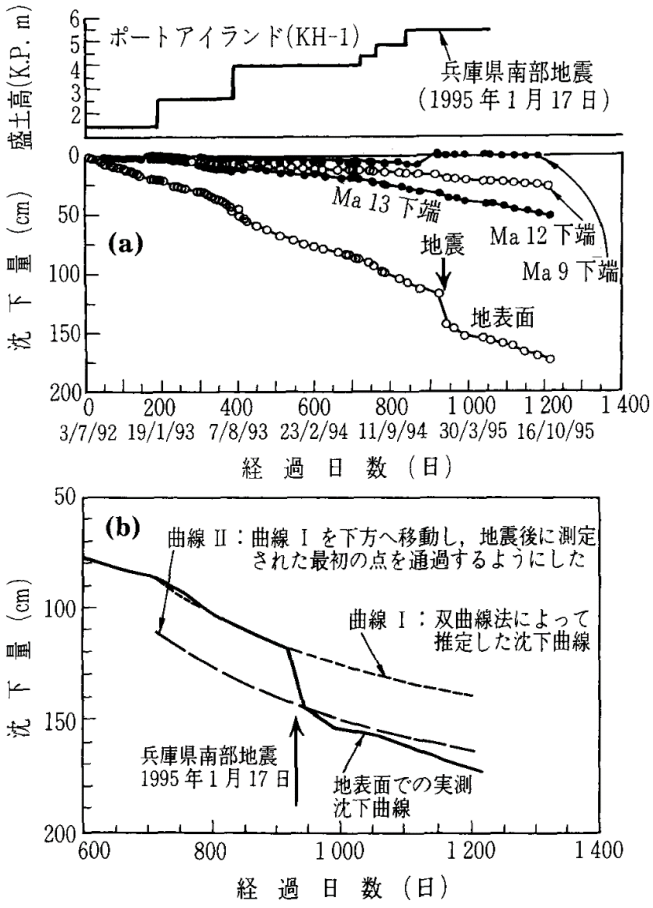

Fig. 5.2 Relationship between the amount of land subsidence and time observed at Port Island during the 1995 Hyogoken Nanbu earthquake.

The sandy ground although not so much as liquefaction damage, there are many reports of earthquake damage of soft land in and outside Japan. However, earthquake damage does not occur in any viscous land, and it is common to viscous land where earthquake damage occurred, that viscous soil has a high water content ratio, "sensitivity",

"softness". Soft clay foundation often shows long-term large settlement under embankment loading as the compressibility is large. On the other hand, the clay foundation has been considered to be safe for the dynamic problem. However, the recently investigated results showed that clay foundation showed remarkable loss of rigidity due to an earthquake, which leads to tremendous seismic damages, as observed in the 1957, 1985 Mexico earthquakes and the 2015 Nepal earthquakes. These areas possess the soft lake deposits consisting of soil types with extremely high water contents, namely, soft and sensitive clays.

Therefore, in addition to the static behavior, it is important to grasp both static and dynamic mechanical properties of naturally deposited clayey materials it is important to understand the dynamic behavior of such soft clay soils, but for that purpose it is possible to use an undisturbed sample collected undisturbed as it is in a naturally deposited state.

To this aim, it is indispensable to carry out various systematic experiments using the undisturbed soil samples. It is difficult to prepare number of homogeneous soft clay sample, due to the problem of variability of quantities during sedimentation, disturbance during sampling and high expense of boring survey. By using the remolded sample, focused on the cementation reaction, in order to artificially produce the soil sample having similar characteristics to those of naturally deposited soft clay. By doing so, while maintaining the reproducibility of the specimen, it might be possible to perform a large number of systematic experiments, and to conduct such model experiments as impossible in the past, in order to artificially produce the sample having similar characteristics to those of naturally deposited soft clay. Although numerous experimental studies have been conducted to reproduce the natural soft clay with cement, the cement was directly added to soil in most cases. As the result, the solidification effect was so strong that localized failure occurred in the soil specimen due to cracking followed by a sudden decrease of shear stress with no increase in excess pore water pressure. So, in terms of the necessity to reduce the solidification effect, a newly attempted methods was introduced “addition of hydration reaction controlled cement” and “calcium leaching” to represent similar characteristics of soft clay material. Various tests were conducted to achieve the required results.

In this chapter, the influence on mechanical properties, when hydration reaction controlled cement is added to clayey soil and also describe the results of examining the influence of calcium leaching on the mechanical properties of cemented cohesive soil will be discussed.

5.2 PREVIOUS STUDIES

Researcher added a small amount of cement to the reconstructed Fukuyama Port cohesive soil sample, added pre-consolidation, prepared the specimen, and performed re-consolidation as shown in Figure 5.3. Due to the structure formed by the solidification reaction of cement, bulky behavior can be confirmed. He also performed the Non-drainage shear test of cement-added reconstituted samples and it might be a localized and brittle loss of strength due to shear plane generation, however, as the confining pressure increases, the axial stress does not decrease [4]. Moreover, at the decrease in the axial differential stress under low confining pressure, shows that it is not a smooth decrease but a rattling and brittle behavior. In addition, the effective stress path clearly shows a "worship behavior "such as a decrease in q with a decrease in p ′after an increase in q with a decrease in p ′greater than that. M of general clay soil is about 1.5, which is to be considered as solidification effect of cement should be too strong as shown in Figure 5.4.

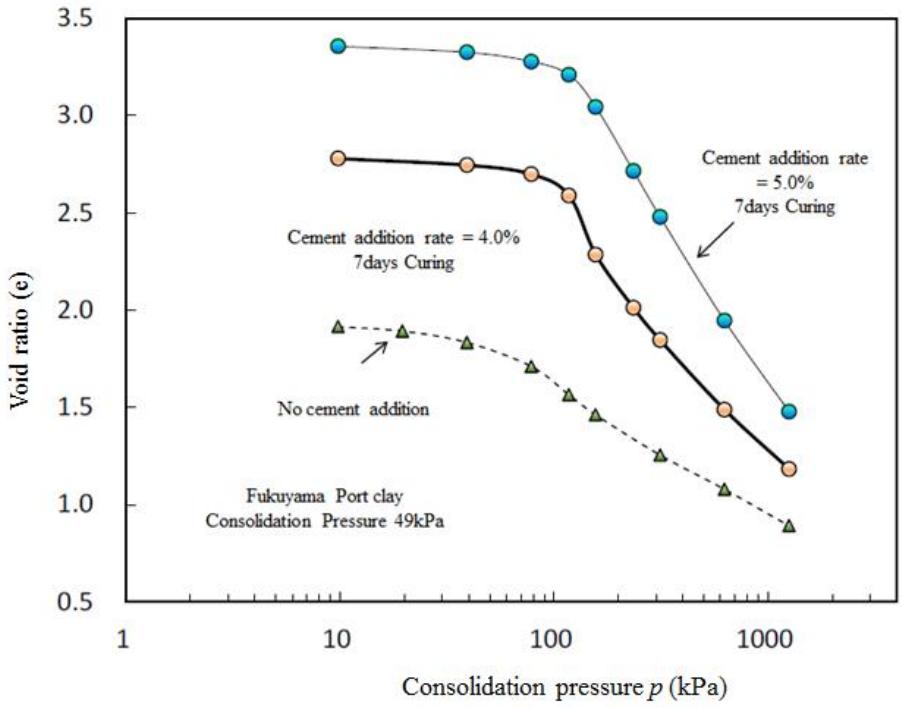

Fig. 5.3 Modified figure of standard consolidation test (Tsuchida et al, 2013).

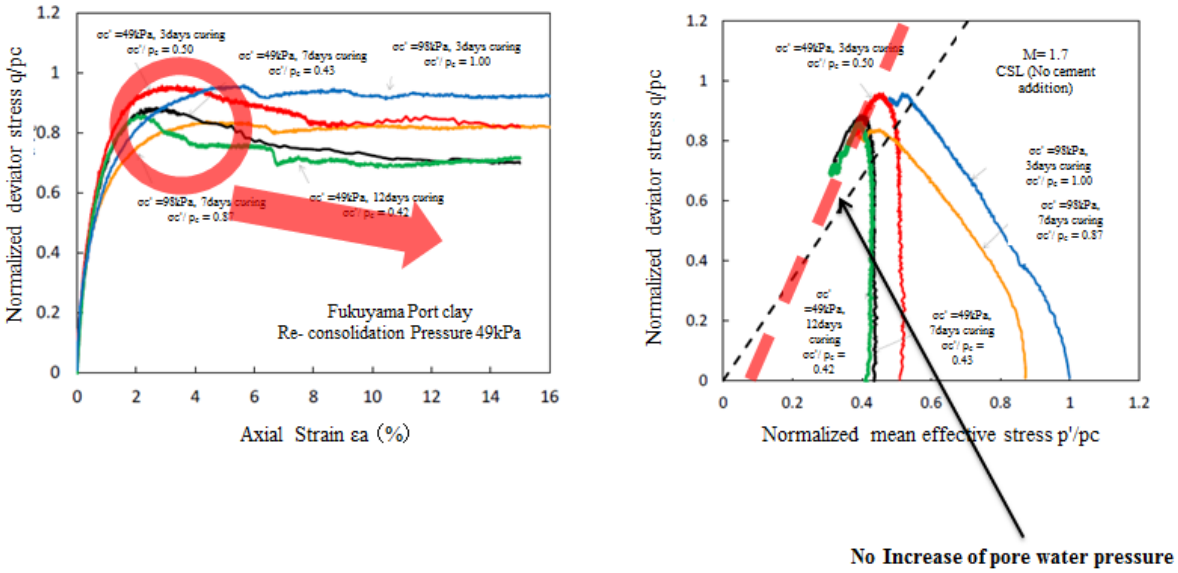

Fig. 5.4 Modified figure of undrained shear test results of cement-added reconstituted samples (Tsuchida et al, 2013)

The behavior based on the concept of skeletal structure and the understanding of the mechanical behavior was analyzed as a fluid with high fluidity assuming the mixed solidification method in the pipe using the cement improved soil of Fujimori clay used in this study. Cement solidification increases the structure and over consolidation. The test result of the cement-improved soil reproduces the bulky behavior outside the normal consolidation line of the tempered improved soil. It can be said that the behavior similar to that of high-viscosity clay soil was reproduced [5].

The axial differential stress decreased after reaching its peak, but the q-εa relationship became brittle and the limit state. The slope of the line is still as large as about 2.0. In the test result of low confining pressure, the specimen reaches to the “tension cut off line” of inclination 3.0 through the origin and shows collapse, because in this research the cement addition rate was 6.9%, so the cement solidification action was strong, and it was considered that the fracture was brittle without showing strength deterioration (softening behavior) as a material property, shown in Figure 5.6. Based on the skeletal structure concept, the addition of cement enhanced the structure, but it was thought that the structure was strong and not easily broken. Therefore, it is necessary to pay attention to physical properties in consideration of the effects of excessive cement addition [6].

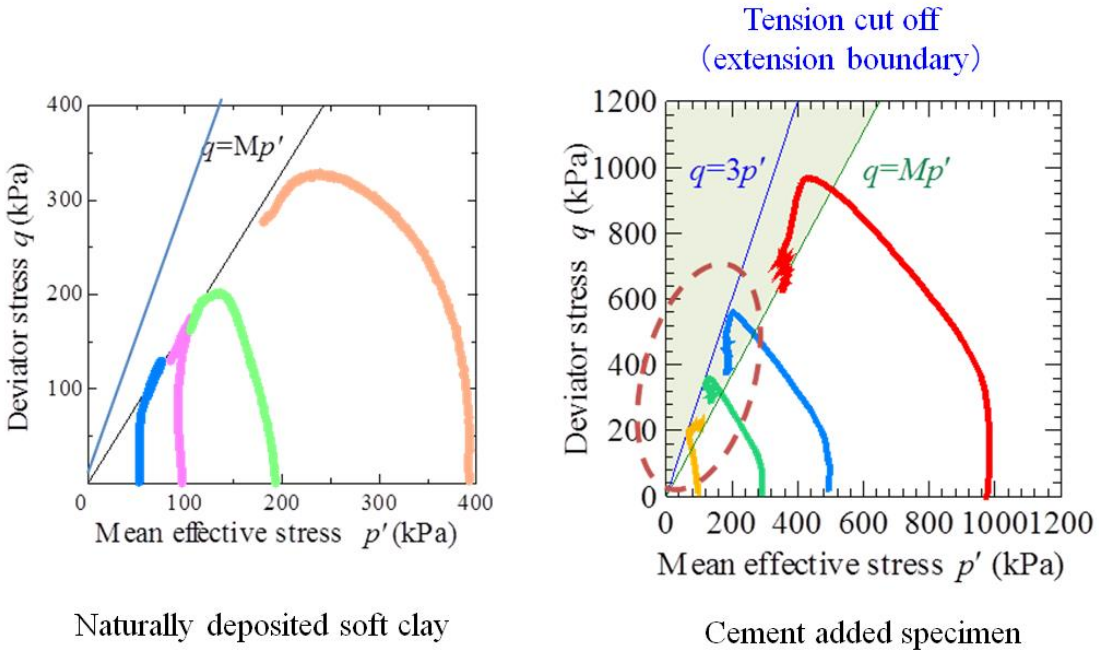

Fig. 5.6 Comparison of naturally and cement added specimen (Fukuwa et al , 2016)

5.3 CHARACTERISTICS OF NATURALLY DEPOSITED SOFT CLAYS

First, we confirmed the mechanical properties of naturally deposited soft clay. Figures 5.7 to 5.9 indicate the typical experimental result of the undisturbed soft clay sample which was sampled from very soft clay layer with its N value about 0 to 2. Figure 5.7 shows the results of unconfined compression tests. Although there are variations, the compressive strength is about 100kPa and shows a clear peak. Since the compressive strength of the remolded sample is about 10kPa, the sensitivity ratio S_t is as large as 10. Figure 5.8 shows the Oedometer test results of the undisturbed and remolded sample. It can be seen that the compression line of the undisturbed sample takes a bulky stress state in the impossible region outside the remolded compression line and the compressibility is also large. Compressibility ratio C_c/C_{cr} is as large as 1.6, where C_c is a compression index of the undisturbed sample and C_{cr} is a compression index of the remolded sample respectively. It was founded that there is a possibility of a large long-term settlement if the sensitivity ratio S_t and compressibility ratio C_c/C_{cr} of the clay layer are equal to or more than 8.0 and 1.5, respectively [7] as shown in Figure 5.10. In that sense, as a characteristic of the soft clayey soil, a large sensitivity ratio and a compression index ratio can be cited. Figure 5.9 shows undrained triaxial compression tests (stress path; deviator stress q ~ mean effective stress p' relation) of undisturbed samples with different confining pressures. Soft clay specimen indicates strain softening behavior with a change of excess pore water pressure. In conclusion soft clays possess high liquidity index, high compressibility and high sensitivity ratio. Moreover reduction

of axial stress due to reduction of effective stress "Softening tendency", “Smooth rise of pore water pressure“

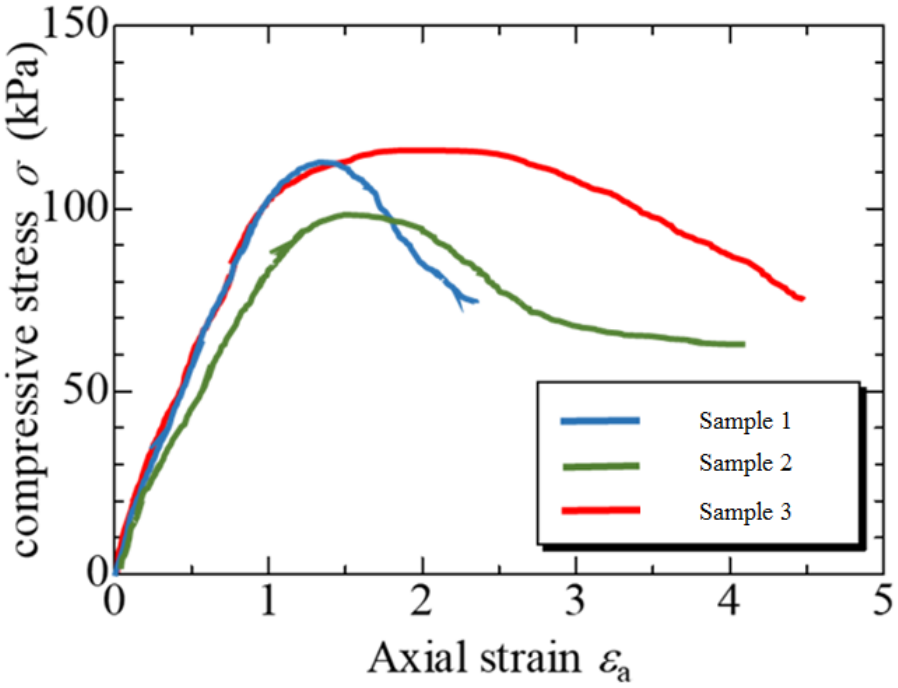

Fig. 5.7 Unconfined compression tests

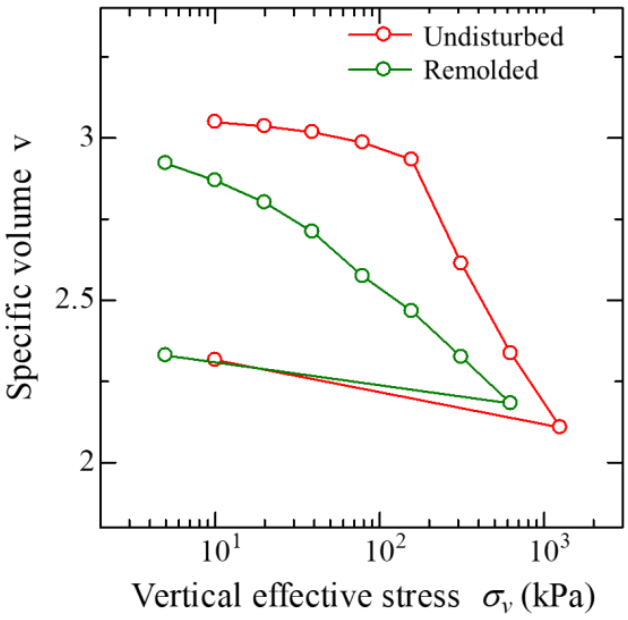

Fig. 5.8 Oedometer test

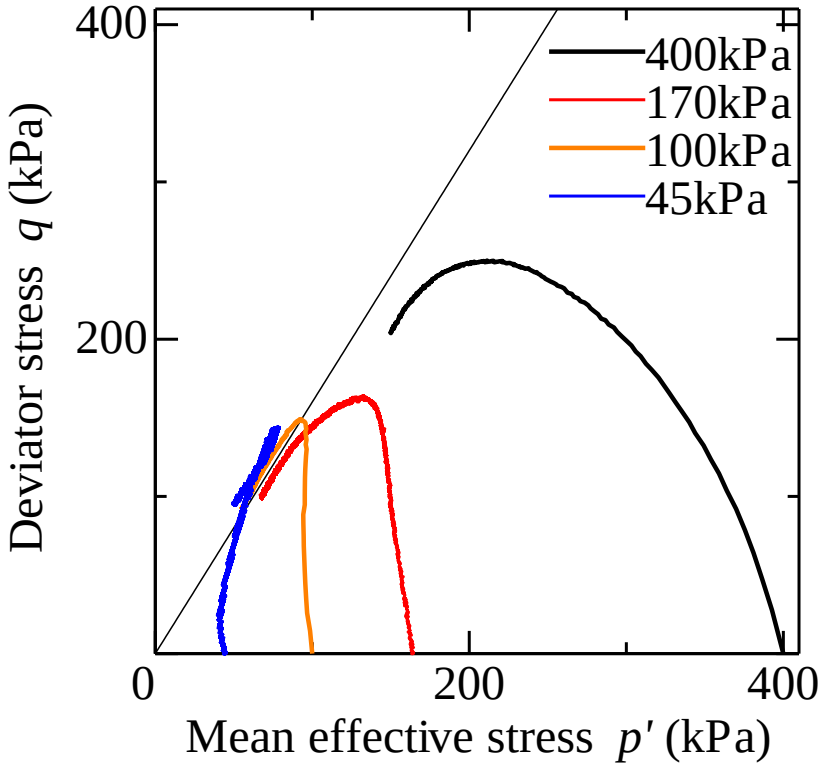

Fig. 5.9 Undrained triaxial compression

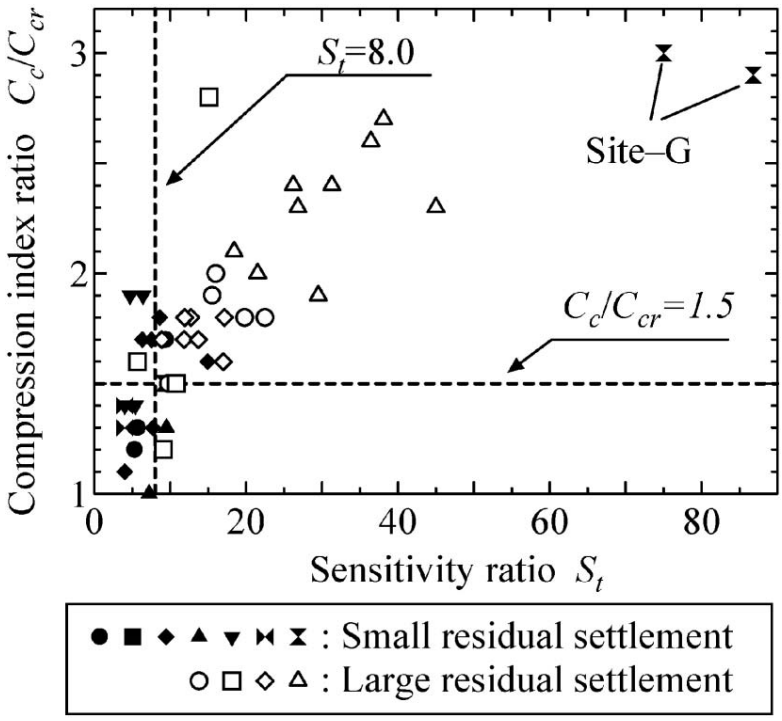

Fig 5.10 Classification based on the sensitivity and compression index ratios (Inagaki, M., etal, 2010)

5.4 PHYSICAL PROPERTIES OF A SPECIMEN

The specimen used for this research is Fujinomori soil. Gradation curve is shown in Figure 5.11 and physical properties are shown in Table 5.1

Table 5.1: Physical Properties of silty Clay

Description	Silty-Clay
Liquid Limit w_L (%)	45.82
Plastic Limit w_p (%)	25.37
Plasticity index I_p	20.44
G_s (g/cm^3)	2.65

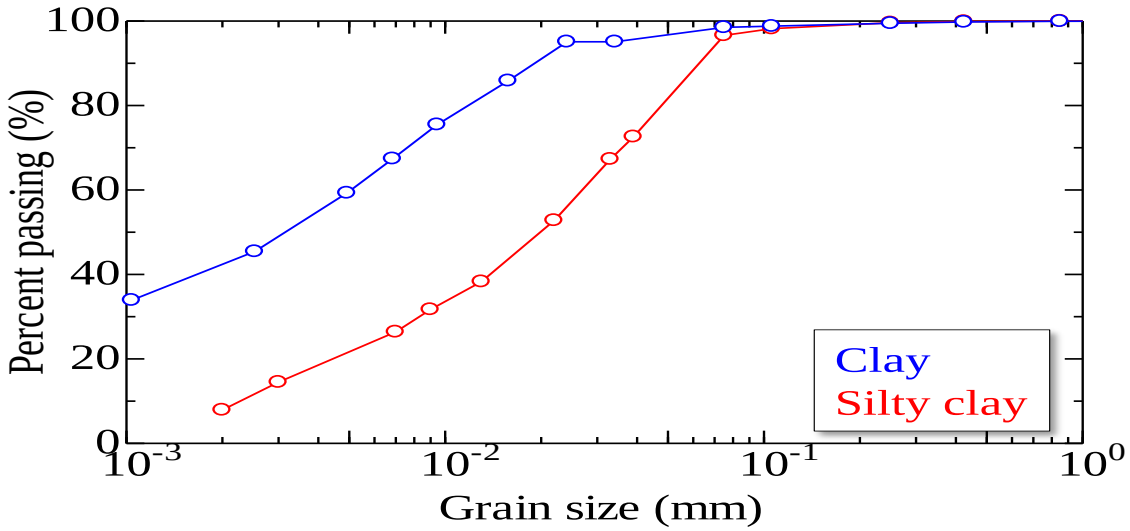

Fig 5.11 Gradation Curve of specimen

5.5 HYDRATION OF CEMENT

In this chapter, the new method hydration controlled cement will be discussed and later on about calcium leaching.

In order to make structure soil, we are using pre-curing cement (early-strength Portland cement (curing 7 days)) in order to reduce the solidification effect and also control PH. Physical properties changes with PH. The Conceptual diagram of hydration reaction of Portland cement shown in Figure 5.12.

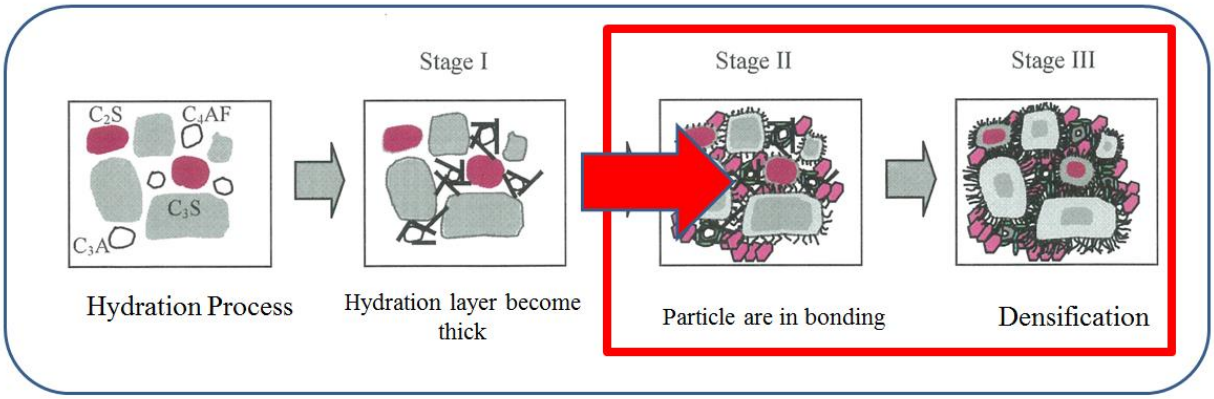

Fig. 5.12 Conceptual diagram of hydration reaction of Portland cement

When cement particles come in contact with water (after water injection), reaction between cement and water starts.
Hydrate forms and the layer of hydrate covering the cement particle surface become thick enough. (Stage 1)
When particles begin to adhere to each other, condensation occurs. (Stage 2)
Densification of cement proceeds by filling the space where water was first present in the hydrate. (Stage 3)

In this chapter, by the above hydration reaction, the bond strength between soil particles was enhanced without going through the density increase (consolidation process) with load loading, and further, the preparation of the specimen in the high water content state was anticipated. Also, this chapter also attempts to control the solidification effect of the hydration reaction that proceeds in stages by continuing agitation during the hydration reaction.

5.5.1 Methodology

In this chapter, the solidification effect of the cement was tired to reduce by stirring clay and cement mixture for a while, for the purpose of destroying the generation of the hydration product. The procedure for preparing specimens is shown below.

1. The cement powder was mixed with the clay and water content ratio was adjusted to be 75% which is approximately 1.5 times the liquid limit of clay, and stir thoroughly for a while. Stirring time is 0, 1, 2, 3 and 6 hours. The amount of 5 specimens was mixed at a time so that there was no significant difference between specimens as shown in Figure 5.13.

2. After properly mixing, the paste was put into a specified plastic mold having a diameter of 50 mm and a height of 100 mm by giving a little vibration while putting

to avoid the intrusion of air.

3. Due to bleeding effect, the moisture rich portion formed on the top of the plastic mold was removed with a spatula and put the mold for curing for 2 weeks in water, so that solidification reaction by early strength Portland cement converged to some extent as shown in Figure 5.14.

4. Since this experiment aims to reproduce soft and viscous soil that can be used in model experiments, all specimens prepared in this experiment were not pre-consolidated.

Fig. 5.13 Flow of sample mixing

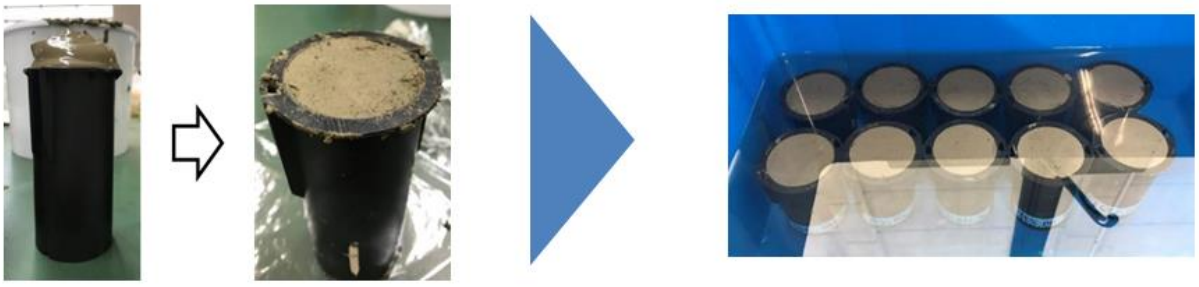

Fig. 5.14 Upper layer of mold is removed and underwater curing

5.5.2 Experimental results and discussion

A viscous soil specimen is prepared, and a physical test, a uniaxial test, a standard consolidation test, and an undrained triaxial test are performed as appropriate, and an attempt is made to grasp their mechanical characteristics. By addition of 5% of cement to specimen with different stirring time, 0, 1,2,3,6 hr., there was not a significant change observed in physical properties with pre-curing time, but it exhibits a high liquidity index that is characteristic of soft clay soils and also the formation of the structure due to the cement solidification reaction is alleviated and the water retention capacity is reduced.

5.5.3 Uniaxial Compression Test

A uniaxial compression test was performed on the artificial cohesive soil specimen with 5% cement added, changing the stirring time, and the characteristics and behavior were investigated. Figure 5.15 shows unconfined compression tests results with different stirring time, and Table 5.2 shows the specific volume, peak strength, residual strength, and specimen appearance. Figure 5.15 shows that the strength and rigidity decrease with increasing the stirring time. Although deformation is brittle, adding cement directly shows high peak strength and high rigidity. As the stirring time increases, the peak strength and the initial stiffness decrease. Moreover, when it exceeds 3 hours, the specimen shows no clear peak. From Table 5.2, the specific volume decreases with increasing stirring time. This is considered to be the influence of bleeding. Looking at the uniaxial compressive strength qu, it also decreases with increasing stirring time. Therefore, it can be considered that the sensitivity ratio St decreases. Looking at the state after shearing, the specimen with a stirring time of 0 hour shows brittle fracture, while the specimen with a stirring time of 6 hours shows ductile fracture.

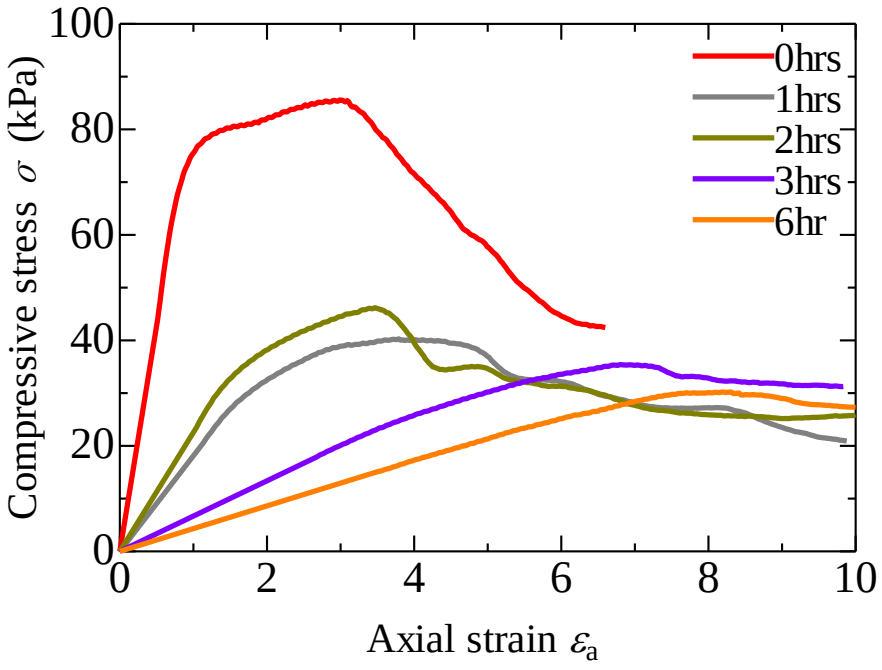

Fig.5.15 Unconfined compression tests

Table 5.2 Specific volume, peak strength, residual strength and specimen appearance

Stirring Time	0hr	1hr	2hr	3hr	6hr
Specimen after shearing	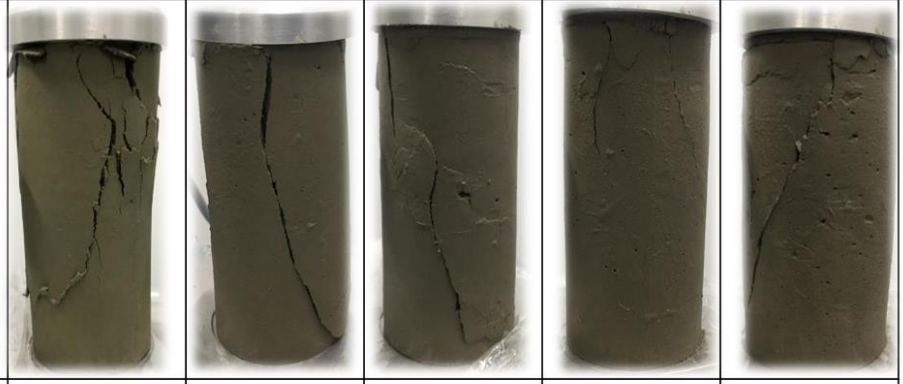				
Specific volume	3.04	2.90	2.84	2.82	2.75
Uniaxial compressive strength q_u	85.6	40.3	46.1	35.4	30.2
Residual Strength	42.4	20.9	27.2	31.3	25.7

Therefore, it was found that by increasing the pre-curing time, both strength and rigidity decreased, and the brittle behavior was relaxed and the sensitivity ratio St was decreased. By prolonging the stirring time, the solidification effect of the cement is reduced.

5.5.4 Standard Consolidation Test

Figure 5.16 shows Oedometer tests with different stirring time. It shows large compressibility while taking a bulky stress state outside the compressed line of the remolded sample by addition of cement. Although the compression index decreases with increasing stirring time, moreover the compressibility ratio is above 1.5, even stirred for 6 hours as shown in Table 5.3.

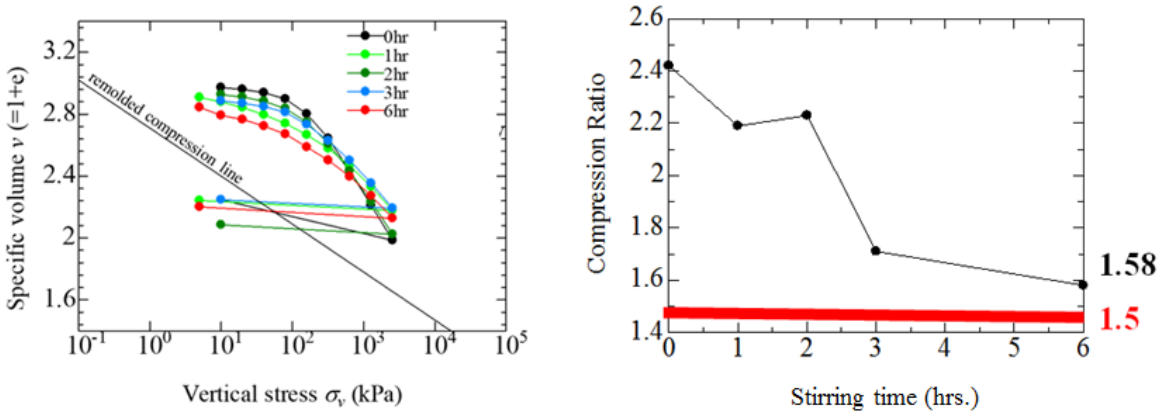

Fig 5.16 Oedometer tests

Table 5.3 Stirring time and compression index

Stirring time (hours)	0hr	1hr	2hr	3hr	6hr
Compression indexC_C	0.75	0.68	0.69	0.53	0.49
Compression index ratio	2.42	2.19	2.23	1.71	1.58

5.5.5 Triaxial compression tests

5.5.5.1 Isotropic consolidation process

The relationship between time and volume strain in the isotropic consolidation process with a Confining pressure of 30 kPa and of 100 kPa, are shown in Figure 5.17 and Figure 5.18 respectively. The axial displacement and volume change are shown in Table 4 and Table 5, respectively. It can be observed that the volumetric strain increases as the stirring time is increased. Furthermore, looking at Table 5.4 and Table 5.5, the longer the stirring time, the larger the axial displacement and volume change.

It can be seen that by increasing the stirring time, it was possible to produce a specimen that was softer and had a larger volume change in a high water content ratio than the specimen only with cement addition.

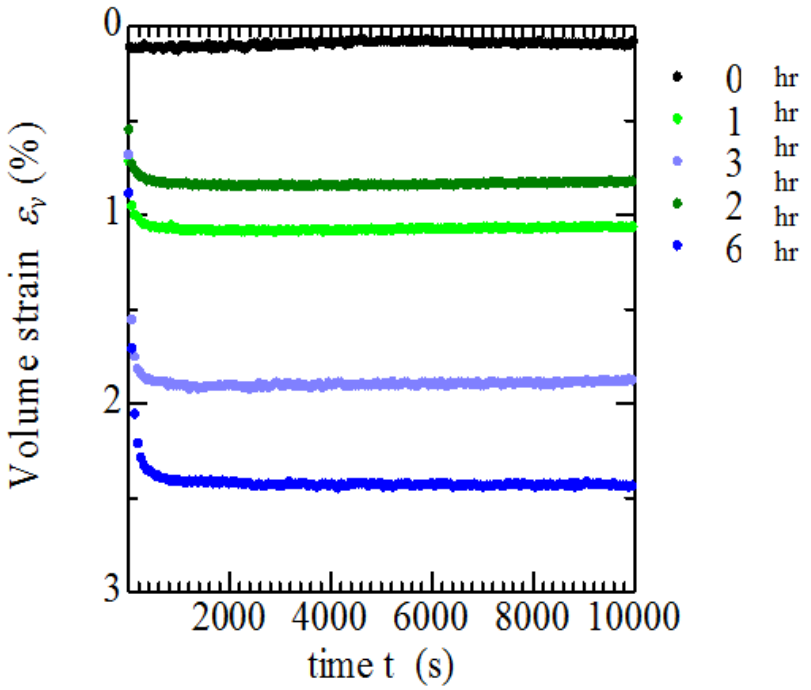

Fig. 5.17 Time-volume strain relation (restraint pressure 30kPa)

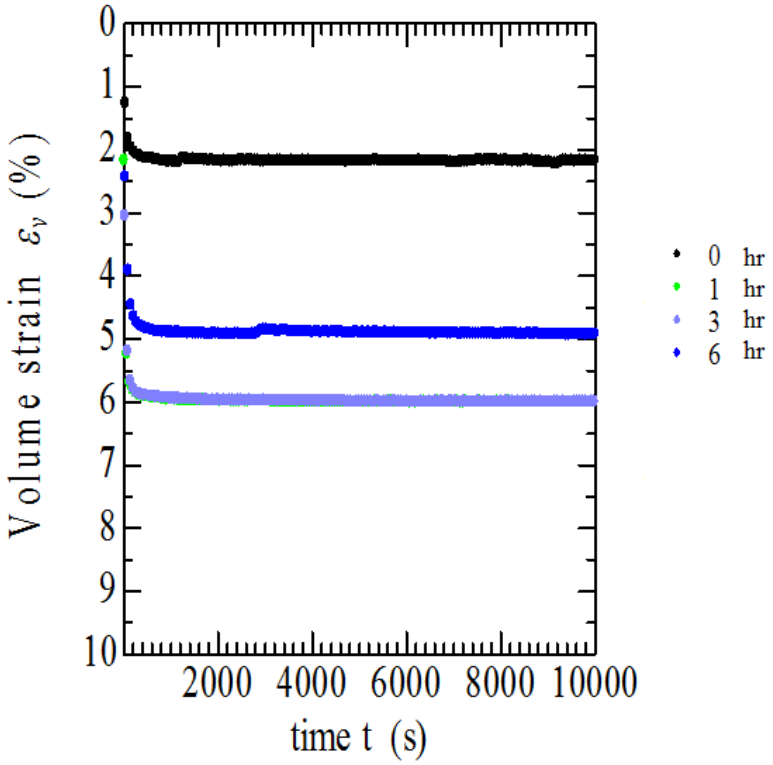

Fig. 5.18 Time-volume strain relation (restraint pressure 100kPa)

Table 5.4 Axial displacement and volume change (confining pressure 30kPa)

Stirring time (hours)	0hr	1hr	2hr	3hr	6hr
Axial displace*ment*(*mm*)	0.24	1.05	0.75	1.53	0.91
Volume change (cm^3)	0.02	1.79	1.21	3.44	4.49

Table 5.5 Axial displacement and volume change (confining pressure 100kPa)

Stirring time (hours)	0hr	1hr	2hr	3hr	6hr
Axial displace*ment*(*mm*)	0.50	1.66	3.83	2.11	0.50
Volume change (cm^3)	4.19	11.7	11.3	8.94	4.19

5.5.5.2 Undrained triaxial compression tests

Undrained triaxial compression tests applying confining pressure of 30kPa with different stirring time are shown in Figure 5.19. The deformation behavior is brittle, when cement is directly added to clay (stirring time is 0hr) and the stress-strain curve is rattling, but when pre-stirring is carried out, the shear strength obviously decreases, the deformation becomes ductile and the stress-strain curve becomes smooth. Moreover, the phase transformation angle decreases with increasing of the stirring time. However, the

longer the stirring time is, the larger the peak intensity is. This is because the volume compression during the isotropic consolidation process is large and the density becomes larger.

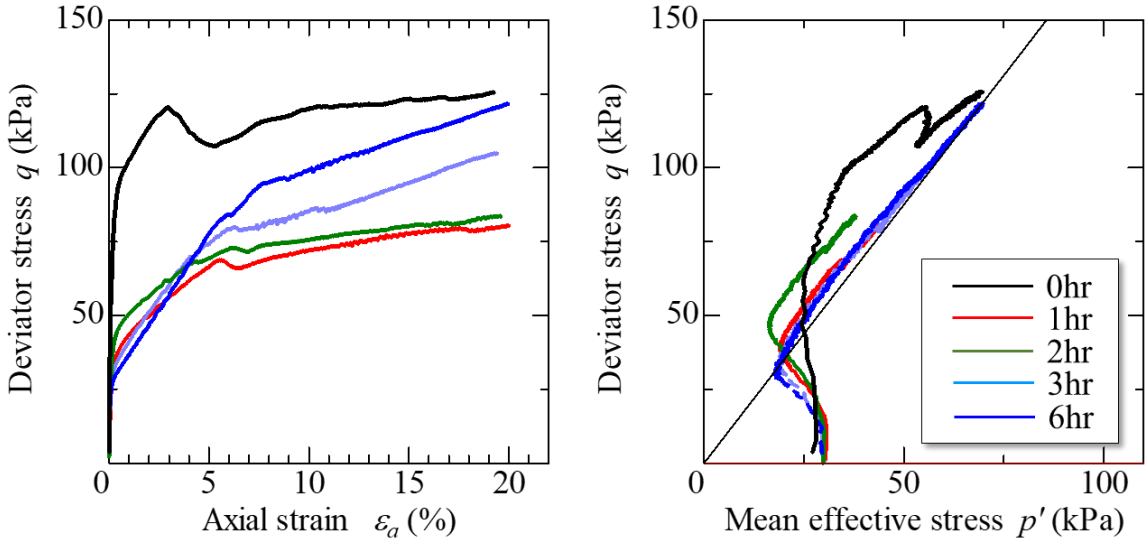

Fig. 5.19 Undrained triaxial compression tests

5.6 CALCIUM LEACHING

Previously, hydration reaction method was adopted during sample preparation and tried to reduce the expression strength. The softening behavior was not achieved properly, so, there was another approach that can be performed on specimens that have already been firmly bonded by adding cement, and attempt to reduce the binding force or increase the void ratio by calcium leaching using ammonium nitrate aqueous solution. Firstly, the background of the leaching with ammonium nitrate will be described with reference to previous studies.

5.6.1 PREVIOUS STUDIES

The immersion of cement paste and mortar in NaCl solution for a long time promotes leaching to reduce the amount of hydrate in the specimen and changes in tensile strength, elastic modulus, and fracture energy is shown [8]. Here, leaching is a phenomenon in which the amount of hydrate in hardened cement is reduced, which a phenomenon is observed in concrete structures in contact with fresh water. The leaching phenomenon is due to the dissolution of calcium ions in CH (calcium hydroxide) and CSH (calcium silicate hydrate) into an aqueous solution with a low concentration of calcium by concentration equilibrium near the surface of the cement and the aqueous solution. The relationship between immersion time and bending strength according to the bending test conducted by Miura et al. is shown in Figure 5.20 and it can be clearly observed that the bending strength decreases with the increase of the immersion time.

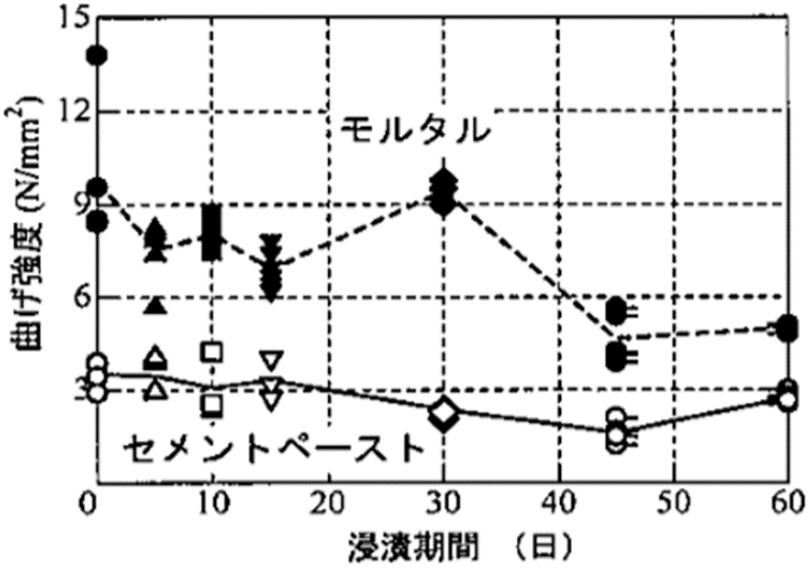

Fig. 5.20 Bending test result (Miura et al.2010)

An ion migration prediction model in cement was built, that takes into account the transformation of the cemented body accompanying Ca leaching, and for verifying the validity of the model, the leaching rate of Ca or the penetration of chloride ions and compared the predicted value and the experimental value of the quantity. The hardened cement was immersed in the leaching accelerator ammonium nitrate to leach out Ca. [9]. The reason is that ammonium nitrate can selectively dissolve Ca $(OH)^2$ and Ca, and there is little influence such as remaining amount in cement. The relationship between the distance from the hardened cement surface and the calcium leaching rate after 7 days of the above leaching. The Figure 5.21 also shows that the calculation results when immersed in water for 1700 days for comparison. From the Figure, it can be seen that the effect of soaking in ammonium nitrate is as effective as 1700 days in water. The study by [8] showed that cement paste and mortar showed strength reduction by Ca leaching, and the study by [9] showed that Ca leaching can be promoted by using ammonium nitrate.

In this section, an artificial viscous soil sample in which 5% of cement is added to Fujimori clay is immersed in an aqueous solution of ammonium nitrate to promote Ca leaching to try to reduce strength, increase the void ratio, and reproduce the strain softening phenomenon during shearing.

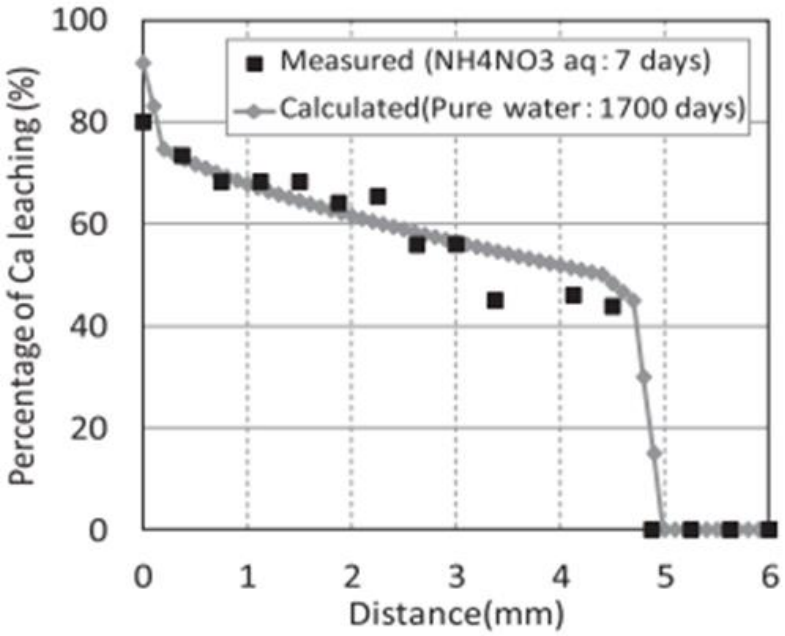

Fig. 5.21 Ca leaching progress (AOYAMA, T., et al.2012)

5.6.2 METHODOLOGY

The methodology from step 1 to 3 is same as in section 5.5.1 but after that just one step was performed,

1. After removing the specimen from the mold, immerse it in a 0.5 mol/L ammonium nitrate aqueous solution for one week. (By soaking for one week, the internal PH value becomes homogeneous and calcium leaching reaches the inside of the specimen.), as shown in Figure 5.22.

Various physical tests and mechanical tests were performed on the specimens thus prepared. The leaching phenomenon referred to here means that the calcium ions in CH (calcium hydroxide) and CSH (calcium silicate hydrate) generated during the hydration reaction of cement depend on the concentration equilibrium between the aqueous solution and the cement surface

Fig.5.22 Concentration and leaching status of ammonium nitrate (1 week immersion)

5.7 EXPERIMENTAL RESULTS AND DISCUSSION

A viscous soil specimen is prepared, and a physical test, a uniaxial test, a standard consolidation test, and an undrained triaxial test are performed as appropriate, and an attempt is made to grasp their mechanical characteristics. By addition of 5% of cement to specimen with different stirring time, 0, 1,2,3,6 hr. and immersed it in a 0.2, 0.5,1 mol/L ammonium nitrate aqueous solution.

5.7.1 PHYSICAL TEST

The results of physical tests with and without calcium leaching are shown in the Table 5.6. The natural water content is the water content at the time of specimen preparation, and the physical test was conducted after refining the specimen once prepared. Although the soil particle density is not changed by calcium leaching (here, the hydrated product is calculated as soil particles), the liquid limit is decreased. The characteristic is that the natural water content is increased by calcium leaching, and as a result, the specimen has very high water content with a liquidity index of 4.0 or more. In fact, the specimens that were self-supporting when turned by hand easily turned into slurry.

Table 5.6 Changes in physical properties due to Ca leaching

	Ca(Without leaching)	Ca(With Leaching)
Soil particle density ρ_s (g/cm^3)	2.77	2.76
Liquid Limit w_L (%)	53.2	42.8
Plastic Limit w_p (%)	30.2	30.8
Plasticity index I_p	23.0	12.0
Natural water content w_n (%)	70.4	80.6
Liquidity Index I_L	1.75	4.15

The particle size accumulation curve is shown in Figure 5.23 and it can be seen that the fine particles are reduced by Ca leaching.

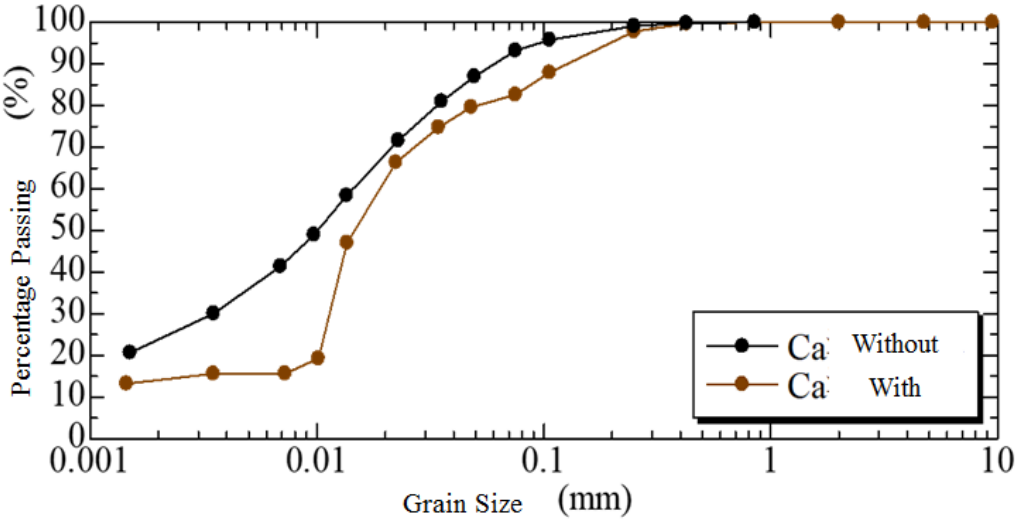

Fig. 5.23 Change in particle size due to Ca leaching

5.7.2 Uniaxial Compression Test

The uniaxial compression test results are shown in Figure 5.24. Here, the ammonium nitrate solution concentration is 0.2, 0.5 and 1.0 mol / l. It can be seen that uniaxial strength and initial stiffness are significantly reduced by calcium leaching. On the other hand, there is no difference due to the solution concentration. This indicates that, when immersed for a sufficient period of time, the degree of calcium leaching occurs to the same extent regardless of the solution concentration.

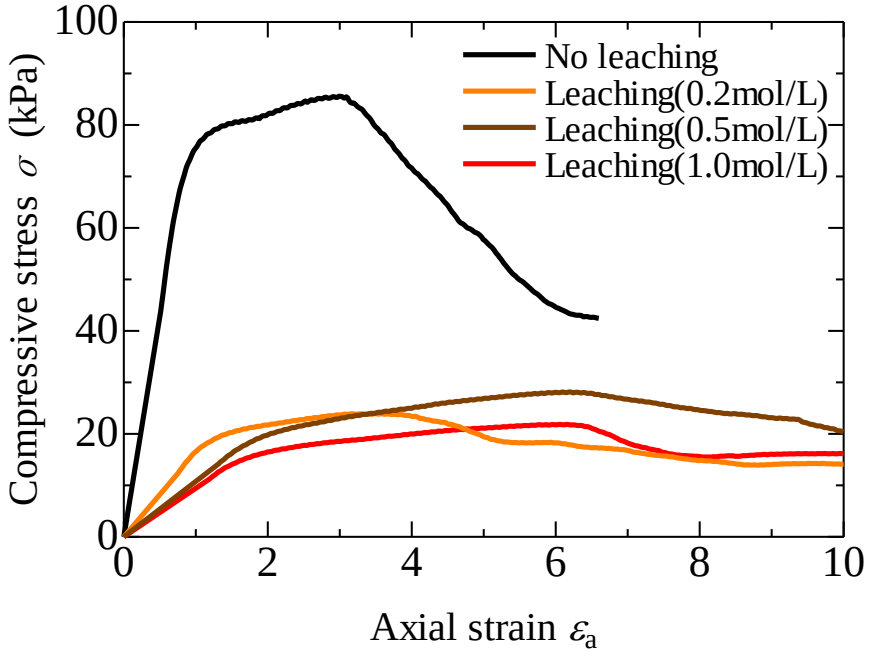

Fig. 5.24 Uniaxial compression test (calcium leaching)

5.7.3 Standard consolidation test

In the standard consolidation test, in addition to a slight increase in specific volume due to calcium leaching, it can be seen that the pre-consolidation pressure is reduced while maintaining high compressibility by adding cement. The Figure 5.25 also shows the standard consolidation test results of a wrought sample prepared by repeatedly kneading calcium-leached samples. The calcium leaching specimen is in a "bulky" state with a large specific volume under the same vertical stress as compared to the tempered sample, and gradually approaches the pulverized compression line as the vertical stress increases.

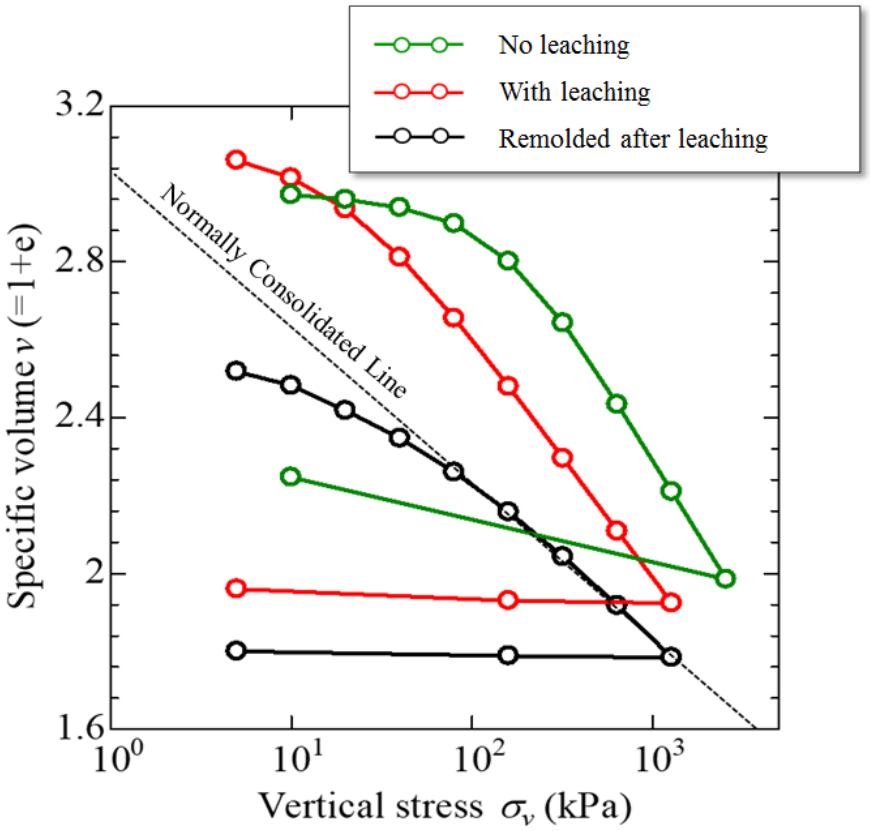

Fig. 5.25 Standard consolidation test

5.7.4 Undrained triaxial compression test

The results of undrained triaxial compression tests conducted at isotropic compaction pressures of 30 kPa and 100 kPa are shown in Figure 5.26. The presence or absence of calcium leaching is also shown. Without calcium leaching (just adding cement directly), the stress-strain curve rattles and shows brittle behavior, but with calcium leaching, draws a smooth curve. Looking at the state of deformation of the specimen during shearing, there is a crack / shear surface that penetrates the specimen longitudinally with axial strain of 3-5% when there is no leaching, but a barrel shape

when there is leaching. It was deformed to show ductile behavior. Looking at the effective stress path, the calcium leached specimen exhibited a slight but smooth softening behavior (decrease in axial differential stress accompanied by excess pore water pressure change).

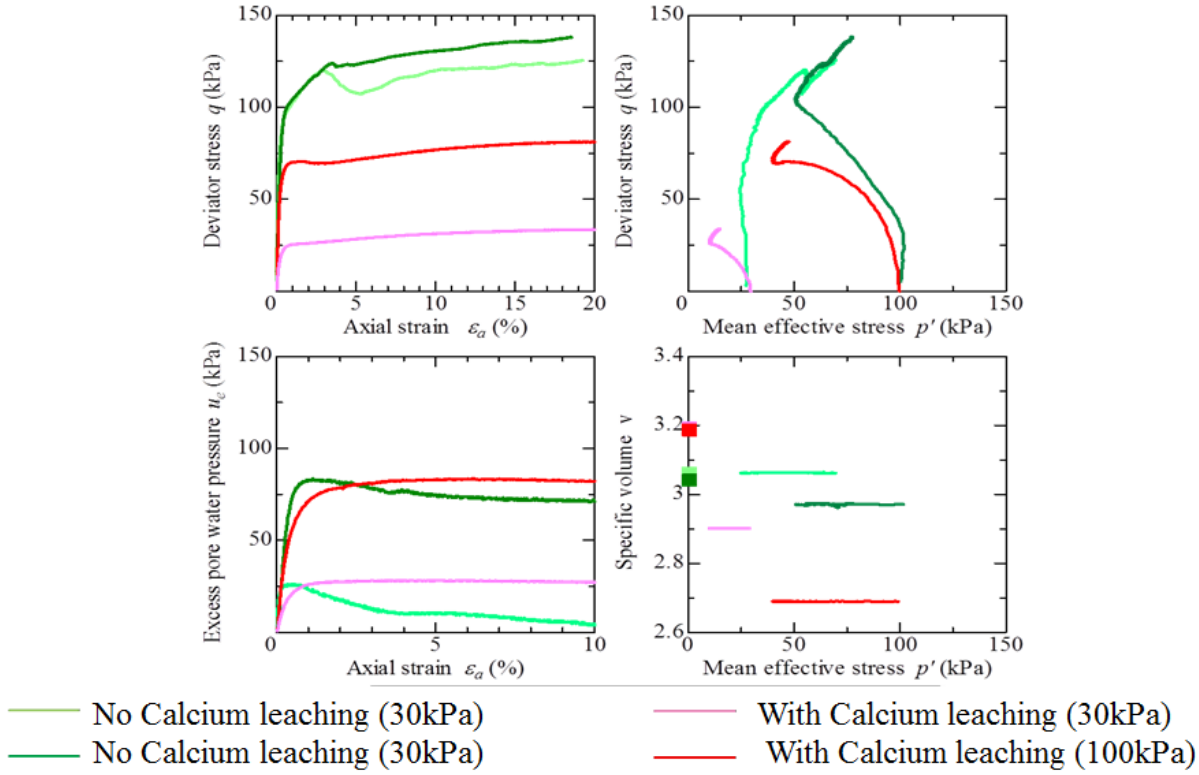

Fig. 5.26 Comparison of triaxial compression test (with and without calcium leaching)

5.8 CONCLUSION

In this chapter, attempted to artificially prepare specimens similar to natural sediment soft clay by adding hydration reaction controlled cement, specifically, by stirring cement and clay mixture for a while, the solidifying action of the hydrated product was destroyed and liquidity index maintains high value. The addition of cement makes it possible to reproduce the characteristics of naturally deposited soft clay to some extent, such as high sensitivity ratio and high compressibility ratio. When cement was added directly, the solidification effect was too strong to show brittle deformation, but by controlling the hydration reaction, it showed ductile behavior. However, it was not possible to reproduce the strain softening behavior which is one of the important characteristics of soft clay.

By using calcium leaching the behavior similar to that of naturally deposited soft

viscous soil was obtained and specimens exhibiting (1) High water content ratio with a high liquidity index, (2) High sensitivity, (3) Bulky behavior outside the normal consolidation line ("impossible region") of the crushed soil in compression behavior, and (4) Smooth stress in shearing behavior -Strain curve and (slight) softening behavior.

From now on, to reproduce the specimens closer to the natural soft clay by searching for the appropriate cement addition amount and stirring time. Moreover, calcium leaching is examined as a method of reducing the solidification action of cement. In future, use finer specimen for experiment like clay, to achieve more good results.

REFERENCES

1. Hirawasa, T., Source mechanism of the Niigata earthquake of June 16, 1964, as derived from body waves. Journal of Physics of the Earth, Vol.13, No.2, 1965, pp 35-66.

2. Wyss, M., and Brune, J. N., The Alaska earthquake of 28 March 1964: A complex multiple rupture. Bulletin of the Seismological Society of America, Vol. 57, No.5, 1967, pp 1017-1023.

3. Hiroshi, M., Estimation of post-earthquake settlement process of clay layer, Journal of Japan Society of Civil Engineers, No. 568 / III-39, 1997, pp 41-48. (Translated from Japanese, “粘土層の地震後沈下過程の推定”).

4. Tsuchida, T., Hirahara, T., Hiramoto, S., and Utaka, k., Shear properties of reconstituted marine clay reconsolidated with the addition of a small amount of cement, Japanese Geotechnical Engineering Journal, Vol.9, No.1, 2004, pp 71-84 (Translated from Japanese, “**少量のセメントを添加し再圧密した再構成海成粘土のせん断特性**”).

5. Ayaka, F., Experimental study on mechanical characteristics of cement- treated clayey soil with high water content. Undergraduate thesis, Nagoya University, Japan, 2015.

6. Ayaka, F., Modeling of mechanical characteristics of cement- treated clayey soil considering cyclic loading characteristics. Master thesis, Nagoya University, Japan, 2017.

7. Inagaki, M., Nakano, M., Noda, T., Tashiro, M., and Asaoka, A., Proposal of a simple method for assessing the susceptibility of naturally deposited clay grounds to

large long-term settlement due to embankment loading, Soils and Foundations, Vol. 50, Vol. 1, 2010, pp 109-122.

8. Yasuto, M., and Yasuhiko, S., Cement paste and mortar immersed in NaCl solution Evaluation of tensile softening properties of concrete, Proceedings of Concrete Engineering, Vol. 21, No.3, 2010, pp 77-86.

9. Aoyama, T., Kurumisawa, K., Nawa, T., and Murakami, Y., Cement hardened material considering calcium leaching Construction of movement prediction model, Cement and concrete papers, Vol.66, No. 1, 2012, pp 311-318.

10. Nakai, K., Khan, I., and Noda, T., Experimental attempt to produce soft clayey specimen by leaching of calcium followed by cement solidification, proceeding of 54th Japan National Conference on Geotechnical Engineering, 2019.

11. Khan, I., Nakai, K., and Noda, T., Experimental attempt to produce soft clayey specimen by adding hydration reaction controlled cement, proceeding of 54th Japan National Conference on Geotechnical Engineering, 2019.

Chapter 6

CONCLUSIONS AND DISCUSSIONS

The conclusions obtained in this research are listed below;

In the chapter 2, to understand the undrained cyclic shear behavior of clayey soil under a drastically changed loading rate is discussed. The loading rate was changed drastically from 1.0Hz to 0.0042Hz by stress control, and 0.01%/min by strain control which was considered to be low enough that pore water migration occurs sufficiently during shearing. Since clay material has low permeability, there is a difference in excess pore water pressure migration depending on the loading rate. Especially when the loading rate is high, the pore water does not migrate sufficiently during cyclic loading and the excess pore water pressure distribution inside the specimen becomes non-uniform. Moreover, observation of the uniformity process of excess pore water pressure after cyclic loading, and a re-compression test after cyclic loading were also conducted. The following conclusion were drawn from the experimental results.

(1) The degree of strain evolution varied depending on the loading rate. Because undrained shear strength is often evaluated by the number of cycles to reach a given DA (double amplitude), this experimental fact indicates that the undrained shear strength also varies depending on the cyclic loading rate. The lower the loading rate is, the weaker the strength becomes.

(2) In the triaxial test apparatus, mean effective stress *p*' is calculated using the excess pore pressure measured at the lower end of the specimen as a representative value. When the cyclic loading rate is high, the pore water does not migrate sufficiently and the distribution of the excess pore water pressure inside the specimen becomes non-uniform (the measured value of the excess pore water pressure becomes small). Therefore, the (apparent) effective stress path varies depending on the loading rate. When the loading rate is high, the effective stress path hardly decreases during the cyclic loading.

(3) During the uniformity process after cyclic loading, the measured value of excess pore water pressure at the end of the specimen increased (mean effective stress decrease). Higher the cyclic loading rates generated, greater excess pore water pressure. However, the final values of excess pore water pressure after the homogenization process was the same regardless of loading rate or slightly larger if the loading rate was lower. This means that if sufficient time is left after cyclic loading, the final mean effective stress value becomes equal regardless of the loading rate.

(4) Slopes of compression lines after cyclic loading were equal regardless of the cyclic loading rate and this value was smaller than the compression index C_c, and equal to or slightly larger than the swelling index C_s. This means that the amount of compression after cyclic loading would be determined based on the swelling index. However, there might be a risk of underestimating the amount of compression unless the decrease in p' due to uniformity process of excess pore water pressure is taken into account.

(5) There are various types of external cyclic forces, such as earthquake motion, coastal waves, and traffic loads, which are actual problems. These all have different loading cycles from rapid loading to slow loading. Since the cyclic shear strength varies depending on the loading rate, it is important to conduct experiments using a suitable loading rate compared with the target problem. In other words, it is important to treat as an initial boundary value problem. In the development of a constitutive equation, it is important to grasp the element characteristics of the material accurately. Therefore, it is important to obtain experimental results at the lowest possible loading rate so that the internal state of the specimen can be treated as homogeneous and uniform. In this chapter reconstructed samples were used, but experiments using undisturbed samples from the naturally deposited condition will be conducted in the future to understand the effects of soil skeletal structure and its disturbance.

In the chapter 3, triaxial tests were carried out using the vertical and the horizontal extraction specimen of the reconstituted clay and silty clay, for accumulating experimental facts of development of anisotropy during the preliminary consolidation process and the influence of the anisotropy on the shear behavior. Pre-consolidation pressure of 200kPa applied to induced initial anisotropy. Undrained shear triaxial test was performed with different isotropic stresses on clay (50 to 1800kPa) and silty clay (50,300 and 600kPa), and undrained shearing was carried out under constant axial strain rate of 0.0056(mm/min) for clay (2 days) and 0.0112(mm/min) for silty clay (6hrs.). Moreover, the comparison of clayey and silty clay and how the grain size affects the development/diminishing of anisotropy are discussed. The following conclusion were drawn from the experimental results.

(1) From a series of experimental results, it is concluded that anisotropy developed in the preliminary consolidation process, and anisotropy disappears due to isotropic consolidation. Nevertheless, it does not completely disappear even under high confining pressure i.e. 1800kPa, especially in case of clay. However, if we compare clay and silty clay soil, silty clay materials lose their anisotropy at lower confining

pressure i.e. 600kPa, as compared to clay materials. Therefore, the grain sizes have significant effect on the developing and diminishing of anisotropy.

(2) Another important fact observed was that critical state index (slope of critical state line) is decreasing and become constant as confining pressure increases. Moreover, modified Cam clay model can considered being more suitable to use as compared to the original Cam clay model in order to represent the work of anisotropy.

(3) Further experiment will be performed to observe the effect of cyclic shear test to evaluate the development/diminishing of anisotropy. Moreover, based on experimental facts, constitutive model will be validated and add some improvement if necessary.

In the chapter 4, the influence of the disturbance of soft clay due to cyclic loading is grasped from undrained triaxial compression tests and importance/implication of soil skeleton structure is discussed. In the past, according to the results of laboratory experiments, it has been found that destabilization such as liquefaction phenomenon does not occur in clayey soil because clayey soil maintains relatively high rigidity and strength even after cyclic loading. It is common that the soil was in the state of "high water content", "high sensitivity", and "soft" where the earthquake damage occurred. The difference between a natural deposited sample and a reconstituted sample is considered to be the degree of development of "soil skeleton structure" that develops over a long period of deposition process over several tens of thousands of years. The following conclusion were drawn from the experimental results.

(1) In this chapter, in the monotonic undrained triaxial test, the strain softening behavior was observed, which is a typical feature of the naturally deposited soft clay.

(2) By applying cyclic loading with strain control, it was possible to give multiple cyclic loading without causing localized deformation of the specimen as compared to stress control which showed the necking failure of the specimen.

(3) It is clearly observed, that with the increase of the cyclic loading history, (1) the initial stiffness smaller, (2) the undrained shear strength decreases, and (3) the degree of strain softening decreases.

(4) It was observed in that in undrained shear isotropic test, as the confining pressure increases, the degree of over consolidation decreases and approaches the normally

consolidated state, but the degree of structure hardly changes, because it has the characteristic that it is difficult to decay by isotropic stress.

(5) The stiffness decreases as the cyclic history increases, and the behavior in which the effective stress decreases can be reproduced. Here, when focusing on the degree of the structure and the degree of over consolidation, it can be seen that the degree of the structure decreases and the degree of over consolidation increases as the cyclic loading history increases. In other words, it can be understood that the degradation of structure and accumulation of over consolidation occur during the cyclic loading.

In the chapter 5, the influence on mechanical properties, when hydration reaction controlled cement is added to clayey soil and also describe the results of examining the influence of calcium leaching on the mechanical properties of cemented cohesive soil will be discussed. By using the remolded sample, and the necessity to reduce the solidification effect, a newly attempted method was introduced “addition of hydration reaction controlled cement” and “calcium leaching”, in order to artificially produce the soil sample having similar characteristics to those of naturally deposited soft clay. Various tests were conducted to achieve the required results. The following conclusion were drawn from the experimental results.

(1) An attempted to artificially prepare specimens similar to natural sediment soft clay by adding hydration reaction controlled cement, specifically, by stirring cement and clay mixture for a while, the solidifying action of the hydrated product was destroyed and liquidity index maintains high value. The addition of cement makes it possible to reproduce the characteristics of naturally deposited soft clay to some extent, such as high sensitivity ratio and high compressibility ratio. When cement was added directly, the solidification effect was too strong to show brittle deformation, but by controlling the hydration reaction, it showed ductile behavior. However, it was not possible to reproduce the strain softening behavior which is one of the important characteristics of soft clay.

(2) When cement is added directly to a clay sample, the solidification effect is too strong and brittle deformation occurs, but the following behavior similar to that of naturally deposited soft viscous soil is obtained by “calcium is leaching” of the cement solidified specimen. It became possible to artificially manufacture specimens exhibiting (1) High water content ratio with a high liquidity index, (2) High sensitivity, (3) Bulky behavior outside the normal consolidation line

("impossible region") of the crushed soil in compression behavior, and (4) Smooth stress in shearing behavior -Strain curve and (slight) softening behavior.

(3) From now on, to reproduce the specimens closer to the natural soft clay by searching for the appropriate cement addition amount and stirring time. Moreover, calcium leaching is examined as a method of reducing the solidification action of cement. In future, use finer specimen for experiment like clay, to achieve more good results.

Appendix 1

A 1.1 INTRODUCTION

This section provides an introduction to the triaxial test, explaining why the test is performed, the stress state of a tested soil, required test system components, and the general procedure for running a triaxial test. It assumes a basic knowledge of soil mechanics for those readers unfamiliar with some terms in this section.

A1.2 WHY TO CONDUCT A TRIAXIAL TEST?

The triaxial test is one of the most versatile and widely performed geotechnical laboratory tests, allowing the shear strength and stiffness of soil and rock to be determined for use in geotechnical design. Advantages over simpler procedures, such as the direct shear test, include the ability to control specimen drainage and take measurements of pore water pressures. Primary parameters obtained from the test may include the angle of shearing resistance ϕ', cohesion c', and undrained shear strength cu, although other parameters such as the shear stiffness G, compression index Cc, and permeability k may also be determined. Figure A1.1 gives an example of the engineering application of the test; here triaxial compression provides strength information at the top of a cut slope, whilst triaxial extension allows parameters for soil elements at the slope base to be determined.

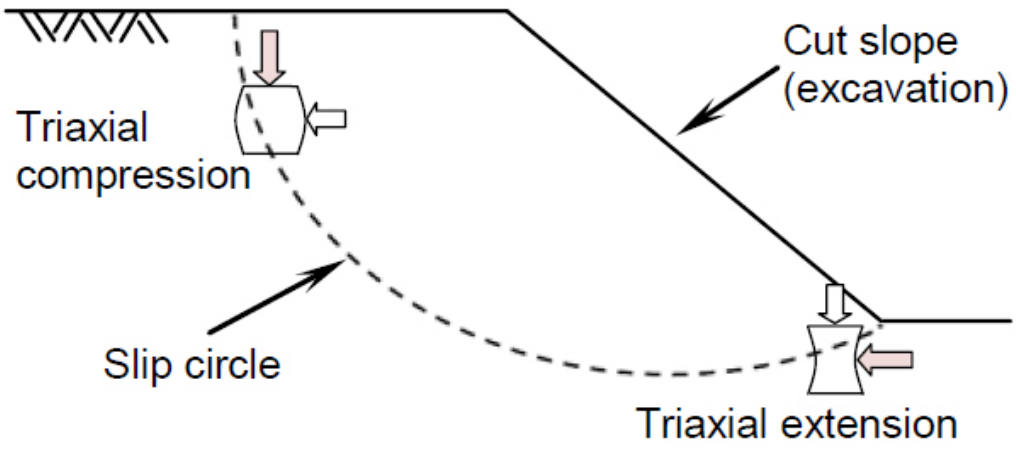

Fig. A.1.1 Example of an engineering application of the triaxial test.

A1.3 WHAT DOES A TRIAXIAL TEST INVOLVE?

The triaxial test typically involves placing a cylindrical specimen of soil, ranging from 35mm to 100mm diameter, into a cell that can be pressurized. The standard height of the specimen shall be 1.5 to 2.5 times the diameter or most specimens have an approximate 2:1 height-to-diameter ratio, and are sealed within a rubber membrane. Following this initial preparation the specimen is saturated, consolidated, and sheared, allowing the soil response to be observed under conditions that may approximate those in-situ. During the shear stage the soil is loaded axially, either in compression, or less-commonly in extension. The general set-up of a triaxial specimen inside a triaxial cell is shown in Figure A.1.2.

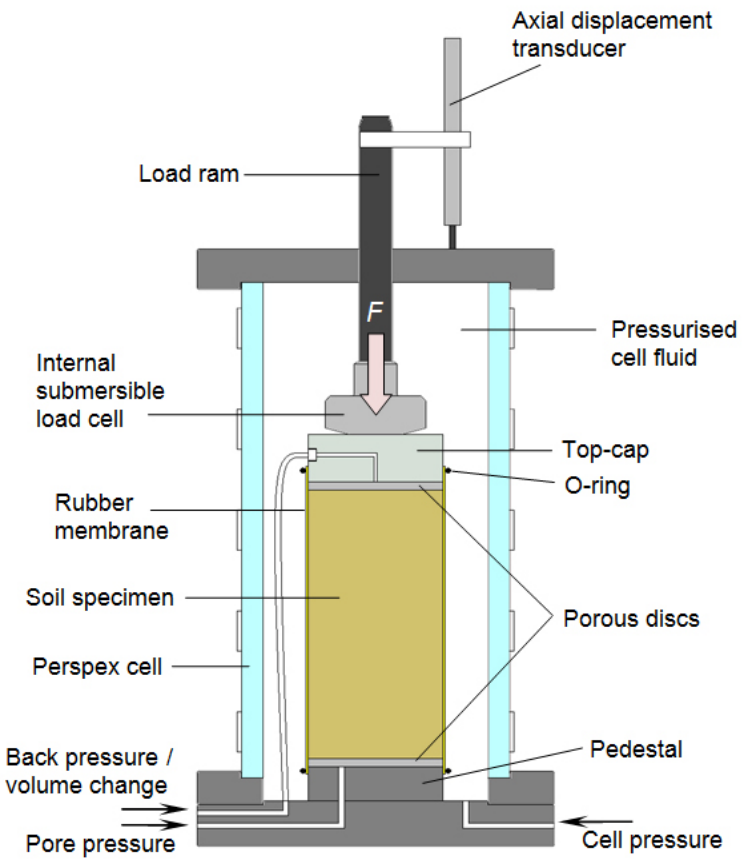

Fig. A.1.2 Schematic diagram of general Set-up of a soil specimen inside a triaxial cell.

A 1.4 WHAT ARE THE TYPES OF TRIAXIAL TEST?

There are three primary triaxial tests conducted in the laboratory, each allowing the soil response for differing engineering applications to be observed. These are:

- Unconsolidated Undrained test (UU)
- Consolidated Undrained test (CU)
- Consolidated Drained test (CD)

The unconsolidated undrained (UU) test is the simplest and fastest procedure, with soil specimens loaded whilst only total stresses are controlled and recorded. This allows the undrained shear strength "*cu*" to be determined, which is suitable for assessing soil stability in the short-term (e.g. during or directly following a construction project). This test is generally performed on cohesive soil specimens.

The consolidated drained (CD) test on the other hand is applicable to describing long-term loading response, providing strength parameters determined under effective stress control (i.e. ϕ' and c'). The test can however take a significant time to complete when using cohesive soil, given the shear rate must be slow enough to allow negligible pore water pressure changes.

Finally the consolidated undrained (CU) test is the most common triaxial procedure, as it allows strength parameters to be determined based on the effective stresses (i.e. ϕ' and c') whilst permitting a faster rate of shearing compared with the CD test. This is achieved by recording the excess pore pressure change within the specimen as shearing takes place.

A 1.5 STRESS STATE DURING A TRIAXIAL TEST

The stresses applied to a soil or rock specimen when running a triaxial compression test are displayed in Figure A.1.3. The confining stress σc is applied by pressurizing the cell fluid surrounding the specimen and it is equal to the radial stress σr, or minor principal stress $\sigma 3$. The deviator stress q is generated by applying an axial strain εa to the soil. The deviator stress acts in addition to the confining stress in the axial direction, with these combined stresses equal to the axial stress σa, or major principal stress $\sigma 1$. The stress state is said to be isotropic when $\sigma 1 = \sigma 3$, and anisotropic when $\sigma 1 \neq \sigma 3$.

Important point is that, in case of extension test, the principal stress directions rotate by 90° and in such a case the radial stress corresponds to the major principal stress direction, with the axial stress providing the minor principal stress.

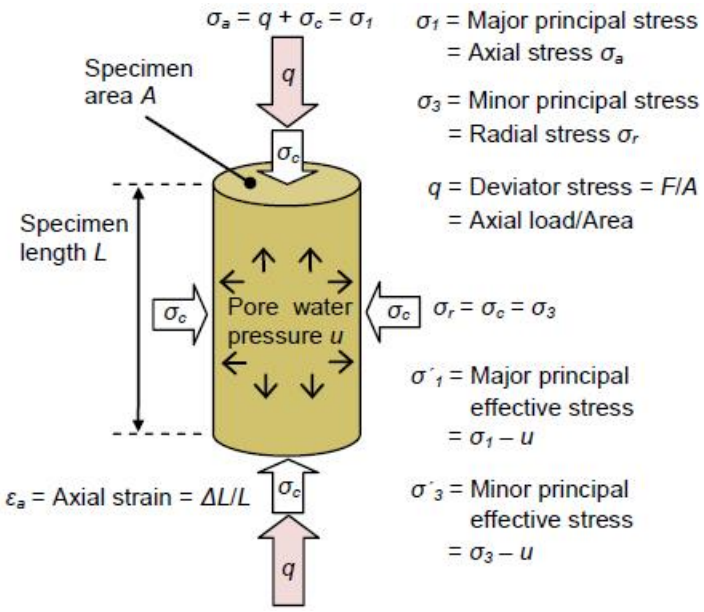

Fig.A.1.4 Specimen stress state during triaxial compression.

A 1.6 GENERAL TRIAXIAL TEST PROCEDURE

As briefly mentioned in the Introduction section of this appendix 1, the triaxial test as described by geotechnical test standards (JGS 0520, 0521, 0522, 0524, 0541:2009 and BS 1377: Part 8: 1990) typically consists of four main stages: specimen and system preparation, saturation, consolidation, and shearing. General outlines of how the experiment performed during this research and each stage are discussed below;

A1.6.1 System check (must be performed before the experiment)

1.) The gauge for the regulator must be maintained at 9MPa.
2.) Water tank must have water and vacuumed for 24hrs.
3.) Initialization must be performed for the areas where water will flow.
    a. Back pressure and Excess pore water pressure transducer/sensor (make sure voltage amplifier is set to zero)
    b. Top cap hole check for saturation (Figure A 1.5)
    c. Base hole check for saturation (Figure A 1.6)
    d. Cell pressure hole (after sample preparation)
    e. Cell pressure transducer/sensor (after sample preparation)

The triaxial used for the experiment is shown in Figure A 1.7 below;

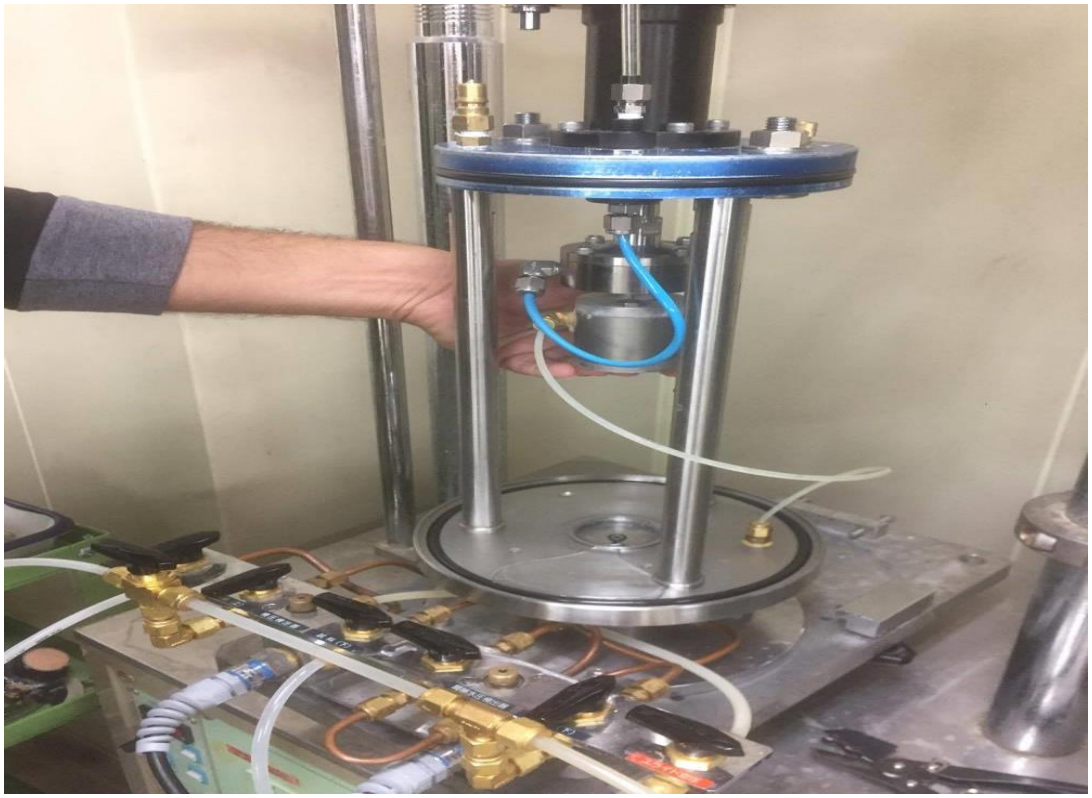

Fig A 1.5 Top cap hole check for saturation

Fig A 1.6 Base hole check for saturation

A 1.7 Triaxial used for the experiment

A 1.6.2 Steps in initialization

Water needs to flow so the step for A.1.6.1 (3) is the same. The difference is the switch that needs to be opened)

1. Open the screw for the Back pressure and Excess pore water pressure transducer/sensor.
2. Let water flow out the Top cap hole (for saturation) and Base hole (for saturation). The initial configuration of the switches connected to the burette is towards the left or towards the cyclic triaxial base. Change the direction towards the burette so that water can be added to the burette.
3. Make sure that the switch for the backpressure is directed towards the positive line not the negative line. Change the direction of the switch towards the negative line only when a negative pressure is being applied to the sample. This instance is performed to let the sandy material stand on its own when the triaxial cell is being placed.

4. Once water is stored inside the burette, change the direction of the switches towards the left or towards the cyclic triaxial base.
5. Open the switch.

A.1.6.3 Adding distilled water to the tank

1. Make sure to use distilled water.
2. Open vacuum so that water can flow into the tank. (Apply maximum pressure)
3. Place the tube connected at the “add water tank” line in the schematic diagram inside the pan where the distilled water is placed.
4. Open the switch at the “add water tank” line and the switch connected at the tank.
5. Vacuum for 24 hrs to de-air the distilled water.
6. To check if the distilled water is completely de-aired tap the container with a tamper. If no bubbles are seen then de-airing is a success as shown in Figure A 1.8

Fig. A1.8 Checking if the distilled water is completely de-aired or not

A 1.6.4 Specimen and System Preparation

The test specimen itself must firstly be prepared from a sample of soil before placing into the triaxial cell. For cohesive soils this may involve trimming undisturbed specimens extruded from Shelby tubes or cut from block samples, whilst for granular soils the specimen may require preparation directly on the pedestal using a split-part

mould. In the case of cohesive specimens such as that shown in Figure A.1.9, a membrane suction stretcher can be used to place the rubber membrane around the soil once in position on the pedestal. It is very important, that disturbance to the specimen should be kept to a minimum during preparation.

Fig. A 1.9 Trimmed cohesive specimen (left); membrane suction stretcher (middle); spilt-part mould for granular specimen preparation (right).

Following placement of the specimen, the triaxial cell and other system components are assembled. During this stage the cell is filled with fluid, pressure / volume controllers connected, and transducer readings set as required. Detailed procedure is listed below;

1. Measure the diameter, height and weight of the specimen Place the membrane on the base. The Performa used for that is shown in Figure A 1.10
2. Seal it with 2 O-rings.
3. Use the split mold to expand the membrane.
4. At the top part of the split mold, the 2 O-rings for the top cap should be placed first. Then, attach the membrane to the split mold.
5. Install the tubes for the vacuum to completely stretch the membrane.
6. Open the vacuum.
7. Place filter paper at the bottom.
8. Place the accessories that prevent the spillage of the sample for the sample preparation.
9. Place the sample by pluviation.
10. Tamp the sides of the split mold in order to densify the sample.
11. Flush water (This step is similar to C)

12. Once water reached the top of the sample, stop flushing the water.
13. Scrape the excess sample with a spatula.
14. Place filter paper at the top part.
15. Attach the sample to the top cap and seal it with 2 O-rings.
16. Make sure to adjust the setting of the axial load so that the sample can fit the cell.
17. Apply a 10kPa negative pressure/vacuum so that the sample will stand. Change the switch of the backpressure towards the negative line.
18. Remove split mold.
19. Place the triaxial cell and connect all the necessary transducers to the cell such as the cell pressure and load cell. Furthermore, open the screw located at the top part of the triaxial cell so that air pressure will not be stored when the triaxial cell is placed.
20. Make sure that it is completely sealed.
21. Initialize the cell pressure transducer.
22. Connect the water line to the water supply.
23. Turn on the switch for the water line that is connected to the line of the triaxial cell.
24. Fill the triaxial cell with water until the bottom part of the load cell. Close the crew located at the top part of the triaxial cell once the water reaches the bottom part of the load cell. Make sure to connect the piston to the triaxial cell. Adjust the jack with the use of the voltage amplifier. Rotate the “Zero knob” in a clockwise direction to lower down the jack. Lock the jack so that it will not move during the shearing part as shown in Figure A 1.11
25. Since there is already water inside the cell the sample can now stand with the use of the cell pressure and because of this, the negative pressure can now be removed. Apply a 10kPa cell pressure first before removing or changing the negative pressure to zero.

	diameter (cm)	height (cm)	thickness (cm)	dummy's height (cm)	dummy's indirect height (cm)
	3.533				
	3.535				
	3.534				
	3.542	8.065	0.057	10.001	2.701
	3.512	8.008	0.057	10.000	2.717
	3.535	7.976	0.058	10.002	2.708
average	3.532	8.016	0.057	10.001	2.709

	name	A	B	C	
	petri dish **mc**	32.22	33.27	32.59	
	petri dish+sample **ma**	50.44	49.02	56.21	
	petri dish+dried sample **mb**	45.88	45.09	50.31	
	water content rario **w**	33.382138	33.2487	33.29571106	average

Fig. A 1.10 Performa sheet for calculating specimen detail

Fig. A 1.11 Specimen in Triaxial cell with Cell pressure 10kPa

A 1.6.5 Saturation

The saturation process is designed to ensure all voids within the test specimen are filled with water, and that the pore pressure transducer and drainage lines are properly de-aired. To check the degree of specimen saturation is sufficiently high before moving to the consolidation stage, a short test is performed to determine Skempton's B-value. This is called a B-check, and requires specimen drainage to be closed whilst the cell pressure is raised by suitable value. However that B is soil-dependent, so whilst normally consolidated soft clay will produce $B \approx 1.00$ at full saturation, a very dense sand or stiff clay may only show $B \approx 0.91$, even if full saturation has been reached. The saturation (B-Values) of each samples were confirmed to be 0.96 or higher in this research and in order to get that following step were followed;

1. Cell pressure must be larger than back pressure by 10kPa (sand/coarse soil) and 20kPa (clay) as shown in Figure A 1.12
2. Always check the units of the gauge and the program and read the volume change. A negative value means water is being added while a positive value means water is being squeezed out.
3. Open the switch for the top cap hole and base hole to read the volume of water.
4. Read the B value to check saturation. (See JGS 0541-2009 Section 5.2.a).
   (a) "Close all the switches at the triaxial base except the switch for the back pressure transducer. It will now serve as the line that will read the change in pore water pressure". Do this for 1 minute."

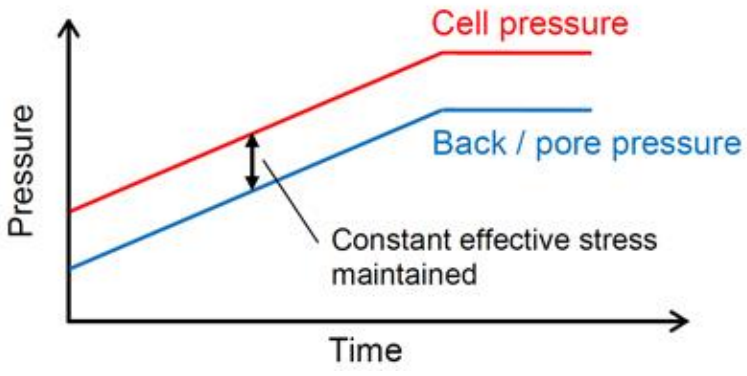

Fig. A 1.12 Specimen saturation by increasing back pressure

	before	after	restraint pressure(kPa)	
side pressure(kgf)	210.938	500.976	300.3	
back pressure(kgf)	200.684	480.460		OK
B value (%)	96.46			

Fig A 1.13 B Value of specimen used in the experiment (Above 0.96)

A 1.6.6 Consolidation

The consolidation stage is used to bring the specimen to the effective stress state required for shearing. It is typically conducted by increasing the cell pressure whilst maintaining a constant back pressure (often equal to the pore pressure reached during the final saturation B-check), as shown in Figure A 1.14. This process is continued until the volume change ΔV of the specimen is no longer significant, and at least 95% of the excess pore pressure has dissipated. The consolidation response can also be used to estimate a suitable rate of strain when shearing cohesive specimens. Fowling procedure were followed while doing consolidation for current research;

1. Open the switch for the top cap hole and base hole to read the volume of water.
2. Do not change the value of the back pressure.
3. Increase the value of the cell pressure to the desired value of the confining pressure.

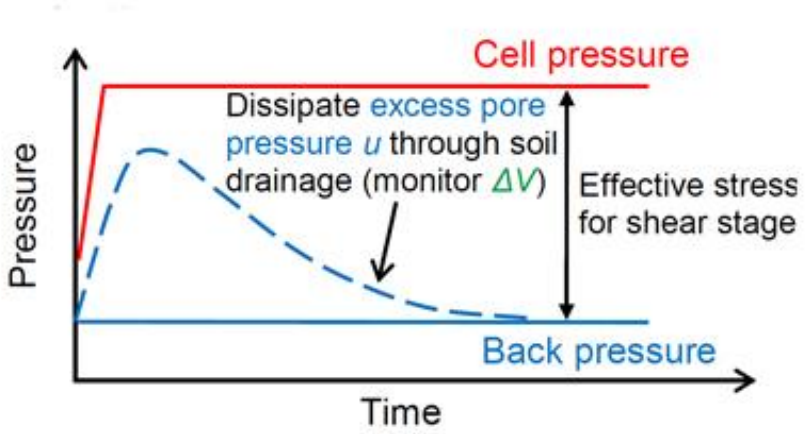

Fig A1.14 Consolidation of test specimen.

Fig. A 1.15 After Consolidation

A 1.6.7 Shearing

The soil is sheared by applying an axial strain εa to the test specimen at a constant rate through upward (compression) or downward (extension) movement of the load frame platen. This rate, along with the specimen drainage condition, is dependent on the type of triaxial test being performed

Table A.1 summarizes the conditions for each test type (*note a constant confining pressure is maintained for each).

Table A .1 Summary of test conditions during shear stage

Test type	Rate of axial strain	Drainage
UU	Typically fastest, reaching failure criterion in 5 – 15 minutes	Closed, no excess pore pressure measurement
CU	Slow enough to allow adequate equalization of excess pore pressures	Closed, record excess pore pressure
CD	Slow enough to result in negligible pore pressure variation	Open, record ΔV & maintain constant back pressure

Specimen response during the shear stage is typically monitored by plotting the deviator stress *q* or effective principal stress ratio *σ′1/σ′3* against the axial strain *εa*. The stage is continued until a specified failure criterion has been reached, which may include identification of the peak deviator stress or peak effective principal stress ratio, observation of constant stress and excess pore pressure / volume change values, or simply a specific value of axial strain being reached (for example *εa* = 20%). Generalised response for normally-consolidated clay is presented in Figure A 1.16, including the excess pore pressure generated during a CU test, and observed specimen volume change during a CD test. The Figure also displays a cohesive specimen after completion of the shear stage, with the plane of failure highlighted (i.e. the plane in which the majority of shear strain occurs).

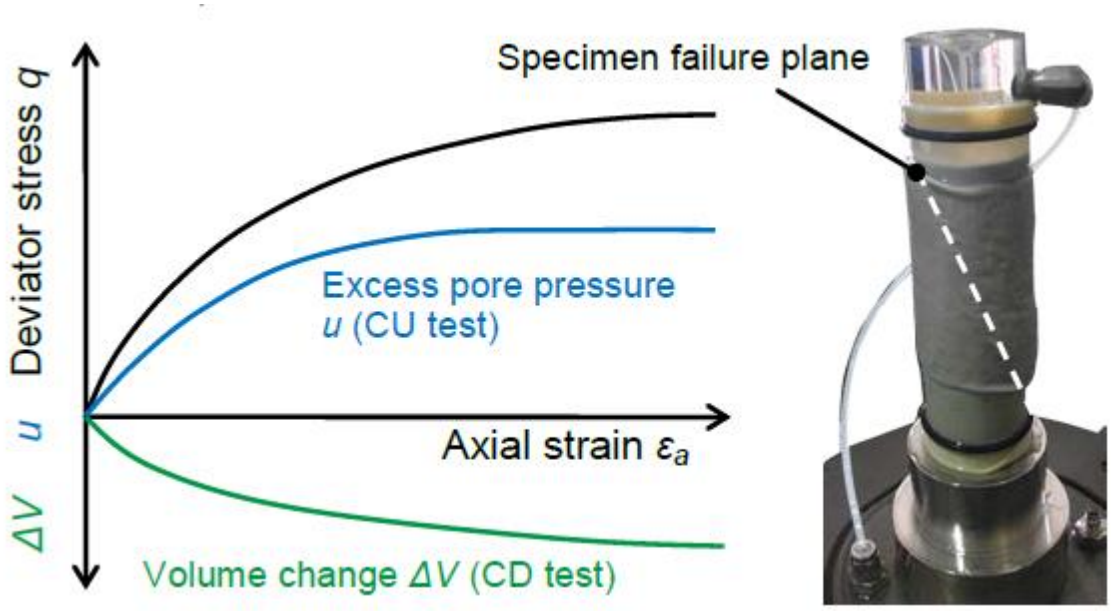

Fig. A 1.16 Generalized specimen response during shear for a normally-consolidated clay (left); cohesive specimen post-shear showing failure plane (right).

Fowling procedure were followed while doing consolidation for current research;

1. Initialize LVDT.
2. Turn on the switch for the loading frame.
3. The undrained shearing was carried out under constant axial strain rate of 0.0056(mm/min) for clay (2 days) and 0.0112(mm/min) for silty clay (6hrs.).

Fig. A 1.15 After Shear

Appendix 2

Superloading/Subloading Yield Surface (SYS) Cam-clay Model

A2.1 INTRODUCTION

In what will always be remembered as an outstanding achievement, the Critical State Soil Mechanics approach (Roscoe et al., 1958, 1963) established some 55 years ago by the Soil Mechanics Group at the University of Cambridge was the first in the world to propose an elastoplastic constitutive equation, the Cam-clay model, capable of integrating both the shear and volume change behaviors of soils. And it is still widely used by many researchers. As the opening, the essences of Cam-clay model will be briefly described in the following, to view the scope of its application.

The essences of Cam-clay model are:

1) Hardening accompanying plastic compression;
2) Softening accompanying plastic expansion;
3) Watershed between hardening and softening (or plastic compression and plastic expansion) denoted by the critical state line $q = \mathrm{M}p'$ in the effective stress space (q - p' space).

In addition, the slope of critical state line (CSL) M is always constant. The fact that the Cam-clay model has rarely been used for analyses of softening/expansion has to do with the limited capabilities of electronic computational technology at that time, and does not reflect any limitations in the model itself. As mentioned above, Cam-clay model is established based on the fully remolded and normally consolidated soil. In other words, it cannot describe the behaviors of

1) Dense sand or overconsolidated clay that behaves hardening accompanying plastic expansion above the CSL;
2) Loose sand or structured clay that behaves softening accompanying plastic compression below the CSL under undrained triaxial tests.

However, we cannot deny the application of Cam-clay model or doubt its validity. Such limitation comes from the fully remolded and normally consolidated soil. If two corresponding concepts, structure and overconsolidation are introduced into Cam-clay model to be the state variables such as plastic volumetric strain, the limitation can be overcome perfectly. Two new yield surfaces, Superloading yield surface and Subloading yield surface, are proposed to represent the concepts of structure and overconsolidation and defined with similar shape as the normal yield surface (plastic potential surface) of

Cam-clay model. During the introduction of structure and overconsolidation, Cam-clay model is still the fundamental theory of soil mechanics and it is a natural but significant progress to deal with the naturally sedimentary soils.
In addition, the state of structure or overconsolidation that is similar to the density or void ratio can be regarded as the mechanical state and varies depending on the loading and unloading. Therefore, based on the Superloading yield surface and Subloading yield surface it is important to clarify that

1) the decrease of overconsolidation
2) and the decay/collapse of structure of sand or naturally sedimentary clay

are persistently developing as the plastic strain progresses. For this reason, the slope of the watershed between softening and hardening could be larger or smaller than the watershed between plastic compression and plastic expansion, which is able to describe not only hardening accompanying plastic compression and softening accompanying plastic expansion but also hardening accompanying plastic expansion and softening accompanying plastic compression.

As for overconsolidation, it is easy to be interpreted by comparing the current loading state with the most severe loading state in the past, while the structure can be represented by the bulky degree of soil, that is how much bulk a certain soil occupies, and it will be illustrated in detail from A2.3. Generally speaking, compared with the soil without structure, the structured soil can sustain a higher load if the void ratio is same or the structured soil can possess larger void ratio if the load is same. There would be no point in pursuing more intuitive interpretations of these terms “overconsolidation” and “soil skeleton structure,” by defining them physically from such visually determined characteristics as the size and configuration of soil particles. We have no need of intuitive definitions at the micro level. What is needed is a mechanical description of overconsolidation and soil structure “at work,” or “in action.” Nothing else matters for soil mechanics as a species of continuum mechanics. For example, we need to understand loss of overconsolidation as acting in the direction of expansion, and decay/collapse of structure as acting in the direction of compression. The introduction of Super/Subloading yield surfaces serves to make mechanical responses of these kinds describable.

The contents mentioned above will be referred sequentially from A2.2 to A2.4. In A2.2, original Cam-clay model is described employing infinitesimal deformation theory, which is for the sake of easy understanding. In A2.4, the formula of Cam-clay model considering the Superloading/Subloading yield surfaces is deduced in the framework of finite deformation theory in which the objectivity of constitutive model is taken into consideration. Moreover, the anisotropy of soil skeleton will be presented at the same time.

The difference between clay and sand will be explained in A2.5. Typical sand is assumed to lose its structure rapidly as the plastic deformation increases while maintain its overconsolidation. However, typical clay is considered to lose its overconsolidation firstly and become normally consolidated clay while maintain its structure. Therefore, not only the behavior of clay but also the behavior of sand can be appropriately reproduced employing the Cam-clay model with the concept of Superloading/Subloading yield surfaces through adjusting the evolutional rates of overconsolidation and structure respectively.

In A2.6, the compaction of loose sand will be simulated under undrained condition by applying small-amplitude cyclic shear stress. Such large volumetric compaction occurs due to not the large mean effective stress but the plastic compression during the decay of structure. Meanwhile the loss of overconsolidation for sand is much smaller than that of structure when loading and the overconsolidation ratio increases again when unloading, which results in the fast accumulation of overconsolidation. On the other hand, because it is easy to lose overconsolidation but difficult to lose structure for clay there is almost no compaction phenomenon in clay. During the various stage of compaction, there will be corresponding sands with different densities and void ratios and their mechanical characteristics will be also different from one another. However, it is obvious that the mechanical response of various sands is able to be described by only one constitutive model and one group of material constants regardless the densities of sand.

A 2.2 CAM-CLAY MODEL

Based on the assumption that all the external work exerted to the soil specimen is transformed into the friction energy of the soil itself, Taylor (1948) made an attempt to explain the soil dilatancy during shearing. Thereafter, by interpreting the plastic work in a similar way, Cambridge school conducted the stress-dilatancy (Taylor's model) and proposed the yield function of Cam-clay model (Roscoe et al., 1958; Schofield and Wroth, 1968).

In this section, different from the assumption of energy, the yield function of Cam-clay model, which takes the plastic volumetric strain as hardening parameter, will be derived based on the basically experimental results: critical state line (CSL) that passes thought the original point in the effective stress space (q - p' space) is of the same slope with that of the normal consolidation line in $\mathrm{v} - \ln p'$ space.

Then the formulation of Cam-clay model will be deduced based on the plastic potential, namely plastic volumetric strain and the associated flow rule.

(1) Derivation of yielding function

The results of triaxial compression test with constant cell pressure employing fully remolded and normally consolidated clay under drained and undrained conditions are shown in **Figures. A2.1** and **A2.2** respectively. Here the mean effective stress p' and deviator stress q is defined as:

$$p' = \frac{1}{3}\mathrm{tr}\boldsymbol{\sigma}' \quad , \quad q = \sqrt{\frac{3}{2}\boldsymbol{S}\cdot\boldsymbol{S}} \quad , \quad \boldsymbol{S} = \boldsymbol{\sigma}' - p'\boldsymbol{I} \qquad \text{(A2.1)}$$

Where $\boldsymbol{\sigma}'$ stands for the effective stress tensor (compression is positive), $\boldsymbol{S}$ represents the deviator stress tensor, $\boldsymbol{I}$ is the unit tensor, $v = 1 + e$ is the specific volume (e: void ratio) and "$\cdot$" represents the inner product.

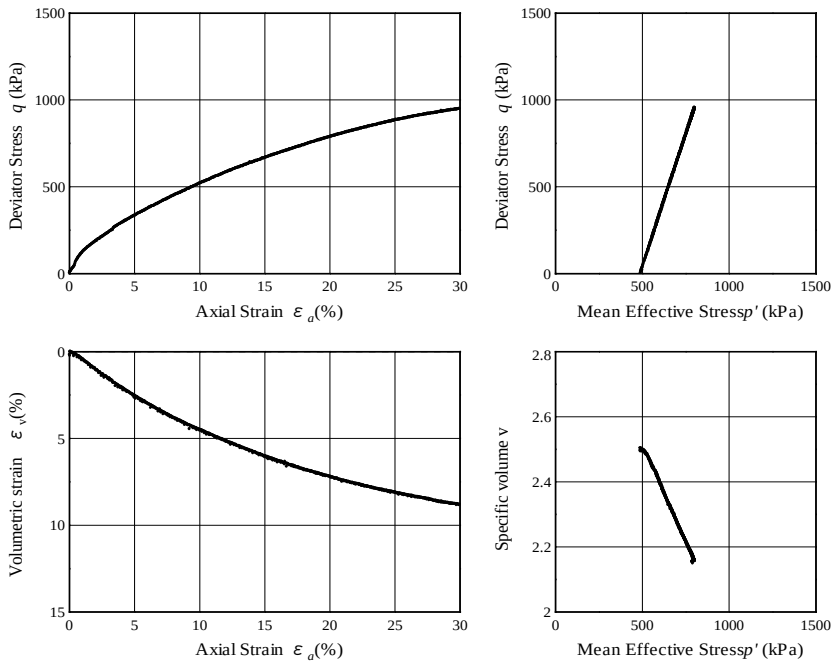

Fig. A2.1 Drained triaxial compression test of fully remolded and normally

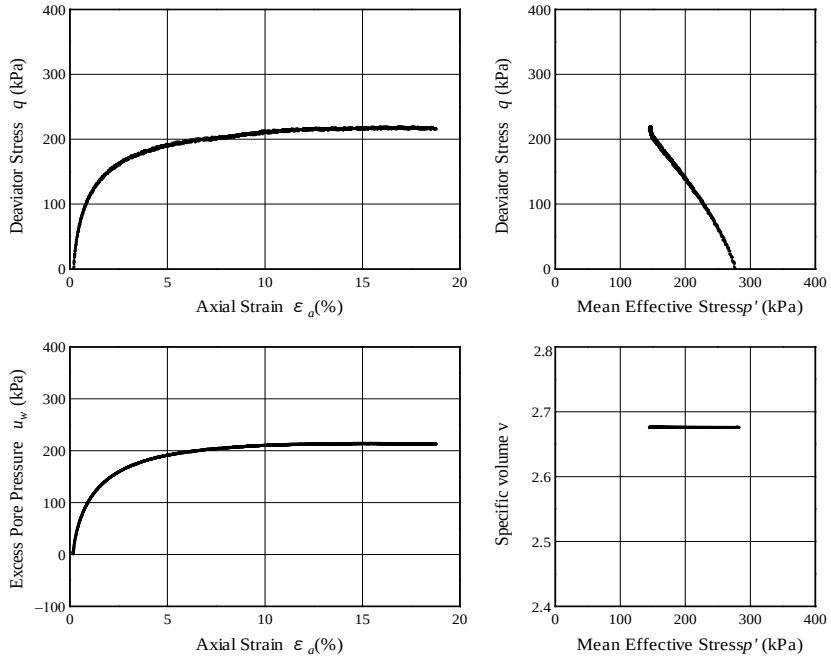

Fig. A2.2 Undrained triaxial compression test of fully remolded and normally

The loading rate is very slow so that the distribution of excess pore water pressure inside the soil specimen is uniform. The effective stress path (q - p' relationship) in **Figure A2.1** follows the total stress path ($dq / dp' = 3$) when the cell pressure is constant. As the axial strain increases, volumetric compression is observed and the specific volume also decreases. On the other hand, there is no volumetric change in the undrained test in **Figure A2.2** and the specific volume keeps constant during shear deformation. Due to the constant-volume condition, positive excess pore water pressure generates to satisfy the undrained condition. Therefore, the effective stress path lies in the left of the total stress path.

If we observe the two results in **Figures A2.1** and **A2.2**, when the axial strain or shear deformation develops adequately a state where there is no change in the effective stress ($\dot{p}' = 0$) and in the specimen volume ($\dot{\varepsilon}_v = 0$) will be finally reached. It is called "Critical State" as the volume change is zero regardless of the shear deformation. If the volumetric strain can be assumed to divide into elastic component and plastic component, because of the constant effective stress ($\dot{p}' = 0$) at Critical State, correspondingly there will be no change in the elastic component of volumetric strain ($\dot{\varepsilon}_v^{\,e} = 0$). In addition, because the total volumetric strain is also zero at Critical State, there will be no change in the plastic component of volumetric strain ($\dot{\varepsilon}_v^{\,p} = 0$) at Critical State. Here, ε_v represents the volumetric strain (compression is positive) and the upper dot is the material time derivative or increment. The superscripts "*e*" and "*p*"

represent the elastic and plastic components of volumetric strain respectively.

$$\dot{\varepsilon}_v = \dot{\varepsilon}_v^{\,e} + \dot{\varepsilon}_v^{\,p} \qquad \text{(A2.2)}$$

In addition, Bishop and Henkel had carried out numerous drained and undrained triaxial compression tests under various isotropic consolidated pressures employing fully remolded and normally consolidated Weald clay. **Figure A2.3** shows the projection of the Critical State to q - p' space and v - p' space respectively. It can be seen that Critical State lies on only one curve at both q - p' and v - p' spaces regardless of the drained or undrained condition. The curve consisting of discrete states of Critical State is called critical state line (CSL) which is actually a line passing through the original point and expressed by $q = \mathrm{M}p'$ in q - p' space. Here M is called critical state constant and represents the material constant. In v - p' space, CSL is a curve but if it is drawn in v - $\ln p'$ space, there is a linear relationship in CSL between v and $\ln p'$, as shown in **Figure A2.4**. Moreover CSL is parallel to the normal consolidation line (NCL). NCL and CSL can be presented by the following equations,

$$\mathrm{v} = \mathrm{N} - \tilde{\lambda} \ln p' \quad \text{at} \quad \eta = \frac{q}{p'} = 0 \quad : \quad \text{NCL} \qquad \text{(A2.3)}$$

$$\mathrm{v} = \Gamma - \tilde{\lambda} \ln p' \quad \text{at} \quad \eta = \frac{q}{p'} = \mathrm{M} \quad : \quad \text{CSL} \qquad \text{(A2.4)}$$

Here N, Γ and $\tilde{\lambda}$ are the material constants and $\tilde{\lambda}$ is called compression index. It is obvious that $\mathrm{N} > \Gamma$.

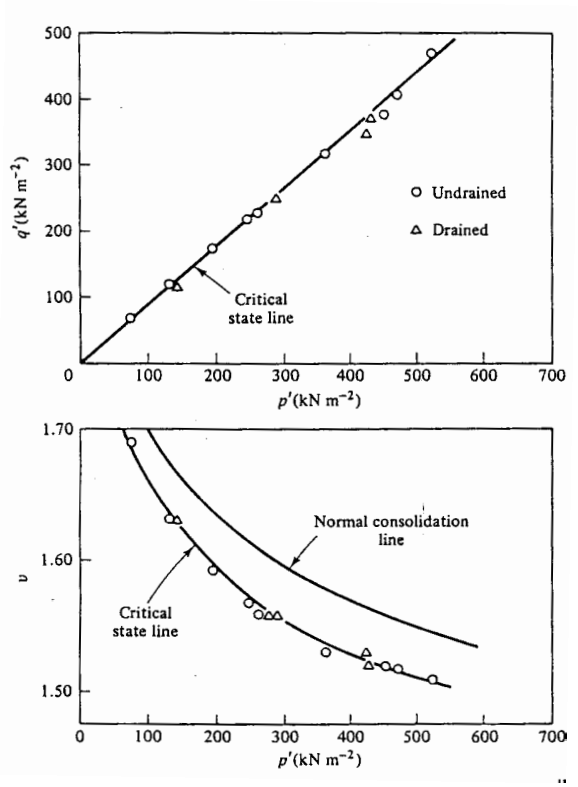

Fig. A2.3 Projection of critical state line (CSL) obtained from drained and undrained triaxial compression tests (after Parry[13], 1960)

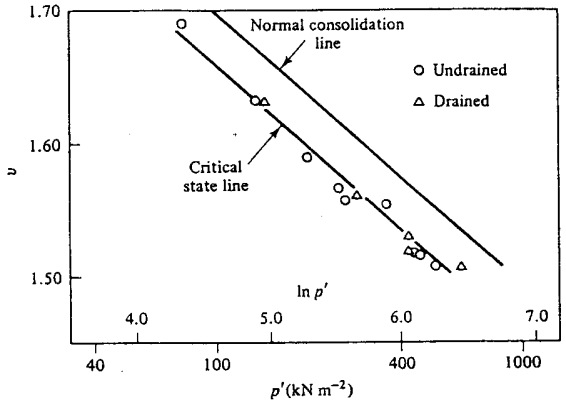

Fig. A2.4 Normal consolidation line (NCL) and critical state line (CSL) (after Parry[13], 1960)

According to **Eqs. (A2.3)** and **A (2.4)**, if the slope of $\tilde{\lambda}$ is independent of the stress ratio η, the intercept of specific volume on the axis of $\ln p'$ can be assumed to be the function of stress ratio $x(\eta)$,

$$\mathrm{v} = x(\eta) - \tilde{\lambda} \ln p' \tag{A2.5}$$

Of course $x(\eta)$ satisfies

$$x(\eta = 0) = \mathrm{N}, \quad x(\eta = \mathrm{M}) = \Gamma \tag{A2.6}$$

For the sake of simplicity, linear interpolation for $x(\eta)$ is assumed and then

$$x(\eta) = \mathrm{N} + \frac{\Gamma - \mathrm{N}}{\mathrm{M}} \eta \tag{A2.7}$$

Therefore, for arbitrary stress ratio η the specific volume will be expressed as

$$\mathrm{v} = \mathrm{N} + \frac{\Gamma - \mathrm{N}}{\mathrm{M}} \eta - \tilde{\lambda} \ln p' \tag{A2.8}$$

According to **Eq. (A2.8)**, the volumetric change (specific volume change) of soil can be ascribed as the variation in $\ln p'$ and variation in stress ratio η. Different from most of matters such as metal for which the volumetric change is only related with isotropic component of stress, the volumetric change of soil is dependent with not only the isotropic component of stress but also the deviator component of stress. The phenomenon of volumetric change due to shear stress if called dilatancy and generally volumetric expansion is positive. From **Eq. (A2.8)**, it is recognized that if the effective stress path follows the constant p' and only the stress ratio η increases from 0 to M, the maximum volumetric change (compression, negative dilatancy) is $\Gamma - \mathrm{N}$.

Next the clay is loaded under normally consolidated state without unloading from the state $(\mathrm{v}_0, p'_0, q_0 = 0)$ to state (v, p', q). Then according to **Eq. (A2.8)**, the relationship between specific volume and stress state is

$$\mathrm{v}_0 = \mathrm{N} - \tilde{\lambda} \ln p'_0 \tag{A2.9}$$

$$\mathrm{v} = \mathrm{N} + \frac{\Gamma - \mathrm{N}}{\mathrm{M}} \eta - \tilde{\lambda} \ln p' \tag{A2.10}$$

During that stage, the volumetric strain ε_v (compression is positive) is

$$\varepsilon_v = \frac{\mathrm{v}_0 - \mathrm{v}}{\mathrm{v}_0} = \frac{1}{\mathrm{v}_0}\left(\frac{\mathrm{N}-\Gamma}{\mathrm{M}}\eta + \tilde{\lambda}\ln\frac{p'}{p'_0}\right) \qquad \text{(A2.11)}$$

Meanwhile, according to the assumption

$$\varepsilon_v = \varepsilon_v^e + \varepsilon_v^p \qquad \text{(A2.12)}$$

and the elastic component of volumetric strain ε_v^e expressed by swelling index $\tilde{\kappa}$

$$\varepsilon_v{}^e = \frac{\tilde{\kappa}}{\mathrm{v}_0}\ln\frac{p'}{p'_0} \qquad \text{(A2.13)}$$

therefore, the plastic component of volumetric strain ε_v^p is

$$\varepsilon_v{}^p = f(p',q) = \frac{1}{\mathrm{v}_0}\left\{\frac{\mathrm{N}-\Gamma}{\mathrm{M}}\left(\frac{q}{p'}\right) + \left(\tilde{\lambda}-\tilde{\kappa}\right)\ln\frac{p'}{p'_0}\right\} = f\left(\boldsymbol{\sigma}'\right) \qquad \text{(A2.14)}$$

Here, $f(p',q) = f(\boldsymbol{\sigma}')$ employs the same f for simplicity. **Eq. (A2.14)** means that the hardening of fully remolded and normally consolidated clay is determined by the plastic volumetric strain ε_v^p. In addition, it is also the yield function of Cam-clay model. Although the volumetric change in **Eq. (A2.7)** is related with the dilatancy, **Eq. (A2.14)** is fundamentally concluded from the two v-$\ln p'$ relationships ($e-\log p'$ relationship) in **Eqs. (A2.3)** and **(A2.4)** and the soil mechanics obtained from **Eq. (A2.14)** can be called $e-\log p'$ soil mechanics (Asaoka et al., 2002).

(2) Plastic potential and associated flow rule

Henkel (1960) had carried out a series of drained and undrained triaxial compression and extension tests employing fully remolded and isotropically consolidated Weald clay. **Figure A2.5** depicts the iso-water-content curves measured from drained and undrained tests on effective stress space and there is no crossover point among the iso-water-content curves. **Figure A2.6** shows the iso-water-content curves if they are redrawn on the q-p' space. Because the soil is saturated, variation of water content can be interpreted as the specific volume change and it can be concluded from Henkel's experiments that once the stress state (p', q) is prescribed, the specific volume v can be determined uniquely. Moreover, if the relationship between stress state and specific volume is drawn in v-p'-q space, the roscoe surface is obtained, which is demonstrated by **Eq. (A2.8)**.

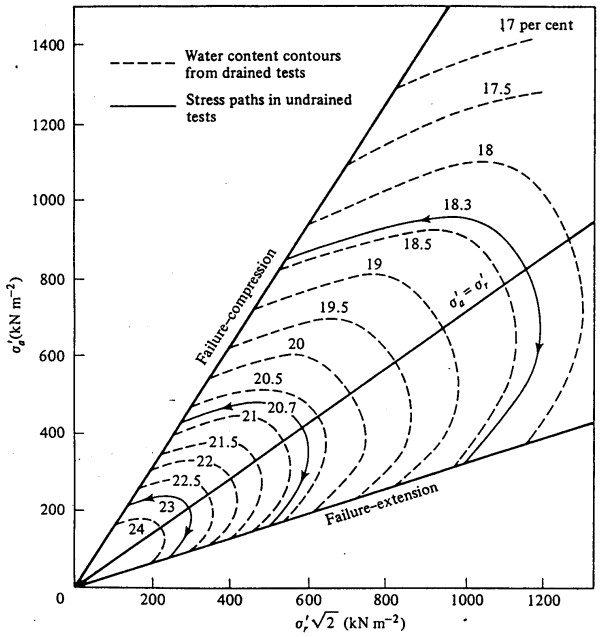

Fig. A2.5 Iso-water-content curve (after Henkel[14], 1960)

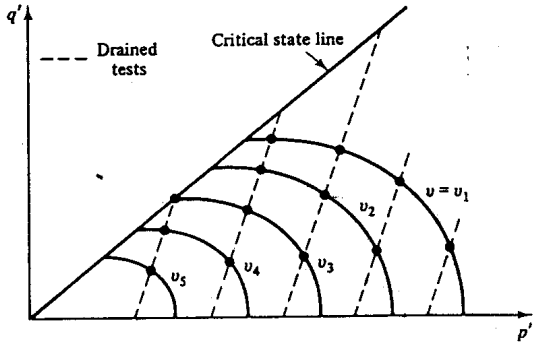

Fig. A2.6 Iso-water-content curve on q - p' space (after Henkel[14], 1960)

Eq. (A2.14) determines the volumetric change of fully remolded and normally consolidated clay only by the initial stress state and final stress state, which can be understood that the volumetric strain is path-independent. If the assumption that the volumetric strain can be divided into elastic and plastic components as shown in **Eq. (A2.12)**, notice the elastic volumetric change is path-independent in **Eq. (A2.13)** and therefore plastic volumetric change in **Eq. (A2.14)** is also path-independent and only determined by the initial and final stress states, which can be analogous to the concept of potential in mathematics. Therefore the plastic potential surface of Cam-clay model can be expressed by **Eq. (A2.14)** and the following associated flow rule

$$\dot{\varepsilon}^p = \lambda \frac{\partial f}{\partial \boldsymbol{\sigma}'} \quad (\lambda > 0) \tag{A2.15}$$

is adopted. Here, λ is the plastic multiplier and $\lambda > 0$ when loading. $\dot{\boldsymbol{\varepsilon}}^p$ is the plastic strain rate tensor and the strain rate $\dot{\boldsymbol{\varepsilon}}$ (compression is positive) is assumed to divide into elastic component $\dot{\boldsymbol{\varepsilon}}^e$ and plastic component $\dot{\boldsymbol{\varepsilon}}^p$,

$$\dot{\boldsymbol{\varepsilon}} = \dot{\boldsymbol{\varepsilon}}^e + \dot{\boldsymbol{\varepsilon}}^p \tag{A2.16}$$

As f is the isotropic scalar function related with the invariants of $\boldsymbol{\sigma}'$ (as well as p' and q), the stress direction and plastic strain rate is coaxial. In order to understand the isotropy of $f(\boldsymbol{\sigma}')$, the following equations that is equivalent to **Eq. (A2.15)** are given

$$\begin{cases} \dot{\varepsilon}_v{}^p = \lambda \dfrac{\partial f}{\partial p'} \\ \dot{\varepsilon}_s{}^p = \lambda \dfrac{\partial f}{\partial q} \end{cases} \tag{A2.17}$$

where $\dot{\varepsilon}_v{}^p$ is the plastic volumetric rate, $\dot{\varepsilon}_s{}^p$ is the plastic shear strain and they are defined by

$$\dot{\varepsilon}_v{}^p \equiv \mathrm{tr}\dot{\boldsymbol{\varepsilon}}^p \quad , \quad \dot{\varepsilon}_s{}^p \equiv \sqrt{\frac{2}{3}\dot{\boldsymbol{e}}^p \cdot \dot{\boldsymbol{e}}^p} \quad , \quad \dot{\boldsymbol{e}}^p = \dot{\boldsymbol{\varepsilon}}^p - \frac{1}{3}(\mathrm{tr}\,\dot{\boldsymbol{\varepsilon}}^p)\boldsymbol{I} \tag{A2.18}$$

If $\dot{\varepsilon}_v{}^p$ and $\dot{\varepsilon}_s{}^p$ is drawn in the $p'-q$ space, as shown in **Figure A2.7** they are found to be the compression component and shear component of the plastic strain rate vector (that is the outward normal direction of plastic potential surface).

It is convenient to understand the results of triaxial compression tests by expressing the associated flow rule in the $p'-q$ space, for example as mentioned above that the plastic volumetric strain rate is zero at the critical state ($\dot{\varepsilon}_v^p = 0$), that is

$$\left.\frac{\partial f}{\partial p'}\right|_{q=\mathrm{M}p'} = 0 \tag{A2.19}$$

according to **Eq. (A2.14)**, there is a relationship between the material constants,

$$\mathrm{N} - \Gamma = \tilde{\lambda} - \tilde{\kappa} \tag{A2.20}$$

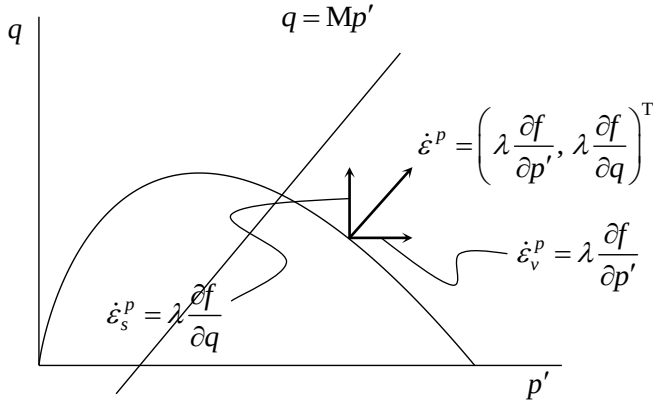

Fig. A2.7 Decomposition of plastic strain rate vector

(3) Plastic compression and plastic expansion

The concrete form of the first equation in **Eq. (A2.17)** can be rewritten by simple calculation

$$\dot{\varepsilon}_v^p = \lambda \frac{\mathrm{D}}{p'} \left(\mathrm{M} - \frac{q}{p'} \right) \tag{A2.21}$$

from which it can be seen that there would be plastic compression below the CSL $q = \mathrm{M}p'$ and plastic expansion above the CSL $q = \mathrm{M}p'$ in the $p' - q$ space. Here $\mathrm{D} = (\tilde{\lambda} - \tilde{\kappa}) / \mathrm{M}\mathrm{v}_0$ is called dilatancy coefficient. The same conclusion can also be easy to read from **Figure A2.7**. The volumetric change of soil expressed by Cam-clay model when loading ($\lambda > 0$) can be classified as the following regions,

$$\begin{aligned}
&\dot{\varepsilon}_v^{\,p} > 0 \quad \text{when} \quad q < \mathrm{M}p' \quad \cdots \quad \text{plastic compression} \\
&\dot{\varepsilon}_v^{\,p} = 0 \quad \text{when} \quad q = \mathrm{M}p' \quad \cdots \quad \text{no plastic volumetric change} \\
&\dot{\varepsilon}_v^{\,p} < 0 \quad \text{when} \quad q > \mathrm{M}p' \quad \cdots \quad \text{plastic expansion}
\end{aligned} \tag{A2.22}$$

which is illustrated in detail in **Figure A2.8**.

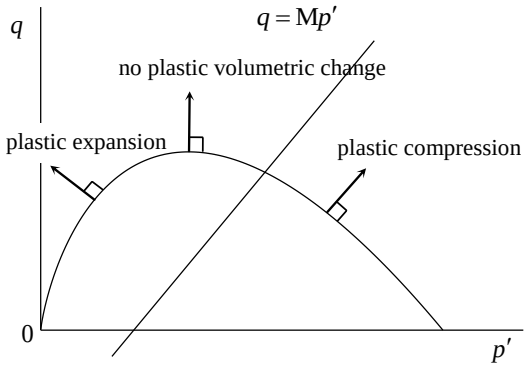

Fig. A2.8 Decomposition of plastic strain rate vector

(4) Hardening and Softening

When we take the total derivative of **Eq. (A2.14)**, the compatibility condition will be obtained

$$\dot{\varepsilon}_v^{\,p} = \frac{\partial f}{\partial p'}\dot{p}' + \frac{\partial f}{\partial q}\dot{q} \tag{A2.23}$$

Substitute **Eq. (A2.21)**, then the plastic multiplier λ is expressed as

$$\lambda = \frac{\dfrac{\partial f}{\partial p'}\dot{p}' + \dfrac{\partial f}{\partial q}\dot{q}}{\dfrac{\partial f}{\partial p'}} = \frac{\dfrac{\partial f}{\partial p'}\dot{p}' + \dfrac{\partial f}{\partial q}\dot{q}}{\dfrac{\mathrm{D}}{p'}\left(\mathrm{M} - \dfrac{q}{p'}\right)} \tag{A2.24}$$

The numerator of **Eq. (A2.24)** represent the inner product of outward normal vector $(\partial f/\partial p', \partial f/\partial q)^{\mathrm{T}}$ of plastic potential surface and stress rate vector $(\dot{p}', \dot{q})^{\mathrm{T}}$. The stress rate vector will point toward the outside of plastic potential surface if the numerator is positive and point toward inside of the plastic potential surface if the numerator is negative. When loading ($\lambda > 0$), the sign of numerator and denominator in **Eq. (A2.24)** should be the same. Therefore, when the current stress state is below the CSL $(q < \mathrm{M}p')$ the subsequent yield surface will enlarge (hardening) and when the current stress state is above the CSL $(q > \mathrm{M}p')$ the subsequent yield surface will reduce (softening), that is the loading condition of Cam-clay model can be divided into three kinds,

$$\begin{aligned}
&\frac{\partial f}{\partial p'}\dot{p}' + \frac{\partial f}{\partial q}\dot{q} > 0 \quad \text{when} \quad q < \mathrm{M}p' \quad \cdots \quad \text{hardening} \\
&\frac{\partial f}{\partial p'}\dot{p}' + \frac{\partial f}{\partial q}\dot{q} = 0 \quad \text{when} \quad q = \mathrm{M}p' \quad \cdots \quad \text{perfectly plastic} \\
&\frac{\partial f}{\partial p'}\dot{p}' + \frac{\partial f}{\partial q}\dot{q} < 0 \quad \text{when} \quad q > \mathrm{M}p' \quad \cdots \quad \text{softening}
\end{aligned} \tag{A2.25}$$

Fig. A2.9 illustrates the enlargement and reduction of subsequent yield surface,

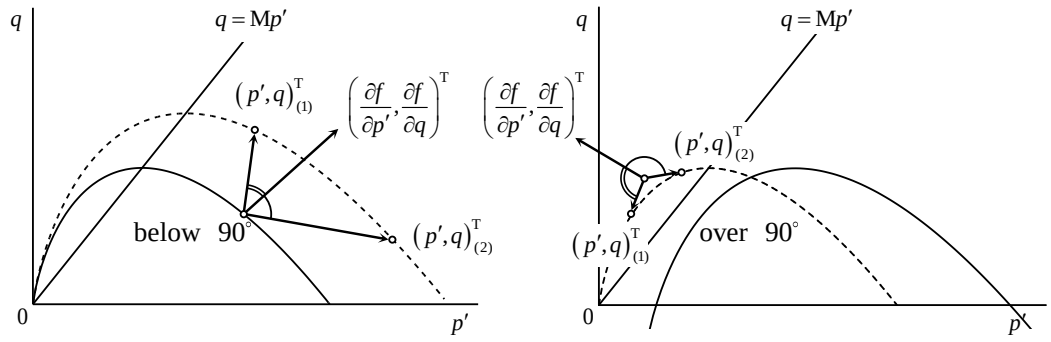

(a) Plastic potential surface enlarge (hardening) (b) Plastic potential surface reduce (softening)

Fig. A2.9 Hardening below $q = \mathrm{M}p'$ and softening above $q = \mathrm{M}p'$

Notice that there is no correspondence that hardening occurs when q increases and softening occurs when q decreases. Some special situations such as $(\dot{p}', q)^{\mathrm{T}}_{(2)}$ in **Figure A2.9** would appear during hardening or softening.

Until now we investigate the aspects of plastic compression/expansion and hardening/softening when the loading behavior of Cam-clay model is considered. It is also helpful to understand the relationship from **Figures A2.8** and **A2.9**. Therefore the characteristics of Cam-clay model, as shown in **Figure A2.10**, is briefly concluded as,

(1) Hardening always accompanying plastic compression and softening always accompanying plastic expansion;

(2) The watershed between hardening and softening is same as watershed between plastic compression and plastic expansion, which is the CSL $q = \mathrm{M}p'$ on $p' - q$ space;

(3) The slope of CSL, M keeps constant when loading.

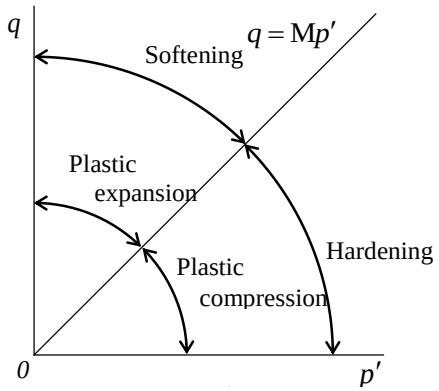

Fig. A2.10 Hardening below $q = \mathrm{M}p'$ and softening above $q = \mathrm{M}p'$

(5) Constitutive equation and loading criterion

The constitutive equation of Cam-clay model will be derived based on the elastoplastic theory. Take total derivative of **Eq. (A2.14)**, that is the compatibility condition, is rewritten as

$$\dot{\varepsilon}_v^p = \frac{\partial f}{\partial \boldsymbol{\sigma}'} \cdot \dot{\boldsymbol{\sigma}}' \tag{A2.26}$$

Considering the associated flow rule (**Eq. A2.15**), the plastic multiplier λ can be expressed by the effective stress rate $\dot{\boldsymbol{\sigma}}'$,

$$\lambda = \frac{\dfrac{\partial f}{\partial \boldsymbol{\sigma}'} \cdot \dot{\boldsymbol{\sigma}}'}{\mathrm{tr}\left(\dfrac{\partial f}{\partial \boldsymbol{\sigma}'}\right)} \tag{A2.27}$$

As for the elastic strain rate, if linear incremental elasticity is assumed, then

$$\dot{\boldsymbol{\varepsilon}}^e = \boldsymbol{E}^{-1}\dot{\boldsymbol{\sigma}}' \tag{A2.28}$$

where $\boldsymbol{E}$ is the elastic coefficient tensor. Substitute the inverse relationship of the above equation and **Eq. (A2.16)** into **Eq. (A2.27)** and use the associated flow rule of **Eq. (A2.15)** once again, the plastic multiplier λ expressed by the strain rate $\dot{\boldsymbol{\varepsilon}}$ is

$$\lambda = \Lambda = \frac{\dfrac{\partial f}{\partial \boldsymbol{\sigma}'} \cdot \boldsymbol{E}\dot{\boldsymbol{\varepsilon}}}{\mathrm{tr}\left(\dfrac{\partial f}{\partial \boldsymbol{\sigma}'}\right) + \dfrac{\partial f}{\partial \boldsymbol{\sigma}'} \cdot \boldsymbol{E}\dfrac{\partial f}{\partial \boldsymbol{\sigma}'}} \tag{A2.29}$$

Here Λ is same as λ in **Eq. (A2.27)**. Then the rate-type elastoplastic constitutive equation of Cam-clay model can be expressed by using Λ as

$$\dot{\boldsymbol{\sigma}}' = \boldsymbol{E}\,\dot{\boldsymbol{\varepsilon}}^e = \boldsymbol{E}(\dot{\boldsymbol{\varepsilon}} - \dot{\boldsymbol{\varepsilon}}^p) = \boldsymbol{E}\,\dot{\boldsymbol{\varepsilon}} - \boldsymbol{E}\Lambda\frac{\partial f}{\partial \boldsymbol{\sigma}'} \qquad \text{(A2.30)}$$

According to the loading condition, the elastic response of **Eq. (A2.28)** and elastoplastic response of **Eq. (A2.30)** can be employed correspondingly. Notice that the second term of the denominator is positive and the denominator is positive for most of soil parameters. In general, the material constants that enable the denominator of **Eq. (A2.29)** to be positive at arbitrary stress state is called Cam-clay parameters (Asaoka et al., 1994). Then the loading condition

$$\Lambda > 0 \qquad \text{(A2.31)}$$

is uniquely determined by the numerator of **Eq. (A2.29)**, and the loading criterion becomes

$$\begin{cases} \text{Loading}(\boldsymbol{D}^p \neq \boldsymbol{0}) & \text{when} \quad \dfrac{\partial f}{\partial \boldsymbol{\sigma}'} \cdot \boldsymbol{E}\dot{\boldsymbol{\varepsilon}} > 0 \\ \text{Unloading}(\boldsymbol{D}^p = \boldsymbol{0}) & \text{when} \quad \dfrac{\partial f}{\partial \boldsymbol{\sigma}'} \cdot \boldsymbol{E}\dot{\boldsymbol{\varepsilon}} < 0 \end{cases} \qquad \text{(A2.32)}$$

If the loading criterion is written by the strain rate, it is necessary to distinguish the softening and unloading. When softening occurs, the current stress state will move toward the inside of the yield surface and the subsequent yield surface will also reduce, as shown in **Figure A2.9**. However when unloading occurs, even thought the current stress state also moves toward the inside of yield surface, the yield surface doesn't move. In Cam-clay model, because the stress state after unloading locates inside the yield surface it is assumed to be elastic response when reloading until the current stress state reaches the previous yield surface.

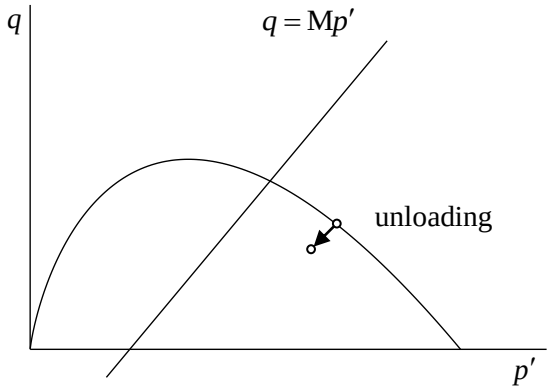

Fig. A2.11 Unloading (yield surface keeps still)

(6) Modified Cam-clay model

As can be seen, **Eq. (A2.6)** is obtained from **Eqs. (A2.3)** and **(A2.4)** by linear interpolation, if the following interpolation relation

$$x(\eta) = \mathrm{N} + \frac{\Gamma - \mathrm{N}}{\ln 2} \ln\left(\frac{\mathrm{M}^2 + \eta^2}{\mathrm{M}^2} \right) \qquad \text{(A2.33)}$$

is adopted, the modified Cam-clay model can be acquired. Compared with the original Cam-clay model of **Eq. (A2.14)**, the yield function of modified Cam-clay model is

$$\varepsilon_v^{\,p} = f(p', q) = \frac{1}{\mathrm{v}_0} \left[\frac{\Gamma - \mathrm{N}}{\ln 2} \ln\left\{ \frac{\mathrm{M}^2 + (q/p')^2}{\mathrm{M}^2} \right\} + (\tilde{\lambda} - \tilde{\kappa}) \ln \frac{p'}{p_0'} \right] = f(\boldsymbol{\sigma}') \qquad \text{(A2.34)}$$

Correspondingly, the relationship between material constants as shown in **Eq. (A2.20)** will be

$$\mathrm{N} - \Gamma = \ln 2 (\tilde{\lambda} - \tilde{\kappa}) \qquad \text{(A2.35)}$$

The plastic potential surface is half-elliptical as shown in **Figure A2.12**. It successfully solves the disadvantage of original Cam-clay model that the gradient of yield function $f(\boldsymbol{\sigma}')$ in plastic volumetric direction is not zero when the stress state is isotropic ($q = 0$). The other characteristics such as hardening accompanying plastic compression below CSL and softening accompanying plastic expansion above CSL is exactly same as the original Cam-clay model. More details about modified Cam-clay model can refer Muir Wood (1955).

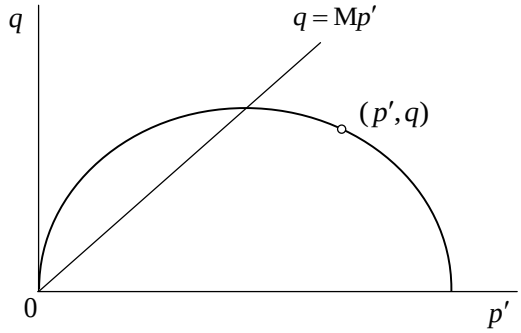

Fig. A2.12 Yield surface of modified Cam-clay model

A 2.3 LIMITATION OF CAM-CLAY MODEL AND ITS MODIFICATION

The mechanical characteristics of soil mainly depend on the three individual factors: density, water content and soil skeleton (Mikasa, 1964). When the research objects are saturated soils, the density has the same meaning as water content as well as specific volume (void ratio). According to **Eq. (A2.8)** that is used to deduce the yield function of Cam-clay model employing fully remolded and normally consolidated soil and **Figure (A2.5)** that is obtained based on fully remolded and normally consolidated soil by Henkel, once the stress state is determined, the density (or specific volume) is also known. Therefore, it is no exaggeration to say that the mechanical response of saturated, fully remolded and normally consolidated soil is determined by its density or water content. On the other hand, it is well-known that mechanical response of naturally sedimentary soil is quite different from that of fully remolded and normally consolidated one, the reason of which, using the words of Mikasa, lies in the different degrees of soil skeleton. Thus, in this section the detailed meaning of soil skeleton including overconsolidation, structure and anisotropy will be exampled in order to illustrate the limitation of Cam-clay model. And in the next section, an elastoplastic constitutive model that includes overconsolidation, structure and anisotropy will be presented.

(1) Loss of overconsolidation

Figure A2.13 shows the typical results of drained triaxial compression test using fully remolded and overconsolidated clay. Since the experimental results of Bishop and Henkel (1962), it is well-known for the researchers that after hardening, there will be softening together with certain volumetric changes from compression to expansion, namely positive dilatancy. Notice that for the drained triaxial tests under constant cell

pressure, if the deviator stress q increases, the plastic potential surface enlarges, that is hardening and if the deviator stress q decreases, the plastic potential surface reduces, that is softening. As can be seen, the result is divided into three regions, A B and C. The left boundary of region B is determined by the beginning of volumetric expansion and the right boundary is determined by the point where stress state becomes softening from hardening. For the region B in **Figure A2.13**, it is obvious that there is volumetric expansion accompanying hardening.

However, the behavior of region B cannot be clarified clearly by Cam-clay model. Considering that the overconsolidation of clay specimen is produced by unloading, the stress point is initially inside the yield surface and after loading until region B, the current stress state maybe still inside the yield surface. Therefore, there will be only elastic response in region B. Meanwhile referring the stress path in $p'-q$ space, p' in region B is successively increasing, which should result in elastic volumetric compression if elastic response is confirmed. However, in region B there is volumetric expansion, which indicates that there should be plastic volumetric expansion and this plastic expansion is larger than elastic compression in region B. In brief, the following conclusions can be obtained: (1) inside the yield surface it is elastoplastic response instead of elastic response; (2) as q increases, there is the possibility of hardening together with plastic expansion. Even if in region B the stress state reaches the yield surface, that is returning to the normal consolidation state, there is still plastic expansion accompanying hardening when the stress state is above CSL. Cam-clay model cannot explain the phenomenon of both (1) and (2).

The calculation result of overconsolidated clay determined by Cam-clay model is shown in **Figure A2.14** to give a further explanation, which is quite different from the practical result. According to Cam-clay model, the larger the overconsolidation ratio (OCR) is, the farer the distance between the initial stress state and the yield surface is. Then, when the overconsolidated clay is reloaded with the assumption that the yield surface keeps still, there is only elastic compression due to the elastic response before the current stress state reaches the yield surface. After the stress state reaches the yield surface, elastoplastic response occurs based on Cam-clay model. But the current stress state is already above CSL and according to Cam-clay model softening accompanying plastic expansion should occur, which corresponds to the sudden decrease in q and increase in ε_v in **Figure A2.14**. The behavior of overconsolidated clay in (2), that is plastic expansion accompanying hardening, cannot be reproduced by Cam-clay model.

In order to reproduce the behavior of overconsolidated clay faithfully, it is necessary for

the proposed model to

(1) allow elastoplastic response when the current stress state is still inside the yield surface;

(2) allow plastic expansion accompanying hardening when the current stress state is above CSL;

which can be perfectly solved by introducing the concept of "Subloading yield surface" proposed by Hashiguchi (1989) into Cam-clay model. The Subloading yield surface that always passes through the current stress state possesses the similar shape to normal yield surface (Cam-clay yield surface) with center of similarity of the original point and ratio of similarity of R which is the reciprocal value of OCR, as shown in **Figure A2.15**. As the plastic deformation progresses, the Subloading yield surface will gradually approach to the normal yield surface and finally these two surfaces combine into one by giving an evolutional rule to the ratio of similarity R. According to Prager's consistency condition (Druker and Prager, 1952), the plastic multiplier is represented by the current stress and the similarity ratio R. Usually, R is always smaller than 1, which means that the Subloading yield surface should not be outside of normal yield surface and when the two yield surfaces become one (R =1), the subsequent response follows Cam-clay model. In addition, during the process of approaching to the normal yield surface, the normal yield surface also increases or decreases due to the plastic deformation, which can reproduce the actual reloading behavior of soils as shown in **Figure A2.16**. Therefore, the concept of Subloading yield surface is able to reasonably demonstrate the converting process of overconsolidated soil into normally consolidated soil when loading. Particularly speaking, (1) plastic deformation inside the normal yield surface is possible; (2) plastic expansion together with hardening above CSL is also possible. Notice that Cam-clay model is only applicable for the loading and unloading of normally consolidated soil and it is not denial but leap of Cam-clay model for introducing Subloading yield surface.

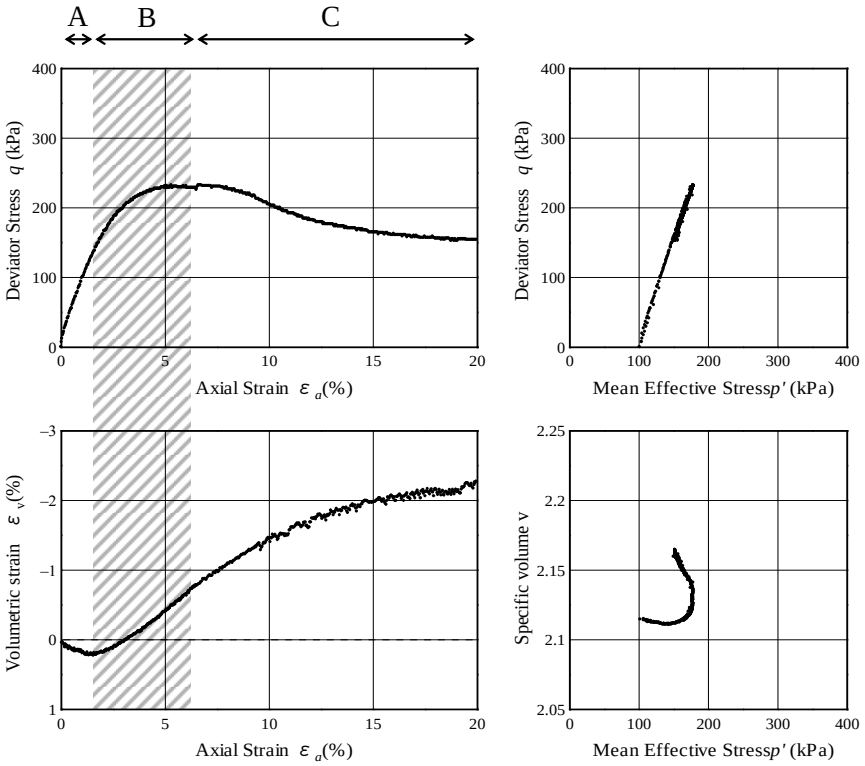

Fig. A2.13 Drained behavior of overconsolidated clay

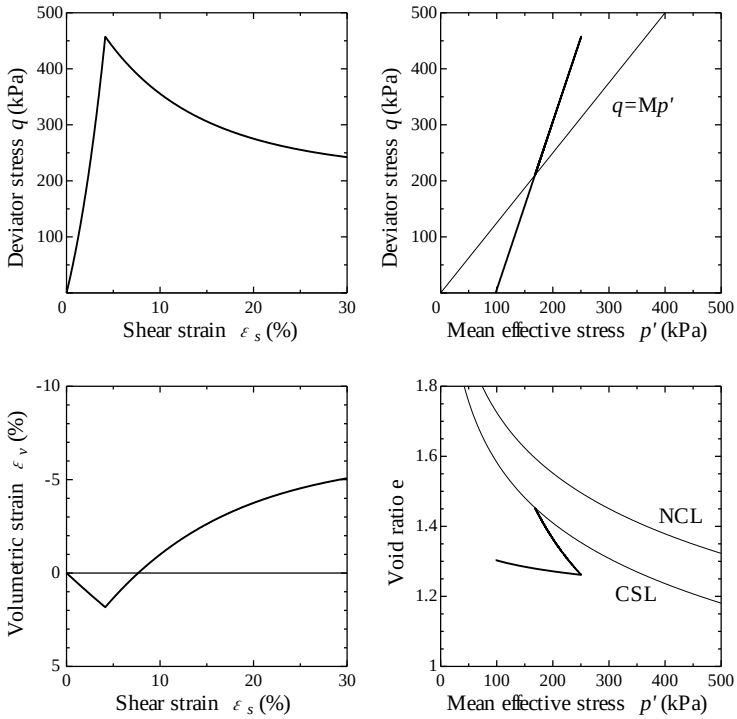

Fig. A2.14 Drained behavior of overconsolidated clay calculated by Cam-clay model

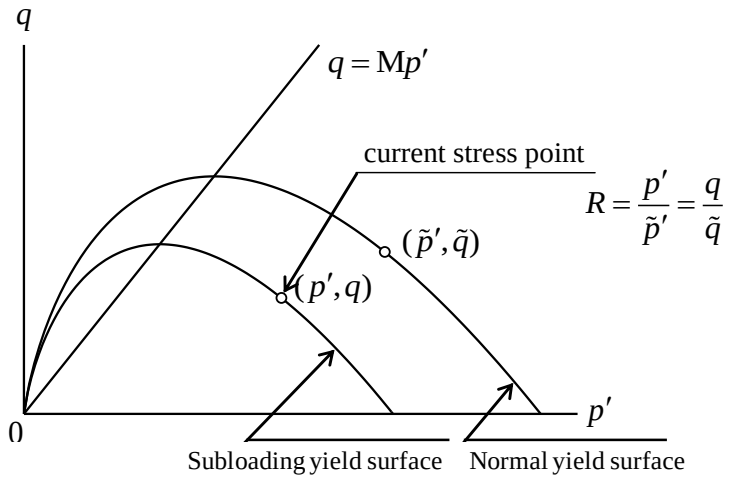

Fig. A2.15 Subloading Cam-clay model

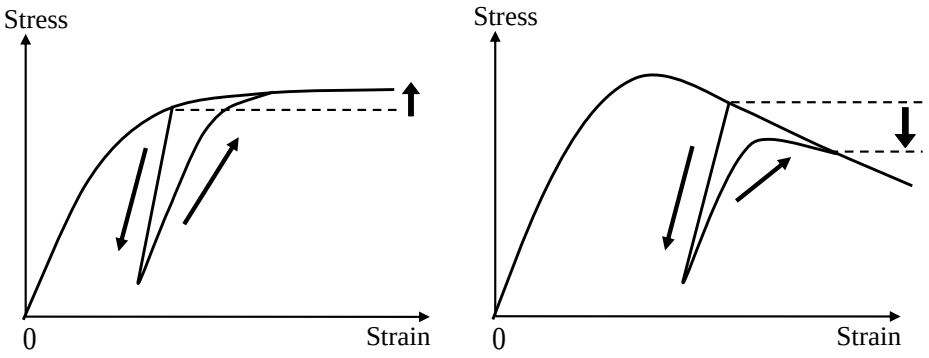

(a) enlarge of yield surface due to hardening (b) diminish of yield surface due to softening

Fig. A2.16 Elastoplastic response and loss of overconsolidation when reloading

(2) Decay/collapse of soil skeleton structure

Figure A2.17 shows the result of standard consolidation test of naturally sedimentary clay with highly structure. The line in **Figure A2.17** represents the normal consolidation line (NCL) of fully remolded clay obtained from standard consolidation test. In terms of Cam-clay model, the area above the normal consolidation line is an impossible region, in other words, it ought to be impossible for a soil to assume this sort of state. But in face we see that the highly structured clay can very well occur in as state of this kind that is not possible for the remolded soil.

As can be seen in **Figure A2.17**, compared with the fully remolded clay without structure, the highly structured clay can sustain larger load when the void ratio is same and similarly it can possess larger void ratio when the loading is same. Therefore the highly structured clay is more "bulky".

It can also be seen from **Figure A2.17** that as the compression load increases, the highly structured soil gradually approaches to the non-structure state (NCL of fully remolded clay) from the impossible region. Such phenomenon can be clarified by the decay/ degradation of structure accompanying plastic deformation when loading.

Together with the above mentioned overconsolidation, Cam-clay model can only describe loading and unloading of the soil under the state:

(1) fully remolded without any structure;

(2) normally consolidated with complete loss of overconsolidation.

Asaoka, Nakano and Noda (1998,2000), based on the mechanical behavior of highly

structured soil in the impossible region, introduced the Superloading yield surface that locates outside of the normal yield surface (Cam-clay yield surface) to describe the structure of soil. Analogically, original point denotes the center of similarity of two surfaces and the similar ratio is represented by R^*, the reciprocal value of which stands for the degree of soil structure. If the Subloading yield surface is also considered, it is set up inside the Superloading yield surface and the similar ratio R which represents the reciprocal of OCR means the ratio of Subloading yield surface to Superloading yield surface, as shown in **Figure A2.18**. Those three similar yield surfaces will gradually become one as the plastic deformation progresses. By defining evolutional rules of R^* and R for the decay of structure and loss of overconsolidation, Superloading/Subloading yield surface Cam-clay model is able to describe the responses of all the soils instead of fully remolded and normally consolidated clay.

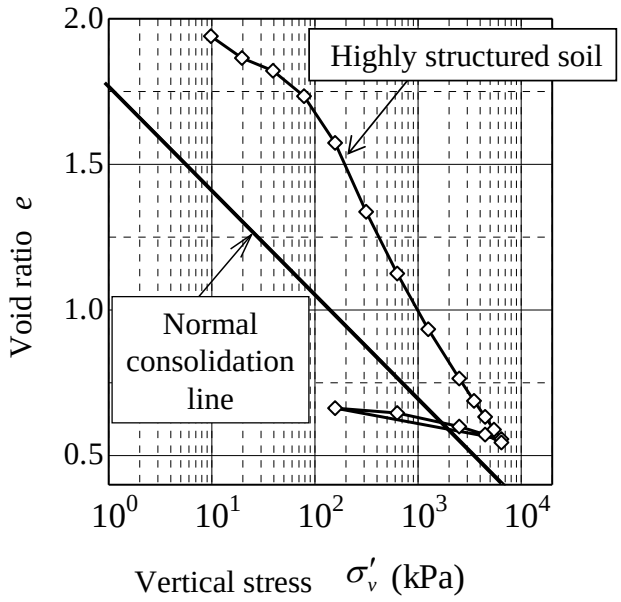

Fig. A2.17 One-dimensional compression behavior of naturally sedimentary clay (after Asaoka et al., 2007)

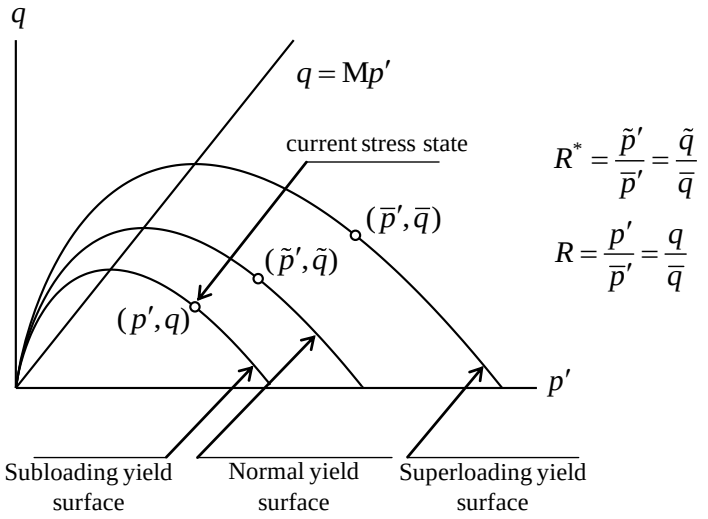

Fig. A2.18 Super/Subloading yield surface Cam-clay model

Figure A2.19 illustrates the undrained behavior of naturally sedimentary clay with high structure. The line in p'-q space represents CSL of fully remolded and normally consolidated clay. As can be seen, mean effective stress p' keeps decreasing all the time, which corresponds to the elastic volumetric expansion. According to the constant-volume condition of undrained tests, there should be plastic volumetric compression to compensate the elastic expansion. Consequently, there will be plastic compression together with softening below CSL, which cannot be explained by Cam-clay model in which there should be always plastic compression together with hardening.

From **Figures A2.17** and **A2.19**, in order to clarify the behavior of soils with high structure, it is necessary for the constitutive model to

(1) describe the state in impossible region defined by the fully remolded soil;

(2) allow plastic compression and softening below CSL;

and it can be solved by introducing Superloading yield surface.

In the next section, based on the loss of overconsolidation and decay of structure during plastic deformation, the slope of watershed between hardening and softening M_s, which corresponds to M in Cam-clay model, will become larger sometimes or smaller sometimes. When the slope of soil becomes still, it is called “dead soil”. If the soil is not “dead” but “live”, it means that there is still certain residual overconsolidation, structure or both of them left. As the loading progresses, the loss of overconsolidation and decay of structure develop due to the plastic deformation and M_s will rise or fall

correspondingly, which will make it possible that plastic expansion accompanies hardening or plastic compression accompanies softening. **Figure A2.20** shows the two possibilities respectively, where

$q = \mathrm{M}p'$: borderline of plastic compression and plastic expansion, M is constant;

$q = \mathrm{M}_s p'$: borderline of hardening and softening, M_s is changing.

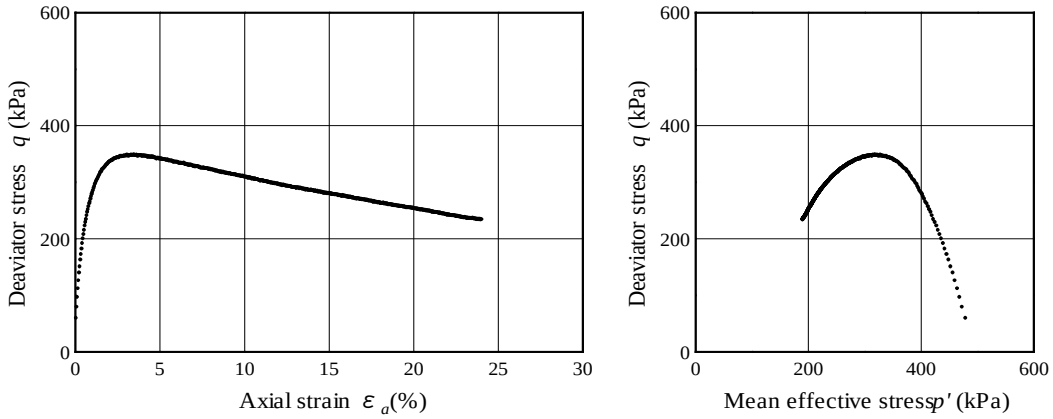

Fig. A2.19 Undrained behavior of naturally sedimentary clay with high structure

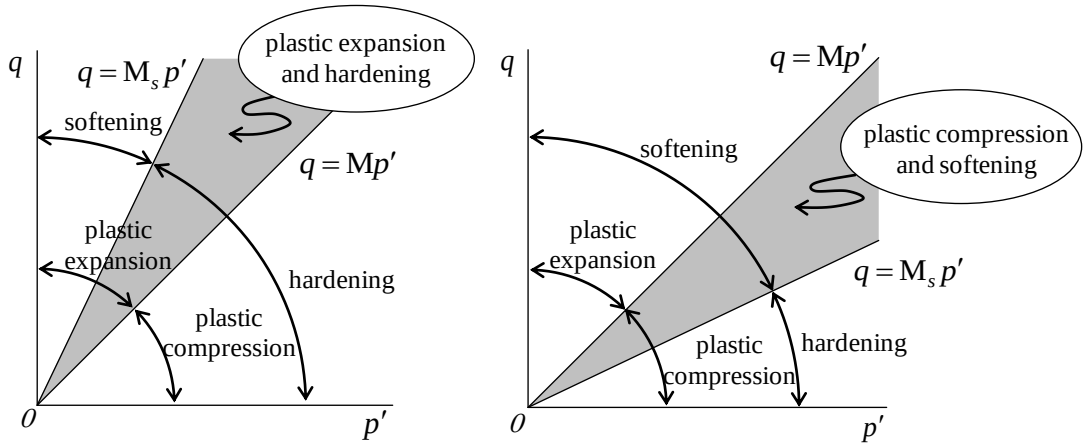

Fig. A2.20 Watersheds of plastic compression/plastic expansion and hardening/softening

(3) Anisotropy

Even though the concept of Superloading yield surface and Subloading yield surface has been introduced into Cam-clay model, it is still impossible to describe the behavior of anisotropy. By introducing Sekiguchi-Ohta model and the rotational

hardening rule of Hashiguchi, Asaoka et al. proposed a three yield surface which can rotate to express the anisotropy (**Figure A2.21**). Notice that this model is based on the modified Cam-clay model instead of the original Cam-clay model. Because the plastic potential surface also rotates as the plastic deformation develops, not only the watershed of hardening and softening M_s but also the watershed of plastic compression and plastic expansion M_a will change. And if the anisotropy is considered, the model becomes non-coaxial. The details about this model will be demonstrated in the next section.

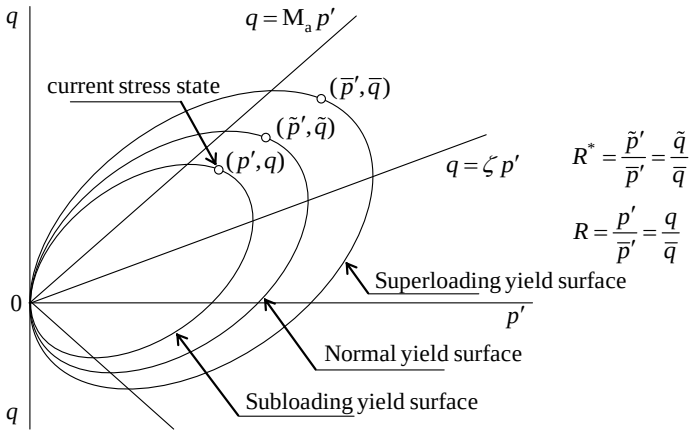

Fig. A2.21 Super/Subloading yield surface Cam-clay model with rotational hardening

A2.4 SUPERLOADING/SUBLOADING YIELD SURFACE (SYS) CAM-CLAY MODEL

In this section, the constitutive equation of SYS Cam-clay model will be presented by concretely defining the evolutional rules of overconsolidation, structure and anisotropy respectively. The concepts of structure, overconsolidation and anisotropy are based on the Superloading yield surface (Asaoka et al., 2002), Subloading yield surface (Hashiguchi, 1989) and Sekiguchi-Ohta model (1977) together with rotational hardening rule (Hashiguchi, 1998). In the following, all the equations are based on the finite deformation theory that satisfies the objectivity.

(1) Decomposition of stretching $\boldsymbol{D}$ and plastic volumetric strain

The stretching $\boldsymbol{D}$ of soil skeleton is assumed to be divided into the sum of elastic component of $\boldsymbol{D}^e$ and plastic component of $\boldsymbol{D}^p$ as:

$$\boldsymbol{D} = \boldsymbol{D}^e + \boldsymbol{D}^p \tag{A2.36}$$

In addition, the volumetric change ΔV of the arbitrary domain of soil skeleton from the reference time (t=0) to current time ($t = t$) can be expressed by the following equation:

$$\begin{aligned}\Delta V &= \int_v dv - \int_V dV \\ &= \int_0^t \left(\int_v dv \right)^{\cdot} d\tau \\ &= \int_0^t \left(\int_V (J \operatorname{tr} \boldsymbol{D}) dV \right) d\tau \\ &= \int_V \left(\int_0^t (J \operatorname{tr} \boldsymbol{D}) d\tau \right) dV \end{aligned} \qquad \text{(A2.37)}$$

Here, J is the Jacobian determinant of deformation gradient $\boldsymbol{F}$ and can be expressed by the specific volume v_0 $(=1+\mathrm{e}_0)$ at reference time and specific volume v $(=1+\mathrm{e})$ at current time:

$$J = \frac{1+\mathrm{e}}{1+\mathrm{e}_0} \qquad \text{(A2.38)}$$

$-\int_0^t (J \operatorname{tr} \boldsymbol{D}) d\tau$ represents the volumetric change (compression amount) per unit volume at reference time and current time, which can be regarded as the general volumetric strain (compression is positive). According to **Eq. (A2.36)**, the volumetric strain is approximately divided into elastic component and plastic component as:

$$-\int_0^t (J \operatorname{tr} \boldsymbol{D}) d\tau = -\int_0^t (J \operatorname{tr} \boldsymbol{D}^e) d\tau - \int_0^t (J \operatorname{tr} \boldsymbol{D}^p) d\tau \qquad \text{(A2.39)}$$

When modified Cam-clay model is extended by finite deformation theory, the plastic volumetric strain that corresponds to the plastic potential surface and yield surface is replaced by $-\int_0^t (J \operatorname{tr} \boldsymbol{D}^p) d\tau$ instead of ε_v^p in infinitesimal deformation theory.

(2) Yield surface of modified Cam-clay model employing η^* (Sekiguchi and Ohta, 1977)

Figure A2.22 gives the triaxial compression and extension result of soils with and without initial anisotropy. When there is no initial anisotropy, the results of triaxial compression and triaxial extension are same. However, when there is initial anisotropy, the results become different and the compression strength seems to be larger. It should also be noticed that by judging the increase/decrease of mean effective stress p', the borderline between plastic compression and plastic expansion M_a becomes larger if the initial anisotropy exists.

In order to explain 1) difference in compression and extension strength 2) difference in M_a when the initial anisotropy exists, an effective way is to rotate the plastic potential

surface respect to p'-axis, as shown in **Figure A2.23**.

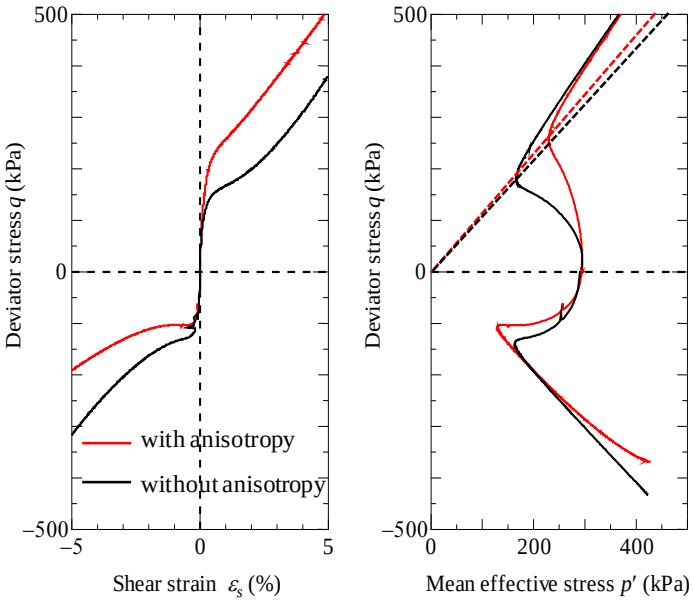

Fig. A2.22 Triaxial compression/extension result of soils with/without initial anisotropy

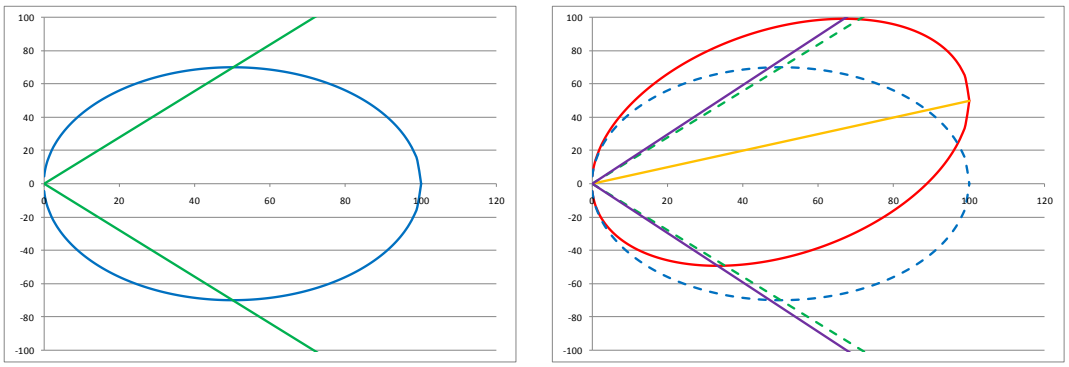

(a) Modified Cam-clay yield surface (b) Rotated yield surface

Fig. A2.23 Rotation of modified Cam-clay yield surface

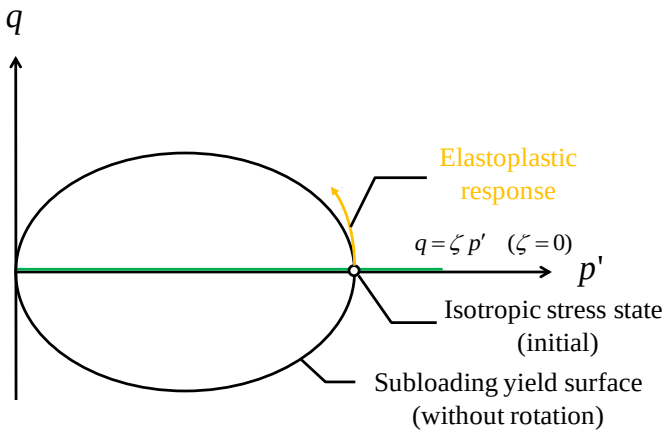

(a) Elastoplastic response and modified Cam-clay yield surface before rotation

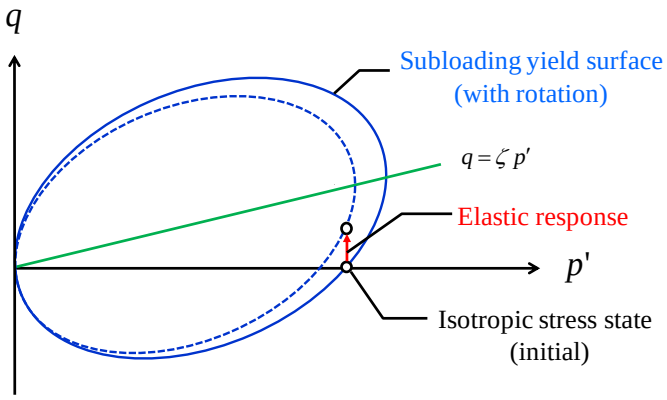

(b) Elastic response and modified Cam-clay yield surface after rotation

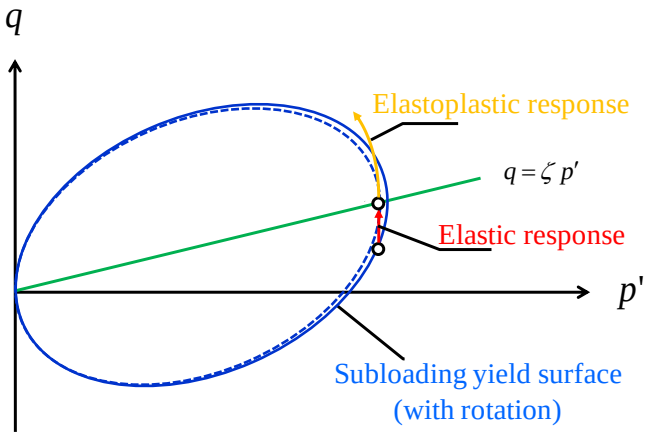

(c) Elastoplastic response and modified Cam-clay yield surface after rotation

Fig. A2.24 Modified Cam-clay yield surface before and after rotation

Next we will explain why the rotation of yield surface can describe the above two points. As shown in **Figure A2.24**, when there is no rotation of yield surface, once loading the soil response will directly go to elastoplastic behavior from the initially isotropic stress

state. However, when the rotation of yield surface is introduced, if the stress state is still initially isotropic there will be only elastic response once loading. And the elastic response would continue until the stress state reaches the central axis of rotation, after which elastoplastic behavior begins to occur. Compared with elastoplastic response, the elastic response can provide larger strength and therefore the difference in strength is reproduced.

Another fact that modified Cam-clay model instead of original Cam-clay model is adopted is clarified in **Figure A2.25**. As can be seen, for the original Cam-clay model there are some exactly same part for the yield surface before and after rotation, which results in the same borderline of plastic compression and expansion before and after the rotation ($M = M_a$). While if the modified Cam-clay yield surface is adopted, the slope of borderline between plastic compression and expansion M_a after rotation becomes larger than M before rotation, which corresponds well to the practical experimental results.

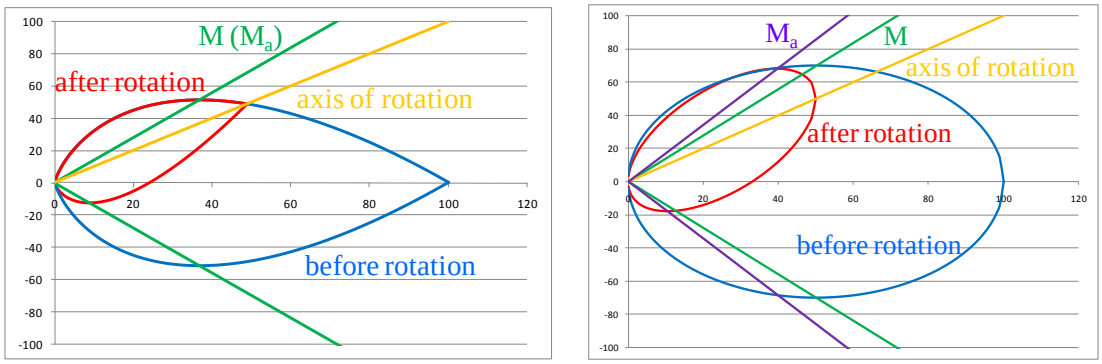

(a) Rotation of original Cam-clay yield surface (b) Rotation of modified Cam-clay yield surface

Fig. A2.25 Rotation of original and modified Cam-clay yield surface

Now that the anisotropy can be described by rotated modified Cam-clay yield surface, the concrete treatment will be given in the following. According to **Eq. (A2.34)**, the stress ratio η $(= q/p')$ is defined by the following equation based on Critical State soil mechanics:

$$\eta = \sqrt{\frac{3}{2}\boldsymbol{\eta}\cdot\boldsymbol{\eta}} \qquad \text{(A2.40)}$$

In order to represent the rotation of yield surface, η is replaced by η^* proposed by Sekiguchi and Ohta (1977):

$$\eta^* = \sqrt{\frac{3}{2}\hat{\boldsymbol{\eta}} \cdot \hat{\boldsymbol{\eta}}} \qquad \text{(A2.41)}$$

where

$$\hat{\boldsymbol{\eta}} = \boldsymbol{\eta} - \boldsymbol{\beta} \quad , \quad \boldsymbol{\eta} = \frac{\boldsymbol{S}}{p'} \quad , \quad q = \sqrt{\frac{3}{2}\boldsymbol{S} \cdot \boldsymbol{S}} \quad , \quad \boldsymbol{S} = \boldsymbol{T}' + p'\boldsymbol{I} \quad , \quad p' = -\frac{1}{3}\mathrm{tr}\boldsymbol{T}' \qquad \text{(A2.42)}$$

Here $\boldsymbol{T}'$ is effective Cauchy stress tensor (tension is positive), $\boldsymbol{S}$ is deviator stress tensor, $\boldsymbol{I}$ is unit tensor and $\boldsymbol{\beta}$ is the tensor named rotational hardening variable. The extent of anisotropy (rotation extent of plastic potential surface) is represented by ζ,

$$\zeta = \sqrt{\frac{3}{2}\boldsymbol{\beta} \cdot \boldsymbol{\beta}} \qquad \text{(A2.43)}$$

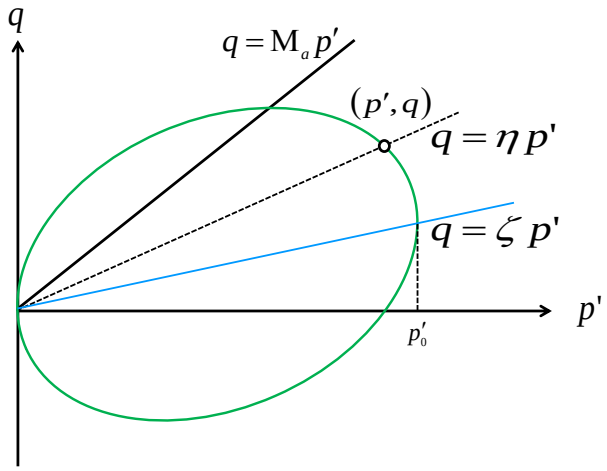

Fig. A2.26 Modified Cam-clay yield surface after introduction of η^* (Seikiguchi and Ohta, 1977)

The plastic potential of modified Cam-clay model after introduction of η^* is given by the following equation. When $\boldsymbol{T}'$ and $\boldsymbol{\beta}$ are under axial-symmetric condition, the plastic potential surface can be drawn in **Figure A2.26** in which the plastic potential surface rotates respect to the axis of hydrostatic pressure.

$$f(p', \eta^*) = \mathrm{MD}\ln\frac{p'}{p'_0} + \mathrm{MD}\ln\frac{\mathrm{M}^2 + \eta^{*2}}{\mathrm{M}^2} = -\int_0^t (J\,\mathrm{tr}\,\boldsymbol{D}^p)d\tau \qquad \text{(A2.44)}$$

Here, D represents the dilatancy coefficient, and can be expressed by $\tilde{\lambda}$, $\tilde{\kappa}$, M, v_0 as:

$$\mathrm{D} = \frac{\tilde{\lambda} - \tilde{\kappa}}{\mathrm{M} v_0} \tag{A2.45}$$

p_0' in **Eq. (A2.44)** is determined by the intersecting point between the initial yield surface and the central axis of normal yield surface $q = \zeta p'$. In addition, the relation between N and Γ is given by:

$$\mathrm{N} - \Gamma = (\tilde{\lambda} - \tilde{\kappa}) \ln 2 \tag{A2.46}$$

As mentioned above, the plastic potential of soil with anisotropy can be represented by replacing η with η^*. The development of anisotropy progresses as the plastic deformation increases (stress-induced anisotropy) and the co-rotational velocity of $\boldsymbol{\beta}$, which is the function of plastic stretching, follow the definition of Hashiguchi and Chen (1998).

(3) Superloading yield surface and Subloading yield surface

Considering that naturally sedimentary soil is generally with structure and overconsolidation, the concept of Superloading/Subloading yield surface is introduced. Here, Superloading yield surface and Subloading yield surface is similar to the normal yield surface (modified Cam-clay model) where the center of similarity locates at the original point in q - p' space. In addition, Superloading yield surface always locates outside of normal yield surface and Subloading yield surface always locates inside of Superloading yield surface. If the stress state located on normal yield surface is expressed by $\tilde{\boldsymbol{T}}'$ and stress states located on Superloading and Subloading yield surfaces are expressed by $\bar{\boldsymbol{T}}'$ and $\boldsymbol{T}'$ respectively, **Eq. (A2.44)** can be rewritten as:

$$\begin{aligned} & f(\tilde{p}', \tilde{\eta}^*) + \int_0^t J \mathrm{tr} \boldsymbol{D}^p d\tau \\ & = \mathrm{MD} \ln \frac{\tilde{p}'}{\tilde{p}_0'} + \mathrm{MD} \ln \frac{\mathrm{M}^2 + \tilde{\eta}^{*2}}{\mathrm{M}^2} + \int_0^t J \,\mathrm{tr}\, \boldsymbol{D}^p d\tau = 0 \end{aligned} \tag{A2.47}$$

where $\tilde{p}_0'$ is the intersection between the normal yield surface and the central axis of normal yield surface $q = \zeta p'$.

Assuming the similar ratio of normal yield surface to Superloading yield surface is R^* ($0 < R^* \leq 1$), then

$$
\begin{aligned}
&\tilde{\boldsymbol{T}}' = R^*\bar{\boldsymbol{T}}' \quad \Rightarrow \\
&\tilde{p}' = -\frac{1}{3}\left(\mathrm{tr}\tilde{\boldsymbol{T}}'\right) = R^*\left\{-\frac{1}{3}\left(\mathrm{tr}\bar{\boldsymbol{T}}'\right)\right\} = R^*\bar{p}' \\
&\tilde{\boldsymbol{S}} = \tilde{\boldsymbol{T}}' + \tilde{p}'\boldsymbol{I} = R^*\left(\bar{\boldsymbol{T}}' + \bar{p}'\boldsymbol{I}\right) = R^*\bar{\boldsymbol{S}} \\
&\tilde{\boldsymbol{\eta}} = \frac{\tilde{\boldsymbol{S}}}{\tilde{p}'} = \frac{R^*\bar{\boldsymbol{S}}}{R^*\bar{p}'} = \bar{\boldsymbol{\eta}} \\
&\tilde{\hat{\boldsymbol{\eta}}} = \tilde{\boldsymbol{\eta}} - \tilde{\boldsymbol{\beta}} = \bar{\boldsymbol{\eta}} - \bar{\boldsymbol{\beta}} = \bar{\hat{\boldsymbol{\eta}}} \\
&\tilde{\eta}^* = \sqrt{\frac{3}{2}\tilde{\hat{\boldsymbol{\eta}}}\cdot\tilde{\hat{\boldsymbol{\eta}}}} = \sqrt{\frac{3}{2}\bar{\hat{\boldsymbol{\eta}}}\cdot\bar{\hat{\boldsymbol{\eta}}}} = \bar{\eta}^*
\end{aligned}
\tag{A2.48}
$$

Substitute it into **Eq. (A2.47)**, the yield function of Superloading yield surface will be expressed as:

$$
\begin{aligned}
&f(\bar{p}', \bar{\eta}^*) + \mathrm{MD}\ln R^* + \int_0^t J\,\mathrm{tr}\,\boldsymbol{D}^p d\tau \\
&= \mathrm{MD}\ln\frac{\bar{p}'}{\tilde{p}_0'} + \mathrm{MD}\ln\frac{\mathrm{M}^2 + \bar{\eta}^{*2}}{\mathrm{M}^2} + \mathrm{MD}\ln R^* + \int_0^t J\,\mathrm{tr}\,\boldsymbol{D}^p d\tau = 0
\end{aligned}
\tag{A2.49}
$$

and **Figure A2.27** gives the two yield surfaces.

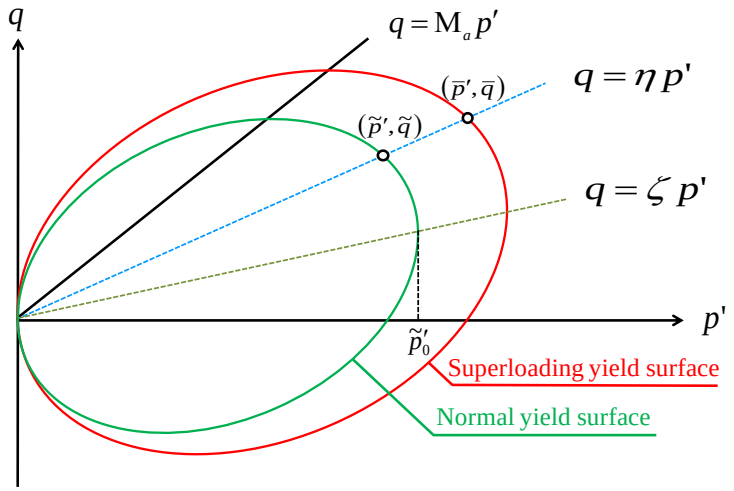

Fig. A2.27 Superloading yield surface and normal yield surface

Analogically, the similar ratio of Subloading yield surface to Superloading yield surface is assumed to be R $(0 < R \le 1)$, then

$$\bar{\boldsymbol{T}}' = \frac{1}{R}\boldsymbol{T}' \quad \Rightarrow$$

$$\bar{p}' = -\frac{1}{3}\left(\mathrm{tr}\bar{\boldsymbol{T}}'\right) = \frac{1}{R}\left\{-\frac{1}{3}\left(\mathrm{tr}\boldsymbol{T}'\right)\right\} = \frac{1}{R}p'$$

$$\bar{\boldsymbol{S}} = \bar{\boldsymbol{T}}' + \bar{p}'\boldsymbol{I} = \frac{1}{R}\left(\boldsymbol{T}' + p'\boldsymbol{I}\right) = \frac{1}{R}\boldsymbol{S} \tag{A2.50}$$

$$\bar{\boldsymbol{\eta}} = \frac{\bar{\boldsymbol{S}}}{\bar{p}'} = \frac{1/R\,\boldsymbol{S}}{1/R\,p'} = \boldsymbol{\eta}$$

$$\hat{\bar{\boldsymbol{\eta}}} = \bar{\boldsymbol{\eta}} - \boldsymbol{\beta} = \boldsymbol{\eta} - \boldsymbol{\beta} = \hat{\boldsymbol{\eta}}$$

$$\bar{\eta}^* = \sqrt{\frac{3}{2}\hat{\bar{\boldsymbol{\eta}}}\cdot\hat{\bar{\boldsymbol{\eta}}}} = \sqrt{\frac{3}{2}\hat{\boldsymbol{\eta}}\cdot\hat{\boldsymbol{\eta}}} = \eta^*$$

Substitute it into **Eq. (A2.49)**, the yield function of Subloading yield surface can be expressed as:

$$\begin{aligned} & f(p',\eta^*) + \mathrm{MD}\ln R^* - \mathrm{MD}\ln R + \int_0^t J\,\mathrm{tr}\,\boldsymbol{D}^p d\tau \\ &= \mathrm{MD}\ln\frac{p'}{\tilde{p}_0'} + \mathrm{MD}\ln\frac{\mathrm{M}^2+\eta^{*2}}{\mathrm{M}^2} + \mathrm{MD}\ln R^* - \mathrm{MD}\ln R + \int_0^t J\,\mathrm{tr}\,\boldsymbol{D}^p d\tau = 0 \end{aligned} \tag{A2.51}$$

and **Figure A2.28** gives the three yield surfaces. In addition, the reciprocal of R^* represents the degree of structure and reciprocal of R represents OCR.

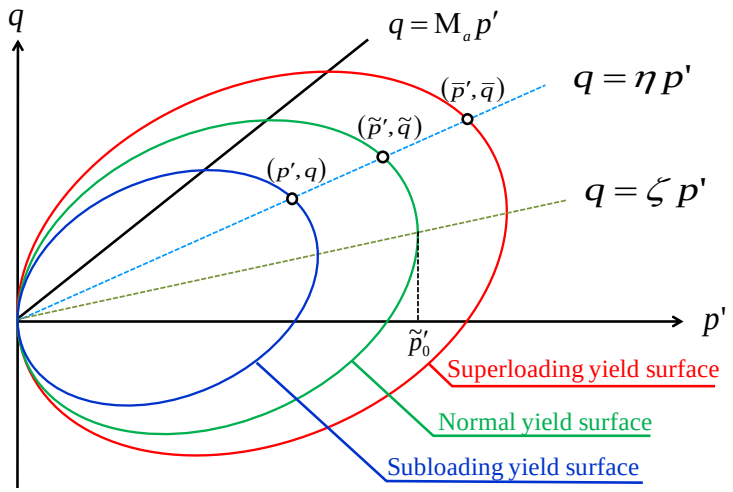

Fig. A2.28 Superloading/Subloading yield surface and normal yield surface

(4) Associated flow rule and compatibility equation

The plastic deformation is assumed to follow the associated flow rule as

$$\boldsymbol{D}^p = \lambda \frac{\partial f}{\partial \boldsymbol{T}'} \quad (\lambda > 0) \tag{A2.52}$$

Where λ is the plastic multiplier. According to the plastic theory and Prager's consistency condition:

$$\frac{\partial f}{\partial \boldsymbol{T}'} \cdot \dot{\boldsymbol{T}}' + \frac{\partial f}{\partial \boldsymbol{\beta}} \cdot \dot{\boldsymbol{\beta}} + J \mathrm{tr}\, \boldsymbol{D}^p + \mathrm{MD} \frac{\dot{R}^*}{R^*} - \mathrm{MD} \frac{\dot{R}}{R} = 0 \tag{A2.53}$$

The magnitude of subsequent plastic potential surface can be determined if the evolutional rates of anisotropy, structure and overconsolidation $\dot{\boldsymbol{\beta}}$, $\dot{R}^*$ and $\dot{R}$ are prescribed. Here, the co-rotational rates $\overset{\circ}{\boldsymbol{T}}'$ and $\overset{\circ}{\boldsymbol{\beta}}$ of $\boldsymbol{T}'$ and $\boldsymbol{\beta}$ are adopted and **Eq. (A2.53)** is rewritten as:

$$\frac{\partial f}{\partial \boldsymbol{T}'} \cdot \overset{\circ}{\boldsymbol{T}}' + \frac{\partial f}{\partial \boldsymbol{\beta}} \cdot \overset{\circ}{\boldsymbol{\beta}} + J \mathrm{tr}\, \boldsymbol{D}^p + \mathrm{MD} \frac{\dot{R}^*}{R^*} - \mathrm{MD} \frac{\dot{R}}{R} = 0 \tag{A2.54}$$

Where

$$\overset{\circ}{\boldsymbol{T}}' = \dot{\boldsymbol{T}}' + \boldsymbol{T}'\boldsymbol{\Omega} - \boldsymbol{\Omega}\boldsymbol{T}' \tag{A2.55}$$

$$\overset{\circ}{\boldsymbol{\beta}} = \dot{\boldsymbol{\beta}} + \boldsymbol{\beta}\boldsymbol{\Omega} - \boldsymbol{\Omega}\boldsymbol{\beta} \tag{A2.56}$$

Here, $\boldsymbol{\Omega}$ is called material spinning. When Green-Naghdi rate is employed as the co-rotational rate, $\boldsymbol{\Omega} = \dot{\boldsymbol{R}}\boldsymbol{R}^{\mathrm{T}}$ in which $\boldsymbol{R}$ represents the rotation tensor derived from the polar decomposition of deformation gradient $\boldsymbol{F}$ and "T" means transpose.

(5) Evolutional rules of overconsolidation, structure and anisotropy

From **Eq. (A2.54)**, it is necessary to define the evolutional rules of overconsolidation, structure and anisotropy in order to determine the magnitude of subsequent yield surface. Assuming that all the evolutional rules are related with plastic deformation, the material time derivative of R^* and R ,and the co-rotational rate of $\boldsymbol{\beta}$ are positive scalar functions involved with plastic stretching. The evolutional rules, based on the various types of soil, are also different, which can determine different mechanical responses. Therefore, the evolutional rules are so important that they are called "the second constitutive equation".

(5-1) Evolutional rule of overconsolidation

The evolutional rule of overconsolidation is assumed to be involved with plastic deformation, specifically the norm of plastic stretching $\left\|\boldsymbol{D}^p\right\| = \sqrt{\boldsymbol{D}^p \cdot \boldsymbol{D}^p}$, and $\dot{R}$ is given by the following equation,

$$\dot{R} = JU\left\|\boldsymbol{D}^p\right\| \tag{A2.57}$$

Here U that is a positive scalar function is related with R and as shown in **Figure A2.29** it also satisfies requirement in **Eq. (A2.58)**,

$$\begin{aligned} U &= \infty \quad \text{when} \quad R = 0 \\ U &= 0 \quad \text{when} \quad R = 1 \end{aligned} \tag{A2.58}$$

The first equation in **Eq. (A2.58)** means that when reloading is applied from the state of completely unloading ($R \cong 0$), there is only elastic response without elastoplastic response as shown in **Figure A2.30**, which requires that $\left\|\boldsymbol{D}^p\right\| \to 0$, that is $U = \dot{R} \Big/ J\left\|\boldsymbol{D}^p\right\| = \infty$. The second equation means that once the stress state reaches the normal yield surface ($R = 1$) there will be no further loss of overconsolidation, which requires that $\dot{R} \to 0$, that is $U = \dot{R} \Big/ J\left\|\boldsymbol{D}^p\right\| = 0$. According to the definition of Hashiguchi (1989), the simplest form of function U is:

$$U = -\frac{m}{\mathrm{D}} \ln R \tag{A2.59}$$

Where m (>0) the material constant that controls the rate of overconsolidation loss and is called normal consolidation index. The larger m is, the faster the loss of overconsolidation is.

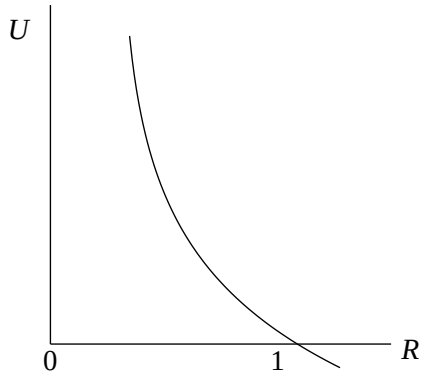

Fig. A2.29 Curve of function U

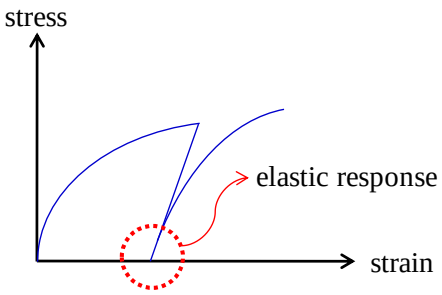

Fig. A2.30 Reloading from completely unloading state

(5-2) Evolutional rule of structure

The evolutional rule of structure is also related with the development of plastic deformation and it can be divided into two types about clay and sand respectively. **Figure A2.31** shows the isotropic consolidation results of overconsolidated and undisturbed clay and sand with various densities respectively. As can be seen in **Figure A2.31(a)**, the consolidation curve gradually approaches to NCL after the stress state passes through consolidation yield stress, which means that the decay of structure in clay still progresses even though the isotropic consolidation is carried out. However from **Figure A2.31(b)**, the consolidation curves keep linear and possess same slope for sands with various densities and difference structure, which means that the decay of structure in sand is kept when the isotropic consolidation is carried out. Therefore, the evolutional rules of structure for clay and sand are:

$$\dot{R}^* = JU^* \left\| \boldsymbol{D}^p \right\| \quad \text{for clay}$$
$$\dot{R}^* = JU^* \sqrt{\frac{2}{3}} \left\| \boldsymbol{D}_s{}^p \right\| \quad \text{for sand} \tag{A2.60}$$

Here $\boldsymbol{D}_s^p$ represents the deviator component of plastic stretching and $\boldsymbol{D}_s{}^p = \boldsymbol{D}^p - \frac{1}{3}(\mathrm{tr}\,\boldsymbol{D}^p)\boldsymbol{I}$, which corresponds to the fact that the decay of structure for sand is independent of the isotropic component of plastic stretching $\mathrm{tr}\,\boldsymbol{D}^p$. U^* that is a positive scalar function is related with R^* and is usable for both sand and clay. As shown in **Figure A2.32**, the function U^* should satisfy:

$$U^* = 0 \quad \text{when} \quad R^* = 0$$
$$U^* = 0 \quad \text{when} \quad R^* = 1 \tag{A2.61}$$

The first equation in **Eq. (A2.61)** means that when the structure is infinite ($R^* \cong 0$), the soil is in a state called colloid and such state can be regarded to be stable without decay of structure. The second equation means that once the stress state reaches the normal yield surface ($R^* = 1$), namely the soil returns to be fully remolded state, there will be no further decay of structure. Accordingly, one of the options satisfying the above requirement is

$$U^* = \frac{a}{\mathrm{D}} R^{*b} (1 - R^*)^c \tag{A2.62}$$

Where a, b, c (>0) are material constants that control the rate of structure decay and are called structure degradation index. In this paper, $b = c = 1.0$ is employed. The larger a is, the faster the decay of structure is. In addition, notice that although R increases once unloading (the soil becomes overconsolidated), R^* still keeps invariable (structure is only related with the effect of decay).

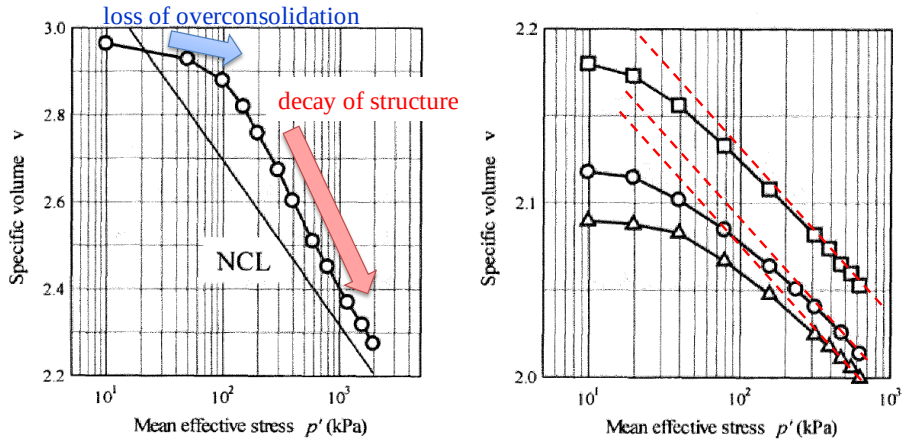

(a) clay (b) sand

Fig. A2.31 Isotropic consolidation results of overconsolidated and undisturbed clay and sand with

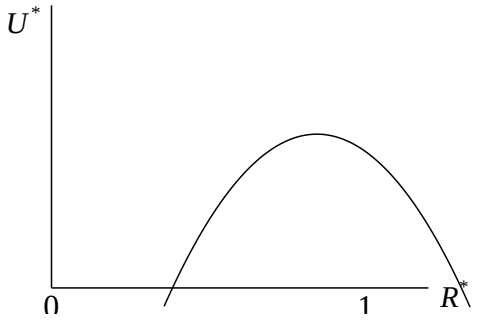

Fig. A2.32 Curve of function U^*

(5-3) Evolutional rule of anisotropy

According to Hashiguchi and Chen (1998), the co-rotational rate $\overset{\circ}{\boldsymbol{\beta}}$ of $\boldsymbol{\beta}$ follows the next 4 assumptions.

(1) The development of anisotropy is independent of the isotropic component of plastic stretching and the co-rotational rate of plastic potential surface is proportional to the magnitude of plastic deviator stretching, where the norm $\left\|\boldsymbol{D}_s^p\right\|$ is employed. Notice that the extent of anisotropy keeps invariable in case of isotropic compression or unloading.

(2) There should be a limitation for the magnitude of central axis of potential surface $\boldsymbol{\beta}$, which is given by:

$$\|\boldsymbol{\beta}\| \le m_b \tag{A2.63}$$

Which means that no matter the initial anisotropy exists or not, the final critical state should be same. In other words, the rotation of plastic potential surface will stop at certain situation, as shown in **Figure A2.33**.

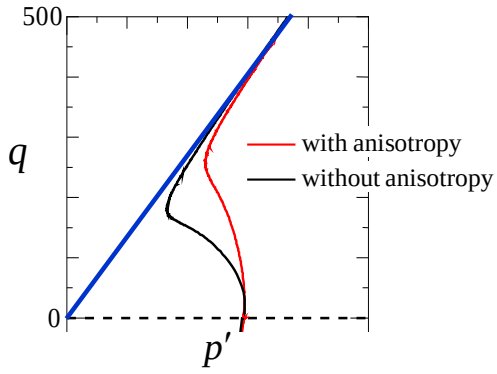

Fig. A2.33 Limitation of rotation of plastic potential surface

Here m_b (≥ 0) is material constant and is called limit constant for rotational hardening. **Eq. (A2.63)** is called limit surface for rotational hardening or rotational limit surface.

$$\eta = \sqrt{\frac{3}{2}} m_b \tag{A2.64}$$

(3) The central axis of plastic potential surface $\boldsymbol{\beta}$ gradually approaches to the line $m_b \hat{\boldsymbol{\eta}}/\|\hat{\boldsymbol{\eta}}\|$ on the rotational limit surface which is the conjugate line corresponding to the line $\hat{\boldsymbol{\eta}}$ on the plastic potential surface. In other words, the rotational rate $\overset{\circ}{\boldsymbol{\beta}}$ is assumed to have the same direction as that of

$$\boldsymbol{\eta}_b = m_b \frac{\hat{\boldsymbol{\eta}}}{\|\hat{\boldsymbol{\eta}}\|} - \boldsymbol{\beta} \tag{A2.65}$$

and **Figure A2.34** gives the detailed description.

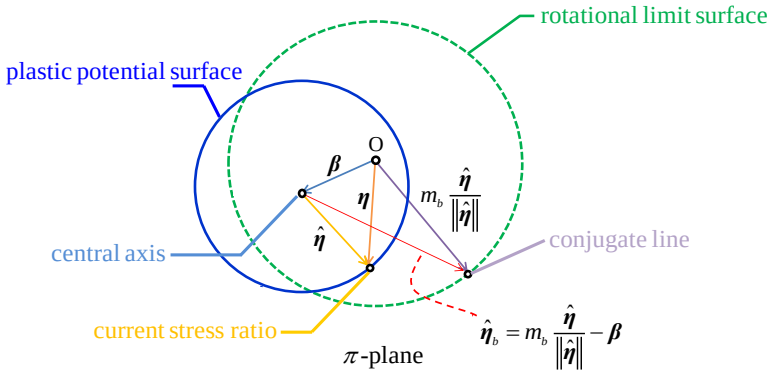

Fig. A2.34 Direction of central axis of plastic potential surface

(4) For the monotonic proportional loading with $\boldsymbol{\eta} = const$, i.e. the so-called

anisotropic consolidation, $\boldsymbol{\beta}$ is naturally considered to reach η gradually, which leads to $\|\hat{\boldsymbol{\eta}}\| \to 0$, as shown in **Figure A2.35**.

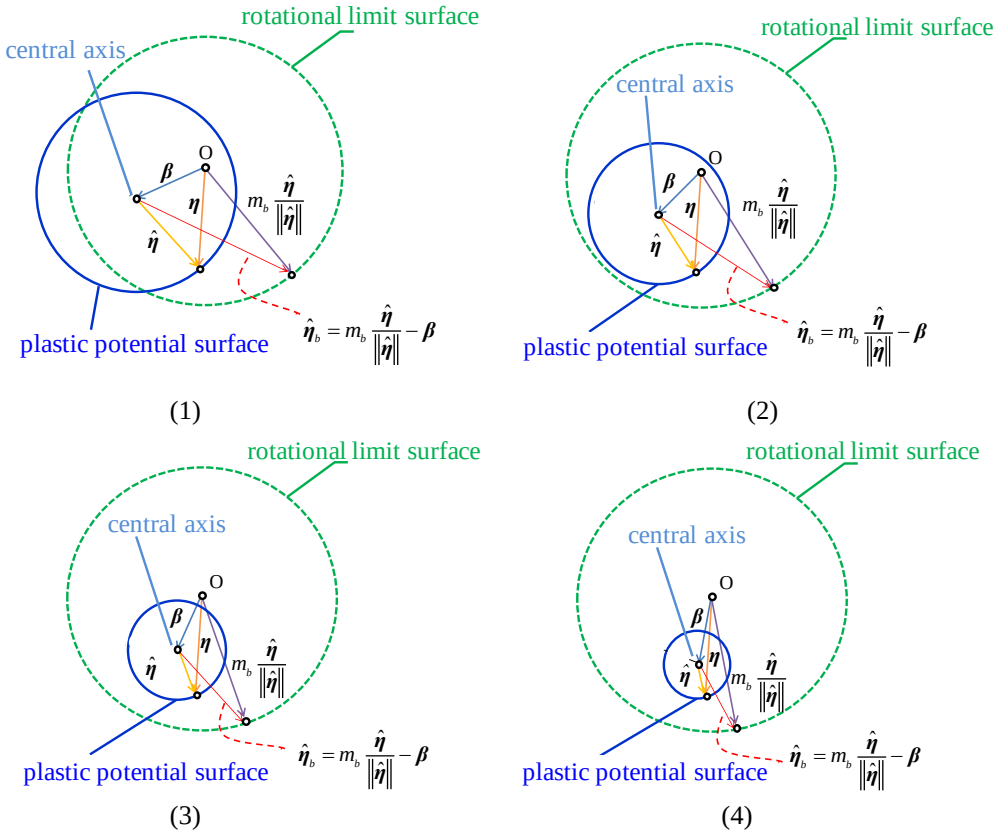

Fig. A2.35 Development of $\boldsymbol{\beta}$ when loading under $\boldsymbol{\eta} = const$

In sum, the evolutional rule of $\boldsymbol{\beta}$ is given by the following equation,

$$\overset{\circ}{\boldsymbol{\beta}} = J \frac{b_r}{\mathrm{D}} \sqrt{\frac{2}{3}} \left\| \boldsymbol{D}_s{}^{p} \right\| \|\hat{\boldsymbol{\eta}}\| \boldsymbol{\eta}_b \qquad \text{(A2.66)}$$

Where b_r is the material constant that controls the rate of the evolution of anisotropy and is called rotational hardening index. The larger b_r is, the faster the anisotropy develops.

(6) Threshold between plastic compression and plastic expansion

Since the plastic potential surface rotates with ongoing plastic deformation, the threshold between plastic volumetric compression and plastic volumetric expansion also moves with ongoing plastic deformation. Note that the plastic volumetric strain rate is expressed by the following equation,

$$\left(-\int_0^t J\,\mathrm{tr}\,\boldsymbol{D}^p d\tau\right)^{\cdot} = -J\,\mathrm{tr}\,\boldsymbol{D}^p = -\lambda J \mathrm{tr}\frac{\partial f}{\partial \boldsymbol{T}'} = \lambda J \frac{\mathrm{MD}}{p'(\mathrm{M}^2+\eta^{*2})}(\mathrm{M}_a{}^2-\eta^2) \quad \text{(A2.67)}$$

Where

$$\mathrm{M}_a{}^2 = \mathrm{M}^2 + \varsigma^2 \quad \text{(A2.68)}$$

Then the watershed between plastic compression and plastic expansion in terms of the stress ratio is given by $\eta = \mathrm{M}_a$, which classifies the volume change behavior as follows:

$$\begin{cases} -\mathrm{tr}\boldsymbol{D}^p > 0 & \text{when} \quad \eta^2 < \mathrm{M}_a{}^2 \quad \cdots \quad \text{plastic compression} \\ -\mathrm{tr}\boldsymbol{D}^p = 0 & \text{when} \quad \eta^2 = \mathrm{M}_a{}^2 \quad \cdots \quad \text{no plastic volumetric change} \\ -\mathrm{tr}\boldsymbol{D}^p < 0 & \text{when} \quad \eta^2 > \mathrm{M}_a{}^2 \quad \cdots \quad \text{plastic expansion} \end{cases} \quad \text{(A2.69)}$$

Figure A2.36 gives the corresponding explanation. According to **Eq. (A2.68)**, M_a increases as the anisotropy develops ($\varsigma \to \sqrt{3/2}m_b$) and M_a decreases as the anisotropy reduces ($\varsigma \to 0$). The existence of rotational limit surface for rotational hardening gives the following constraint to M_a:

$$\mathrm{M}^2 \le \mathrm{M}_a{}^2 \le \mathrm{M}^2 + \frac{3}{2}m_b{}^2 \quad \text{(A2.70)}$$

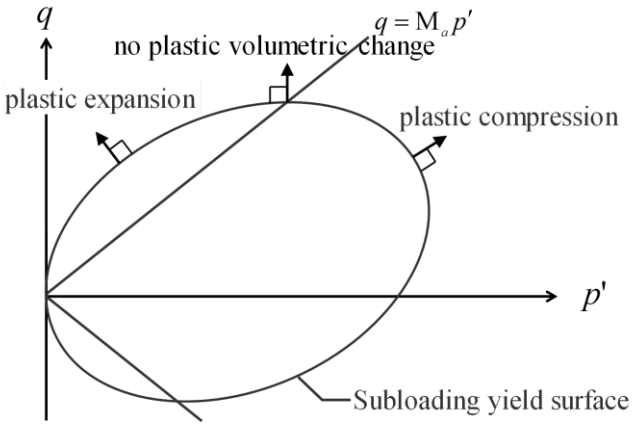

Fig. A2.36 Plastic compression below $q = \mathrm{M}_a p'$ and plastic expansion above $q = \mathrm{M}_a p'$

(7) Threshold between hardening and softening

Substituting the evolutional rules given in **Eqs. (A2.57)**, **(A2.60)** and **(A2.66)** into **Eq. (A2.54)** and applying the associated flow rule, the plastic multiplier λ can be expressed as follows:

$$\lambda = \frac{\frac{\partial f}{\partial \boldsymbol{T}'} \cdot \overset{\circ}{\boldsymbol{T}}'}{J \frac{\mathrm{MD}}{p'(\mathrm{M}^2 + \eta^{*2})}(\mathrm{M}_s{}^2 - \eta^2)} \tag{A2.71}$$

In which M_s can be given according to clay or sand because the different evolutional rules for clay and sand in **Eq. (A2.60)**, when clay

$$\begin{aligned} \mathrm{M}_s{}^2 = \mathrm{M}_a{}^2 + br\frac{4\mathrm{M}\eta^{*2}}{\mathrm{M}^2 + \eta^{*2}}(m_b\eta^* - \sqrt{\frac{3}{2}}\hat{\boldsymbol{\eta}} \cdot \boldsymbol{\beta}) \\ - \mathrm{MD}(\frac{U^*}{R^*} - \frac{U}{R})\sqrt{6\eta^{*2} + \frac{1}{3}(\mathrm{M}_a{}^2 - \eta^2)^2} \end{aligned} \tag{A2.72}$$

When sand

$$\begin{aligned} \mathrm{M}_s{}^2 = \mathrm{M}_a{}^2 + br\frac{4\mathrm{M}\eta^{*2}}{\mathrm{M}^2 + \eta^{*2}}(m_b\eta^* - \sqrt{\frac{3}{2}}\hat{\boldsymbol{\eta}} \cdot \boldsymbol{\beta}) \\ - \mathrm{MD}\left\{\frac{U^*}{R^*}2\eta^* - \frac{U}{R}\sqrt{6\eta^{*2} + \frac{1}{3}(\mathrm{M}_a{}^2 - \eta^2)^2}\right\} \end{aligned} \tag{A2.73}$$

Based on the theory of plasticity, when soil is under loading, it holds that $\lambda > 0$. Given that λ is positive, **Eq. (2.71)** suggests that η=M_s is the threshold of softening and hardening and there exist the following three cases for loading:

$$\begin{cases} \frac{\partial f}{\partial \boldsymbol{T}'} \cdot \overset{\circ}{\boldsymbol{T}}' > 0 \quad \text{when} \quad \eta^2 < \mathrm{M}_s{}^2 \quad \cdots \quad \text{hardening} \\ \frac{\partial f}{\partial \boldsymbol{T}'} \cdot \overset{\circ}{\boldsymbol{T}}' = 0 \quad \text{when} \quad \eta^2 = \mathrm{M}_s{}^2 \quad \cdots \quad \text{perfectly plastic} \\ \frac{\partial f}{\partial \boldsymbol{T}'} \cdot \overset{\circ}{\boldsymbol{T}}' < 0 \quad \text{when} \quad \eta^2 > \mathrm{M}_s{}^2 \quad \cdots \quad \text{softening} \end{cases} \tag{A2.74}$$

Figure A2.37 illustrates the detailed response. According to **Eqs. (A2.72)** and **(A2.73)**, when the loss of overconsolidation, decay of structure, development/reduction of anisotropy as well as the stress ratio vary due to loading, M_s also varies. Moreover, M_s also varies as the overconsolidation and stress ratio changes due to unloading. $\mathrm{M}_s = \mathrm{M}_a$ if and only if the soil reaches fully remolded and normally consolidated state ($R^* = 1$, $R = 1$) and the development of anisotropy stops ($\|\hat{\boldsymbol{\eta}}\| = 0$ or $\boldsymbol{\eta}_b = \boldsymbol{0}$).

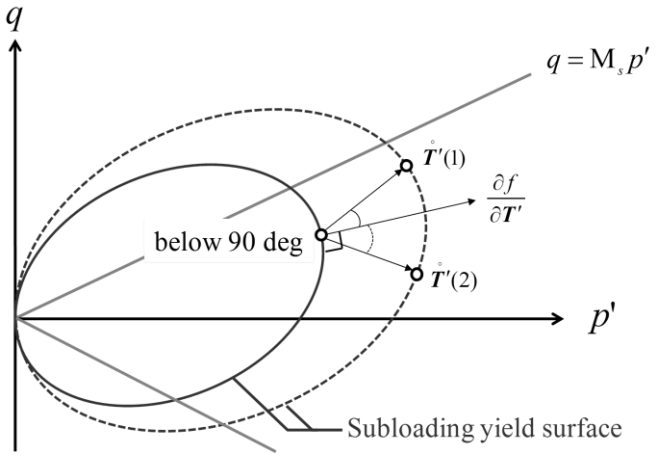

(a) Enlarging of plastic potential surface (hardening)

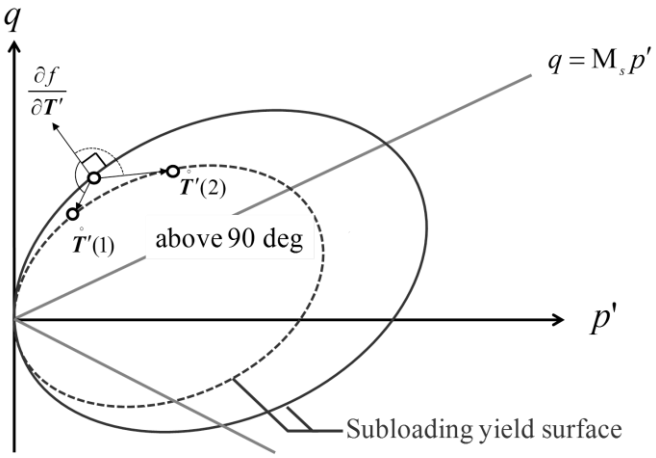

(b) Diminishing of plastic potential surface (softening)

Fig. A2.37 Hardening below $q = \mathrm{M}_s p'$ and softening above $q = \mathrm{M}_s p'$

(8) Constitutive equation and loading criterion

The elastic response is expressed by

$$\overset{\circ}{\boldsymbol{T}}' = \boldsymbol{E}\boldsymbol{D}^e \tag{A2.75}$$

where $\boldsymbol{E}$ is the elastic coefficient tensor. Substituting the evolutional rules **Eqs. (A2.57)**, **(A2.60)** and **(A2.66)**, elastic constitutive equation **Eq. (A2.75)** and decomposition of stretching **Eq. (A2.36)** into the compatibility condition **Eq. (A2.54)** and considering the associated flow rule in **Eq. (A2.52)**, the plastic multiplier Λ in term of stretching will be:

$$\Lambda = \lambda = \frac{\dfrac{\partial f}{\partial \boldsymbol{T}'} \cdot \boldsymbol{E}\boldsymbol{D}}{\dfrac{\partial f}{\partial \boldsymbol{T}'} \cdot \boldsymbol{E} \dfrac{\partial f}{\partial \boldsymbol{T}'} + J \dfrac{\mathrm{MD}}{p'(\mathrm{M}^2 + \eta^{*2})}(\mathrm{M}_s{}^2 - \eta^2)} \qquad (\Lambda > 0) \qquad \text{(A2.76)}$$

Substitute **Eqs. (A2.36)** and **(A2.52)** into **Eq. (A2.75)**, then the elastoplastic constitutive equation employing the plastic multiplier Λ in terms of stretching will be:

$$\overset{\circ}{\boldsymbol{T}}' = \boldsymbol{E}\boldsymbol{D} - \Lambda \boldsymbol{E} \frac{\partial f}{\partial \boldsymbol{T}'} \qquad \text{(A2.77)}$$

If the elastic response is assumed to obey the non-linear isotropic Hooke' law, then

$$\overset{\circ}{\boldsymbol{T}}' = (\tilde{K} - \frac{2}{3}\tilde{G})(\mathrm{tr}\,\boldsymbol{D}^e)\boldsymbol{I} + 2\tilde{G}\boldsymbol{D}^e \qquad \text{(A2.78)}$$

Where $\tilde{K}$ represents the elastic volumetric modulus and $\tilde{G}$ represents the elastic shear modulus. For the soil skeleton when the swelling index is given by $\tilde{\kappa}$ it is necessary for **Eq. (A2.78)** to satisfy:

$$-J\,\mathrm{tr}\,\boldsymbol{D}^e = -\frac{\tilde{\kappa}}{1+\mathrm{e}_0}\frac{\dot{p}'}{p'} \qquad \text{(A2.79)}$$

Therefore, $\tilde{K}$ and $\tilde{G}$ can be expressed in terms of J and p':

$$\begin{aligned} \tilde{K} &= \frac{1+\mathrm{e}}{\tilde{\kappa}}p' \ \left(= \frac{J(1+\mathrm{e}_0)}{\tilde{\kappa}}p'\right) \\ \tilde{G} &= \frac{3(1-2\nu)}{2(1+\nu)}\tilde{K} \end{aligned} \qquad \text{(A2.80)}$$

Where ν is Poisson's ratio.

When **Eq. (A2.78)** is employed as the elastic constitutive equation, the concrete form of rate-type constitutive equation of SYS Cam-clay model (**Eq. (A2.77)**) is given by the following equation:

$$\overset{\circ}{\boldsymbol{T}}' = (\tilde{K} - \frac{2}{3}\tilde{G})(\mathrm{tr}\boldsymbol{D})\boldsymbol{I} + 2\tilde{G}\boldsymbol{D} - \frac{(6\tilde{G}\hat{\boldsymbol{\eta}} \cdot \boldsymbol{D} - \tilde{K}\alpha\,\mathrm{tr}\boldsymbol{D})(6\tilde{G}\hat{\boldsymbol{\eta}} - \tilde{K}\alpha\boldsymbol{I})}{12\eta^{*2}\tilde{G} + \tilde{K}\alpha^2 + h} \qquad \text{(A2.81)}$$

In which

$$\begin{aligned} \alpha &= \mathrm{M}_a{}^2 - \eta^2 \\ h &= Jp'\frac{\mathrm{M}^2 + \eta^{*2}}{\mathrm{MD}}(\mathrm{M}_s{}^2 - \eta^2) \end{aligned} \qquad \text{(A2.82)}$$

Notice that soil parameters that make the denominator of Λ in **Eq. (A2.76)** to be positive for arbitrary stress state is called Cam-clay parameters (Asaoka et al., 1994), then the loading criterion

$$\Lambda > 0 \tag{A2.83}$$

can be rewritten simply in terms of the numerator of Λ as follows:

$$\begin{cases} \text{Loading} \quad (\boldsymbol{D}^p \neq \boldsymbol{0}) \quad \text{when} \quad \dfrac{\partial f}{\partial \boldsymbol{T}'} \cdot \boldsymbol{E}\boldsymbol{D} > 0 \\ \text{Unloading} \, (\boldsymbol{D}^p = \boldsymbol{0}) \quad \text{when} \quad \dfrac{\partial f}{\partial \boldsymbol{T}'} \cdot \boldsymbol{E}\boldsymbol{D} < 0 \end{cases} \tag{A2.84}$$

(9) Additional evolutional rule of structure

In the previous definition of evolutional rule of structure, it is assumed that the structure is independent of unloading. However, according to the recent researches the structure will not decay but increase (upgradation of structure). Then the following evolutional rule is adopted:

$$\dot{R}^* = JU^* \left\{ (1 - c_s)\left(-D_v^p\right) + c_s \sqrt{\frac{2}{3}} \left\| \boldsymbol{D}_s^p \right\| \right\}$$

$$\begin{cases} -D_v^p > 0 : \ \text{compression} \\ -D_v^p < 0 : \ \text{expansion} \end{cases} \tag{A2.85}$$

Where c_s is a material constant that represents the ratio of plastic shear deformation to plastic compression deformation ($0 \le c_s \le 1$). $c_s \to 0$ for clay which means the decay of structure is mainly due to compression and $c_s \to 1$ for sand which means the decay of structure is mainly due to shear deformation.

When there is plastic expansion ($-D_v^p < 0$) it is possible for $\dot{R}^*$ to be negative. In other words, the upgradation of structure is possible when the plastic volumetric expansion exists.

A2.5 CHARACTERISTICS OF SYS CAM-CLAY MODEL

In conventional critical state soil mechanics, the critical state stress ratio M is the threshold both for hardening and softening and for plastic volumetric compression and plastic volumetric expansion. Therefore, hardening is always associated with plastic volumetric compression and softening is always associated with plastic volumetric expansion. Furthermore, the threshold value M is constant throughout the loading procedure. However, when the evolutional rules of the soil structure and overconsolidation are considered, the threshold between hardening and softening given by M_s is a variable of ongoing plastic deformation. The same is true for the threshold between plastic volumetric compression and plastic volumetric expansion. When the rotational hardening rule is considered, the evolution of anisotropy gives the threshold

M_a also as a variable of ongoing plastic deformation. Furthermore, **Eqs. (A2.72)** and **(A2.73)** suggest that it is not always trivial whether M_s is larger than M_a, or not. In other words, hardening is possible even with plastic volumetric expansion and softening is also possible during plastic volumetric compression. In this section, the effects of structure, overconsolidation and anisotropy will be illustrated one by one with an emphasis on the relation between M_s and M_a.

The soil parameters employed in the calculation is shown in **Table A2.1**.

Table A2.1 Soil parameters of a typical clay

〈Elastoplastic parameters〉	
Compression index $\tilde{\lambda}$	0.250
Swelling index $\tilde{\kappa}$	0.045
Critical state constant M	1.25
Intercept of NCL* N	2.73
Poisson's ratio υ	0.3
〈Evolutional parameters〉	
Degradation index of structure a ($b = c = 1.0$)	0.5
Normal consolidation index m	10.0
Rotational hardening index b_r	0.001
Rotational hardening limit constant m_b	1.0

∗ specific volume on NCL of fully remolded when q = 0, p' =

(1) Effect of overconsolidation (Subloading yield surface)

Assuming that the soil is under overconsolidation ($0 < R < 1$) and fully remolded ($R^* = 1$) state and there is no development of anisotropy ($br = 0$), then the threshold between hardening and softening M_s in **Eq. (A2.72)** is expressed as follows (although only the behavior of clay is discussed, there is no difference when sand is adopted):

$$M_s^2 = M_a^2 + MD\frac{U}{R}\sqrt{6\eta^{*2} + \frac{1}{3}(M_a^2 - \eta^2)^2} \qquad \text{(A2.86)}$$

Because U is a positive scalar function, it is obvious that M_s is larger than M_a, that is:

$$M_s \geq M_a \qquad \text{(A2.87)}$$

In other words, there is a new region where plastic volumetric expansion accompanying hardening exists for the fully remolded and overconsolidated soil, as shown in **Figure**

A2.38. Based on **Eq. (A2.59)**, the concrete form of U/R is as follows:

$$\frac{U}{R} = -\frac{1}{\mathrm{D}}\frac{m\ln R}{R} \tag{A2.88}$$

From **Eq. (A2.88)**, it is obvious that U/R is monotonically decreasing as R increases and becomes 0 when $R=1$. Therefore, as the loss of overconsolidation due to ongoing plastic deformation develops, M_s descends gradually toward M_a and finally keeps consistent with M_a.

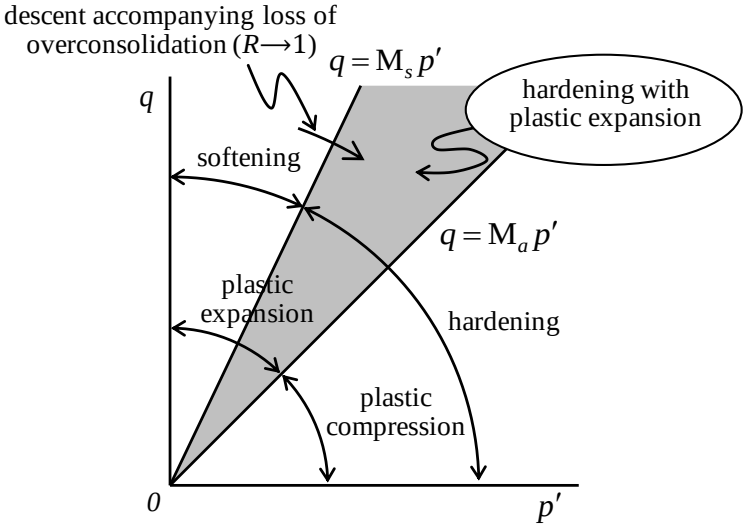

Fig. A2.38 Change of M_s based on the effect of Subloading yield surface (plastic expansion together with hardening)

Table A2.2 Initial values

Vertical effective stress σ_{v0}' (kPa)	98.1
Structure $1/R_0$ *	1.00
OCR $1/R_0$	8.00
Anisotropy $\zeta_0 = \sqrt{3/2\,\boldsymbol{\beta}_0 \cdot \boldsymbol{\beta}_0}$	0.00
Coefficient of lateral stress $\sigma_{h0}'/\sigma_{v0}'$	1.00

Figure A2.39 presents the simulation result of drained behavior on fully remolded and overconsolidated soil, which corresponds to the experimental result shown in **Figure A2.13**. The initial values are shown in **Table A2.2**. The characteristic for overconsolidated soil that expansion together with hardening is clearly shown in **Figure**

2.39. In other words, as discussed above, Cam-clay model with introduction of Subloading yield surface is able to reproduce:

(1) elastoplastic behavior inside the normal yield surface;

(2) plastic expansion together with hardening.

Figure A2.40 illustrates the enlarging/diminishing of Subloading and normal yield surfaces and change of borderline between hardening and softening $q = \mathrm{M}_s p'$ in q - p' space. The corresponding structure $1/R^*$ and OCR $1/R$ at different stages are also presented. When

$$\mathrm{M}_a < \eta < \mathrm{M}_s \tag{A2.89}$$

the behavior of plastic expansion together with hardening does occur. Even thought the state of $\mathrm{M}_a < \eta < \mathrm{M}_s$ has already reaches just after stage (b), there is total volumetric expansion until stage (c) where we should take the elastic volumetric compression due to increase of p' into consideration.

(2) Effect of structure (Superloading yield surface)

Assuming that the soil is under highly structured ($0 < R^* < 1$) and normally consolidated ($R = 1$) state and there is no development of anisotropy ($br = 0$), then the threshold between hardening and softening M_s in **Eq. (A2.72)** is expressed as follows (the behavior of clay is discussed here):

$$\mathrm{M}_s{}^2 = \mathrm{M}_a{}^2 - \mathrm{MD}\frac{U^*}{R^*}\sqrt{6\eta^{*2} + \frac{1}{3}(\mathrm{M}_a{}^2 - \eta^2)^2} \tag{A2.90}$$

Because U^* is a positive scalar function, it is obvious that M_s is smaller than M_a, that is:

$$\mathrm{M}_s \le \mathrm{M}_a \tag{A2.91}$$

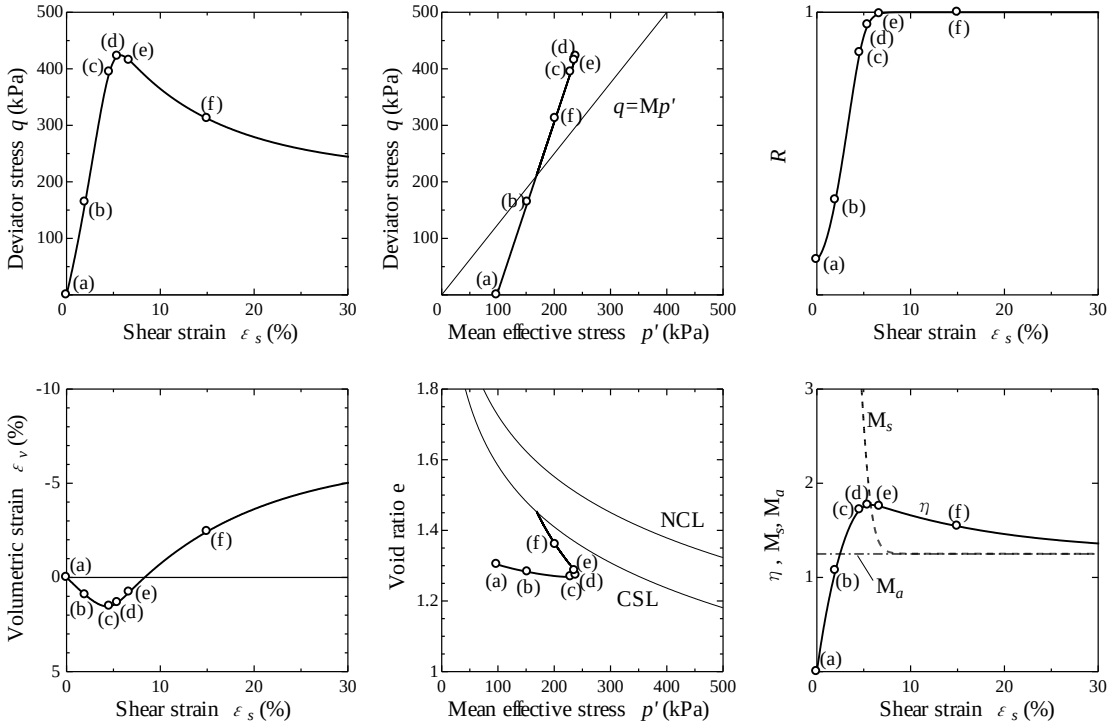

Fig. A2.39 Simulation of drained behavior of fully remolded and overconsolidated soil

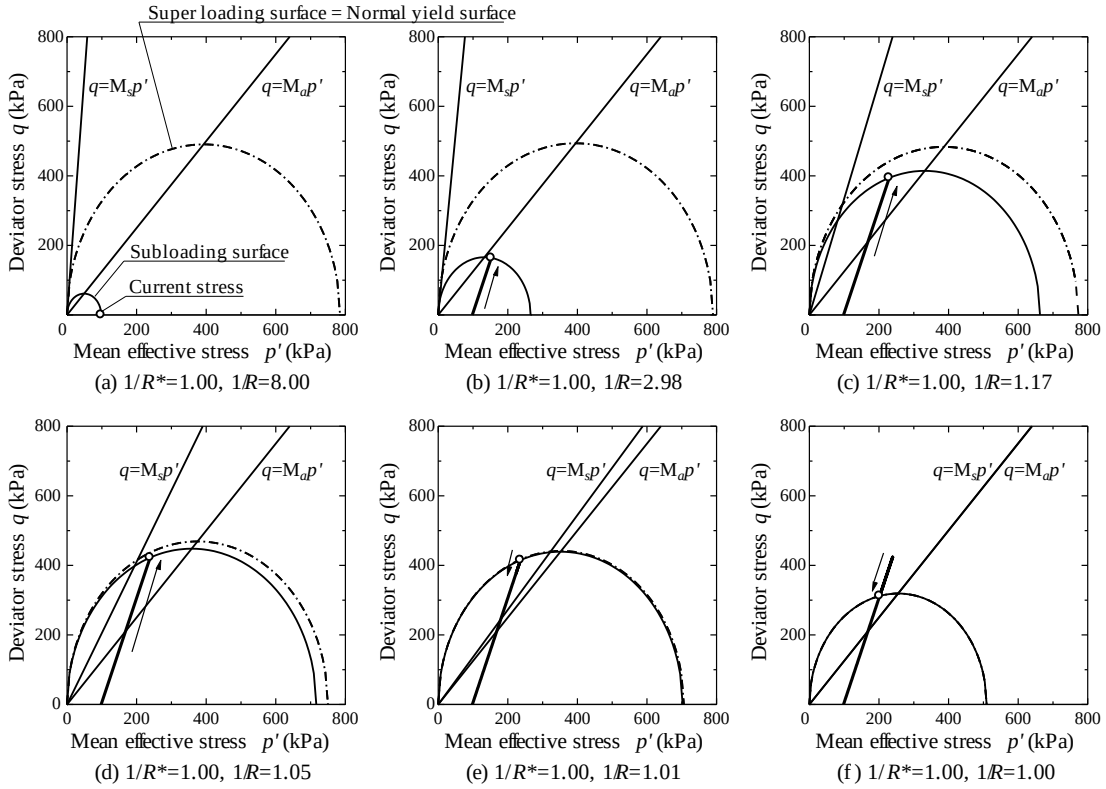

Fig. A2.40 Enlarging/diminishing of Subloading and normal yield surfaces, and change of M_s

In other words, there is a new region where plastic volumetric compression accompanying softening exists for the highly structured and normally consolidated soil, as shown in **Figure A2.41**. Based on **Eq. (A2.62)**, the concrete form of U^*/R^* where $b=1$ for simplicity is as follows:

$$\frac{U^*}{R^*}=\frac{a}{\mathrm{D}}(1-R^*)^c \qquad \text{(A2.92)}$$

From **Eq. (A2.92)**, it is obvious that U^*/R^* is monotonically increasing as R^* increases and becomes 0 when $R^*=1$. Therefore, as the decay of structure due to ongoing plastic deformation develops, M_s ascends gradually toward M_a and finally keeps consistent with M_a.

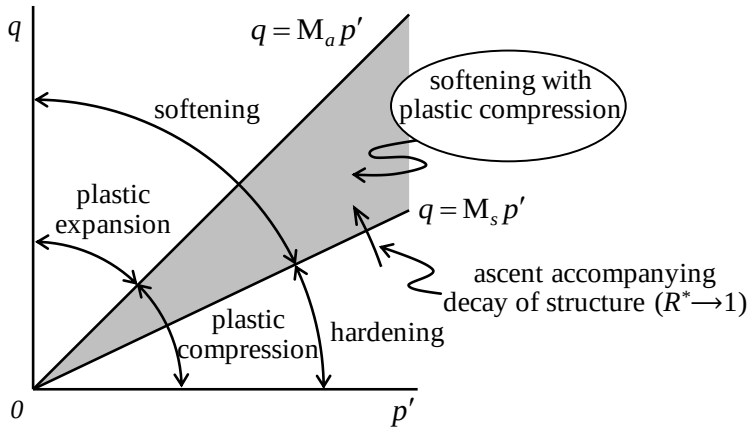

Fig. A2.41 Change of M_s based on the effect of Superloading yield surface (plastic compression together with softening)

Table A2.3 Initial values

Vertical effective stress σ_{v0}' (kPa)	294
Structure $1/R_0$ *	4.59
OCR $1/R_0$	3.80
Anisotropy $\zeta_0=\sqrt{3/2\,\boldsymbol{\beta}_0\cdot\boldsymbol{\beta}_0}$	0.009
Coefficient of lateral stress $\sigma_{h0}'/\sigma_{v0}'$	1.00

Figure A2.42 presents the simulation result of undrained behavior on highly structured and normally consolidated soil, which corresponds to the experimental result shown in **Figure A2.19**. The initial values are shown in **Table A2.3**. NCL and CSL are also drawn in **Figure 2.42**. As discussed above, Cam-clay model with introduction of Superloading yield surface is able to reproduce:

(1) the behavior outside of the impossible region of fully remolded soil;

(2) plastic compression together with softening.

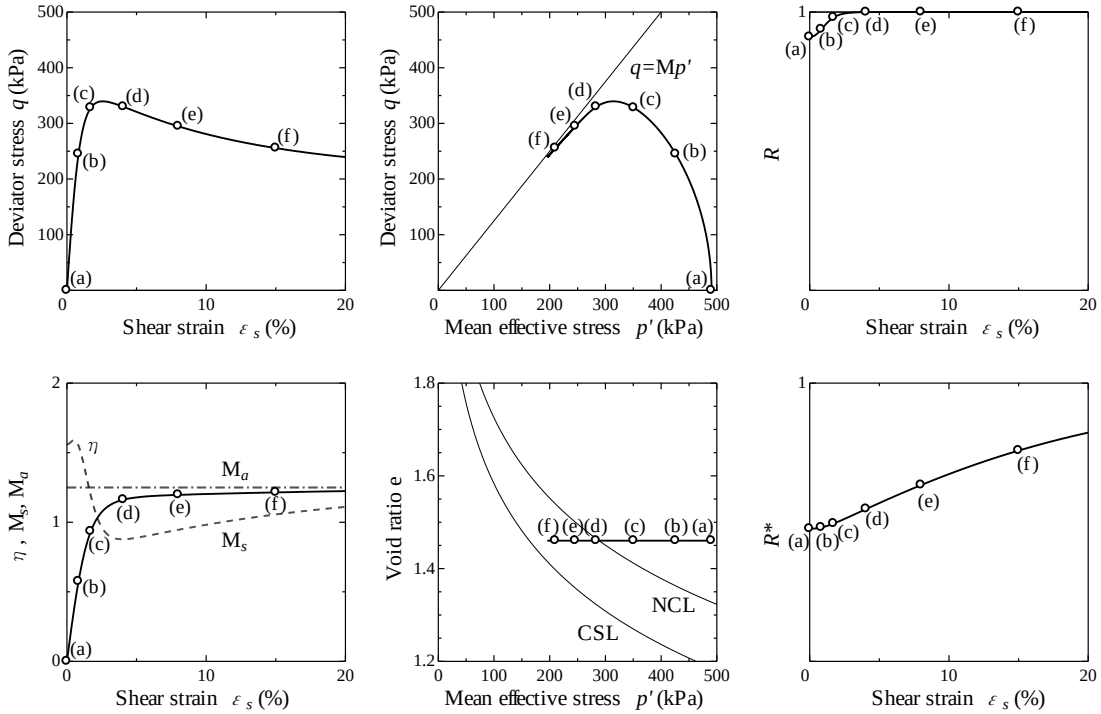

Fig. A2.42 Simulation of undrained behavior of highly structured and normally consolidated soil

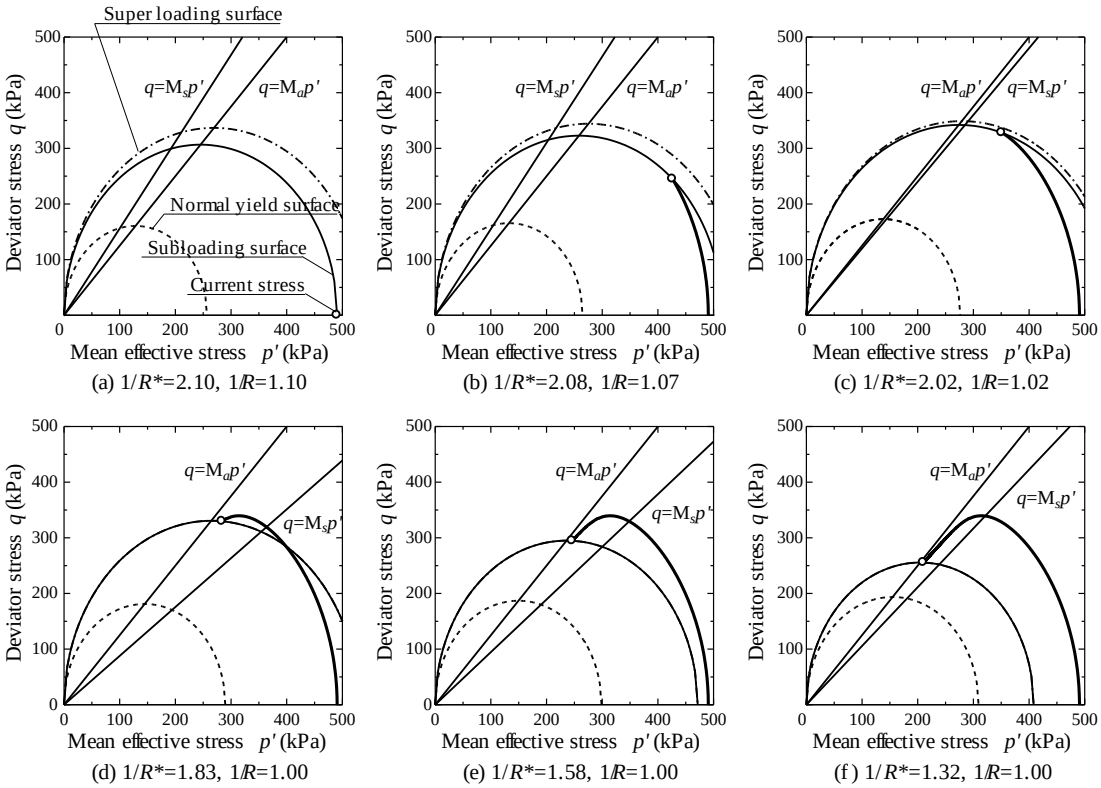

Fig. A2.43 Enlarging/diminishing of Superloading and normal yield surfaces, and change of M_s

Figure A2.43 illustrates the enlarging/diminishing of Superloading and normal yield surfaces and change of borderline between hardening and softening $q = \mathrm{M}_s p'$ in q - p' space. The corresponding structure $1/R^*$ and OCR $1/R$ at different stages are also presented. When

$$\mathrm{M}_s < \eta < \mathrm{M}_a \tag{A2.93}$$

the behavior of plastic compression together with softening does occur. In addition, as can be seen if the soil is under both structured and overconsolidated state, M_s may be above M_a or below M_a as the loss of overconsolidation and decay of structure develop accompanying ongoing plastic deformation. The details will be discussed in the next section about the difference between sand and clay.

(3) Effect of anisotropy (η^* and rotational hardening)

The effect of the evolution of anisotropy upon M_s and M_a is clearly observed when fully remolded and normally consolidated state ($R^* = 1, R = 1$) soil is considered. According to **Eq. (A2.68)**, M_a is always larger than critical state constant M as long as there is anisotropy and the value range of M_a is determined by **Eq. (A2.70)**.

On the other hand, M_s is given by the following equation:

$$\mathrm{M}_s{}^2 = \mathrm{M}_a{}^2 + br\frac{4\mathrm{M}\eta^{*2}}{\mathrm{M}^2 + \eta^{*2}}\left(m_b\eta^* - \sqrt{\frac{3}{2}}\hat{\boldsymbol{\eta}}\cdot\boldsymbol{\beta}\right) \tag{A2.94}$$

here

$$m_b\eta^* - \sqrt{\frac{3}{2}}\hat{\boldsymbol{\eta}}\cdot\boldsymbol{\beta} \geq \|\boldsymbol{\beta}\|\eta^* - \sqrt{\frac{3}{2}}\hat{\boldsymbol{\eta}}\cdot\boldsymbol{\beta} = \|\boldsymbol{\beta}\|\eta^*\left(1 - \frac{\hat{\boldsymbol{\eta}}}{\|\hat{\boldsymbol{\eta}}\|}\cdot\frac{\boldsymbol{\beta}}{\|\boldsymbol{\beta}\|}\right) \geq 0 \tag{A2.95}$$

then

$$\mathrm{M}_a \leq \mathrm{M}_s \tag{A2.96}$$

Which indicates that hardening is still possible during plastic volumetric expansion when the stress ratio satisfies $\mathrm{M}_a < \eta < \mathrm{M}_s$. Since hardening during plastic volumetric expansion at high stress ratio is a typical nature of overconsolidated soils, it is called the "quasi-overconsolidation effect". In other words, when high levels of stress-induced anisotropy develop, normally consolidated soil still exhibits overconsolidation-like behavior at high stress ratio.

Here, the important thing is that all the effects on the movements of M_s and M_a are the combined effects of the following three factors: decay of the structure, loss of

overconsolidation and evolution of anisotropy that occur as plastic deformation proceeds.

A2.6 DIFFERENCE BETWEEN SAND AND CLAY

(1) Classification of soil states respect to structure and overconsolidation

According to the degree of structure and overconsolidation, the soil state can be divided into the following 4 categories:

(1) structured and overconsolidated state $(0<R^*<1,\ 0<R<1)$

(2) structured and normally consolidated state $(0<R^*<1,\ R=1)$

(3) non-structured and overconsolidated state $(R^*=1,\ 0<R<1)$

(4) non-structured and normally consolidated state $(R^*=1,\ R=1)$

Soils under states ①, ② or ③ will gradually approach to and finally reach state ④ as the ongoing plastic deformation develops.

Naturally sedimentary soils including clay and sand are generally at state ①, namely a highly structured and more or less overconsolidated state, and due to the ongoing plastic deformation turn to state ④, namely a normally consolidated state without structure. In principle there are two different paths for the soils from the initial state to the final state. One is a path passing through an almost normally consolidated state with structure, and the other through an overconsolidated state without structure.

Route C: ① overconsolidation & structure ⟶ ② normal consolidation & structure ⟶ ④ normal consolidation & non-structure

Route S: ① overconsolidation & structure ⟶ ③ overconsolidation & non-structure ⟶ ④ normal consolidation & non-structure

As can be seen, Route C represents that the loss of overconsolidation is earlier than the decay of structure as the ongoing plastic deformation proceeds. Contrarily, Route S represents that the decay of structure is earlier than the loss of overconsolidation.

The conclusion that typical clay is considered to follow Route C and typical sand is considered to follow Route S will be presented in advance, which is shown in **Figure A2.44** (The evolutional rate of anisotropy also influences the behavior of sand and clay, but it is out of scope).

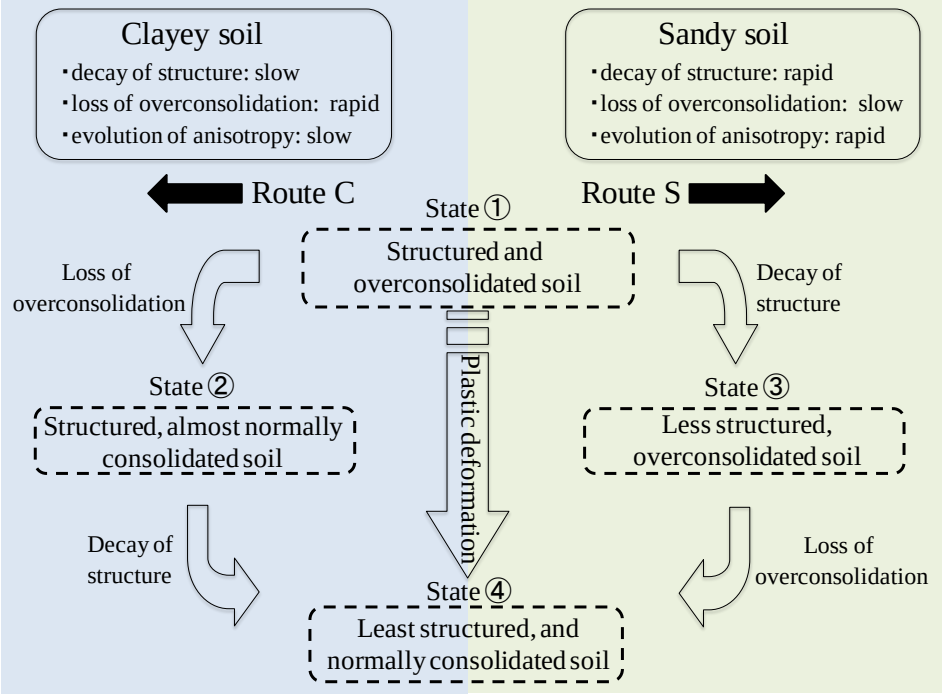

Fig. A2.44 Route C and Route S

(2) Undrained behavior of highly structured and overconsolidated clay and medium dense sand

The above conclusion can be observed from **Figures A2.45** and **A2.46** which depict undrained behaviors of highly structured and overconsolidated clay and medium dense sand respectively (assume that both clay and sand are under state ①). As can be seen, the behavior of clay follows:

(I) plastic compression & hardening; (II) plastic expansion & hardening; (III) plastic compression & softening; and the behavior of sand follows:

(I) plastic compression & hardening; (II) plastic compression & softening; (III) plastic expansion & hardening;

From section A2.5, it is known that "plastic expansion & hardening" is a typical response due to the loss of overconsolidation and "plastic compression & softening" is a typical response due to the decay of structure. Therefore, the structured and overconsolidated clay under state ① firstly loses the overconsolidation to state ② and then degrades the structure until state ④, namely Route C; while the medium dense sand under state ① firstly degrades the structure to state ③ and then loses the overconsolidation until state ④, namely Route S.

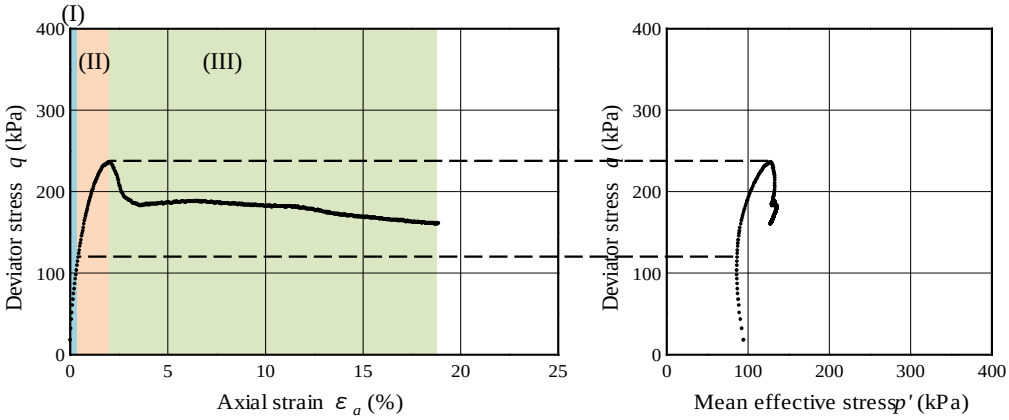

Fig. A2.45 Triaxial undrained behavior of highly structured and overconsolidated clay (after Asaoka et al., 2000)

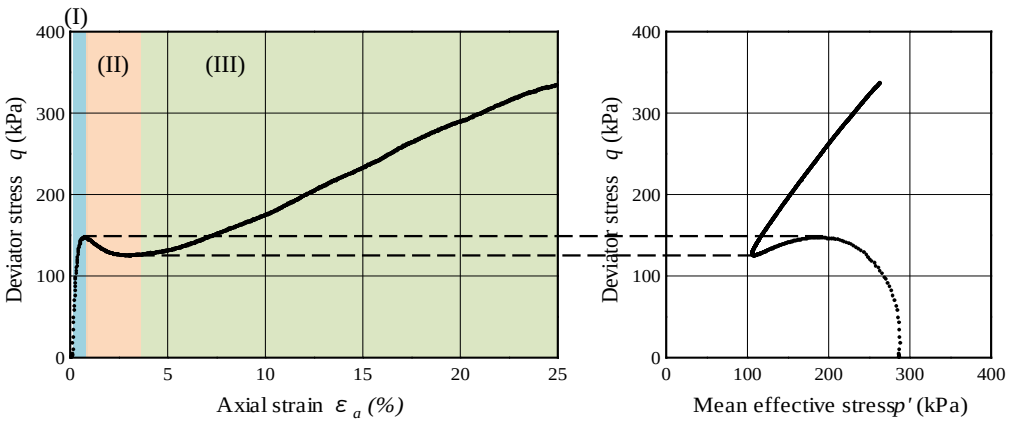

Fig. A2.46 Triaxial undrained behavior of dense sand (after Nakano et al., 2004)

(3) Simulation of clay and sand based on SYS Cam-clay model

In SYS Cam-clay model, the degradation rate of overconsolidation is dominated by a parameter m in the evolution law for R, while the structure decay rate is dominated by the parameters a, b and c (of which b and c generally have a value 1) in the evolutional law for R^*. Depending on the value differences on these parameters, the model is therefore capable of describing a development either on Route C or on Route S. In other words, there is no need to provide separate model for clay and for sand. In the following, the numerical simulations will be carried out to reproduce the undrained shear behaviors of highly structured and overconsolidated clay and medium dense sand

in **Figures. A2.45** and **A2.46** respectively.

(3-1) Simulation of undrained behavior of highly structured and overconsolidated clay

The elastoplastic parameters and evolution parameters are same as those in **Table A2.1**. Using these evolution parameters, while a rapid loss in overconsolidation per unit plastic deformation can be seen, there is virtually no decay in soil structure. The same is also evident from the calculation result. Thus, the parameters in **Table A2.1** are indicative of typical clay. The initial values, prior to subjecting it to an undrained triaxial compression test, are shown in **Table A2.4**, which indicates a highly structured and overconsolidated state.

Table A2.4 Initial values of highly structured and overconsolidated clay

Vertical effective stress σ_{v0}' (kPa)	98.1
Structure $1/R_0$ *	4.50
OCR $1/R_0$	2.20
Anisotropy $\zeta_0 = \sqrt{3/2\boldsymbol{\beta}_0 \cdot \boldsymbol{\beta}_0}$	0.00
Coefficient of lateral stress $\sigma_{h0}'/\sigma_{v0}'$	1.00

The corresponding undrained behavior employing SYS Cam-clay model is shown in **Figure A2.47**, where the loss of overconsolidation ($R \to 1$) develops firstly and then the decay of structure ($R^* \to 1$) slowly proceeds. Another important point is that because of the residual structure that remains even after the loss of overconsolidation, the clay in the latter half of the test displays a softening behavior together with plastic compression. This is called "rewinding" (Tatsuoka and Kohata, 1995), which corresponds to **Figure A2.45** and **Figure A2.48** demonstrates the effective stress path, enlarging/diminishing of three yield surfaces and changes of M_a and M_s. Given that initially $\mathrm{M}_s > \mathrm{M}_a$, even at a point where

$$\mathrm{M}_a p' < q < \mathrm{M}_s p' \qquad \text{(A2.97)}$$

The clay will still go on exhibiting hardening, in spite of the plastic expansion that accompanies this. However, the loss of overconsolidation in the clay then proceeds rapidly, and as M_s steeply decreases to a level where $\mathrm{M}_s < \mathrm{M}_a$, the stress eventually comes to a state

$$\mathrm{M}_s p' < q < \mathrm{M}_a p' \qquad \text{(A2.98)}$$

where the behavior switches to softening together with plastic compression. If the

plastic deformation is allowed to proceed further, the decay of structure (approach between Superloading yield surface and normal yield surface) also develops and M_s will rise again. Finally, M_s will of course settle at $M_s = M_a$, and the clay will attain a steady state of $q = M_a p'$. In other words, stress, volume and excess pore water pressure will all cease to vary in response to the ongoing development of shear strain at $q = M_a p'$.

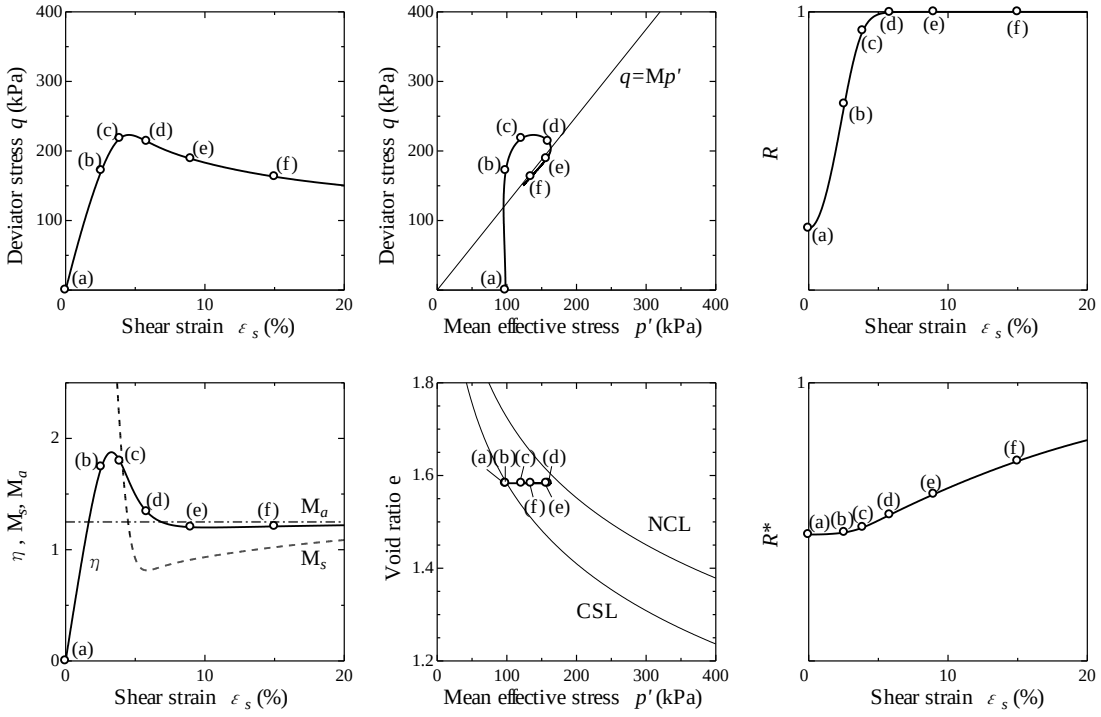

Fig. A2.47 Simulation of undrained behavior of highly structured and overconsolidated clay

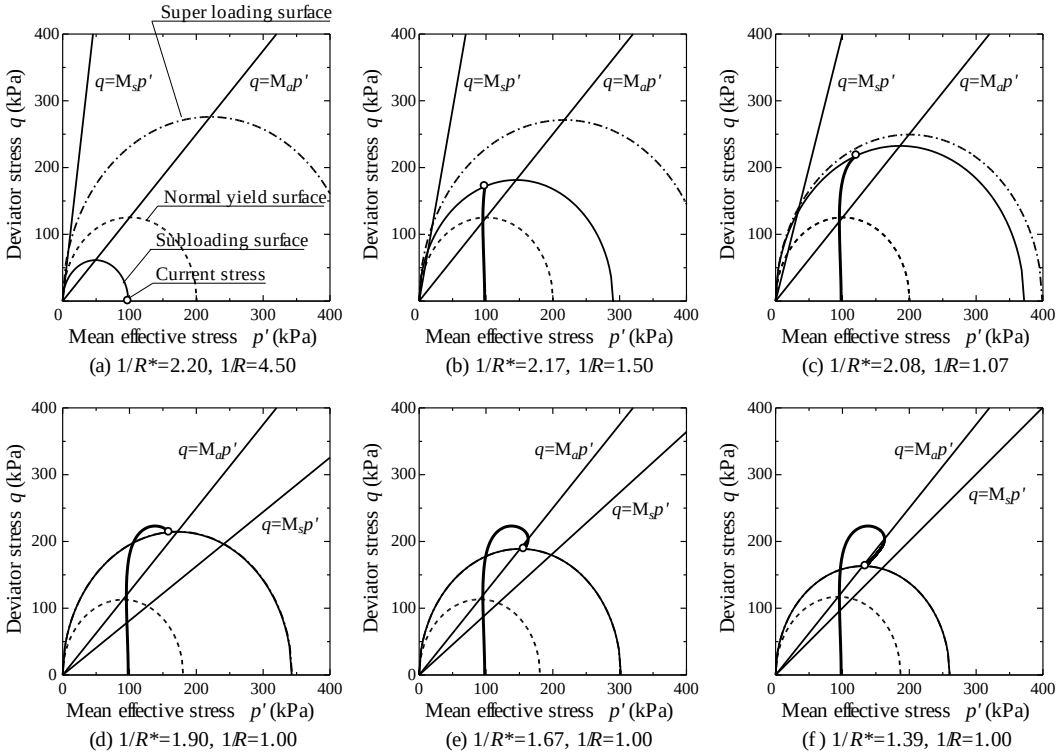

Fig. A2.48 Enlarging/diminishing of three yield surfaces and changes of M_a and M_s

Figure A2.49 gives the movement of M_s of the highly structured and overconsolidated clay. As can be seen, the typical clay exhibits plastic expansion accompanying hardening firstly and then plastic compression accompanying softening.

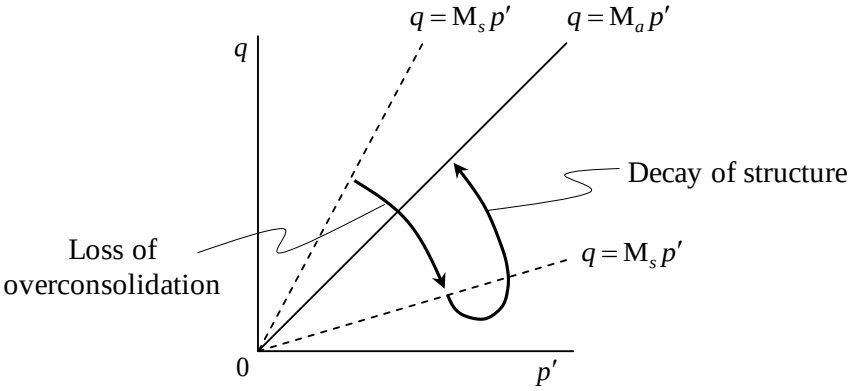

Fig. A2.49 Movement of M_s

(3.2) Simulation of medium dense sand

The elastoplastic parameters and evolution parameters are shown in **Table A2.5**. Using these evolution rule parameters, it can be seen that while a rapid collapse in

structure occurs per unit plastic deformation, there is next to no loss in overconsolidation. This will also be evident from the calculation. The parameters in **Table A2.5** are thus indicative of typical sand. The initial conditions of this sand, prior to its investigation in an undrained triaxial compression test, are shown in **Table A2.6**. The initial values indicate a highly structured and overconsolidated state and the reason why such sand is medium dense sand will be clarified in section A2.7.

The corresponding undrained behavior employing SYS Cam-clay model is shown in **Figure A2.50**, where the decay of structure ($R^* \to 1$) develops firstly and then the loss of overconsolidation ($R \to 1$) slowly proceeds. The phenomenon that plastic compression together with softening occurs firstly and then plastic expansion together with hardening is observed in the latter half of simulation corresponds to the experimental result in **Figure A2.46**. **Figure A2.51** demonstrates the effective stress path, enlarging/diminishing of three yield surfaces and changes of M_a and M_s. Given that initially $\mathrm{M}_s < \mathrm{M}_a$, even at a point where

$$\mathrm{M}_s p' < q < \mathrm{M}_a p' \qquad \text{(A2.99)}$$

the sand will still go on exhibiting softening , in spite of the plastic compression that accompanies this. However, the decay of structure (approach between Superloading yield surface and normal yield surface) in the sand then proceeds rapidly, and as M_s steeply increases to a level where $\mathrm{M}_a < \mathrm{M}_s$, the stress eventually comes to a state

$$\mathrm{M}_a p' < q < \mathrm{M}_s p' \qquad \text{(A2.100)}$$

where the behavior switches to hardening together with plastic expansion. If the plastic deformation is allowed to proceed further, the loss of overconsolidation (approach between Superloading yield surface and Subloading yield surface) also develops and M_s will fall again. Finally, M_s will of course settle at $\mathrm{M}_s = \mathrm{M}_a$, and the sand will attain a steady state of $q = \mathrm{M}_a p'$. In other words, stress, volume and excess pore water pressure will all cease to vary in response to the ongoing development of shear strain at $q = \mathrm{M}_a p'$.

Figure A2.52 gives the movement of M_s of the medium dense sand. As can be seen, compared with the movement of M_s of the typical clay in **Figure A2.49**, the typical sand exhibits plastic compression accompanying softening firstly and then plastic expansion accompanying hardening.

Table A2.5 Elastoplastic and evolution parameters of a typical sand

〈Elastoplastic parameters〉	
Compression index $\tilde{\lambda}$	0.05
Swelling index $\tilde{\kappa}$	0.012
Critical state constant M	1.0
Intercept of NCL* N	1.97
Poisson's ratio υ	0.3
〈Evolutional parameters〉	
Degradation index of structure a $(b = c = 1.0)$	2.75
Normal consolidation index m	0.08
Rotational hardening index b_r	3.50
Rotational hardening limit constant m_b	0.7

∗ specific volume on NCL of fully remolded when q = 0, p' =

Table A2.6 Initial values of a medium dense sand

Vertical effective stress σ_{v0}' (kPa)	294
Structure $1/R_0$ *	4.59
OCR $1/R_0$	3.80
Anisotropy $\zeta_0 = \sqrt{3/2\boldsymbol{\beta}_0 \cdot \boldsymbol{\beta}_0}$	0.009
Coefficient of lateral stress $\sigma_{h0}'/\sigma_{v0}'$	1.00

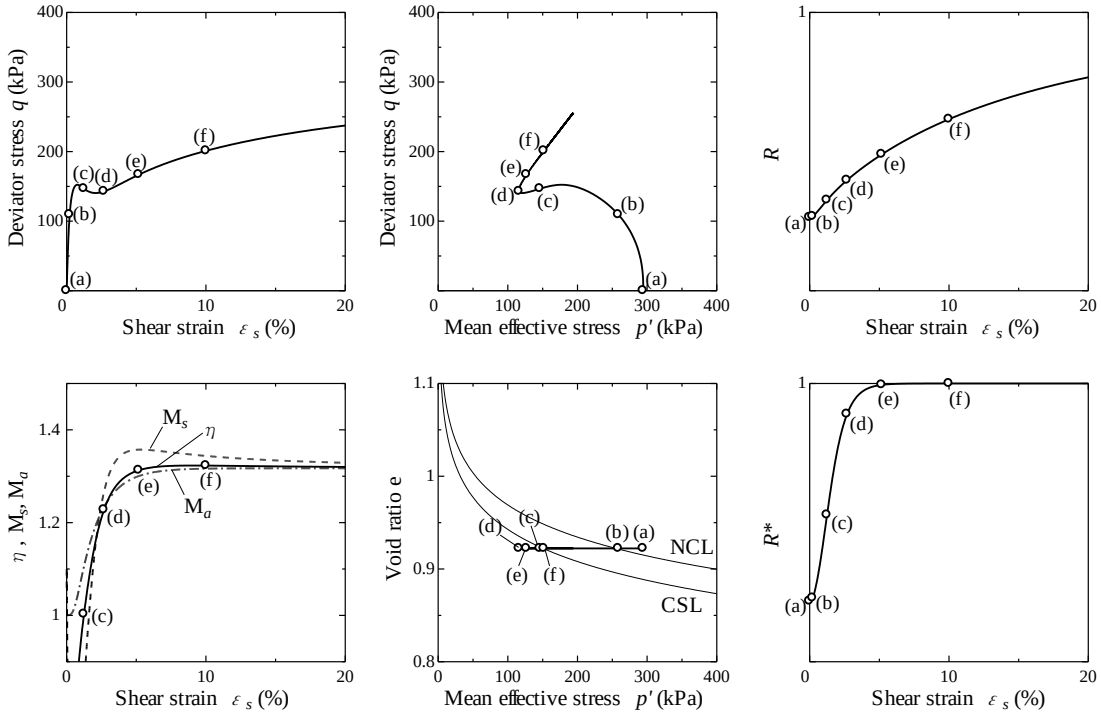

Fig. A2.50 Simulation of undrained behavior of medium dense sand

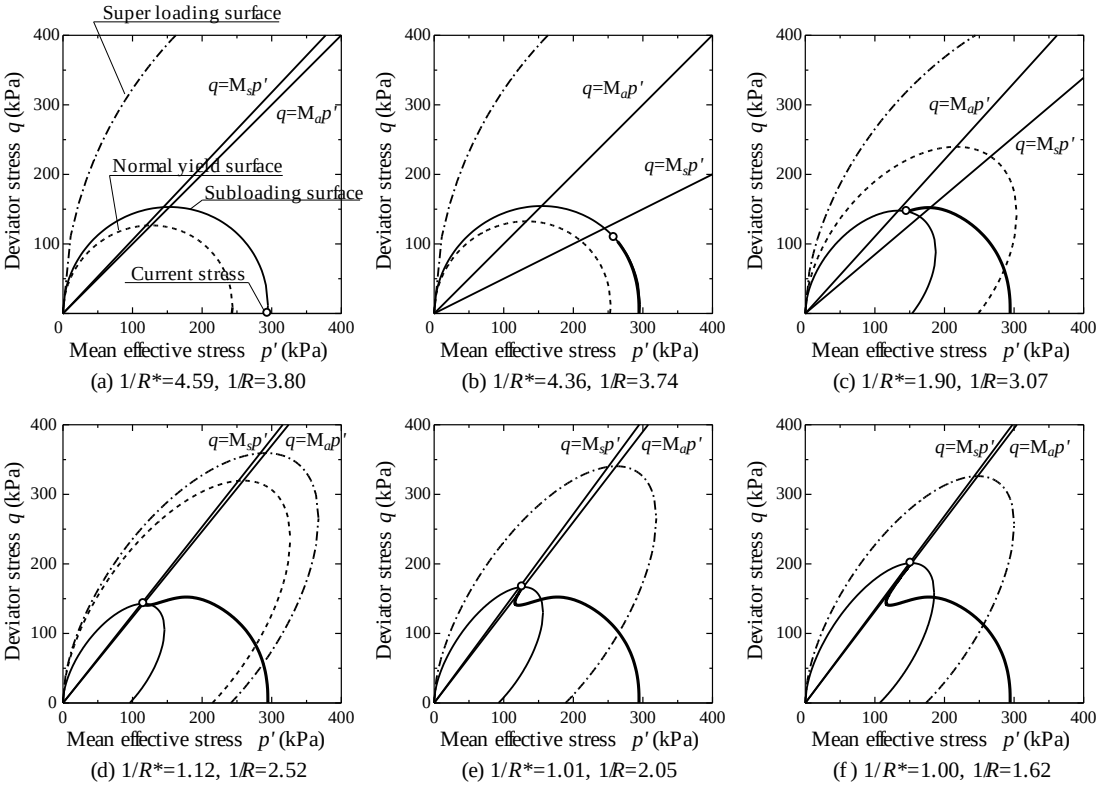

Fig. A2.51 Enlarging/diminishing of three yield surfaces and changes of M_a and M_s

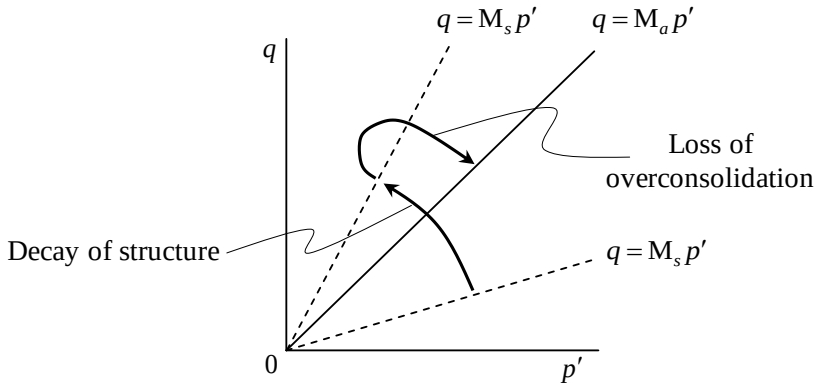

Fig. A2.52 Movement of M_s

The brief conclusion can be summed up as: when the overconsolidated and highly structured soil in State ① turns to be normally consolidated and fully remolded soil in State ④, the loss of overconsolidation outruns the decay of structure in the typical clay, namely Route C as shown next; whereas in typical sand the opposite is true: the decay of structure proceeds faster than the loss of overconsolidation, namely Route S as shown next. By manipulating the parameters for the rates of evolution of these two states of structure and overconsolidation, it becomes possible to reproduce the behaviors of typical sands and typical clays by one single constitutive model.

Route C: ① overconsolidation & structure ⟶ ② normal consolidation & structure ⟶ ④ normal consolidation & non-structure

Route S: ① overconsolidation & structure ⟶ ③ overconsolidation & non-structure ⟶ ④ normal consolidation & non-structure

In addition, it is not impossible to conceive of a soil in which loss of overconsolidation and decay of structure might proceed together at the same rate, with the result that the state of soil would change directly from ① to ④, without passing through either state ② or state ③. A clayey sand or a sandy clay might perhaps fit this description. That is why the adjective "typical" is attached to clay and sand in the above conclusion statement. It is both difficult and unnecessary to draw an absolutely precise dividing line between clay and sand.

A2.7 COMPACTION/Ddensification OF LOOSE SAND

(1) Mechanism of volume change (compression) that differs from $\mathrm{e} - \log p'$

Prager's consistency condition **Eq. (A2.54)** can be rewritten as:

$$\dot{\varepsilon}_v^p (= -J\,\mathrm{tr}\boldsymbol{D}^p) = \dot{f} + \mathrm{MD}\frac{\dot{R}^*}{R^*} - \mathrm{MD}\frac{\dot{R}}{R} \qquad \text{(A2.101)}$$

which indicates that

(1) the decay of the soil structure ($\dot{R}^* > 0$, $R^* \to 1$) acts in the direction of the soil's plastic volume compression;

(2) the loss of overconsolidation ($\dot{R} > 0$, $R \to 1$) acts in the direction of the soil's plastic volume expansion.

(3)

However, plastic compression or plastic expansion is determined by the relationship between η and M_a. There is also possibility that the decay of structure accompanies plastic expansion and the loss of overconsolidation accompanies plastic compression.

The soil mechanics for volume change obtained from **Eq. (A2.14)**, that is $\dot{\varepsilon}_v^p = \dot{f}$, can be called "e-log$p'$" soil mechanics. The volume change due to decay of structure or loss of overconsolidation is regarded to be another volume change mechanism which is different from $\mathrm{e} - \log p'$ mechanism. The volume change analysis based on the new mechanism including dilatancy will be carried out in the following:

According to the completely inverse process of obtaining Cam-clay model's yield surface or plastic potential surface (**Eq. (A2.14)**) from **Eq. (A2.8)**, the reverse result that is equivalent to **Eq. (A2.8)** can be obtained from Subloading yield surface (**Eq. (A2.51)**) where the current stress state locates:

$$\mathrm{v} = \mathrm{N} - \tilde{\lambda}\ln p' - (\tilde{\lambda} - \tilde{\kappa})\ln\frac{\mathrm{M}^2 + \eta^{*2}}{\mathrm{M}^2} - (\tilde{\lambda} - \tilde{\kappa})\ln R^* + (\tilde{\lambda} - \tilde{\kappa})\ln R \qquad \text{(A2.102)}$$

If the 4th and 5th term is removed from **Eq. (A2.102)**, the equation represents the roscoe surface of modified Cam-clay model. Therefore, the highly structured soil ($0 < R^* < 1$) locates the upper side of the roscoe surface. In other words, the stress state can reach the impossible region of fully remolded soil. Contrarily, the overconsolidated soil ($0 < R < 1$) locates the lower side of the roscoe surface. In other words, even if the stress state is same, various void ratio will be obtained due to the degree of soil structure and the ratio of overconsolidation. From **Eq. (A2.102)**, in order to reduce the void ratio (specific volume), it is necessary to make the soil structure decayed or the soil overconsolidated.

The densification due to the decay of structure or the increase of overconsolidation may

occur in both clay and sand. However, for clay there are a relatively smaller decay rate of structure and a larger loss of overconsolidation, and thus the densification through large amount of loading or action of unloading is much difficult to realize. For sand, the decay of structure is easy to occur and the loss of overconsolidation is difficult, so the densification can be realized by small-amplitude repeated loading, which corresponds to the compaction of loose sand. As the phenomenon of the densification of drained loose sand under repeated shear stress is a complicated thing to grasp, let's explain it in the following with the aid of numerically computated examples obtained from SYS Cam-clay model.

(2) Compaction/Densification of loose sand under repeated drained shear stress application

It will be recalled that the sand in section A2.6 was initially in a medium dense state (State ①), and that the investigation concerned the undrained application of shear stress. The sand under consideration here is the same as in section A2.6 (all the parameters are same as those in **Table A2.5**), but its initial state is different, in that before undergoing repeated shear stress under drained conditions it is as indicated in **Table A2.7**. The significance of this is that, in the terms of section A2.6, the sand in the present test begins in the "normally consolidated and structured state," namely State ②. It will be easy to see that the values in **Table A2.7** correspond to the classic initial considerations for loose sand.

Table A2.7 Initial values of a loose sand

Vertical effective stress σ_{v0}' (kPa)	294
Structure $1/R_0$ *	130
OCR $1/R_0$	1.00
Anisotropy $\zeta_0 = \sqrt{3/2\boldsymbol{\beta}_0 \cdot \boldsymbol{\beta}_0}$	0.00
Coefficient of lateral stress $\sigma_{h0}'/\sigma_{v0}'$	1.00

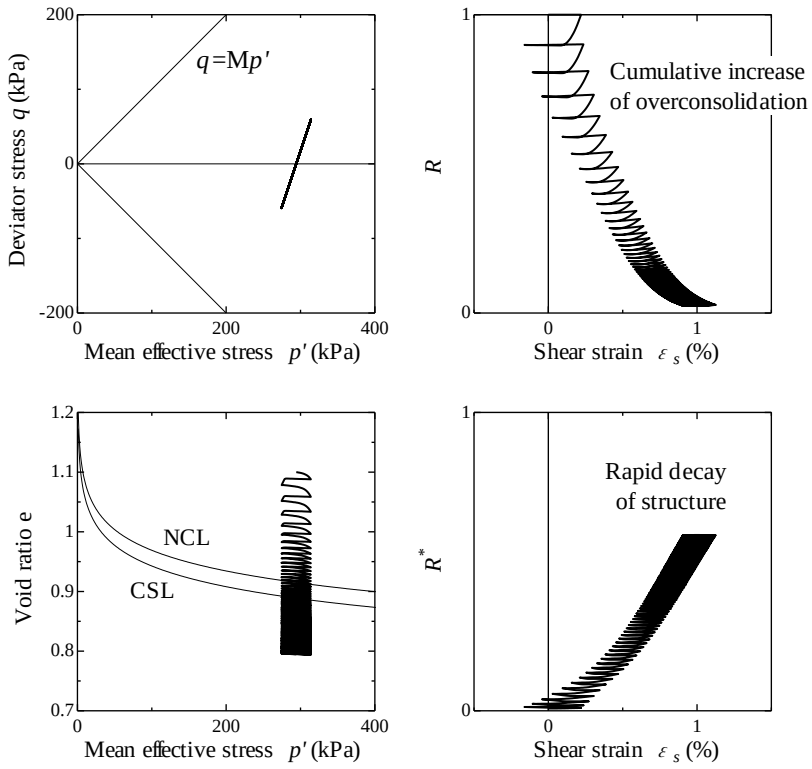

Fig. A2.53 Overall behavior of "compaction" of a loose sand under repeated shear stress application

A triaxial repeated compression/extension test was performed on the loose sand, under drained conditions, at a constant lateral pressure ($\sigma_2 = \sigma_3 = 294$ kPa) and a relatively low shear stress amplitude q. The deviator stress amplitude is 58.9 kPa. The elastoplastic response to this, according to SYS Cam-clay model, can be seen in **Figure A2.53**. The extreme degree of volume compression undergone with the loose sand is shown by $\mathrm{e} - p'$ axes. The two lines drawn in the Figure represents the normal consolidation and critical state lines from the modified Cam-clay model, using the elastoplastic parameters: $\tilde{\lambda}$, $\tilde{\kappa}$, N and Γ ($= \mathrm{N} - (\tilde{\lambda} - \tilde{\kappa})\ln 2$). Looking at these results, it can be seen that the soil compression theory of classical soil mechanics, based on the $\mathrm{e} - \log p'$ relation and dilatancy $\mathrm{N} - \Gamma \propto \tilde{\lambda} - \tilde{\kappa}$, is powerless to deal with the compaction/densification of sand.

Figure A2.54 is an enlargement of $\mathrm{e} - p'$ relationship in **Figure A2.53**. This illustrates vividly the impossibility of trying to compact loose sand under monotonic loading. At a pressure above 2000 kPa, the sand particles are finally crushed to destruction. **Figure A2.54** is also important for showing that no concept of "maximum past loading" is needed for a definition of the overconsolidation ratio. Let's next look more closely at that aspect.

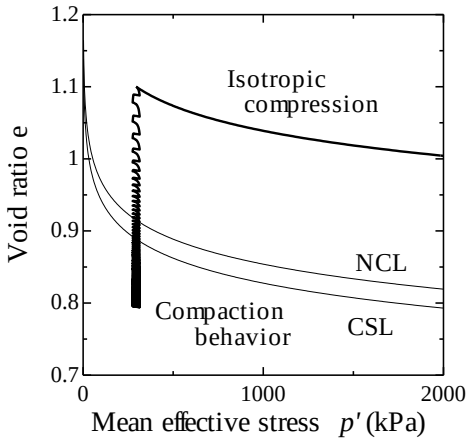

Fig. A2.54 Compaction and isotropic compression of loose sand

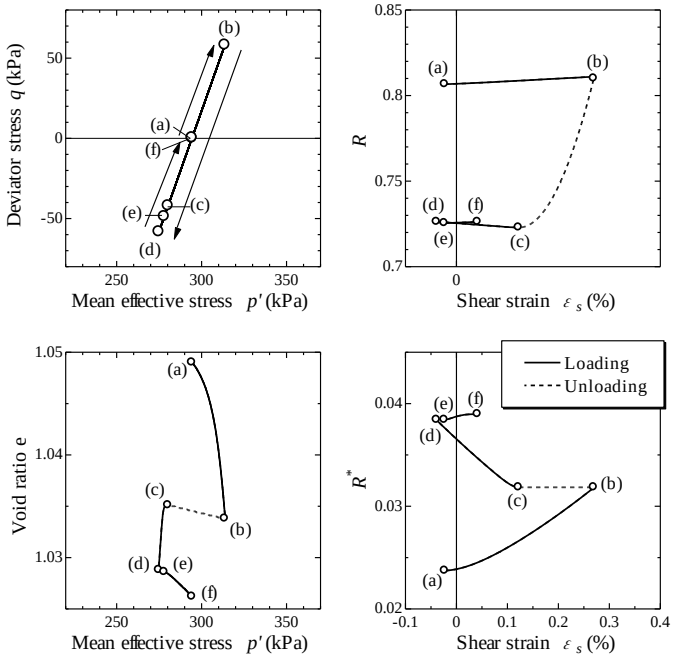

Fig. A2.55 Detailed behavior during "compaction" procedure

The changes in void ratio and in R and R^* are shown enlarged in **Figure A2.55**, for the third cycle of the repeated shear stress. Although these Figures are simply a blowing up of **Figure A2.54**, the larger scale does aid comprehension. There are significant compressions during the loading stages (a)□(b), (c)□(d) and (e)□(f). How large a compression occurs can be appreciated from **Eq. (A2.101)** as well as from the increase of R^*. However, the loss of overconsolidation accompanying the loading process is extremely small. By contrast, the increase in overconsolidation that occurs in the unloading states (b)□(c) and (d)□(e) of the repeated loading is highly conspicuous. In this way, while the structure is destroyed early on by the repeated loading, overconsolidation goes on accumulating, leading to a diminution in R. The same

tendency can be gleaned from **Figure A2.53**.

The fact that there is so little loss of overconsolidation in the loading stage implies that the increases in size of the Subloading and Superloading yield surfaces under loading must be comparable, so that there is almost no change in the ratio between them. However, whereas the Superloading yield surface, after increasing in size under loading, hardly alters its position in response to the subsequent unloading, the Subloading yield surface follows the response of diminution in the current stress and reduces its shape in turn. Since the overconsolidation ratio is determined as the size ratio between the Superloading and Subloading yield surfaces, and since every repeated cycle of loading means that the Superloading yield surface will increase in size while the size of the Subloading yield surface will remain tied to the position of current stress, the overconsolidation ratio, in a case of sand like this, will go on and on rising, as shown in **Figure A2.56**.

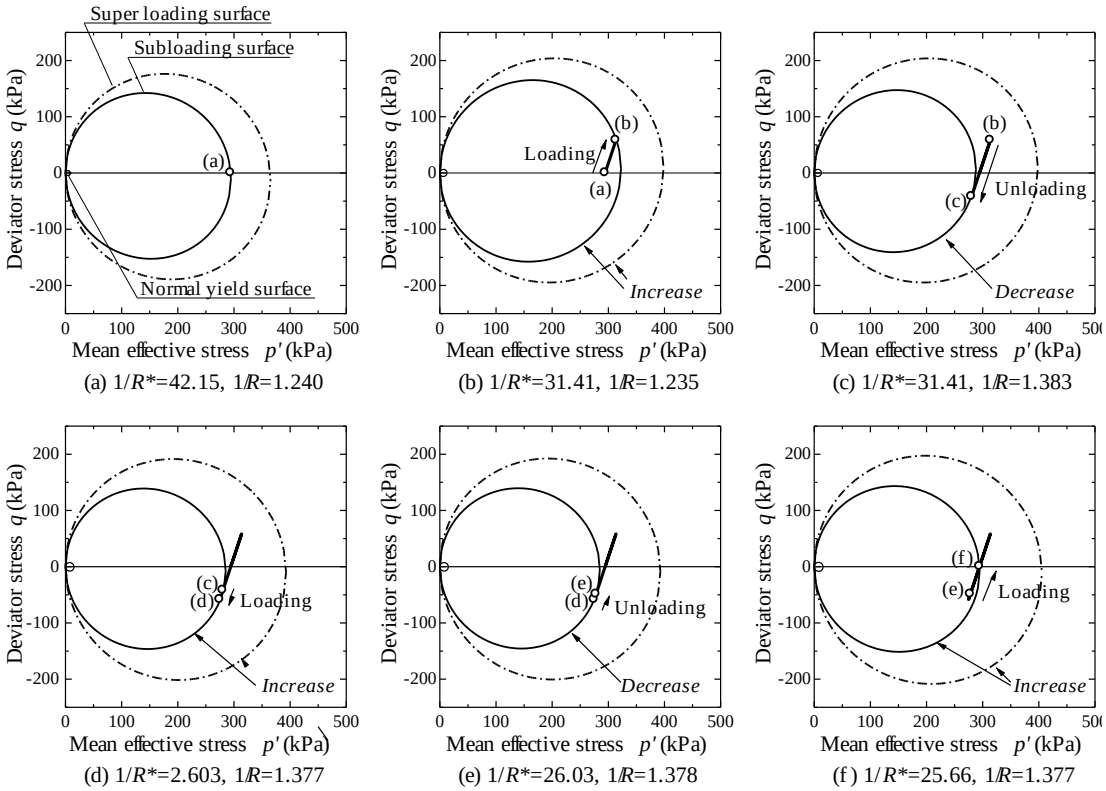

Fig. A2.56 Enlargement of Superloading yield surface due to repeated loading

(3) Drained and undrained behaviors of sand with various densities

The $e - p'$ in **Figure A2.53** is relabeled here as **Figure A2.57**. **Figure A2.57** shows five states of the sand, [1]□[5], as indicated by void ratio e, R and R^*, obtained in the course of compaction at five stages of repeated loading, beginning at

initial state [1]. (n indicates the number of each shear cycle.) Looking at the five states, we recognize them as:
[1]: loose sand
[2]: medium loose sand
[3]: medium dense sand
[4]: dense sand
[5]: very dense sand

These five states of sand are all obtained from the same sand. That is to say, the five states [1]□[5] of this sand have all been generated spontaneously by assigning the elastoplastic and evolution parameters of **Table A2.5** to SYS Cam-clay model and then computing the responses to repeated shear stresses on the basis of the initial conditions shown in **Table A2.7**. It is to be stressed that they are not simply five states that are invented arbitrarily. (The initial values of medium dense sand in previous section are regarded to be [3].)

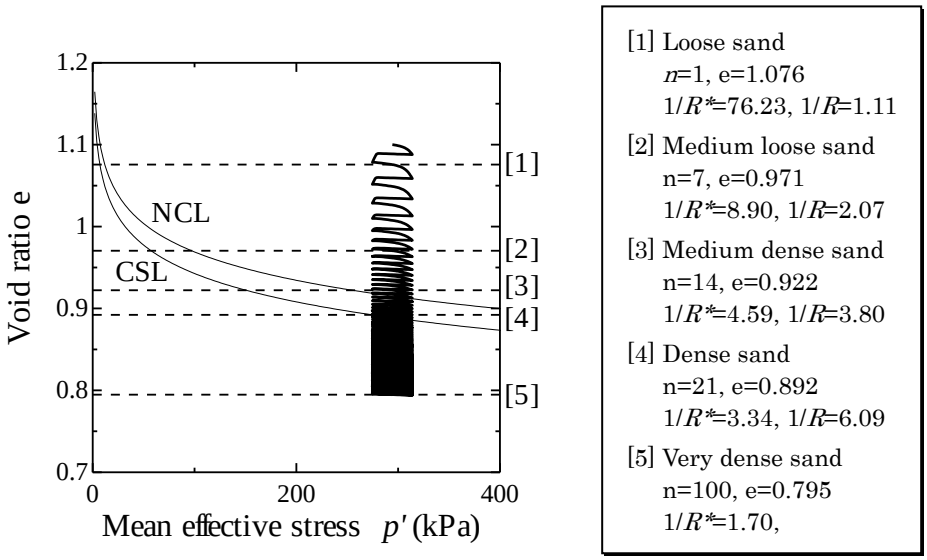

Fig. A2.57 Five different sand specimens as distinguished by “compaction” procedure

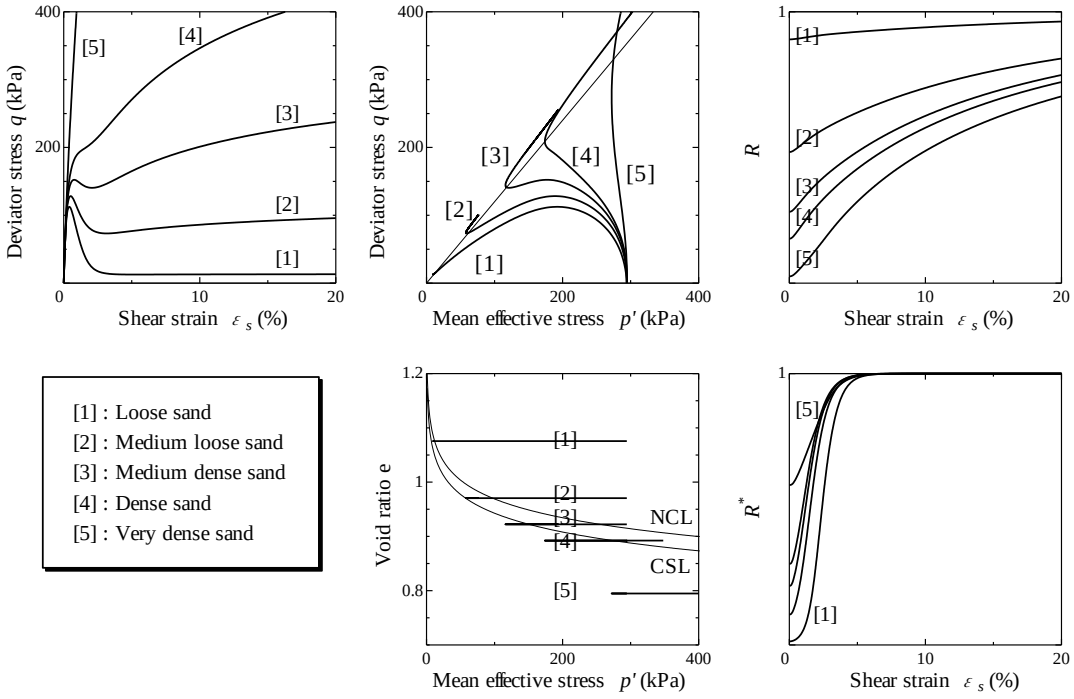

Fig.

A2.58 Undrained triaxial compression behaviors of the five and specimens of different densities

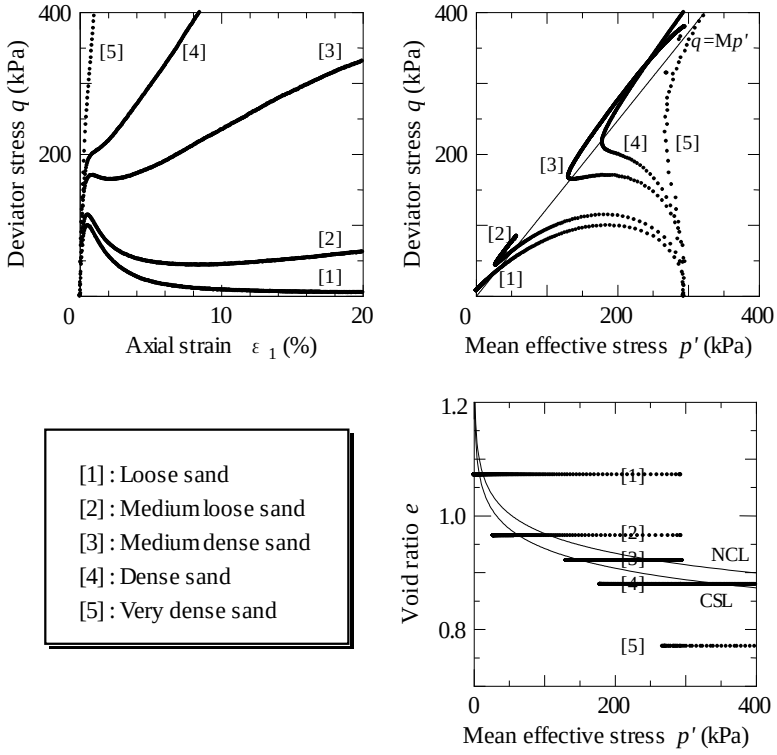

Fig. A2.59 Experimental results corresponding to Fig. A2.58

(after Nakano and Nakai, 2004)

Table A2.8 Physical properties of the sand tested in laboratory

Specific gravity of grains G_s	2.65
Maximum void ratio $e_{\max}$	1.06
Minimum void ratio $e_{\min}$	0.64

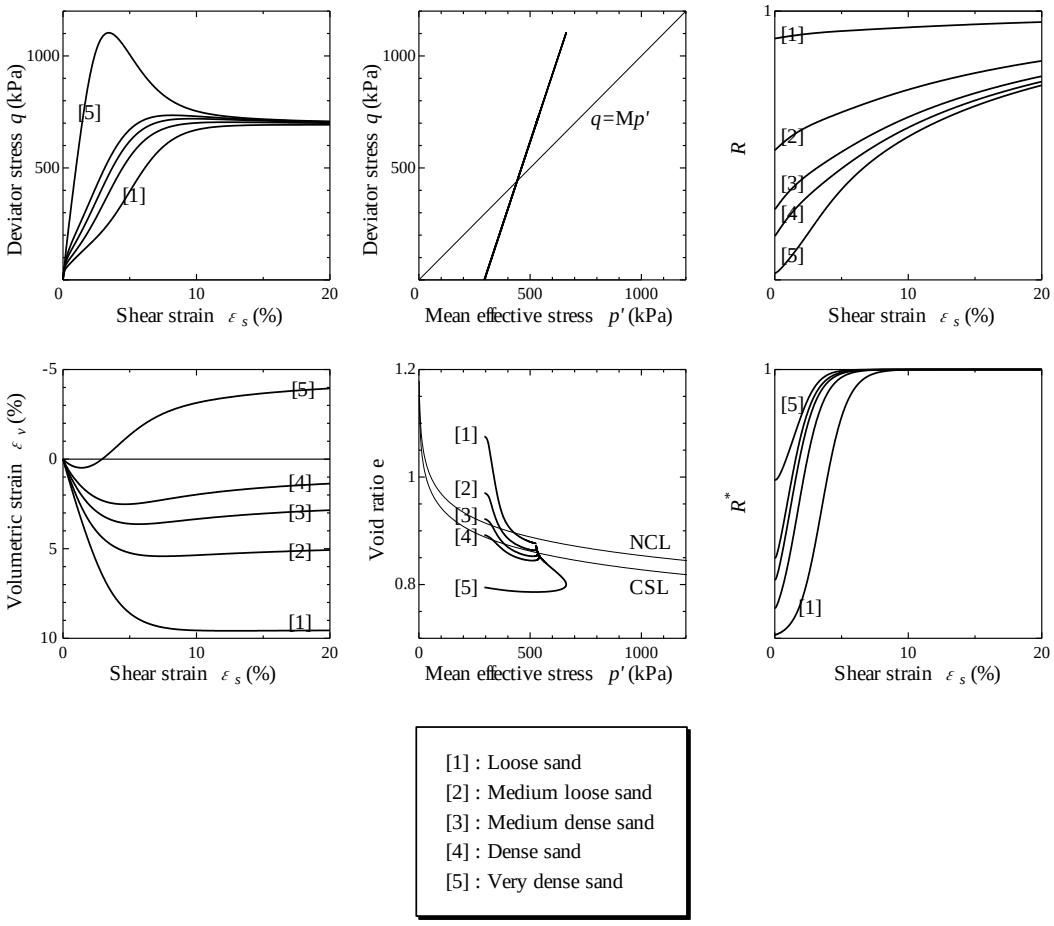

Fig. A2.60 Drained triaxial compression behaviors of the five and specimens of different densities

In the next, how these five different kinds of sand will respond to undrained and drained triaxial tests will be computated. **Figure A2.58** shows the elastoplastic response obtained from SYS Cam-clay model for an undrained triaxial compression test with constant lateral cell pressure. All of these sand responses are derived from the same elastoplastic and evolution parameters (**Table A2.5**). Moreover, as was stressed above, the initial conditions of the specimen in each of the five cases are obtained by successive calculations from the original loose state of the same sand. It will therefore be evident that the undrained shear responses in **Figure A2.58** are all the results of a

variation of void ratio, overconsolidation ratio, degree of structure and anisotropy in the same sand specimen. What happens when the test is actually performed in a laboratory is shown in **Figure A2.59**. These test results come from work by Nakano and Nakai (2004). The physical specifications of the sand used are given in **Table A2.8.** It is important to notice the good qualitative and quantitative match between **Figures A2.58** and **A2.59**. The qualitative tendencies of the test finding in **Figure A2.59** have long been familiar in experimental soil mechanics (Castro, 1969). In addition, there is also a line called "phase transformation line" in **Figure A2.59**. The slope of this line is 1.2 that is larger than the critical state constant $M=1.0$. Finally, when the stress ratio is high enough, the so-called "failure line" can also be depicted. The changes in the slopes of these lines lie in that the watershed of plastic expansion and plastic compression M_a varies as extent of anisotropy develops during the shear action. From the experimental results that the phase transformation line and failure line appear, we can conclude that the evolutional rate of anisotropy for sand is relatively rapid.

There have been attempts by some researchers and research groups to explain the experimental findings of **Figure A2.59** by setting up separate models or separate elastoplastic parameters. However, they have virtually nothing to say on the subject of the drained shearing of sand. This is because, in drained conditions, both loose and dense sand undergo very noticeable changes in sedimentation through shearing.

Figure A2.60 shows the elastoplastic response of 5 sands corresponding to **Figure A2.57** for a drained triaxial compression test with constant lateral cell pressure. The qualitative tendency in **Figure A2.60** is already well-known from the classic experiments of soil mechanics (Bishop and Henkel, 1962).

REFERENCES

1) Asaoka A. (2003): Consolidation of clay and compaction of sand, An elasto-plastic description –, Keynote lecture, Proc.of 12th Asian Regional Conf. on Soil Mechanics and Geotechnical Engineering, Leung et al. Singapore, Aug., Vol.2, pp.1157-1195.
2) Roscoe, K. H., Schofield, A. N. and Wroth, C. P. (1958): On the yielding of soils, Geotechnique, Vol.8, pp.22-53.
3) Roscoe, K. H., Schofield, A. N. and Thurairajah, A. (1963): Yielding of clays in states wetter than critical, Geotechnique, Vol.13, pp.211-240.
4) Asaoka, A., Nakano, M. and Noda, T. (1994): Soil-water coupled behaviour of saturated clay near/at critical state, Soils and Foundations, Vol.34, No.1, pp.91-105.

5) Noda, T., Asaoka, A. and Nakano, M. (2008): Soil-water coupled finite deformation analysis based on a rate-type equation of motion incorporating the SYS Cam-clay model, Soils and Foundations, Vol.48, No.6, pp.771-790.
6) Asaoka, A., Nakano, M. and Noda, T. (1998): Super loading yield surface concept for the saturated structured soils, Proc, of the fourth European conference on numerical methods in geotechnical engineering NUMGE98, pp.232-242.
7) Asaoka, A., Nakano, M. and Noda, T. (2000): Superloading yield surface concept for highly structured soil behavior, Soils & Foundations, No.40, Vol.2, pp.99-110.
8) Asaoka, A., Noda, T., Yamada, E., Kaneda, K. and Nakano, M. (2002): An elasto-plastic description of two distinct volume change mechanisms of soils, Soils and Foundations, Vol.42, No.5, pp.47-57.
9) Hashiguchi, K. (1978): Plastic constitutive equations of granular materials, Proc. of US-Japan Seminar on Continuum Mechanics and Statistical Approaches in the Mechanics of Granular Materials (Cowin, S.C. and Satake, M. eds.), Sendai, JSSMFE, pp.321-329.
10) Taylor, D. W. (1948): Fundamentals of soil mechanics, John Wiley, New York, pp.700.
11) Schofield, A. N. and Wroth, C. P. (1968): Critical state soil mechanics, McGRAW-HILL, London.
12) Parry, R. H. G. (1960): Triaxial compression and extension tests on remoulded saturated clay, Geotechnique, 10, pp.166-180.
13) Henkel, D. J. (1960): The relationships between the effective stresses and water content in saturated clays, Geotechnique, Vol.10, pp.41-54.
14) Atkinson, J. H. and Henkel, D. J. (1978): The mechanics of soils, McGRAW-HILL.
15) Muir Wood, D (1955): Soil behavior and critical state soil mechanics, Cambridge.
16) Mikasa M. (1964): A classification chart for engineering properties of soils, Soils and Foundations, Vol.12, No.4, pp.17-24.
17) Bishop, A. W. and Henkel, D. J. (1962): The measurement of soil properties in the triaxial test, Edward Arnold, London.
18) Asaoka, A., Nakano, M. and Noda, T. (1997): Soil-water coupled behavior of heavily overconsolidated clay near/at critical state, Soils & Foundations, Vol.37, No.1, pp.13-39.
19) Druker, D. C. and Prager, W. (1952): Soil mechanics and plastic analysis on limit design, Quarterly of applied mechanics, Vol.10, No.2, pp.157-165.
20) Sekiguchi, H. and Ohta, H. (1977): Induced anisotropy and time dependency in clays, Constitutive Equations of Soils（Proc, 9th Int. Conf. Soil Mech. Found. Eng., Spec. Session9）, Tokyo, p.229-238.
21) Hashiguchi, K. and Chen, Z. P. (1998): Elastoplastic constitutive equations of soils

with the subloading surface and the rotational hardening, Int. J. Numer. Anal. Meth. Geomech., Vol.22, pp.197-227.

22) Green, A. E. and Naghdi, P. M. (1965): A general theory of elasto-plastic continuum, Archive for Rational Mechanics and Analysis, Vol.18, pp.251-281.

23) Hashiguchi, K. (1989): Subloading surface model in unconventional plasticity, Int. J. of Solids and Structures, Vol.25, pp.917-945.

24) Nakano, M., Nakai, K. and Asaoka, A. (2004): A description of mechanical behavior of clay and sand based on evolutions of soil structure and overconsolidation, Workshop on Testing Modeling and Simulation in Geomechanics, ASCE.

25) Asaoka, A., Nakano, M. and Noda, T. (2001): The loss of structure and the decay of overconsolidation, Proc. 15th Int. Conf. on Soil Mechanics and Geotechnical Engineering, Istanbul, Turkey, pp.19-22.

26) Tatsuoka, F. and Kohata, Y. (1995): Stiffness of hard soils and soft rocks in engineering applications, Proc. of 1st Int. Conf. on Pre-failure Deformation Characteristics of Geomaterials, Sapporo, Japan, 2, pp.947-1063.

27) Castro, G. (1969): Liquefaction of sands, ph.D. Thesis, Harvard Soil Mech. Series, No. 81.